AD0275395

ASD-TR-61-207

OFFICIAL FILE COPY

CRACK STRENGTH AND CRACK PROPAGATION CHARACTERISTICS OF HIGH STRENGTH METALS

TECHNICAL DOCUMENTARY REPORT No. ASD-TR-61-207

JANUARY 1962

20080818 029

DIRECTORATE OF MATERIALS & PROCESSES
AERONAUTICAL SYSTEMS DIVISION
AIR FORCE SYSTEMS COMMAND
UNITED STATES AIR FORCE
WRIGHT-PATTERSON AIR FORCE BASE, OHIO

PROJECT Nr 7381, TASK Nr 738103

OFFICIAL FILE COPY

(Prepared under Contract Nr AF 33(616)-7444
by the Douglas Aircraft Company, Inc., Long Beach, California;
R. H. Christensen and P. H. Denke, authors.)

NOTICES

When Government drawings, specifications, or other data are used for any purpose other than in connection with a definitely related Government procurement operation, the United States Government thereby incurs no responsibility nor any obligation whatsoever; and the fact that the Government may have formulated, furnished, or in any way supplied the said drawings, specifications, or other data, is not to be regarded by implication or otherwise as in any manner licensing the holder or any other person or corporation, or conveying any rights or permission to manufacture, use, or sell any patented invention that may in any way be related thereto.

Qualified requesters may obtain copies of this report from the Armed Services Technical Information Agency, (ASTIA), Arlington Hall Station, Arlington 12, Virginia.

This report has been released to the Office of Technical Services, U. S. Department of Commerce, Washington 25, D. C., for sale to the general public.

Copies of ASD Technical Reports and Technical Notes should not be returned to the Aeronautical Systems Division unless return is required by security considerations, contractual obligations, or notice on a specific document.

600 - April 1962 - 28-1215 & 1216

AD275395

FOREWORD

The USAF contract, AF 33(616)-7444, was initiated under Project Nr 7381, Task Nr 738103, "Crack Strength and Crack Propagation Characteristics of High Strength Metals", Aeronautical Systems Division. The work was administered under the direction of the Directorate of Materials and Processes, Deputy for Technology, Aeronautical Systems Division with Mr. Sidney O. Davis, Major John A. Fiorillo and Mr. C. L. Harmsworth acting as project engineers.

The Douglas program was conducted under the direction of L. S. Mull, Chief of Strength and Dynamics Section, Long Beach Transport Aircraft Engineering, with R. H. Christensen acting as the Douglas project engineer. Analysis methods were directed by P. H. Denke, assisted by J. O'Kelly.

The design, planning and operation of all structural tests and testing fixtures were under the direction of W. W. Bradley, Senior Strength Test Engineer, assisted by H. A. Bellows, Jr.

The mechanical, metallurgical and fatigue testing laboratories were under the supervision of J. L. Waisman, Chief Metallurgist. Work in these laboratories was administered by A. Phillips, T. Conmy, C. S. Yen, R. Engel and J. W. Clark.

This report contains the results of the tests performed between 1 August 1960 and 31 May 1961.

ABSTRACT

The purpose of this program has been to obtain engineering data on the crack propagation and residual strength characteristics of structural materials suitable for use in aerospace systems. Results of a fracture testing program for high strength sheet metals are presented. More than 500 sheet stock panels ranging in width from one to 18 inches and in thickness from .020" to .100" were tested. These panels contained centrally located cracks which were generated principally by fatigue loading at various exposure times under a variety of environments. In general the fatigue crack is shown to be a more severe stress raiser than any manufactured notch yet investigated. Fracture strengths of the cracked panels were determined for rupturing temperatures ranging from -340°F. to 2,500°F.

The experimental results were studied analytically. A semi-empirical expression for residual strength is derived. This expression is based on a modification of the formula given by Crichlow for the effective width of the plastic zone. An expression for the rate of crack propagation also is presented. The crack rate formula is based on the plastic zone concept, and accounts for the observed approach to infinite cracking rates as the crack length approaches critical. These formulas are shown to agree well with test results and are suitable for design applications.

A digital analysis of the elastic and plastic stress and strain distribution in the cracked plate was performed. The analytical method is discussed and results are presented.

PUBLICATION REVIEW

This report has been reviewed and is approved.

FOR THE COMMANDER:

W. P. Conrardy

W. P. CONRARDY
Chief, Materials Engineering Branch
Applications Laboratory
Directorate of Materials and Processes

TABLE OF CONTENTS

SECTION		PAGE
1	INTRODUCTION	1
2	OUTLINE AND REVIEW OF TEST PROGRAM	3
3	TEST PROCEDURE	5
4	SUMMARY OF TEST RESULTS ON PH15-7 MO RH950 STEEL SHEET (-320°F to +900°F)	13
5	SUMMARY OF TEST RESULTS ON AM355 STEEL SHEET (-320°F TO +900°F)	47
6	SUMMARY OF TEST RESULTS ON A.I.S.I.4340 STEEL SHEET (-320°F TO +600°F)	68
7	SUMMARY OF TEST RESULTS ON UNITEMP (RENE' 41) NICKEL CR-MO-CO ALLOY SHEET (-340°F TO +1,810°F)	82
8	SUMMARY OF TEST RESULTS ON B120 VCA TITANIUM ALLOY SHEET (-320°F TO +600°F)	113
9	SUMMARY OF TEST RESULTS ON WROUGHT-SINTERED MOLYBDENUM (COATED) SHEET (-340°F TO +2,500°F)	127
10	RESIDUAL STRENGTHS OF CRACKED PANELS UNDER BIAXIAL STRESSING	147
	(a) PH15-7 MO RH950 STEEL PANELS	147
	(b) RENE' 41 NICKEL ALLOY PANELS	147
11	RESIDUAL STRENGTH OF STRUCTURALLY-STIFFENED STEEL PANELS CONTAINING CRACK SLITS	166
12	RESIDUAL STRENGTH OF FATIGUE CRACKED PANELS AS A FUNCTION OF SHEET THICKNESS	174
13	PROGRESSIVE FORMATION OF CRACKS LEADING TO FRACTURE	180
14	ANALYSIS	199
	(a) RESIDUAL STRENGTH	199
	(b) CRACK PROPAGATION RATE	202
	(c) STRESS DISTRIBUTION AROUND A CRACK IN THE ELASTIC AND PLASTIC STATES OF STRAINING	205

TABLE OF CONTENTS (Cont'd)

SECTION		PAGE
15	CONCLUSIONS AND RECOMMENDATIONS.....	219
16	REFERENCES.....	223
	APPENDIX A - ELECTRON MICROSCOPY IN EXAMINING CRACKED AND FRACTURED METAL SURFACES....	224
	APPENDIX B - MATHEMATICAL DERIVATIONS.....	235
	APPENDIX C - ELECTRIC-ARC DISCHARGE METHOD OF FORMING STARTER-CRACKS.....	239
	APPENDIX D - RESULTS OF THE PLASTIC ANALYSIS.....	242
	APPENDIX E - USE OF THE EMPIRICAL FORMULAS.....	248
	APPENDIX F - SUPPLEMENTARY ANALYSIS OF RESIDUAL STRENGTH.....	253
	BIBLIOGRAPHY.....	256

LIST OF ILLUSTRATIONS

FIGURE		PAGE
1	Test Specimen Shearing Schedule	8
2	Test Specimens	9
3	Test Panel Temperature Distribution Survey	10
4	Fatigue machine	11
5	Test Set-up in Low-Cycle Hydraulic Fatigue Test Machine	12
6	Residual Strength vs Degree of Cracking	17
7	Residual Strength vs Degree of Cracking	18
8	Residual Strength vs Degree of Cracking	19
9	Un-notched Tensile Strength as a Function of Test Temperature	20
10	Fracture Toughness vs Test Temperature	21
11	Residual Strength vs Test Temperature	22
12	Residual Strength vs Test Temperature	23
13	Residual Strength vs Degree of Cracking	24
14	Residual Strength vs Degree of Cracking	25
15	Residual Strength vs Degree of Cracking	26
16	Residual Strength vs Degree of Cracking	27
17	Net Fracture Strength vs Degree of Cracking	28
18	Net Fracture Strength vs Degree of Cracking	29
19	Fatigue Crack Growth.	30
20	Fatigue Crack Growth.	31
21	Fatigue Crack Growth.	32
22	Residual Strength vs Degree of Cracking	33
23	Notch Strength vs Test Temperature.	34
24	Net Area Fracture Strength vs Test Temperature	35

FIGURE		PAGE
25	Fatigue Crack Growth	36
26	Load-Strain Curve	37
27	Residual Strength vs. Degree of Cracking	50
28	Fatigue Crack Growth	51
29	Fatigue Crack Growth	52
30	Interrupted Fatigue Crack Growth	53
31	Fatigue-Creep Crack	54
32	Residual Strength vs. Degree of Cracking	55
33	Fatigue Crack Growth	56
34	Fatigue Crack Growth	57
35	Fatigue Crack Growth	58
36	Stress Intensity vs. Rate of Cracking	59
37	Accumulative Fatigue Crack Growth	60
38	Stress Intensity vs. Rate of Cracking at Elevated Temperatures	61
39	Accumulative Fatigue Crack Growth	62
40	Load-Strain Curves	63
41	Residual Strength vs. Degree of Cracking	70
42	Residual Strength vs. Degree of Cracking	71
43	Residual Strength vs. Length of Micro Cracks	72
44	Micro-Crack Specimens	73
45	Fracture Surfaces of Micro-Cracked Specimens	74
46	Residual Strength as a function of Cycles of Loading	75
47	Fatigue Crack Growth	76
48	Load-Strain Curve	77

LIST OF ILLUSTRATIONS (Cont'd)

FIGURE		PAGE
49	Residual Strength vs. Degree of Cracking	85
50	Residual Strength vs. Degree of Cracking	86
51	Fracture Toughness vs. Test Temperature	87
52	Fatigue Crack Growth	88
53	Fatigue Crack Growth	89
54	Fatigue Crack Growth	90
55	Fatigue Crack Growth	91
56	Fatigue Crack Growth	92
57	Fatigue Crack Growth	93
58	Fatigue Crack Growth	94
59	Programmed Fatigue Crack Growth	95
60	Programmed Fatigue Crack Growth	96
61	Programmed Fatigue Crack Growth	97
62	Programmed Fatigue Crack Growth	98
63	Programmed Fatigue Crack Growth	99
64	Theoretical Crack Growth Curves	100
65	Stress Intensity vs. Rate of Cracking	101
66	Unnotched Tensile Strength as a function of Test Temperature	102
67	Load-Strain Curve	103
68	Residual Strength vs. Degree of Cracking	115
69	Residual Strength vs. Degree of Cracking	116
70	Fatigue Crack Growth	117
71	Fatigue Crack Growth	118
72	Fatigue Crack Growth	119

LIST OF ILLUSTRATIONS (Cont'd)

FIGURE		PAGE
73	Load-Strain Curve	120
74	Residual Strength vs. Degree of Cracking	130
75	Residual Strength vs. Degree of Cracking	131
76	Residual Strength vs. Degree of Cracking	132
77	Fatigue Crack Growth.	133
78	Fatigue Crack Growth.	134
79	Fatigue Crack Growth.	135
80	Stress Intensity vs. Rate of Cracking	136
81	Environmental Breakdown of Molybdenum Panel	137
82	Environmental Breakdown of Molybdenum Panel	138
83	Load-Strain Curve	140
84	Center notched Molybdenum Test Panel at 2500 ^{o}F	141
85	Detail of High Temperature Test Set-up	142
86	Residual Strength vs. Crack Length under Biaxial Loading	149
87	Residual Strength vs. Crack Length under Biaxial Loading	150
88	Residual Strength vs. Crack Length under Biaxial Loading	151
89	Safe to Unsafe Fracture	152
90	Straight Running Fracture	153
91	Curved Running Fracture	154
92	Curved Running Fracture	155
93	Cross-Section of Bulge Specimen Test Apparatus	160
94	Bulge Arc-Height Measuring Device-Type 1	161
95	Bulge Arc-Height Measuring Device-Type 2	162

LIST OF ILLUSTRATIONS (Cont'd)

FIGURE		PAGE
96	Test Recording and Preliminary Calibration Equipment	163
97	Block Diagram of Bulge Panel Arc-Height Vs. Pressure Recording System	164
98	Typical XY Recording of Bulge Arc-Height Change Vs. Pressure Increase	165
99	Residual Strength Vs. Degree of Cracking	167
100	Stiffened Steel Panel - Uniaxial Loading	168
101	Panel Fabrication Details	169
102	18 Inch Wide Unstiffened Panel in Testing Machine (Heat Lamps Shown on One Side Only)	170
103	Test Set-Up of Center Slotted 20 Inch Panel	171
104	Enlarge View of Stiffened Panel. Insert of Unstable Crack	172
105	Residual Strength Vs. Degree of Cracking	175
106	Residual Strength Vs. Degree of Cracking	176
107	Residual Strength Vs. Degree of Cracking	177
108	Residual Strength Vs. Degree of Cracking	178
109	Residual Strength Vs. Degree of Cracking	179
110	Crack Growth Vs. Number of Load Cycles	185
111	Micro and Macro Cracking	186
112	Coarse and Fine Fracture	187
113	Fatigue Crack Growth in Later Stages	188
114	Fatigue Fracture	189
115	Progressive Fracture	190
116	Progressive Crack Growth Temperature Effects	191
117	Electron Microfractographs	192

FIGURE		PAGE
118	Creep-Fatigue Crack	193
119	Micro-Metal Quakes	194
120	Fracture Appearance	195
121	Heat Tinted Fatigue Cracked Surfaces	196
122	Fracture Transition	197
123	Sinusoidal Fracture Path	198
124	Cracked Plate in Equilibrium	207
125	Comparison of Residual Strength Formula With Test For PH15-7 Mo RH950	208
126	Comparison of Residual Strength Formula With Test For B120 VCA Titanium	209
127	Comparison of Residual Strength Formula With Test For RENE' 41	210
128	Comparison of Residual Strength Formula With Test For 2024-T3 Alclad	211
129	Comparison of Residual Strength Formula With Test For 7075-T6 Alclad	212
130	Notch Resistance as Function of Material Ductility	213
131	Comparison of Theoretical and Experimental Crack Propagation Rates	214
132	Idealized Structure for Crack Analysis	215
133	σ_y, Elastic Distribution	216
134	Comparison with Westergaard's Result	217
135	Elastic Distribution of Equivalent Stress	218
136	Electron Microscope	227
137	Electron Microfractograph of Fatigue Fractured Surface - RENE' 41 Nickel Alloy Sheet Material	228
138	Electron Micrograph of Microstructure - PH15-7 Mo RH950	229
139	Electron Microfractograph of Fatigue Fractured Surface in Tantalum Sheet Stock	230

LIST OF ILLUSTRATIONS (Cont'd)

FIGURE		PAGE
140	Electron Microfractograph of Fatigue Fractured Surface Aluminum	231
141	Stereoscopic Electron Microfractograph of Fatigue Fractured Surface - RENE' 41	232
142	Electron Microfractograph of Fatigue Fractured Surface of Pure Molybdenum Wrought-Sintered Sheet. .	233
143	Fatigue Crack Growth "Arrest" Lines as a Function of Net Area Fatigue Cracking Stress	234
144	Agietron Machine Tool	240
145	View Showing a Bulge Panel in Position for Forming Fine (.006 inch) Slit in Crown of Test Specimen . .	241
146	Equivalent Stress-Equivalent Plastic Strain Curve .	243
147	Convergence of the Newton-Raphson Process	244
148	Distribution of Longitudinal Stress at a Transverse Section Through the Crack	245
149	Residual Stress at Zero Load	246
150	Longitudinal Residual Stress Distribution	247
151	Example of Fatigue Crack Propagation	252
152	Modified Assumption for Stress Distribution	257

LIST OF TABLES

TABLE		PAGE
1	Test Material	7
2	Mechanical Properties of PH15-7 Mo RH950 Steel	38
3	Mechanical Properties of AM355 Steel	64
4	Chemical Analysis - AM355 Steel	64
5	Cumulative Crack Growth Under Programmed Loads	104
6	Cumulative Crack Growth Under Programmed Loads	105
7	Mechanical Properties of UNITEMP (RENE' 41)	107
8	Mechanical Properties of B120 VCA Titanium	121
9	Environmental Schedule of a Molybdenum Panel	137
10	Environmental Schedule of a Molybdenum Panel	138
11	Mean Crack Rates	250
12	Calculation of Crack Propagation Curve	251

NOMENCLATURE, SYMBOLS, AND DEFINITIONS

a	$= \frac{\ell}{2}$ or one-half the crack length.
b	= number of blocks in a programmed spectrum of loads and temperatures.
$\mathcal{B}$	= reciprocal of R, or $\sigma_{max}/\sigma_{min}$.
R_p	= plastic zone notch resistance factor.
R	$= \sigma_{min}/\sigma_{max}$
σ_{crk}	= maximum cracking stress in fatigue load cycle.
σ_R	= residual gross area strength of a crack damaged sheet panel.
σ	= gross section stress
$\sigma_{y.s.}$	= same as F_{ty} to unnotched material yield strength.
σ_u	= same as F_{tu} to unnotched material tensile strength.
i	= subscript denoting the ith case.
T_{rupt}	= temperature of specimen at rupture, degree Fahrenheit.
T_{crk}	= cracking temperature of specimen during fatigue crack growth, degree Fahrenheit.
ℓ	= crack length, inches.
ℓ_o	= initial length of starter crack, inches.
ℓ_c	= critical crack length for instability.
$\Sigma\ell$	= total length of crack damage, slot length plus crack length, inches.
ℓ_i	= length of crack at end of ith environmental block.
μ	= slope of theoretical crack-growth curve at $\ell = \ell_c/2$
n	= number of stress cycles.
n_o	= number of stress cycles at ℓ_o.
N	= number of stress cycles to reach ℓ_c or fracture.
k	= constant of proportionality.
K	= stress intensity factor.

K_{cl}	= fracture toughness.
$\mathcal{G}_c$	= critical driving force to fracture specimen at the point of instability.
$\mathcal{G}_{Ic}$	= same as above for plane strain condition.
Δ	= an incremental quantity of ℓ,n, etc.
λ	= spacing between "growth arrest lines" of fatigue fractured surface, micro-inches.
W,w	= plate or panel width, inches.
y	= ℓ_c/W, nondimensional.
P	= axial applied load, pounds.
psi	= pounds per square inch.
ksi	= thousands of pounds per square inch.
t	= time, minutes.
thk.	= thickness, inches.
$\frac{d\ell}{dn}$	= crack growth in micro-inches per cycle, or mils per cycle
ℓn	= natural logarithm.
crack propagation	= the micro-invisible as well as the macro-visible progressive growth of a crack under fatigue or creep load environments.
residual strength	= the impaired or reduced ultimate strength of a panel or member containing a crack, notch or some form of physical material damage.
crack strength	= (a misnomer) sometimes used in lieu of residual strength.

SECTION 1

INTRODUCTION

The complete elimination of fatigue cracks and minute defects in airframe and missile structures is not practical in the present state of technology. Therefore, the "fail safe" design concept has been developed to provide adequate structural safety in the presence of such conditions. According to this concept, multiple load paths are provided, so that a propagating crack can not destroy the load-carrying ability of the structure.

A knowledge of fatigue crack propagation and the strength remaining at any stage of development is important in the application of the fail safe concept. The need for this knowledge becomes more acute as vehicle performance increases and the consequences of structural failure (as in manned space craft) become continually more serious.

The purpose of the present study is to add to the knowledge of crack propagation and residual strength, especially for the newer high strength metals at elevated and cryogenic temperature.

Experimental and analytical investigations of crack propagation and residual strength were conducted. In the experimental phase, testing was done on the steels PH15-7 Mo, AM355 and AISI 4340; the titanium alloy B120 VCA; the nickel-base alloy RENE' 41; and coated molybdenum. Test temperatures ranged from -340°F to 2,500°F.

Cracks were propagated in plate specimens containing centrally located saw cuts. The rate of cracking was observed. Studies of cumulative crack growth under programmed loads and temperatures also were conducted.

Most of the residual strength measurements were made on fatigue cracked specimens, rather than on specimens containing manufactured slots. The fatigue crack was found to reduce residual strength more severely than a slot of any type. Some test results are included on the crack strength under biaxial stressing of the sheet materials RENE' 41 and PH15-7 Mo at 70°F.

A number of observations were made regarding the conjoint action of fatigue with creep and other time dependent phenomena. The effect of the prior history of load and temperature on the subsequent development of fatigue cracks was investigated.

Studies of crack growth based on the appearance of the fracture surface were undertaken. In this work the techniques of electron microscopy and color photography were utilized. These observations are expected to be useful in contributing toward a better understanding of fracture mechanics.

In the analytical phase, semi-empirical expressions were obtained for residual strength and rate of crack propagation. These expressions are based on considerations which emphasize the significant role played by plasticity in the fracture of ductile metals.

Manuscript released by the authors May 1961 for publication as an ASD Technical Report.

The expression for residual strength is a modification of a formula derived by Crichlow based on the effective width of the plastic zone existing at the end of a crack. Good agreement with test results is demonstrated. The formula contains a parameter called the plastic zone notch resistance factor, R_p, which is a measure of the notch resistance of the material.

The expression for rate of crack propagation also is based on considerations of plasticity. The expression accounts for the observed fact that the rate of cracking tends to approach infinity as the crack length approaches critical. Values predicted by the formula correlate well with test results for crack propagation under steady cyclic and programmed loads.

Both formulas are suitable for design applications. A set of design curves for the residual strength of fatigue cracked sheet materials at various rupture temperatures, based on the empirical formula, is presented. Appendix E presents examples of the use of the empirical formulas.

Any empirical approach to fracture mechanics, such as the above, involves undetermined parameters which must be established by other means, usually experimental. However, additional more rigorous analysis also can throw light on the nature of fracture, and assist in the determination of empirical constants. Such an analysis should account for plasticity, which must play a significant part in the fracture of a ductile metal. Accordingly a digital analysis of the elastic and plastic distributions of stress and strain in the cracked plate was performed. The analysis utilized the Redundant Force Method for statically indeterminate systems, and the Reuss equations for biaxial plasticity. Results are reported.

The findings of the crack growth study support the general conclusion that the crack propagation phase of fatigue damage is more predictable and less subject to scatter than the nucleation phase. Most of the scatter in fatigue data results from scatter in the microcrack nucleation period.

At elevated temperatures the cracking is more uniform than at low temperatures, where the cracking of less ductile materials tends to be sporadic. Uniformity of cracking increases with material ductility.

Visible-crack growth periods at elevated temperatures were found to be greater than at low temperatures under the same stress conditions, even though the total fatigue life at the higher temperatures is less. This effect may be related to improved ductility at elevated temperature.

Creep cracking under steady state elevated temperature conditions has marked effects on subsequent fatigue crack progression. The disruption of the leading edge of a fatigue crack and the surrounding material as a significant effect on residual strength of panels ruptured at lower temperatures.

Protective coatings for molybdenum such as W-2 and Durak-B are effective under steady loading. Under cyclic loading, cracks form in the coating, and at temperatures from 1,300° to 2,500°F, the molybdenum oxidizes and burns at extremely rapid rates.

SECTION 2

TEST PROGRAM

This section briefly reviews and outlines the various phases of the testing program. Since fracture strength in material evaluations is a relatively new field a completely fixed or universally accepted terminology has not yet been set. For the purposes of following this report it is suggested that the reader refer to the symbols and definitions on page xiv. The term "crack propagation" for example, has been widely used in industry to describe all conditions from the micro-progressive slow-growth of a fatigue crack to the catastrophic course of fracture during unstable rupture. In this report "crack propagation" has been taken to mean crack-growth only during a fatigue or creep loading environment.

The "residual strength" or crack strength (a misnomer) is defined as the impaired ultimate strength of the material, panel or member containing a crack. This strength is the highest strength attained prior to the onset of unstable fracture originating from the initial cracks in a part.

Many other terms may be found that are not yet common to this field, however, it is hoped that either their usage will be self-explanatory or that referral to the "definitions" will be made.

The reporting as well as the test program for each material investigated has been divided into separate evaluations. Therefore, rather than repeat discussions of the testing phase outline, which was nearly identical for each metal, it will be presented only once and in this section of the report.

PROGRAM OUTLINE

Crack propagation and residual strength tests on high strength metals are principally for small panel specimens. Some large panels are also included in an attempt to demonstrate that safe and reasonable estimates of residual crack strength of large components can be made.

Crack growth and residual strength properties of B120VCA titanium; RENE' 41, nickel base alloy; and three high strength steels, PH15-7 Mo, AM355 and 4340 have been investigated. In addition, a limited amount of testing of the refractory metal molybdenum (coated) has been undertaken.

Inasmuch as elevated temperature is an important environmental consideration in the design of present and future vehicles, the crack studies were expanded to investigate this paramter. Data was obtained on high strength steels up to 1,000°F. on the nickel alloy to 1,800°F. and on the refractory metal up to 2,500°F. A few low temperature tests, to -320°F., were made.

Specifically the program included an investigation of the following variables and their effects on the strength of the metals.

PHASE I. RESIDUAL STRENGTHS OF CRACKED PANELS

(a) effect of length of crack
(b) effect of type of crack
(c) effect of panel width
(d) effect of panel thickness
(e) effect of temperature on dimensions of fatigue grown cracks
(f) effect of temperature on crack strength (short time)
(g) effect of soak temperature
(h) effect of biaxial stressing
(i) comparison of ASTM edge-notched material screening specimen with fatigue cracked panels
(j) correlation of (i) with $\mathcal{G}_c$ and K_c, fracture toughness

PHASE II. FATIGUE CRACK GROWTH RATES

(a) rate of growth as function of cracking stress
(b) rate of growth as function of panel width
(c) rate of growth as function of panel thickness
(d) rate of growth as function of testing temperature
(e) rate of growth as function of interrupted test load levels - programmed spectrum.
(f) rate of growth as function of time of exposure (vary testing speed) at temperature
(g) fractographic examination by electron microscope to correlate "growth line spacing" with stress levels and temperature levels.

SECTION 3

TESTING PROCEDURES

TEST SPECIMENS, EQUIPMENT AND TEST SET-UP

The conditions and heat treatments of the test materials are described in the various sections of this report. In general, the large sheet panels were received and heat treated to the tensile strength ranges as given in Table 1 on page 7.

Prior to heat treatment however, the large sheets were sheared into test specimens and small panels according to the schedule in Figure 1 on page 8. The test panels were milled to nominal widths and slotted centrally with a .006" to .010" thick jewelers circular slotting saw. The slot was machined from both sides of the panel. See Figure 2. The starter crack or central slot was made in this way on over 80% of the test panels. The slot in the remaining panels was performed by the electric arc discharge method. See Appendix C.

Varying lengths of cracks were then grown in the panels by cyclical loads in a fatigue testing machine. The maximum fatigue cracking stress, cycles of loading, and final crack lengths that were grown are itemized in the "Tabulation of Data" within the material "SECTIONS". In most cases the fatigue cracks were grown at +75° to +80° Fahrenheit. Some steel panels were fatigued at cracking temperatures as high as +600° Fahrenheit.

Due to the inconvenience of measuring gross crack growth in wide sheet panels enclosed within a furnace, it was the plan to heat the panels by radient heat lamp reflectors. Preliminary tests indicated the method to be the most accessible for test specimen observation and data recording. Clamp-on thermocouples indicated that a temperature control of +2° at the 800°F. level could be easily maintained for periods greater than forty minutes. The use of a Powerstat in maintaining a steady and continuous current to the lamps was responsible for this accuracy. The control of temperature throughout the actual testing period and the temperature distribution across the panel width was held within $\pm$ 2%. A typical test temperature distribution is shown on a 4" wide panel in the sketch of Figure 3. It is believed that the thermal stresses, due to the temperature gradients both width and thicknesswise in these panels, are too small to have any significant effect on the crack growth characteristics.

The 2" wide to 6" wide test panels were fatigue tested and fatigue cracked in a 15,000 pound capacity Krouse fatigue testing machine. All tests in this testing machine were conducted at a testing frequency of 500 cpm. (Figures 4 and 5).

The majority of the 8" wide test panels were fatigue cracked in a Douglas designed axial loading resonant-type fatigue machine at a testing frequency of 800 cpm. A few 8" wide test panels were cyclically loaded with the aid of the hydraulic jack and a pressure cycling stand at loading rates from 20 to 50 cpm.

All of the fatigue testing machines incorporated calibrated strain-gauge loading rings in series with the test panels. The dynamic loading of the panels was constantly monitored throughout the testing phase with the aid of visual recording oscilloscope. It is believed that the accuracy of the dynamic load as well as the drift in load due to cracking of the panel was within $\pm$ 3% of the nominal value throughout the entire testing period. The stress ratio ($R = \sigma_{min}/\sigma_{max}$) used in fatigue cracking the test panels was held constant throughout the entire program. The value selected was an R value of +.20.

After fatigue cracking, the panels were statically ruptured in either a 60,000 pound capacity Southwark-Emery hydraulic testing machine or a 30,000 pound capacity Riehle testing machine. All panels were loaded to fracture at a loading rate of between 5,000 and 15,000 pounds per minute.

The heating of the panels, in the rupture testing, similar to the fatigue testing, was accomplished with high density quartz-lamp radiant heat reflectors.

The sub-zero tests were conducted as follows: For the panels tested at -240°F. to -340°F. liquid nitrogen was used. A slotted metal container was placed around the panels and the slit to specimen was sealed with "vacuum bag sealing compound." The container was then filled with liquid nitrogen and the panel temperature allowed to reach an equilibrium temperature before testing.

Iron constantan thermocouples pulse-welded to the panels were used for the low-temperature tests. Chromel-alumel thermocouples were used in the elevated temperature tests.

After fracture the initial fatigue crack lengths were measured under ten-power magnification to the nearest hundredth of an inch. See Section 13, page 195.

At the outset of this program there was some doubt as to the importance of using naturally grown fatigue cracks instead of the simpler and more economic forms of sharp machined notches. It was decided that if the fatigue cracks were found to be the severest form of notch then this method would be adhered to in obtaining test specimens for the residual strength or fracture studies.

In the majority of materials investigated, it was found that the fatigue crack was the severest form of notch and for this reason it has been used extensively throughout this testing program. A few machined sharp notch specimens were made for comparison purposes.

The general design of the simple uniaxial loaded sheet panels is shown in the sketches on page 9.

TABLE 1

TEST MATERIAL

Material	As-Received Condition	Heat Treat (U.T.S.)	Maximum Short Time Temperature (8-30 Minutes)	Maximum Long Time Temperature (2-4 Hours)
PH15-7 Mo (Steel)	Condition A	240,000	900° F	600° F
AM355 (Steel)	Condition A	215,000	900° F	650° F
4340 (Steel)	Normalized	280,000	600° F	
B120 VCA (Titanium)	Soln. Treated Cold Rolled	207,000	900° F	600° F
Rene' 41 (Nickel)	Cold formed	196,000	1,800° F	900° F
Comm. Pure Molybdenum (W-2 Coating)	Unannealed 120/130,000		2,500° F	1,350° F

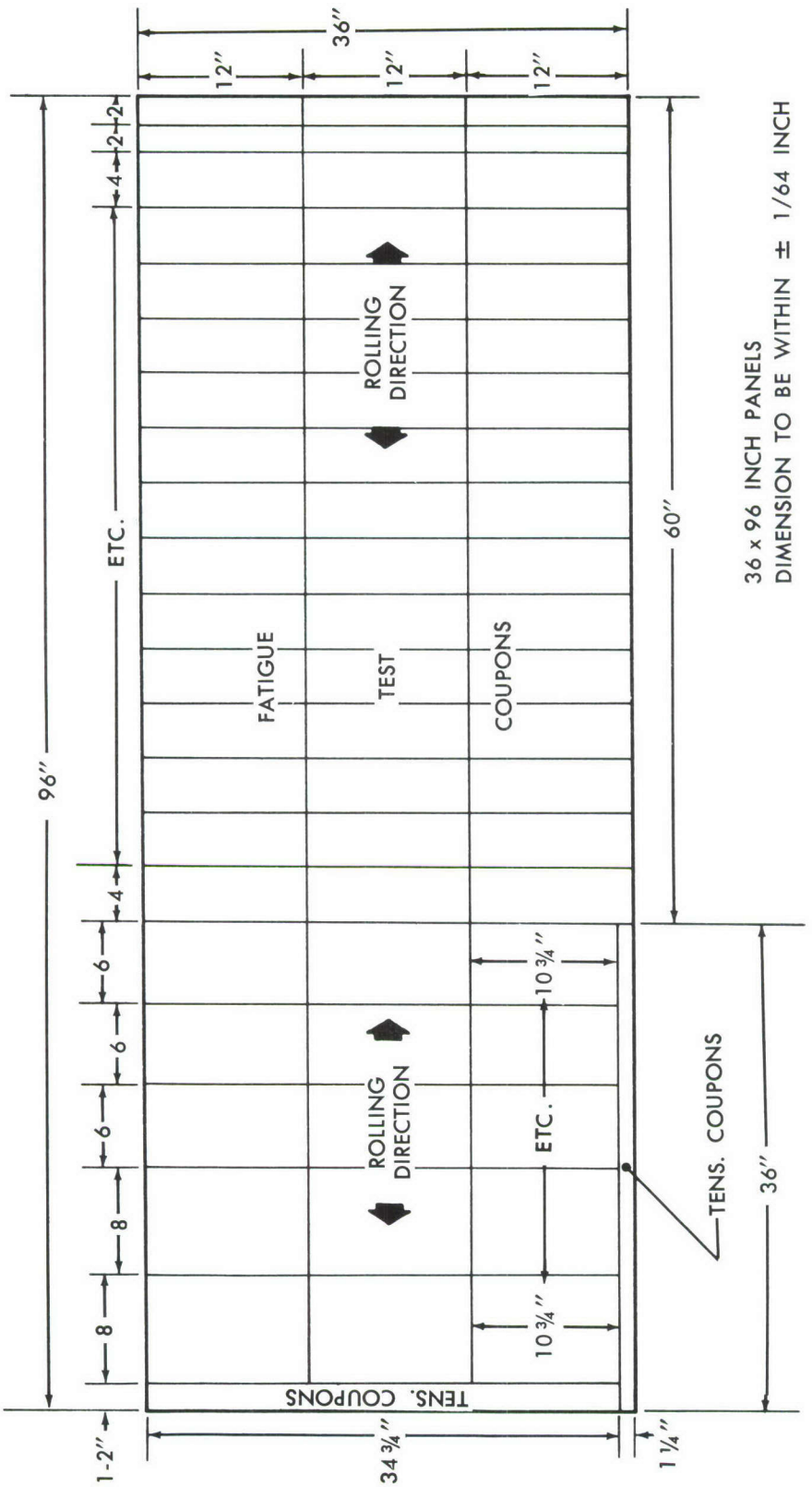
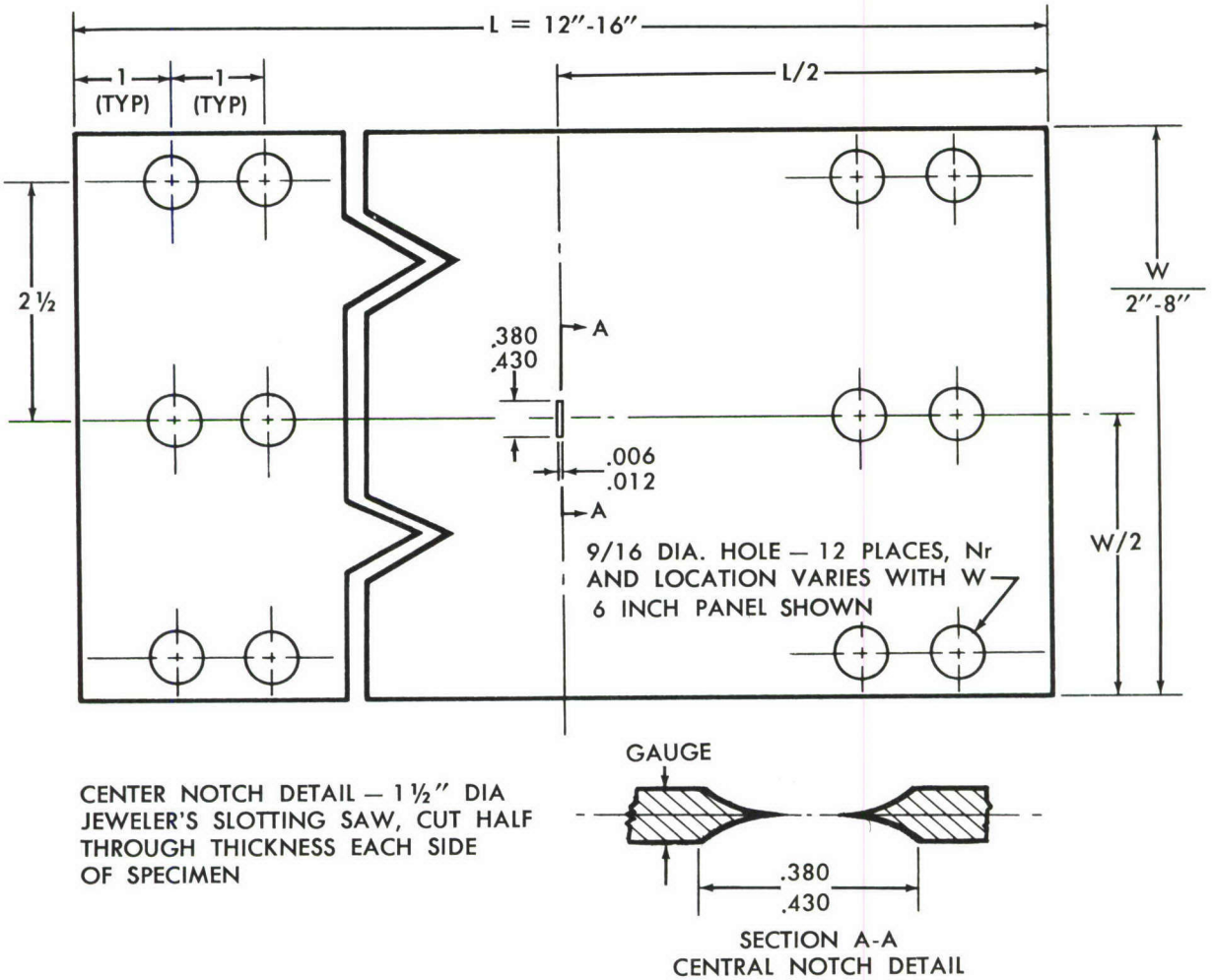


Figure 1. TYPICAL TEST SPECIMEN SHEARING SCHEDULE



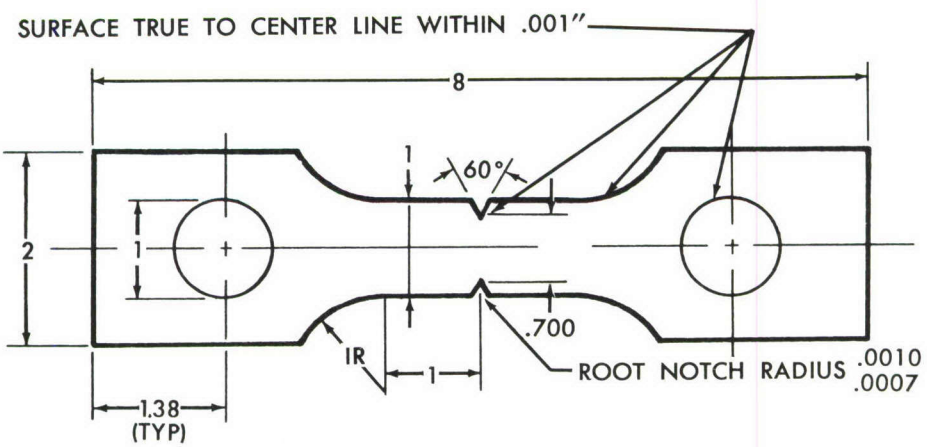


Figure 2. TEST SPECIMENS

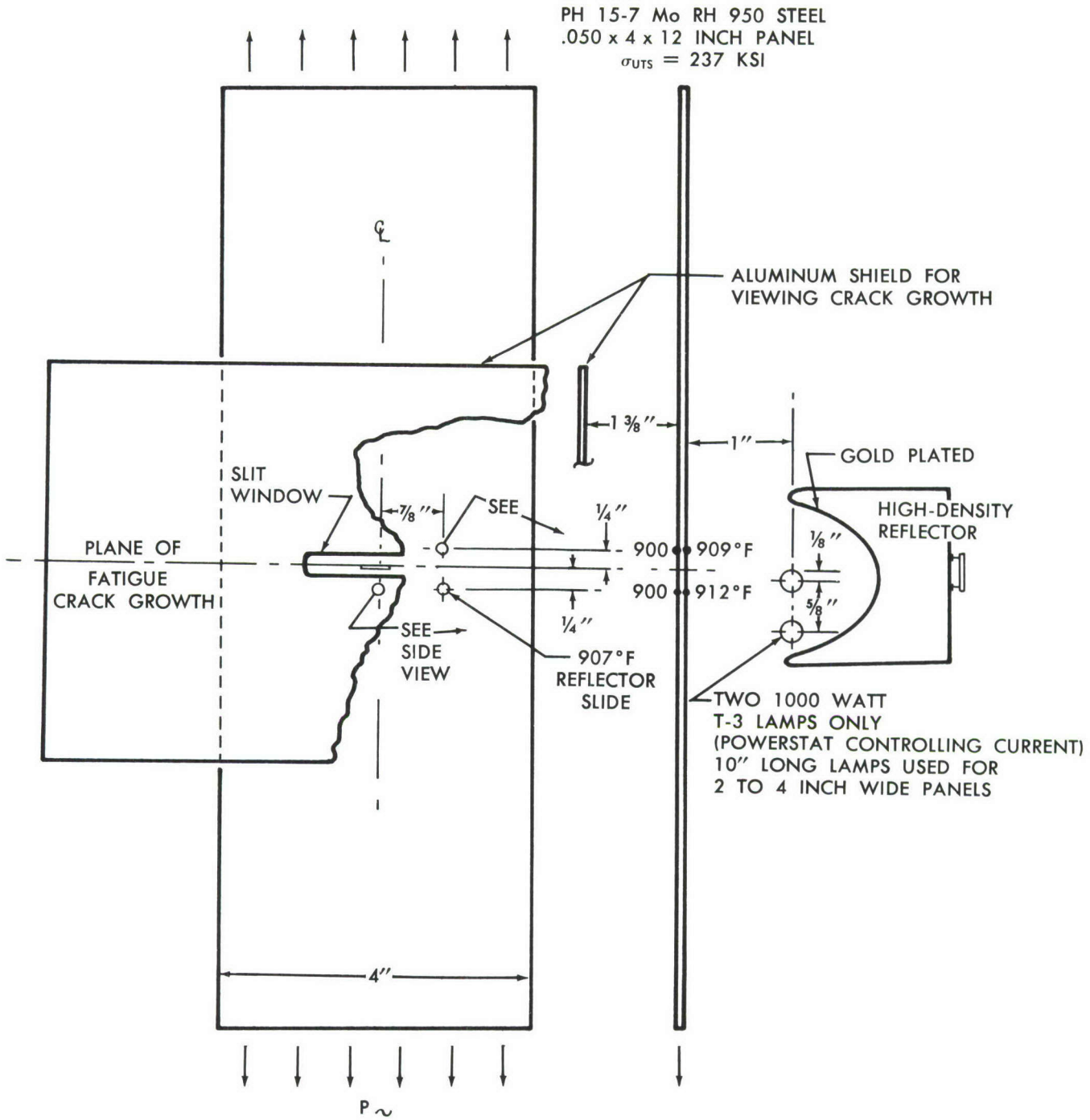


Figure 3. TEST PANEL TEMPERATURE DISTRIBUTION SURVEY

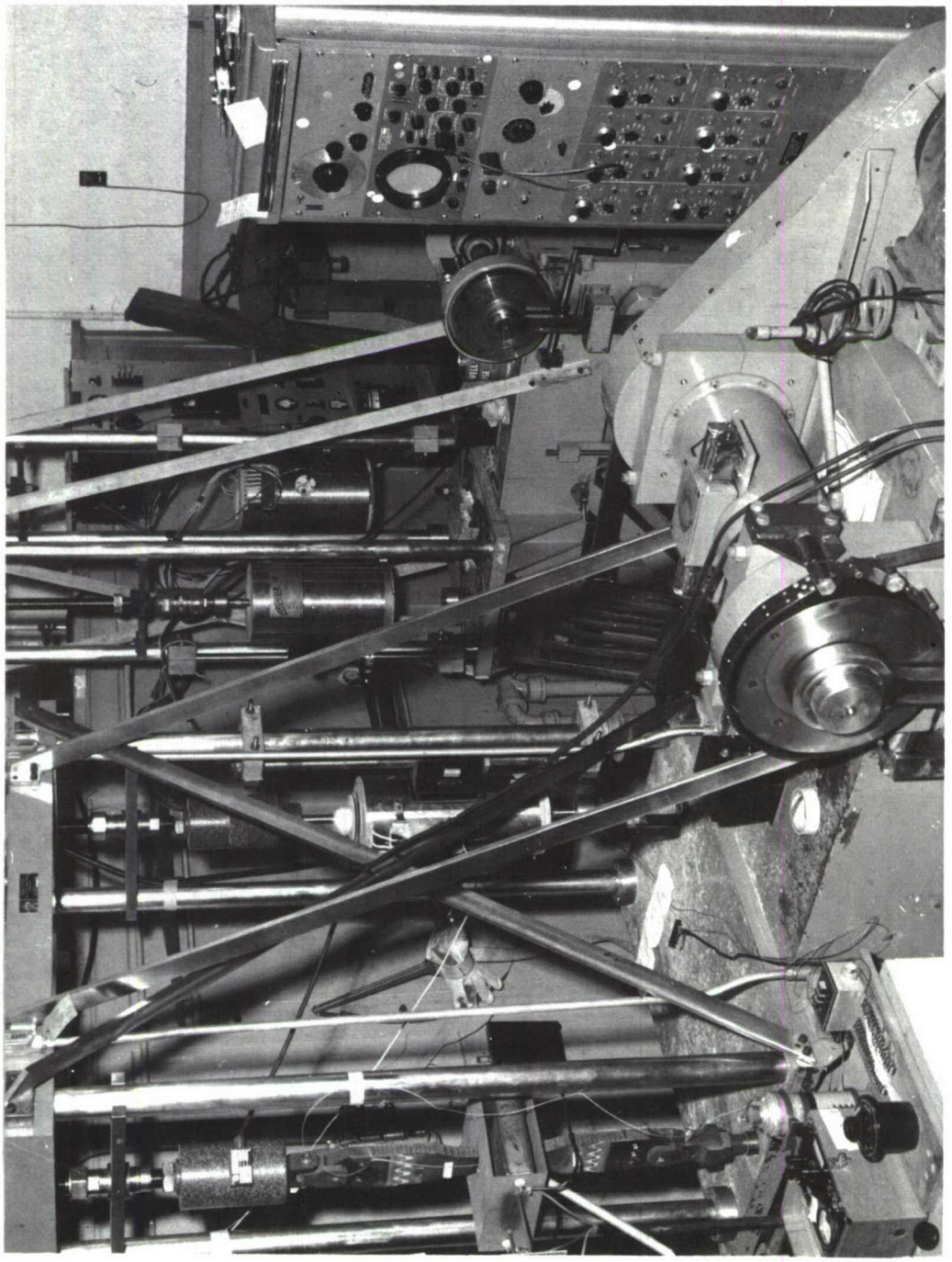


Figure 4. KROUSE FATIGUE MACHINE

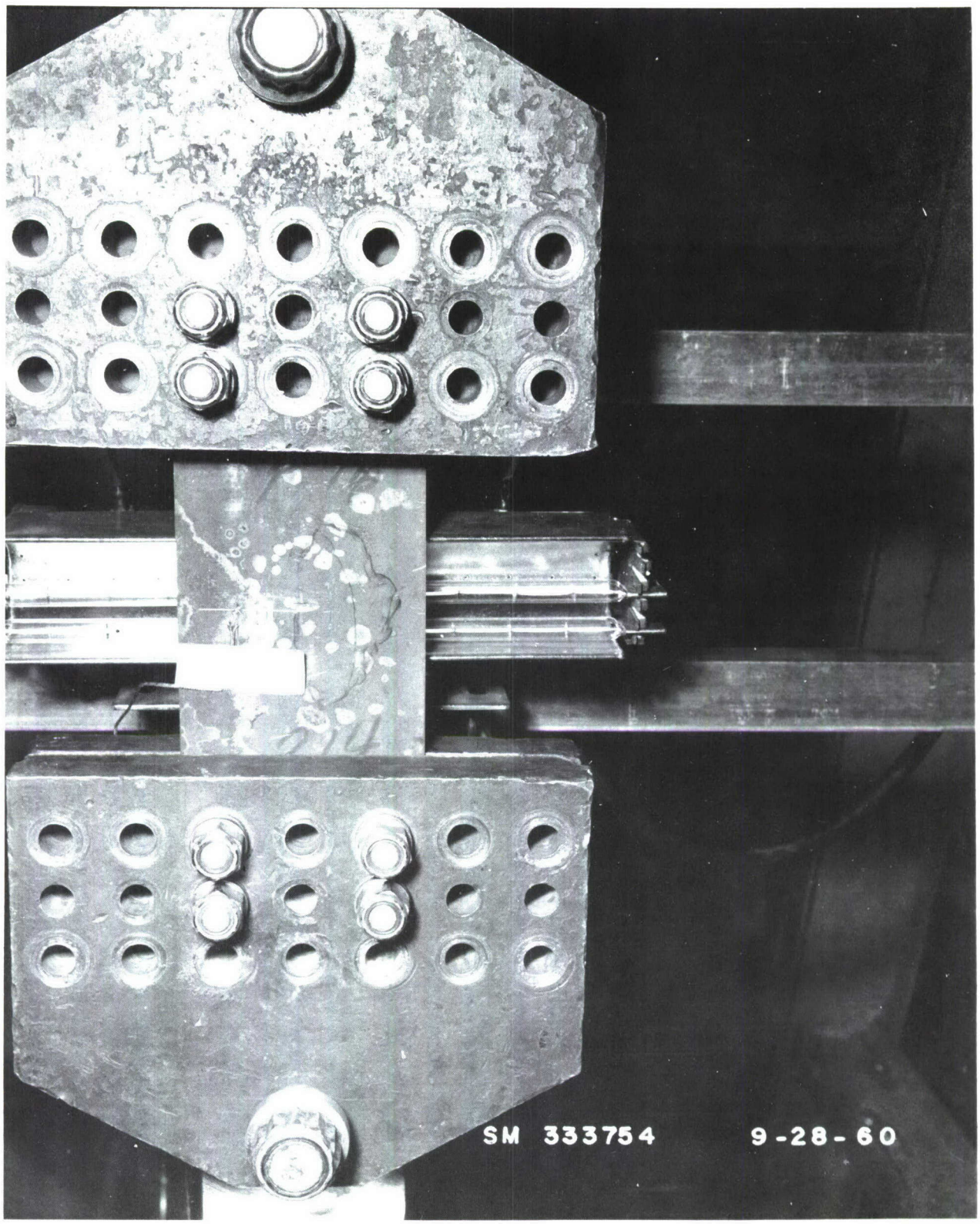


Figure 5. TEST SET-UP IN LOW-CYCLE HYDRAULIC FATIGUE TEST MACHINE

SECTION 4

SUMMARY OF TEST RESULTS ON PH15-7 MO - RH950 STEEL SHEET

Descriptions and the mechanical properties of the material reported in this section are given on page 38.

1. In general, data have indicated that the load carrying capacity of the cracked metal panels is significantly less for the case of naturally grown fatigue cracks than for the coarser forms of damage such as jeweler's saw slots or milled notches. This is graphically shown in Figure 6. It is also believed that the great amount of data generated within this program has significantly revealed subtle differences in fracture strengths of fatigue cracked metal panels as a function of the environment used to generate the crack. Figures 7 and 8 show some of these differences.

   a. The residual strength of fatigue cracked sheet panels tends to increase as the rupture temperature increases for cracks greater in length than a certain critical value. For cracks shorter than this critical length, the residual strength decreases as temperature increases.

   b. The residual strengths of the fatigue cracked sheet panels varied with the conditions of generating the fatigue crack.

      (1) Residual strengths are lowest when the cracks are grown at the lower stresses.

      (2) Residual strengths are greater for cracks generated in elevated temperature environments.

      (3) Fatigue cracks grown at 600° F. are more severe when statically ruptured at 75° F. than when ruptured at 600° F. (a notch softening effect when ruptured at 600° F.), Figure 7.

      (4) The notch softening effect at rupture is further emphasized by the difference (though slight) between curves I and III on Figure 8. All cracks on these curves were grown at a fatigue cracking stress of 34,000 psi and an R value, $\sigma_{min}/\sigma_{max}$, of +.2.

      The test panels on curve III of Figure 8 were held at temperature and load for one hour, whereas the panels on curves I and II were at temperature for only two to three minutes.

      (5) A comparison between curves I and II of Figure 8 indicates that fatigue cracks grown at lower stresses are more severe than cracks grown at higher stresses (lower stress means finer slip; fine slip leads to finer and sharper crack tips).

2. Tensile ultimate and yield strengths for PH15-7 Mo and other steels have been plotted on the chart of Figure 9. In order to calculate "fracture

toughness", K_{c_1} for central cracks in sheet materials at various temperatures (+600°F. to -340°F.) it is necessary to know the values of $\sigma_{y.s.}$ at these temperatures. The data plotted on this figure are necessary to approximate the values of yield strength in the K_c calculations at varying rupture temperatures. The F_{tu} curve has also been extrapolated to obtain the Figure 10 plot.

3. Few data similar to that shown in Figure 10 can be found in the literature. The plot of fracture toughness vs. rupture temperature indicates (by the discontinuity) the suggestion of a "transition temperature" similar to that shown by other forms of testing. It is believed that the K_c method* of making material evaluation should be expanded to testing at temperatures other than the usual 75° F. laboratory conditions.

   It is interesting to note that the value of K_c, fracture toughness, is also reduced for panels initially cracked at the lower temperatures. This is only conclusive for panels ruptured at equivalent or higher temperatures than the crack growing temperatures. The two-inch panels at +100° F. and -320° F. are unexplained.

4. A suggested form for eventually presenting design data is shown in the graph of Figures 11 and 12. One of the most pronounced characteristics of the material behavior is the relatively constant strength values at low and cryogenic temperatures for a variety of crack sizes. This effect has been observed on a limited number of test panels and should be investigated further. However, if found to be true the implications are that for some materials there will be little tolerance for even the most minute crack lengths when low temperature environments have to be considered.

5. At elevated temperatures there is a definite effect of degree of cracking on the residual strength. There also appears to be a greater tolerance for allowable crack sizes. It will soon be necessary to correlate and tie all of these findings into the "fail safe" structural design problems. It may also be necessary to develop new fail safe structural features since the old ones may not apply in the regions of higher design stress fields.

6. Evidence of crack-front blunting due to elevated temperature testing is shown in Figures 13 through 15. The data indicates a greater notch resistance for panels ruptured at elevated temperatures. Figure 7 also indicates this notch blunting of the crack front grown at elevated temperature followed by tensile rupture at a lower temperature.

7. The curves drawn through the test points on Figures 6 through 16 are all represented by an equation. The equations are not noted on the figures of this section. The analytical derivation of the equations for residual strength characteristics are given in Section 14, Analysis.

* Readers not familiar with "fracture toughness" measurements and calculations are referred to Reference 1 and 2 for a thorough discussion and sample evaluation.

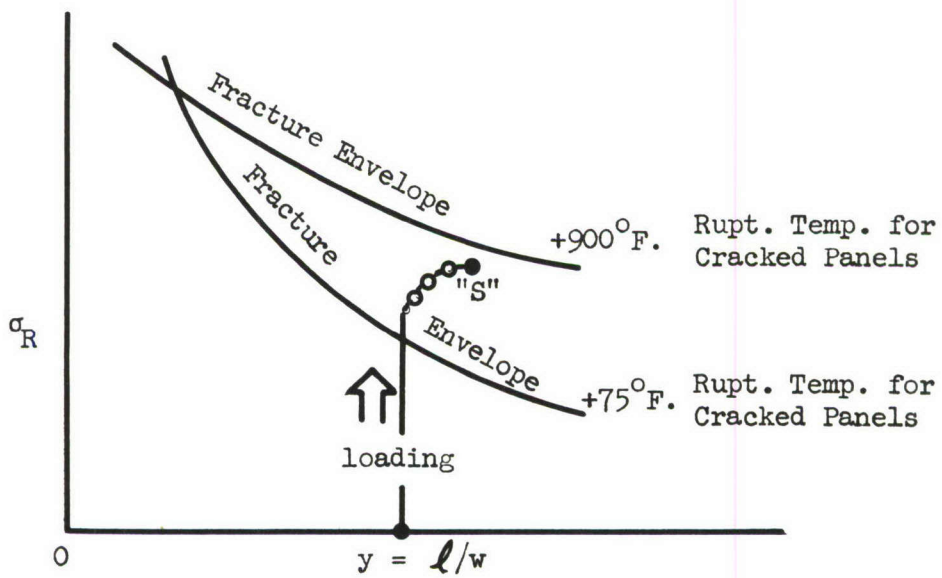
a. A comparison of the data of Figures 13, 14 and 15 at a given rupture temperature, indicates an increase in notch sensitivity for a given degree of crack damage as the panel width increases. This has been observed on materials in the past and has been one of the greatest drawbacks for using small specimen screening data for predicting the behavior of larger structures.

b. The empirical analysis of data from different widths of panels now indicates that residual strengths can be predicted for a wide range of panel widths from test data on one panel size. See Analysis, Section 14.

8. Figures 17 and 18, on 4" and 6" wide panels, show data presented on a net-area stress basis rather than the usual gross-area (σ_R) method. This method reduces the scatter somewhat but still does not normalize the data for various panel widths as given in Section 14.

9. Figures 19 through 21 show crack growth curves as a function of panel width and testing temperature. Additional data and discussions of this phase are reported in Section 14.

It is becoming more and more evident that it is necessary to conduct crack growth tests at temperatures which are at the useful operating limits of the materials. It has been demonstrated that some large differences in residual strength can result depending on crack growing temperatures as well as fracture testing temperatures. The design strength significance and the importance of such studies may best be introduced by the following discussion of some observations. Refer to the figure below.



During the loading of a panel that has been heated to +900° F. one can observe, under moderate magnification, the slow growth (shear cracking and plastic flow) and extension of the blunted crack front. At point "S" the load was suddenly but only slightly reduced, and the temperature then lowered to +75° F. The panel did not fracture. This demonstrated (1) that temperature alone is not responsible for the increased notch strength, since the panel at +75° F. was loaded far above the previously established fracture envelope; (2) that the temperature is primarily responsible for a blunting of the crack front which reduces the notch severity, or for creep strain in the region of the crack tip which alleviates the stress concentration.

10. The residual strengths of three fatigue cracked and prestrained panels in the above described sequence for the material PH15-7 Mo RH950 are shown in Figure 22. These panels were prestrained at 600° F. and 900° F. to the rupture strength envelope of the +75° F. tested panels. The panels were then retested to rupture at a +75° F. test temperature. The data may not be wholly conclusive but does indicate a 20% increase over the average strength with no pre-straining. These tests have been repeated on the other materials in this program with similar results and are described in the following sections.

11. Results of the ASTM edge-notched specimens, ($r = .0007"$ and $K_T = 17+$) shown in Figure 23, were as expected for this material. The ASTM standard edge notch specimen does not have as severe a stress raiser as a naturally grown fatigue crack and for many materials the fracture strength data would be unconservative from the design standpoint. The data presented on Figure 23 indicates this to be true especially from the low to the medium rupture temperatures which could be normal environmental temperatures for this material.

12. Figure 24 shows fracture strength as a function of testing temperature for a series of ageing temperatures in the air-hardening PH15-7 Mo steel specimens. All specimens tested in these conditions are of the ASTM edge-notch type.

13. Crack growth and residual strength tests have been performed on a variety of sheet gauges in the 6" panel widths. Typical crack growth curves for the different gauges are shown in Figure 25. Although the general trend has been for heavier gauges to exhibit slightly greater rates of crack growth ($\Delta \ell / \Delta n$), it does not appear significant in this plot. Residual strength tests on the various sheet gauges are discussed in Section 12.

14. Electron microfractographs have been made for two samples of the progressively fatigue cracked material PH15-7 Mo. These replicas are shown on page 192 of Section 13.

15. The effect of cracks in elevated temperature environments does not appear to be as serious a problem as some may have originally thought. Probably it is less of a problem than at normal temperatures. Sub-zero environments, however, are far different situations and many material problems may arise. Techniques to mitigate these effects may be necessary.

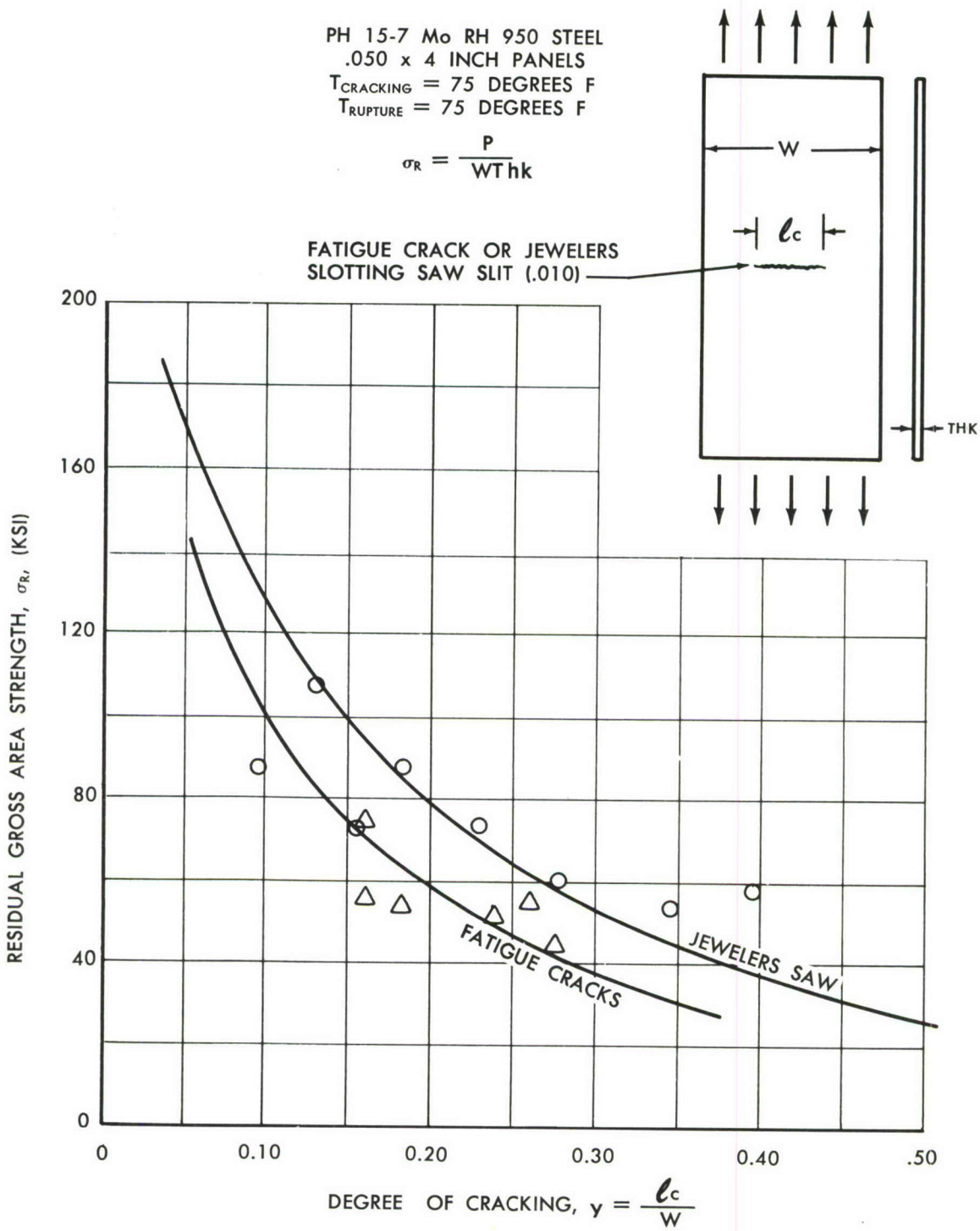


Figure 6. RESIDUAL STRENGTH vs DEGREE OF CRACKING

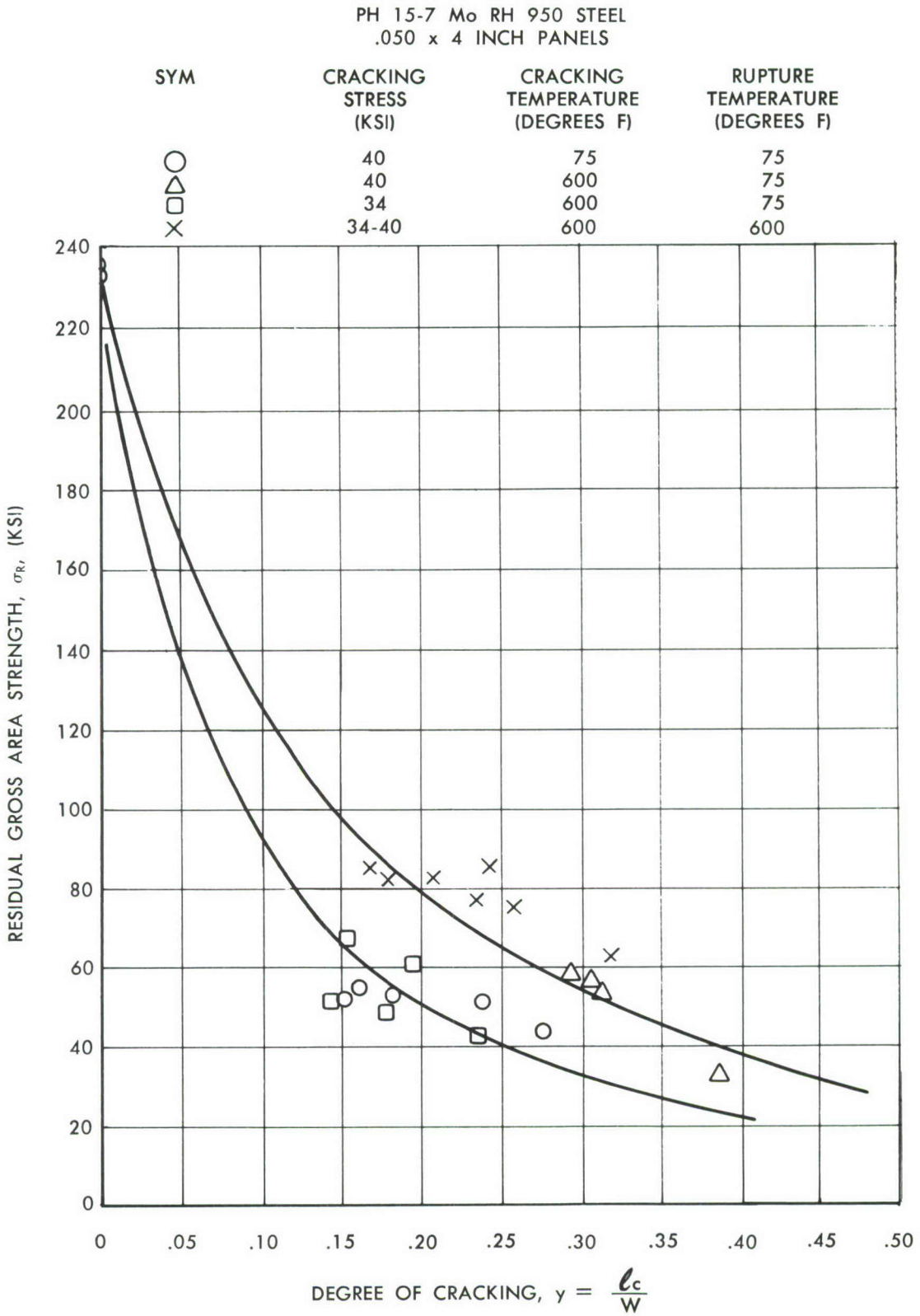


Figure 7. RESIDUAL STRENGTH vs DEGREE OF CRACKING

PH 15-7 Mo RH 950 STEEL
.050 x 4 INCH PANELS
$T_{CRACKING}$ = 600 DEGREES F
NUMBER IN ( ) DENOTES
FATIGUE CRACKING STRESS KSI

I, II TENSILE RUPTURE TEMPERATURE = 600°F
2 TO 3 MIN EXPOSURE AT 600°F

III TENSILE RUPTURE TEMPERATURE = 600°F
60 MIN EXPOSURE TO 600°F PLUS 80%
OF CURVE I STRENGTH ENVELOPE AS
A SUSTAINED STRESS

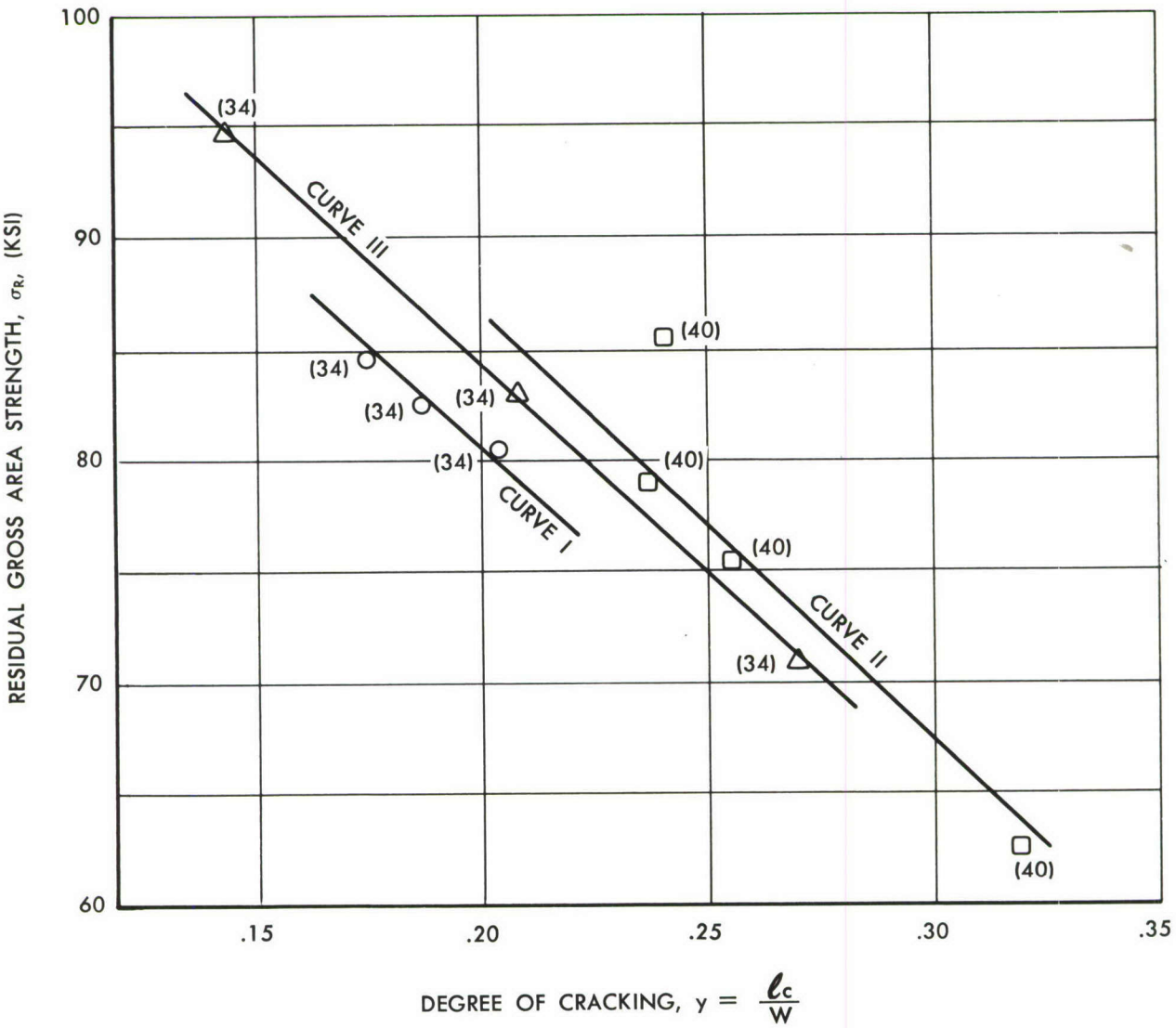


Figure 8. RESIDUAL STRENGTH vs DEGREE OF CRACKING

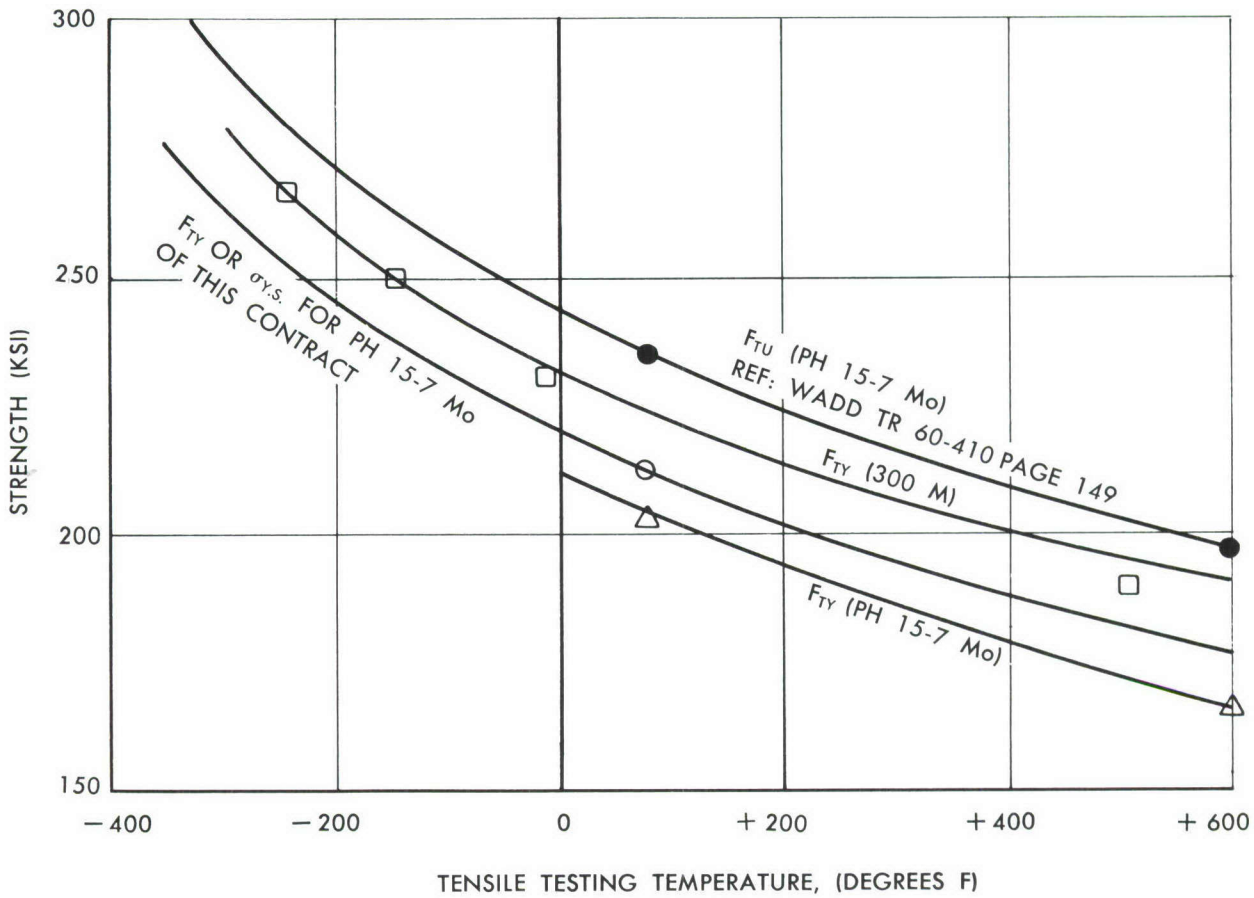


Figure 9. UN-NOTCHED TENSILE STRENGTH AS A FUNCTION OF TEST TEMPERATURE

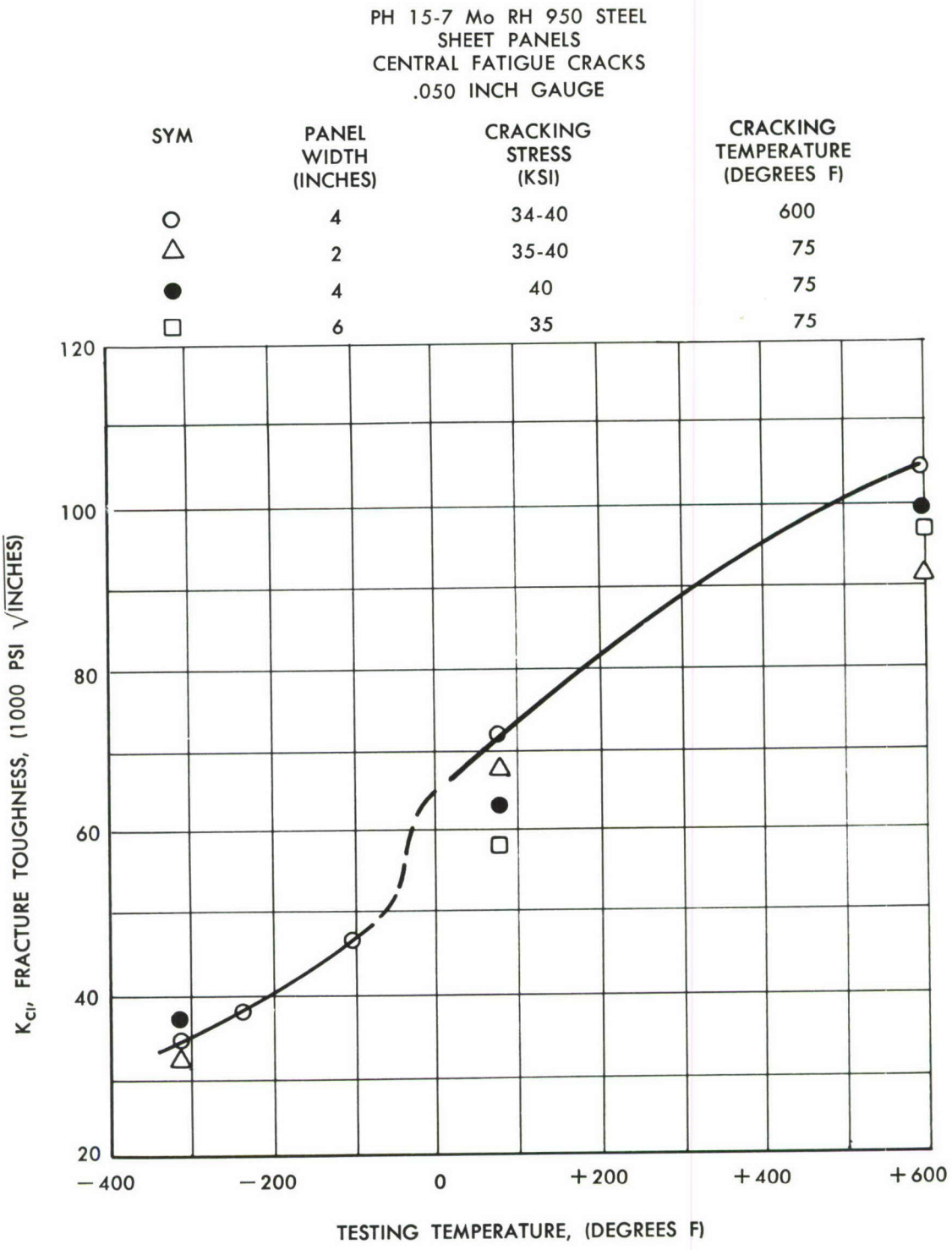


Figure 10. FRACTURE TOUGHNESS vs TEST TEMPERATURE

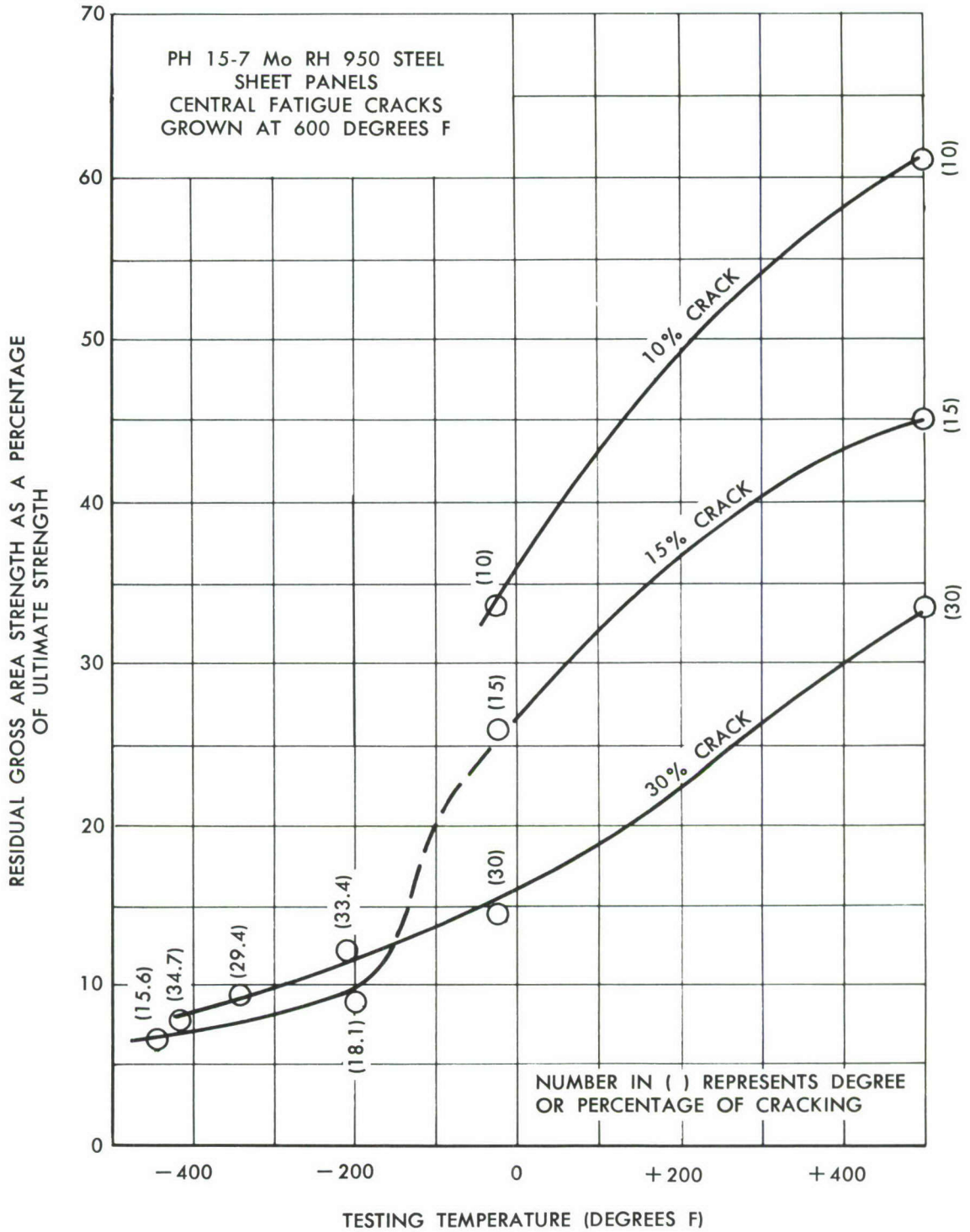


Figure 11. RESIDUAL STRENGTH vs TEST TEMPERATURE

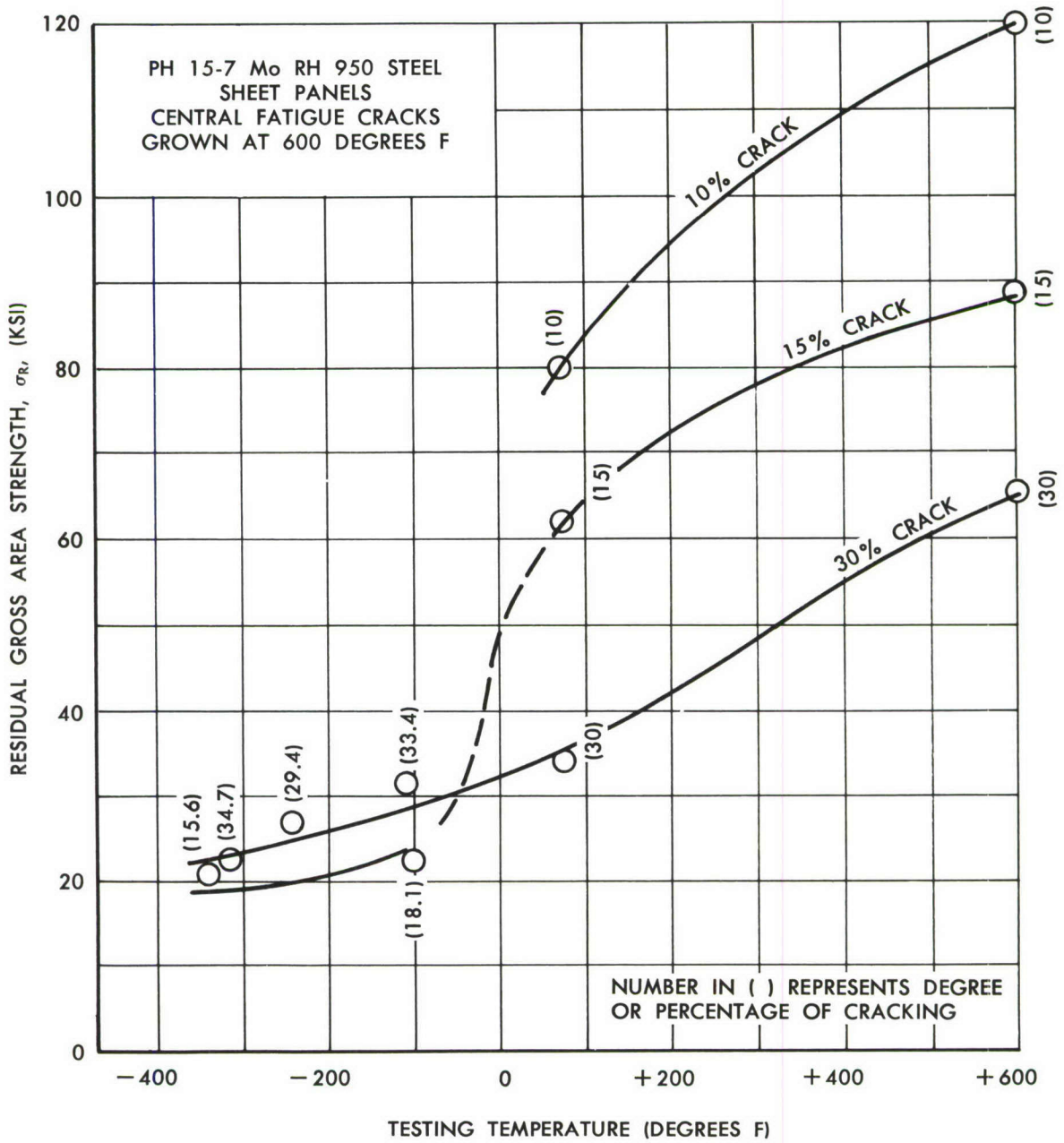


Figure 12. RESIDUAL STRENGTH vs TEST TEMPERATURE

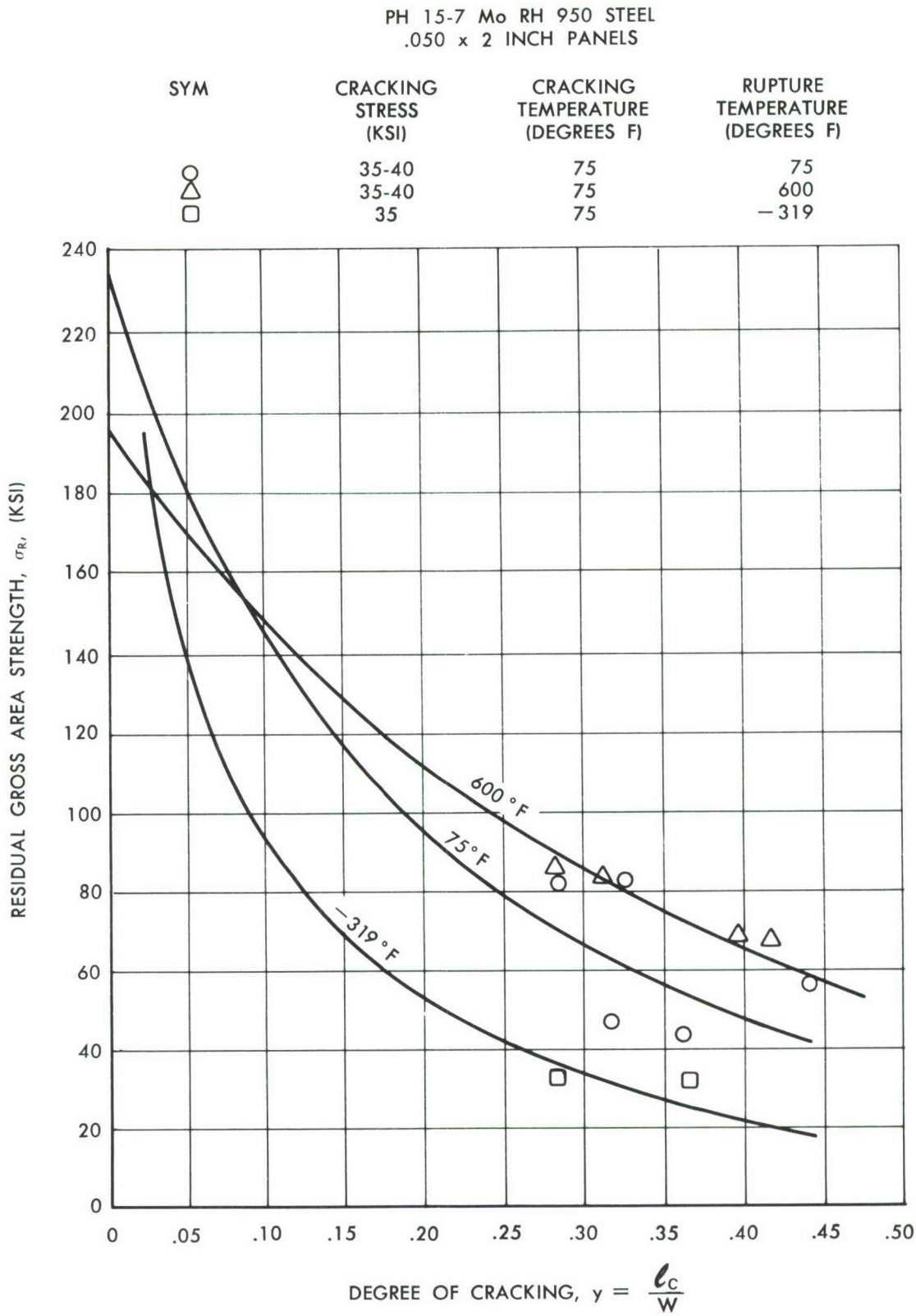


Figure 13. RESIDUAL STRENGTH vs DEGREE OF CRACKING

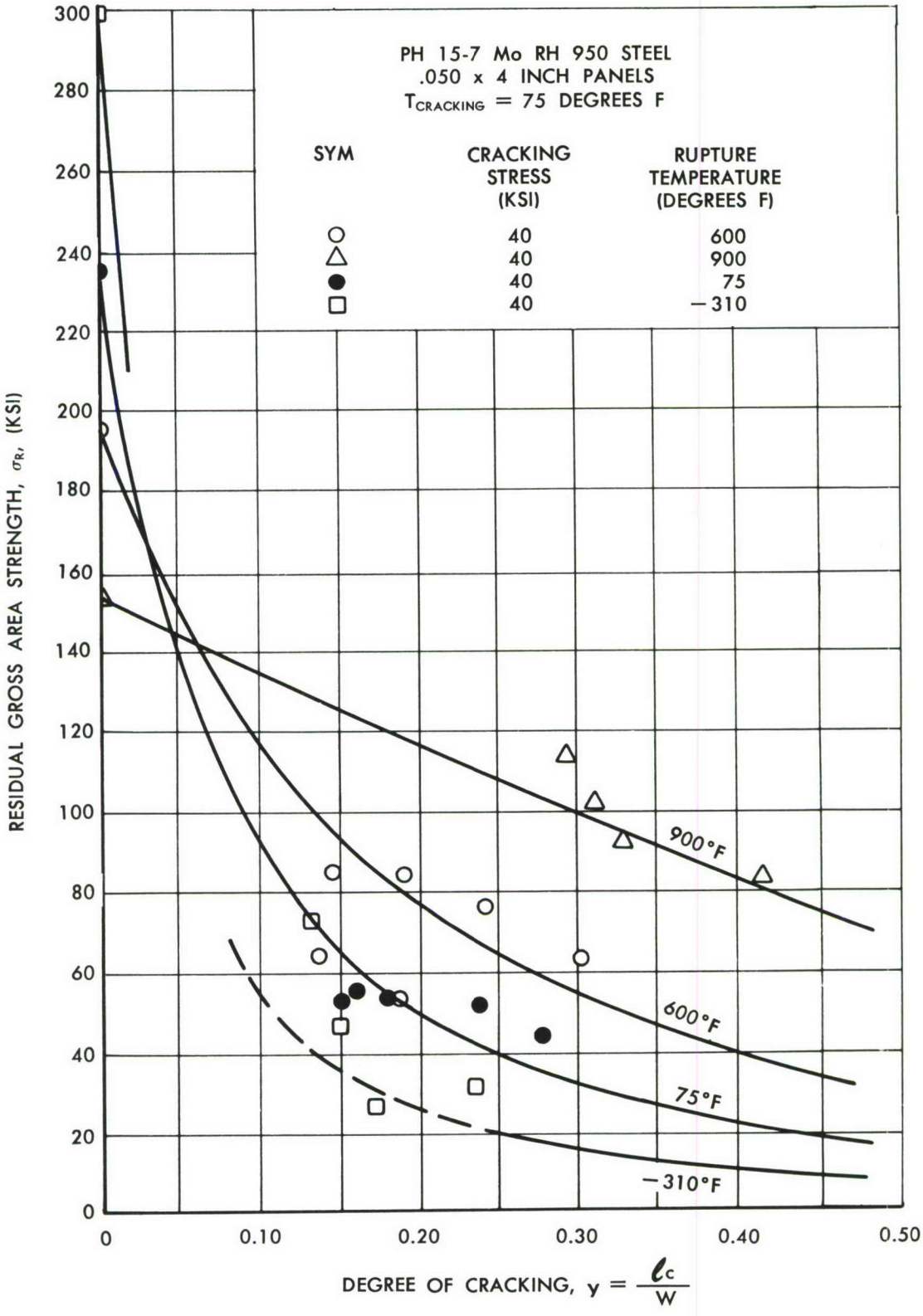


Figure 14. RESIDUAL STRENGTH vs DEGREE OF CRACKING

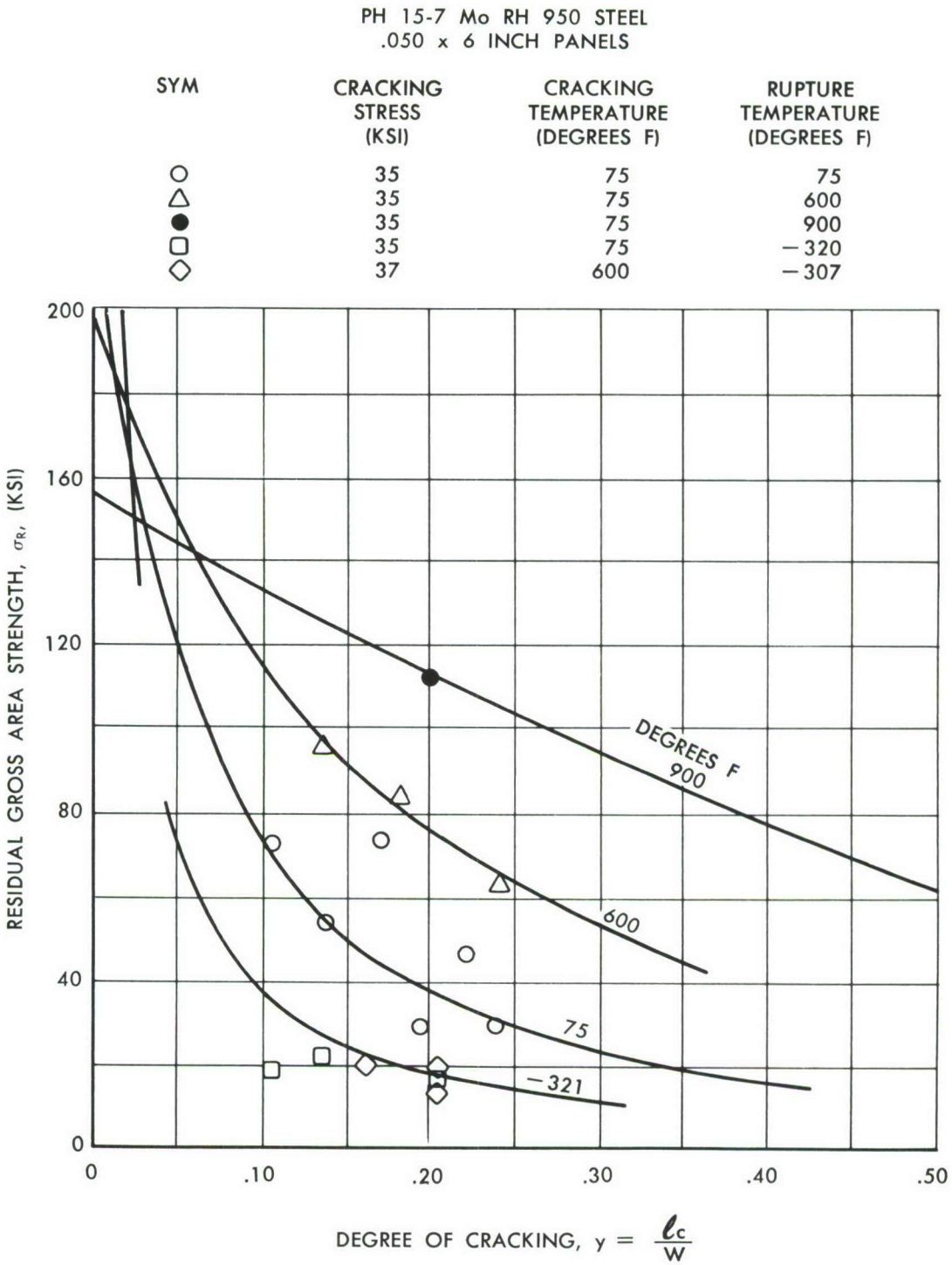


Figure 15. RESIDUAL STRENGTH vs DEGREE OF CRACKING

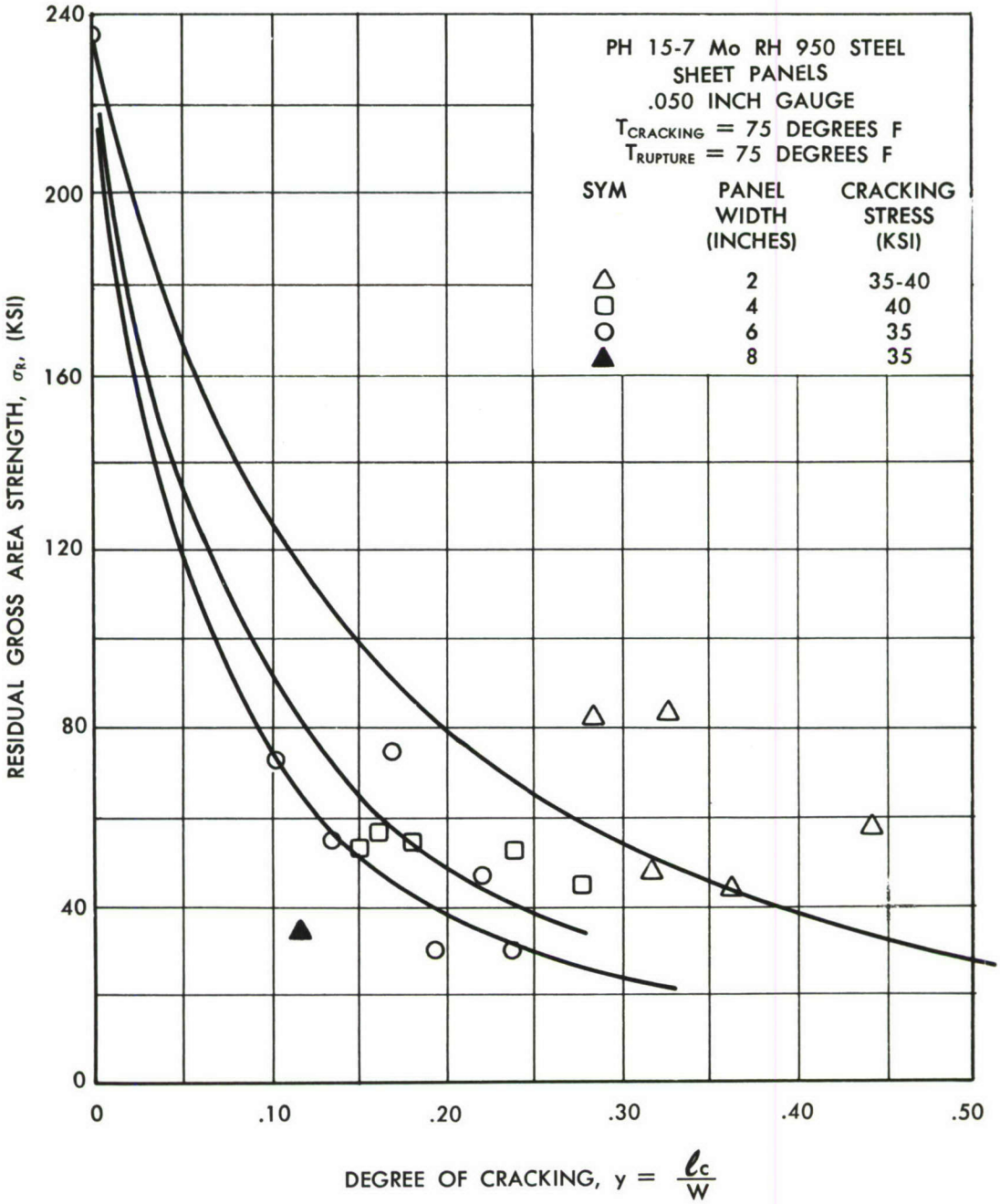


Figure 16. RESIDUAL STRENGTH vs DEGREE OF CRACKING

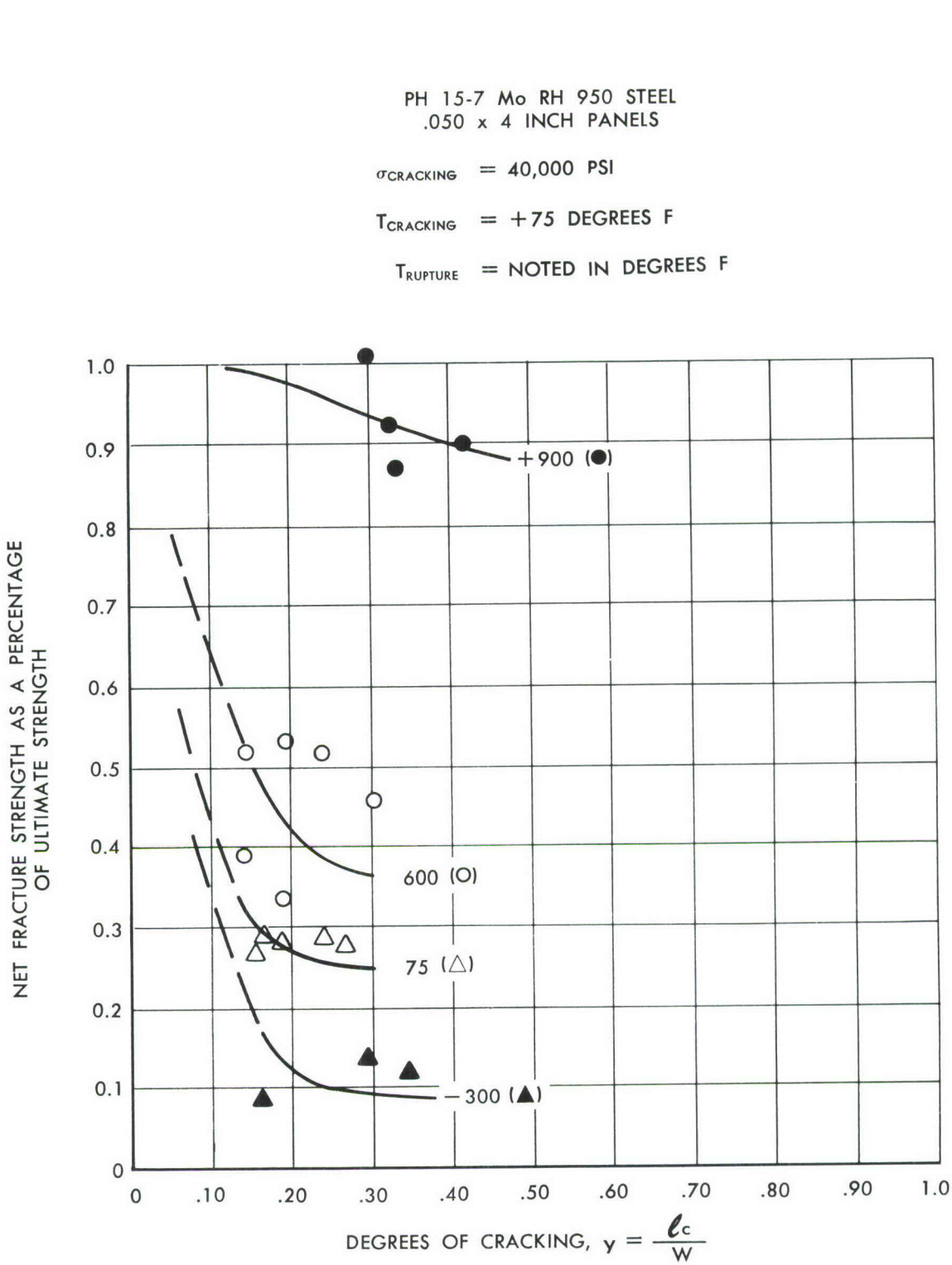


Figure 17. NET FRACTURE STRENGTH vs DEGREE OF CRACKING

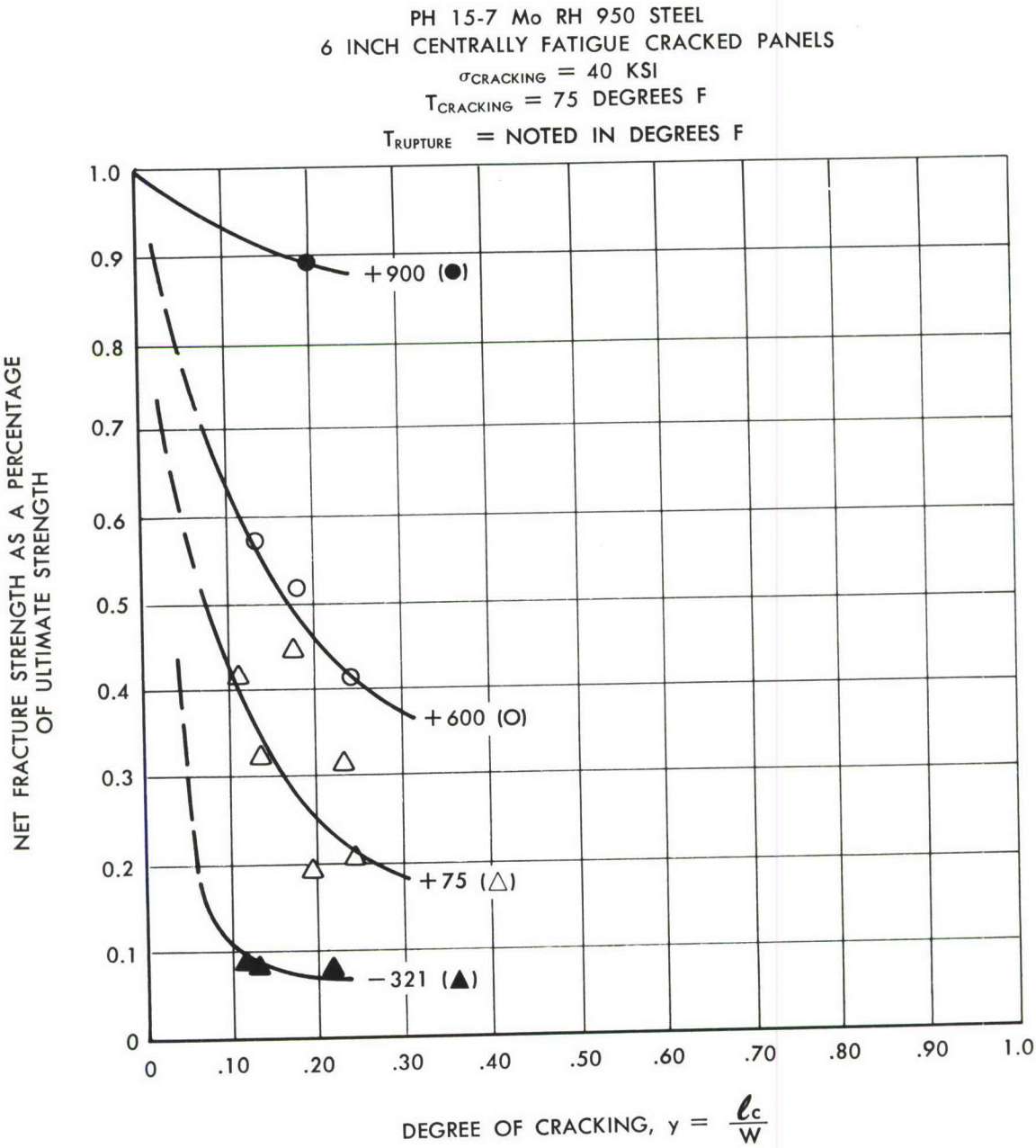


Figure 18. NET FRACTURE STRENGTH vs DEGREE OF CRACKING

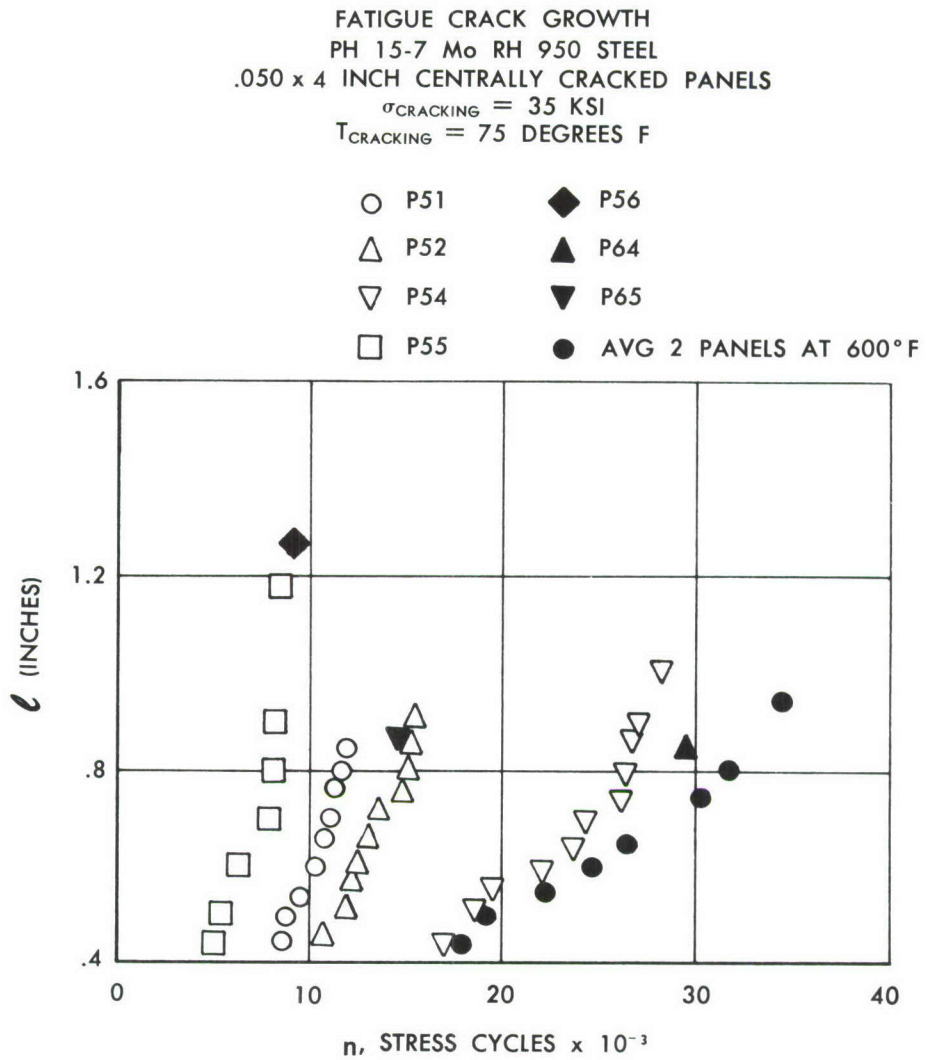


Figure 19. FATIGUE CRACK GROWTH

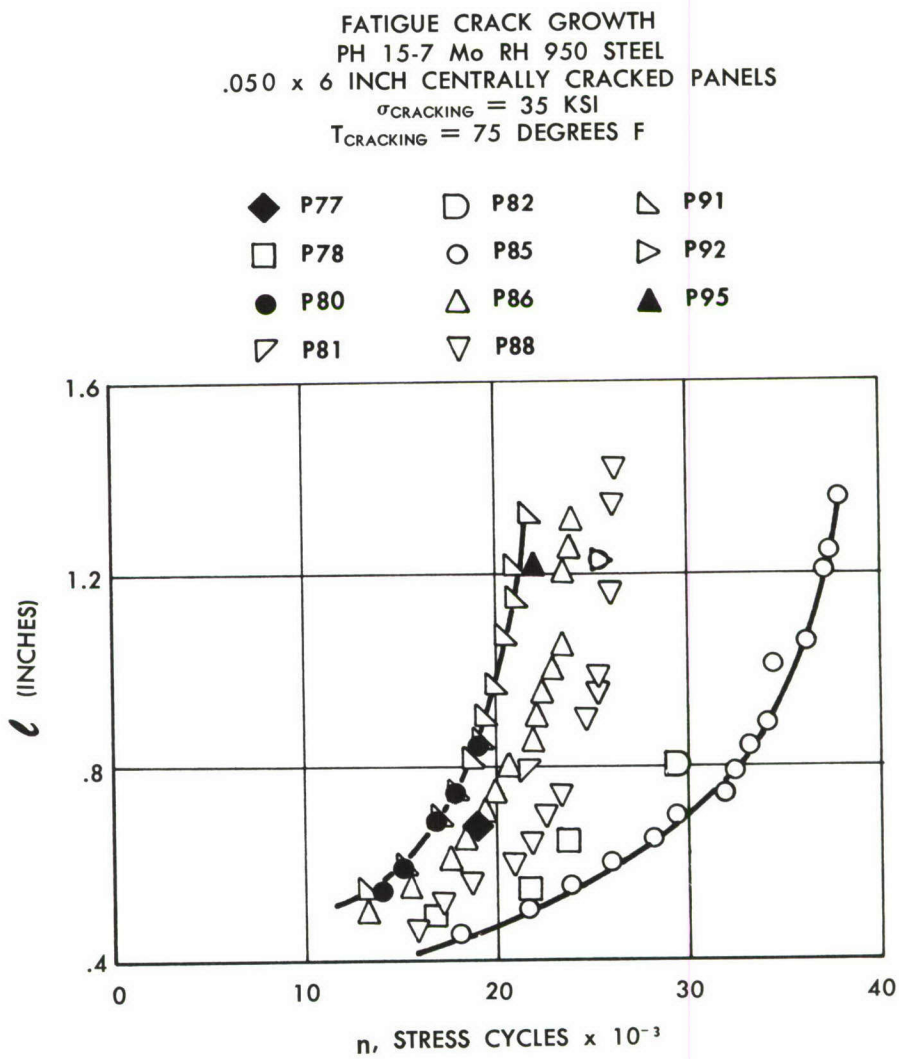


Figure 20. FATIGUE CRACK GROWTH

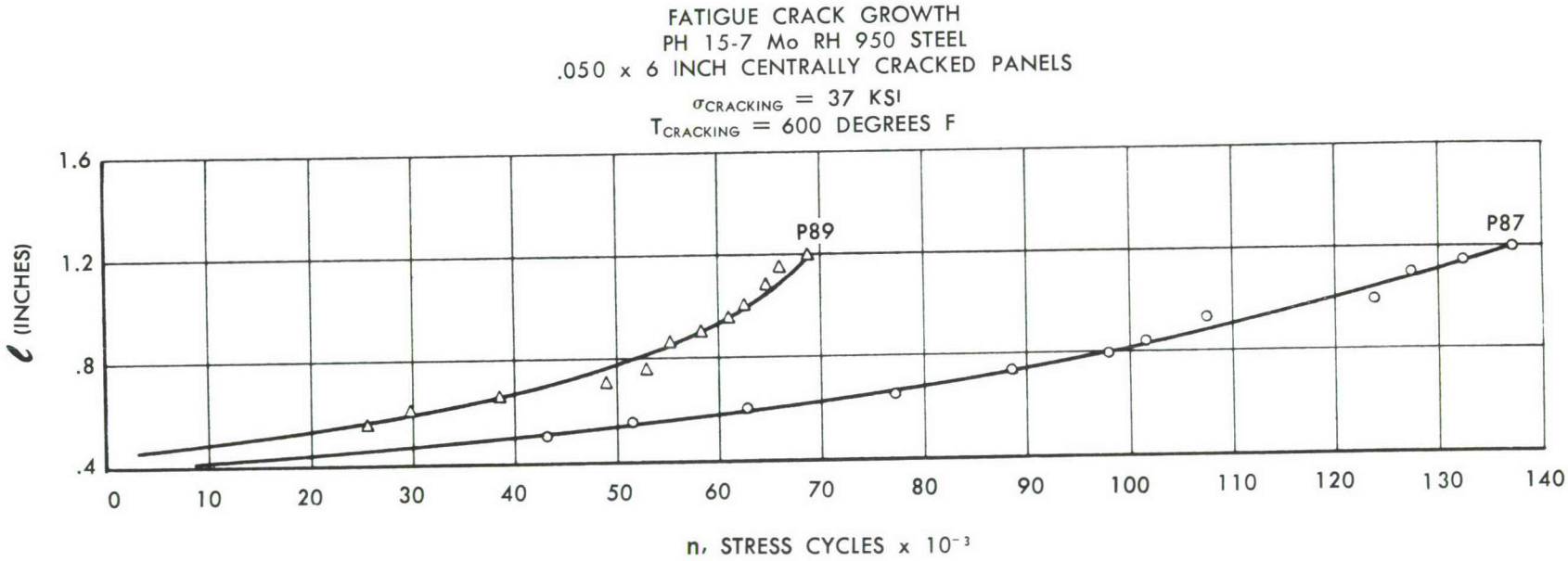


Figure 21. FATIGUE CRACK GROWTH

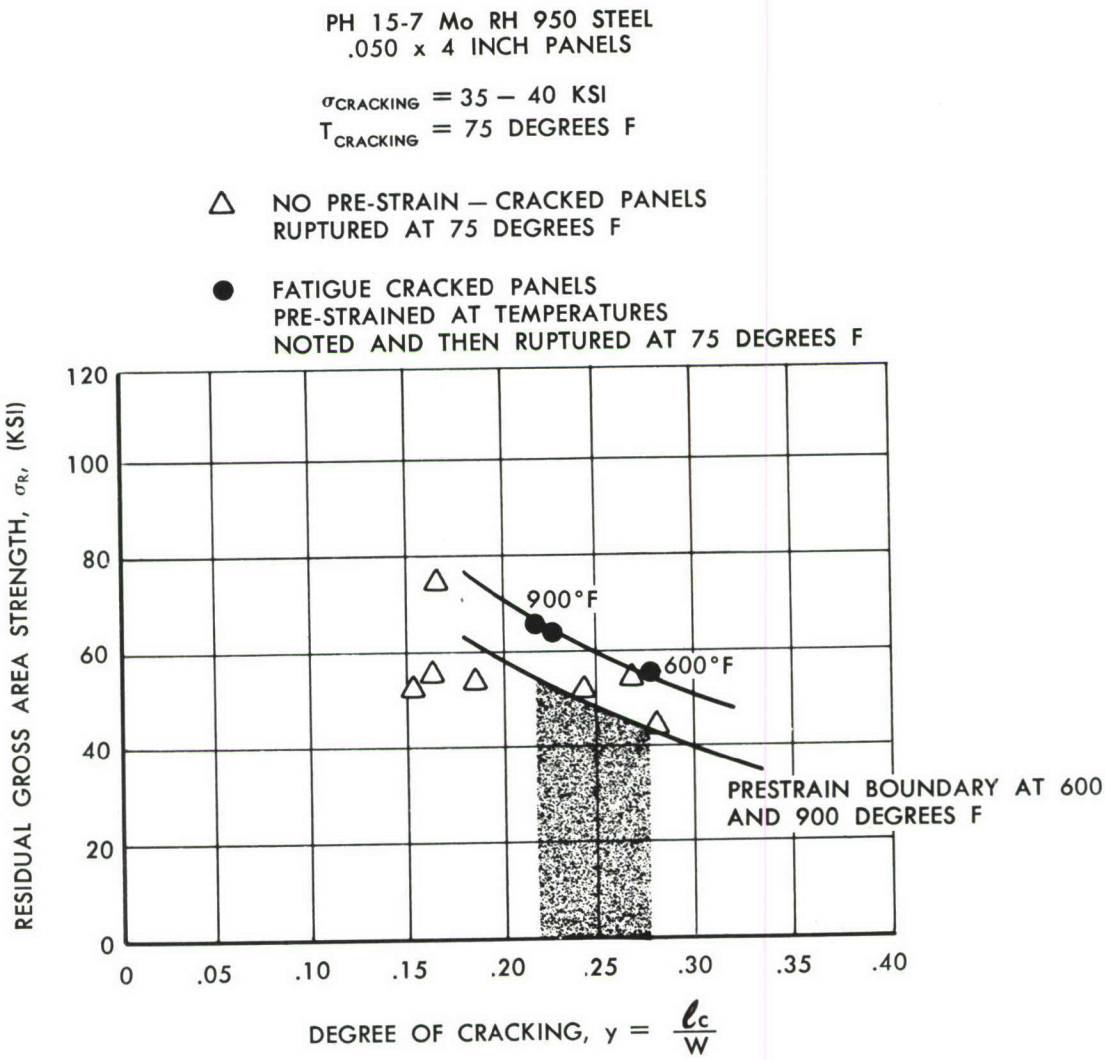


Figure 22. RESIDUAL STRENGTH vs DEGREE OF CRACKING

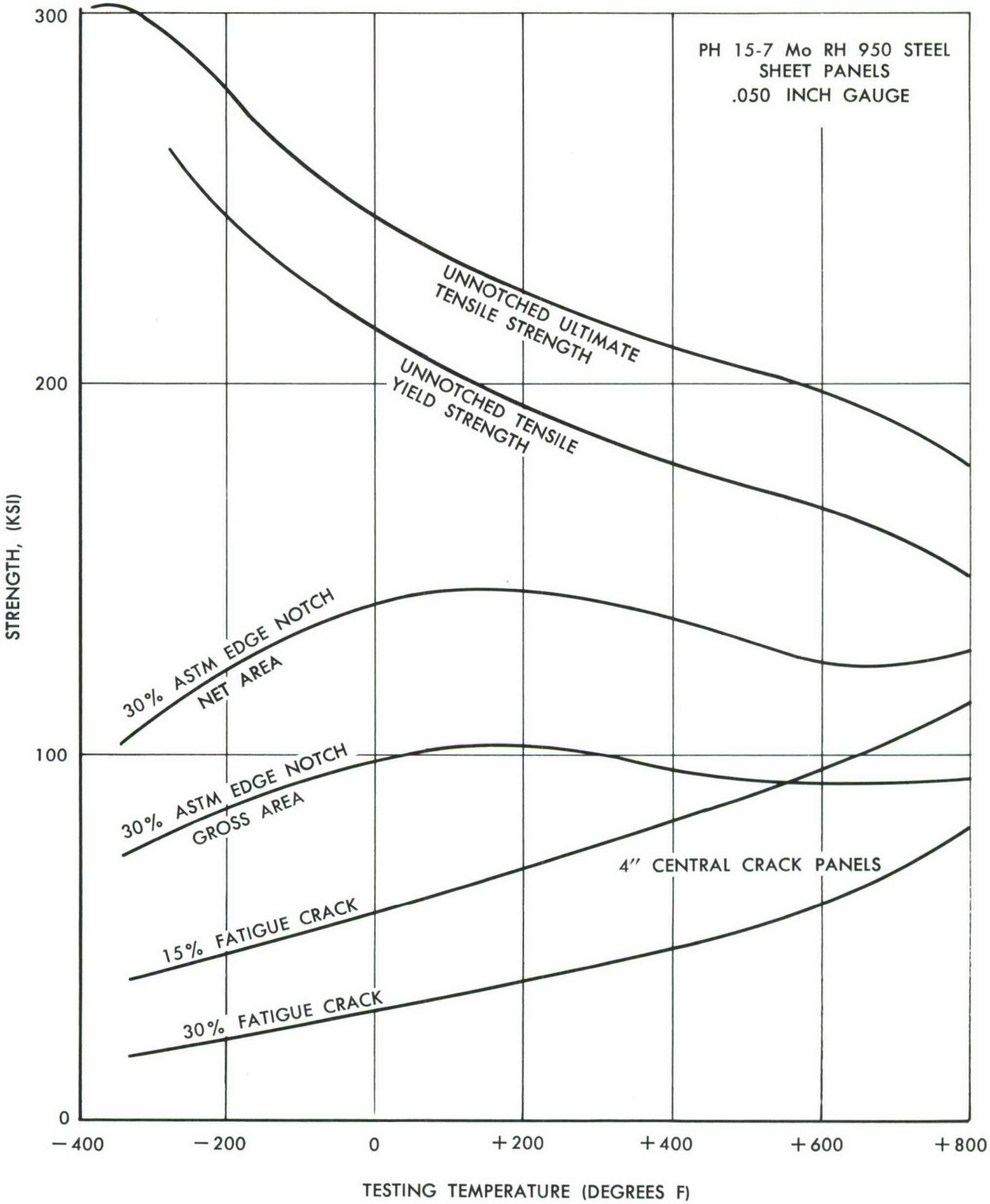


Figure 23. NOTCH STRENGTH vs TEST TEMPERATURE

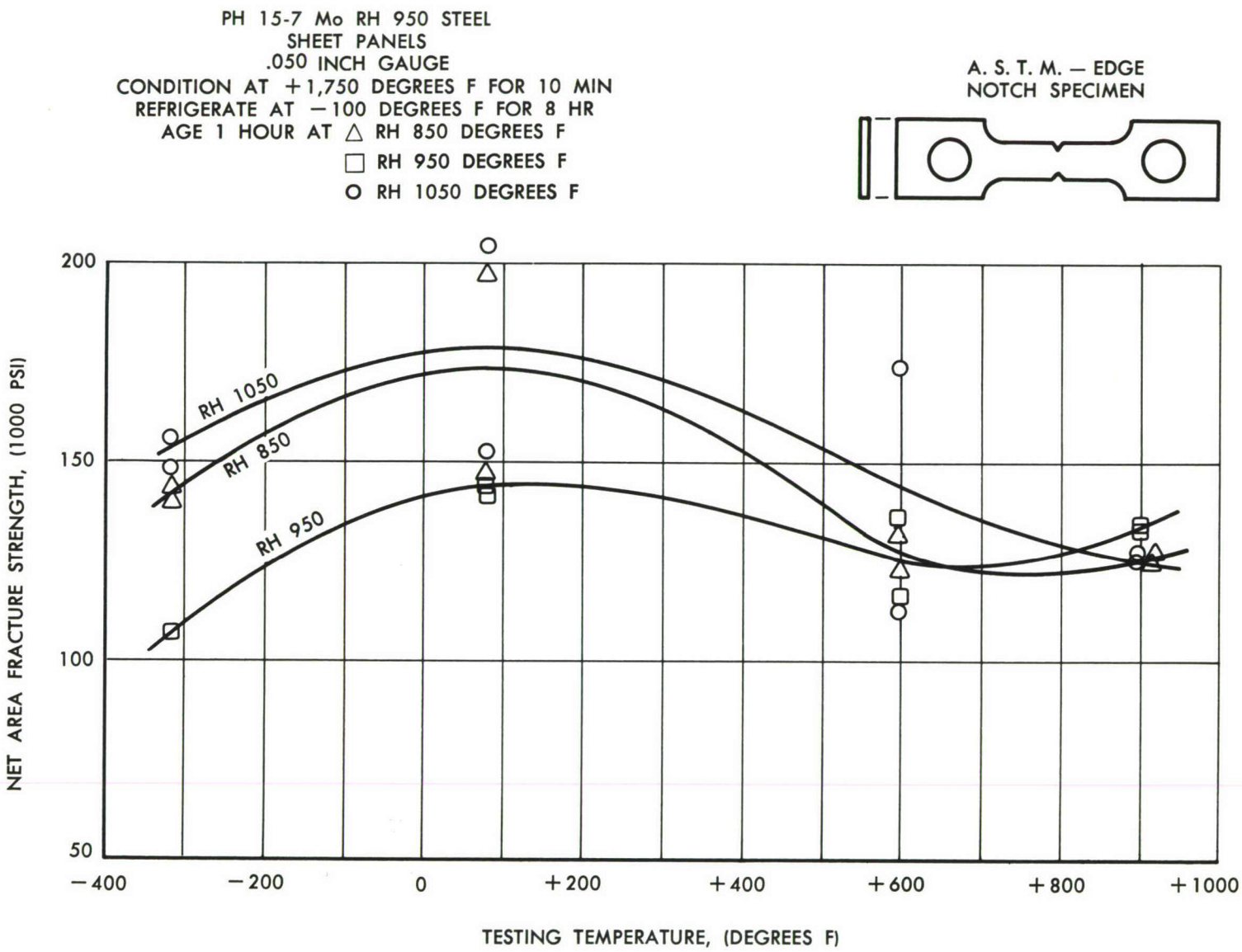


Figure 24. NET AREA FRACTURE STRENGTH vs TEST TEMPERATURE

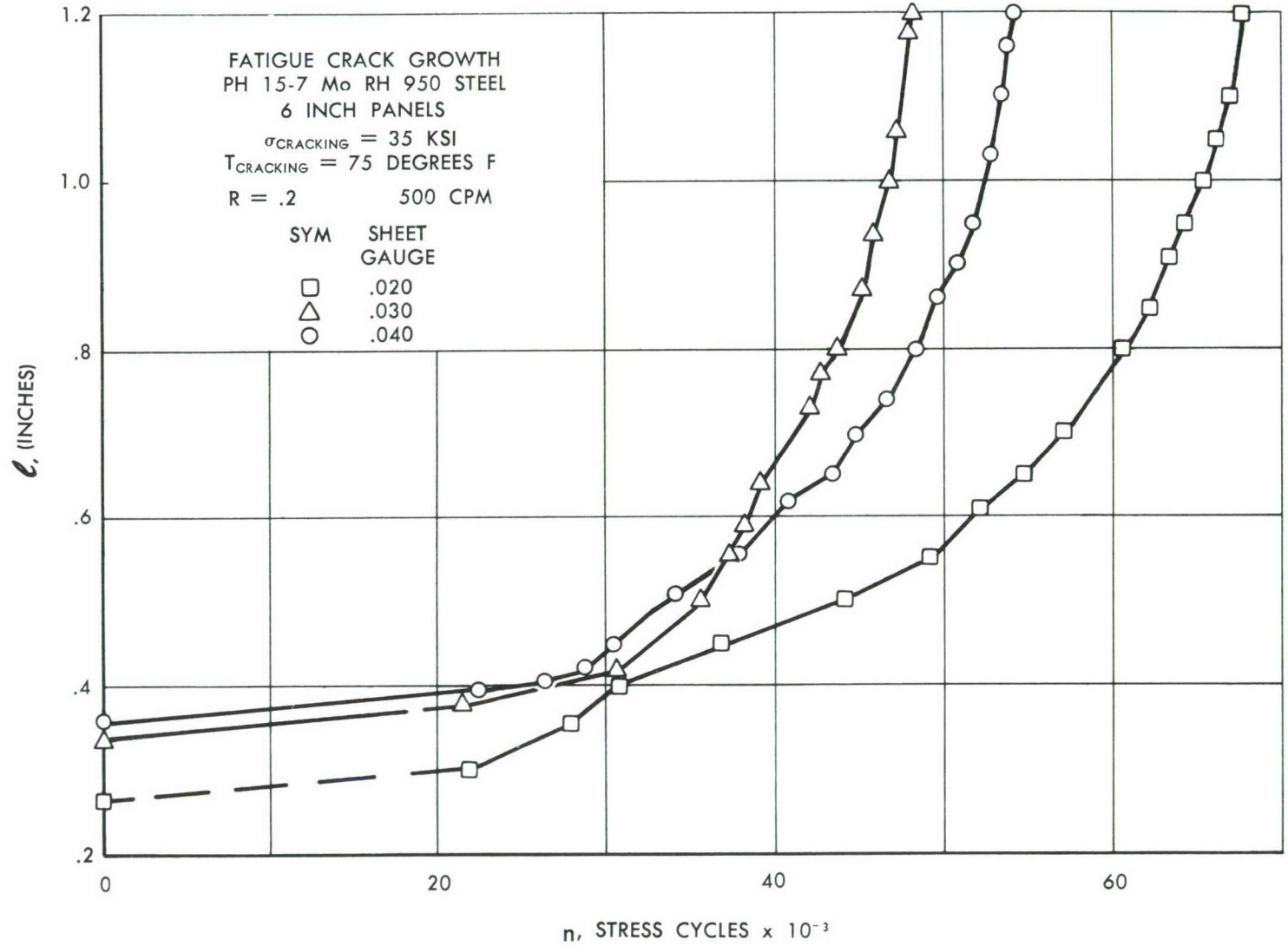


Figure 25. FATIGUE CRACK GROWTH

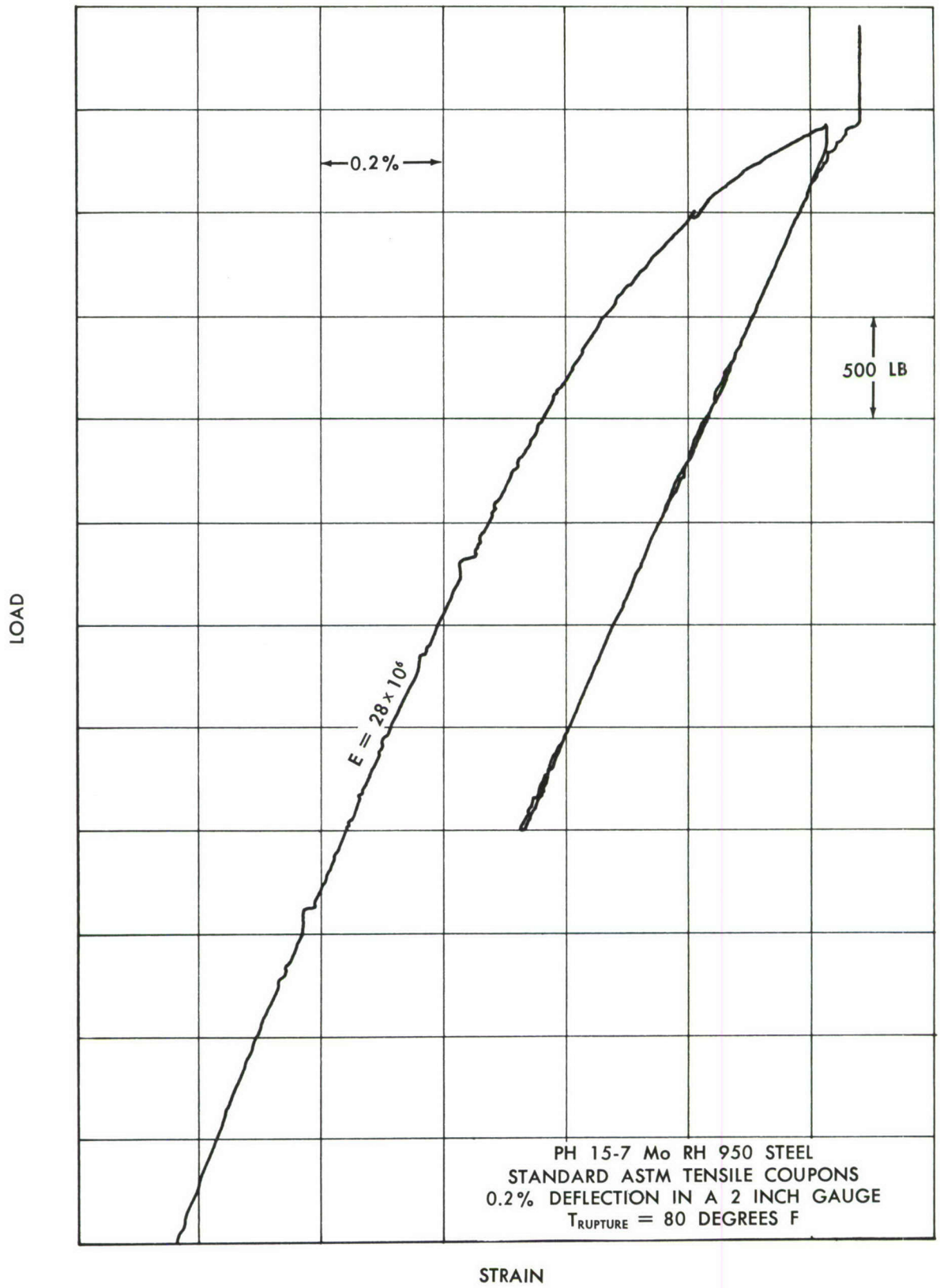


Figure 26. LOAD-STRAIN CURVE

MECHANICAL PROPERTIES

The coupons and panels tested in the program were made from the precipitation-hardening stainless steel, PH15-7 Mo. All panels reported here are .050 sheet stock and were milled, slotted, and drilled in the "A" condition. The panels were then heat-treated as follows:

Condition at 1,750° F for 10 minutes
Air Cool
Refrigerate at -100° F for 8 hours
Age at 950° F for 1 hour
Air Cool

TABLE 2

PH15-7 Mo
ARMCO
HEAT NO 890681

Code	Width	Thick	Area	Yield Load	$\sigma_{y.s.}$ psi	Ult. Load	F_{tu} psi	% Elong.	Grain Direc.
1	.505	.0497	.0251	5230	208,365	5,905	235,260	4.0	Cross
2	.505	.0496	.0250	5210	208,400	5,930	237,200	5.0	
3	.505	.0436	.0250	5285	211,400	5,900	236,000	4.0	
4	.505	.0494	.0249	5200	208,835	5,900	236,945	4.0	
5	.505	.0496	.0250	5340	213,600	5,980	239,200	4.0	
6	.505	.0494	.0249	5325	213,855	5,985	240,360	4.0	
7	.506	.0488	.0247	5130	207,690	5,820	235,625	5.0	with
8	.505	.0488	.0246	4790	194,715	5,800	235,775	5.5	
9	.505	.0489	.0247	5290	214,170	5,850	236,845	5.5	
10	.505	.0488	.0246	5180	210,570	5,840	237,400	5.5	

TABULATION OF TEST DATA

Spec	W (in)	T_{crk} °F	T_{rupt} °F	σ_{crk} (ksi)	ℓ_c	y	σ_r (psi)	n (cyc)	$\sigma_{y.s.}$ ** (psi)	$\left(\frac{\sigma_r}{\sigma_{y.s.}}\right)^2$	$\frac{\pi \ell_c}{2W}$	Q_1*	$\sqrt{Q_1 W}$	K_{c1}
P101	2.02	+ 75	+ 75	40	.57	.282	81,200	10,600	205,250	.157	.442	.525	1.03	83.6
102	2.02	75	600	40	.555	.277	86,000	11,450	165,000	.270	.435	.650	1.06	91.0
103	2.02	75	75	40	.64	.317	47,500	9,700	205,250	.054	.482	.545	1.05	50.0
104	2.03	75	600	40	.63	.310	83,500	13,350	165,000	.255	.486	.560	1.07	89.4
106	2.0	75	600	35	.79	.395	69,250	20,250	165,000	.176	.620	.825	1.28	88.6
107	2.0	75	+600	35	.83	.415	68,880	21,225	165,000	.173	.650	.890	1.33	91.6
108	2.0	75	75	35	.88	.440	57,000	21,800	205,250	.0772	.690	.880	1.33	76.0
109	2.0	75	+ 75	35	.72	.36	43,250	19,600	205,250	.0445	.565	.660	1.15	49.8
110	1.77	75	-319	35	.50	.282	33,400	15,450	275,000	.146	.443	.52	0.96	32
111	1.63	75	+ 75	35	.53	.325	82,000	13,250	205,250	.160	.510	.625	1.01	82.7
112	1.47	75	-319	35	.54	.367	33,400	13,500	275,000	.146	.576	.73	1.03	34.5
P35A	4	+ 75	+ 75	40	.465	.116	59,250	25,600	205,250					
P41	4	+ 75	+ 75	40	.63	.158	56,000	13,100	205,250					
44	4	+ 75	+ 75	40	.60	.150	52,200	10,300	205,250					
47	4	+ 75	+ 75	40	.71	.178	52,800	15,300	205,250					

* Values of Q extrapolated slightly outside of ASTM recommended region.
** Extrapolated from ASTM data, see figure 9

TABULATION OF TEST DATA

Spec	W (in)	$T_{crk.}$ °F	T_{rupt} °F	σ_{crk} (ksi)	ℓ_c	y	σ_r (psi)	n (cyc)	$\sigma_{y.s.}$ (psi)	$\left(\frac{\sigma_r}{\sigma_{y.s.}}\right)^2$	$\frac{\pi \ell_c}{2w}$	Q_1	$\sqrt{Q_1 W}$	K_{c1}
50	4	+ 75	+ 75	40	.95	.238	50,900	14,800	205,250	.0614	.375	.410	1.28	65.0
54	4	+ 75	+ 75	40	1.10	.275	44,250	27,300	205,250	.0467	.432	.480	1.39	61.5
34A	4	+ 75	+600	40	.54	.135	64,750	10,300	165,000					
33A	4	+ 75	+600	40	.58	.145	86,250	7,300	165,000					
42	4	+ 75	+600	40	.74	.185	53,500	10,300	165,000	.105	.290			
48	4	+ 75	+600	40	.75	.187	85,250	10,800	165,000	.266	.294	.350	1.18	101.
52	4	+ 75	+600	40	.95	.24	77,500	15,500	165,000	.22	.275	.450	1.34	104.
55	4	+ 75	+600	40	1.20	.30	62,875	8,500	165,000	.145	.470	.555	1.49	93.7
P37A	4	+ 75		40				8,000						
39A	4	+ 75	+900	40	1.16	.29	114,550	7,400	114,000	1.00	.455			
45	4	+ 75		40				9,600						
49	4	+ 75	+900	40	1.23	.308	101,750	11,500	114,000	.79	.484			
53	4	+ 75	+900	40	1.30	.325	92,750	13,400	114,000	.657	.510			
P50	4	+ 75	+900	40	1.65	.412	84,275	9,150	114,000	.543	.647			
P30A	4	+ 75	-306	40	.54	.13	73,150	13,500	275,000					
40A	4	+ 75	-318	40	.59	.15	47,700	37,100	275,000					

TABULATION OF TEST DATA

Spec	W (in)	T_{crk} °F	T_{rupt} °F	σ_{crk} (ksi)	ℓ_c	y	σ_r (psi)	n (cyc)	$\sigma_{y.s.}$ (psi)	$\left(\frac{\sigma_r}{\sigma_{y.s.}}\right)^2$	$\frac{\pi \ell_c}{2w}$	Q_1	$\sqrt{Q_1 W}$	K_{c_1}
43	4	+ 75	-295	40	.66	.165	71,200	81,600	? soft					
46	4	+ 75	-325	40	.69	.173	26,500	12,900	275,000	.0092	.272			
51	4	+ 75	-325	40	.935	.234	30,500	11,950	275,000	.0123	.367	.380	1.23	37.5
57	4	+ 75	-305	40	1.10	2.75	57,650	64,450	? soft					
P76	6	+ 75	+ 75	40	.61	.103	71,500	8,020	205,250	.121	.162			
81	6	+ 75	+ 75	35	.80	.133	54,800	21,000	205,250	.071	.209			
83	6	+ 75	+ 75	35	1.05	.172	74,300	22,960	205,250	.131	.270			
86	6	+ 75	+ 75	35	1.31	.222	46,600	24,000	205,250	.0515	.349	.370	1.49	69.5
88	6	+ 75	+ 75	35	1.43	.237	29,670	26,200	205,250	.0210	.372	.390	1.53	45.5
92	6	+ 75	+ 75	35	1.23	.197	29,830	25,350	205,250	.0212	.309			
P77	6	+ 75	+600	35	.67	.135	95,915	19,000	165,000	.336	.222			
79	6	+ 75	600	35	1.04	.180	83,670	18,560	165,000	.257	.282			
80	6	+ 75	900	35	.85	.20	110,580	19,000	114,000	.940	.314			
85	6	+ 75	+600	35	1.36	.238	60,830	37,700	165,000	.135	.374	.425	1.60	97.3
P82	6	+ 75	-320	35	.80	.133	20,500	29,100	275,000					
78	6	+ 75	-322	35	.63	.105	19,930	23,750	275,000					

TABULATION OF TEST DATA

Spec	W (in)	T_{crk} °F	T_{rupt} °F	σ_{crk} (ksi)	ℓ_c	y	σ_r (psi)	n (cyc)	$\sigma_{y.s.}$ (psi)	$\left(\frac{\sigma_r}{\sigma_{y.s.}}\right)^2 \frac{\pi \ell_c}{2w}$	Q_1	$\sqrt{Q_1 W}$	K_{c_1}
93	6	+ 75	-321	35	1.22	.203	16,867	25,700	275,000				
P71	4	+600	+600	35				29,350					
P75	4	+600	+600	35				39,950					
P87	6	600	-305	37	1.20	.200	13,300	137,100					
P89	6	600	-313	37	1.21	.201	18,330	68,900					
P84	6	600	-302	37	.94	.157	19,670	0					
PA	18	jewelrs	+ 75		5.625	.312	48,060	0					
PB	18	sloting	+ 75		1.687	.0937	74,340	0					
PC	18	saw	+ 75		3.187	.177	63,720	0					
PD	18		-325		3.20	.178	22,860	0					
P3	4	600	75	34	0.59	.151	67,900	40,030					
P19	4	600	75	40	1.51	.385	33,550	23,060		.0253	.605	.710	1.67	56.0
P18	4	600	75	40	1.19	.304	57,700	28,570		.0750	.477	.550	1.47	85.0
P14	4	600	75	34	.92	.235	41,700	66,620		.0392	.369	.385	1.23	51.3

Blank spaces for K_c values denote no calculation made since crack lengths were too short for parameter, $\pi a/w$, to fall within ASTM recommended region of use.

TABULATION OF TEST DATA

Spec	W (in)	T_{crk} °F	T_{rupt} °F	σ_{crk} (ksi)	ℓ_c	y	σ_r (psi)	n (cyc)	$\sigma_{y.s.}$ (psi)	$\left(\frac{\sigma_r}{\sigma_{y.s.}}\right)^2$	$\frac{\pi \ell_c}{2w}$	Q_1	$\sqrt{Q_1 W}$	K_{c_1}
P6	4	600	75	34	.695	.177	49,900	25,080						
P31	4	75	75	35	1.11	.283	67,500	24,030		.102	.444	.505	1.41	95.2
P28	4	75	75	66	.63	.161	73,000	1,030						
P30	4	75	75	40	1.03	.263	54,800	10,780						
P33	4		75	jewelrs	.40	.099	86,500	0						
P34	4		75		1.12	.279	59,200	0		.079	.438	.480	1.37	81.1
P35	4		75	saw	.66	.164	72,400	0						
P36	4		75		1.35	.344	51,600	0		.060	.540	.625	1.565	80.8
P37	4		75	cuts	.51	.130	106,600	0						
P38	4		75		1.54	.392	57,000	0		.0735	.615	.750	1.71	97.5
P39	4		75	(slots)	.90	.230	72,400	0		.118	.361	.402	1.25	90.5
P40	4		75		.72	.184	85,800	0						
P12	4	600	75	34	.56	.143	51,300	26,510						
P23	4	600	75	40	1.22	.312	54,500	42,000		.067	.490	.560	1.48	80.7
P22	4	600	75	40	1.15	.294	59,300	40,570		.0795	.461	.525	1.44	85.5
P13	4	600	75	34	.77	.196	60,100	92,050						

TABULATION OF TEST DATA

Spec	W (in)	T_{crk} °F	T_{rupt} °F	σ_{crk} (ksi)	ℓ_c	y	σ_r (psi)	n (cyc)	$\sigma_{y.s.}$ (psi)	$\left(\frac{\sigma_r}{\sigma_{y.s.}}\right)^2$	$\frac{\pi \ell_c}{2w}$	Q_1	$\sqrt{Q_1 W}$	K_{c_1}
P25	4	600	600*	40	1.25	.319	62,500	26,000		.127	.500	.595	1.53	95.7
P20	4	600	600*	40	1.00	.255	75,600	32,020		.186	.400	.495	1.36	103.0
P15	4	600	600*	40	.93	.237	78,800	26,000		.202	.372	.445	1.32	104.0
P4	4	600	600*	34	.68	.173	84,400	25,380						
P7	4	600	600*	34	.80	.204	80,600	47,500						
P10	4	600	600*	34	.73	.186	82,400	38,080						
P16	4	600	600*	40	.94	.240	85,700	37,000		.240	.377	.470	1.36	116.4
P11	4	600	600+	34	.56	.140	94,600≠	28,000						
P9	4	600	600+	34	.82	.205	83,800≠	46,000						
P2	4	600	600+	34	1.06	.265	70,700≠	41,570						
P5	4	600	-340	34	.61	.156	20,200	39,760						
P21	4	600	-244	40	1.15	.294	26,700	26,710	250,000	.0114	.461	.50	1.40	37.4
P27	4	600	-320	40	1.36	.347	22,450	25,900	270,000	.0069	.545	.61	1.54	34.6
P8	4	600	-100	34	.71	.181	22,340	27,000						
P26	4	600	-105	40	1.31	.334	31,000	29,935	230,000	(.182)	.525	.58	1.50	46.5

* 600°F tensile test held at temperature two to three minutes while being fractured.
\+ Temperature held 60 minutes under 80% load prior to fracture.
≠ Prior to failure panels were held at approximately 80% of this stress.

TABULATION OF TEST DATA

Spec	W (in)	T_{crk} °F	T_{rupt} °F	σ_{crk} (ksi)	ℓ_c	y	σ_r (psi)	n (cyc)	$\sigma_{y.s.}$ (psi)	$\left(\frac{\sigma_r}{\sigma_{y.s.}}\right)^2$	$\frac{\pi \ell_c}{2w}$	Q_1	$\sqrt{Q_1}$	K_{c_1}
P150	4	+ 75	+ 75	35	.79	1.97	65,000	23,100						
151	4	+ 75	+ 75	35	1.03	.257	57,700	23,300						
152	4	+ 75	+ 75	35	1.22	.305	49,500	46,250						
158	4	+ 75	+ 75	Welded	.40	.10	72,800	0						
159	4	+ 75	+ 75	slot	.40	.10	78,000	0						
162	4	+ 75	+ 75	slot	.40	.10	100,000	0						
163	4	+ 75	+ 75	only	.40	.40	96,600	0						
P99	6.01	+ 75	+ 75		.81	.134	49,500							
P97	6.03	+ 75	+ 75		.81	.134	66,000							
P94	6.05	+ 75	+ 75		.795	.132	75,000							
P153	4	+ 75	+ 75	35	.92	.23	48,300**	22,350						
154	4	+ 75	+ 75	35	.96	.24	49,700	17,650						
155	4	+ 75	+ 75	35	.90	.225	45,600**	31,550						
156	4	+ 75	+ 75	35	1.20	Variable		42,600						
P157	4	+ 75	+ 75	20	.50	Variable		107,325						
P100	4	+ 75	+ 75		1.18	.196	56,900							

** Preloaded at +700°F and 60,000 psi = σ_{gross} (25 to 90 minutes)

TABULATION OF TEST DATA

Spec	W (in)	T_{crk} °F	T_{rupt} °F	σ_{crk} (ksi)	ℓ_c	y	σ_r (psi)	n (cyc)	$\sigma_{y.s.}$ (psi)	$\left(\frac{\sigma_r}{\sigma_{y.s.}}\right)^2 \frac{\pi \ell_c}{2w}$	Q_1	$\sqrt{Q_1 W}$	K_{c_1}
96	4	+ 75	+ 75		1.20	.198	43,050						
P98	4	+ 75	+ 75		1.22	.205	55,200						
P200	4	+ 75	+ 75	35	.92	.115	35,000	Fract. in fatigue					

SECTION 5

SUMMARY OF TEST RESULTS ON AM355 STEEL SHEET

The test program on the 215,000 tensile strength steel is briefly discussed. Over sixty panels were tested (2" to 8" widths) in a program similar to that for the PH15-7 Mo steel. The test results are presented in the accompanying graphs and are discussed below.

Difficulty was encountered in sawing the starter notch in panels of this material in both the annealed as well as the heat-treated condition. The electric-arc discharge method, see Appendix C, was used to perform the 0.4" long by .005" to .009" wide starter cracks in this material.

1. Figure 27 illustrates the residual strength characteristics of the centrally fatigue cracked panels. Similar to the PH15-7 Mo steel panels, it can be seen that notch sensitivity increases with a decrease in rupturing temperature. Although this material does not appear to be as notch resistant as the material Rene' 41 (Section 7), it does exhibit greater crack strengths than the PH15-7 Mo steel having higher tensile strengths.

2. Figure 28 is a graph of fatigue crack growth versus number of stress cycles. The four inch wide test panels in this graph were tested at two values of maximum cyclic cracking stress and cracking temperature. A discussion of crack growth rate as a function of temperature is given in Section 13.

3. Figure 29 shows fatigue crack growth versus stress cycles for eight inch wide panels tested at cycling rates of 20 to 50 cpm. No pronounced difference in cracking characteristics can be observed as a function of rate of cyclic loading at normal testing temperatures (75-80°F). This effect, however, can be very pronounced at elevated temperatures.

4. To expand further the crack-growth investigations, an additional yet realistic parameter has been added to the program. Figure 30 illustrates the effect of a high preload in an elevated temperature environment on the interrupted crack growth characteristics of the metal. This step in the program has resulted in an extension of the crack which may be termed "creep-cracking" under the steady state conditions. See Figure 31, page 54 and Appendix A. The resulting blunter front of the crack tip under these conditions is evidenced by a slower rate of crack-growth. Note the delay in growth on resuming the cyclic stressing. The beneficial delaying period is not long however, since the prior crack-growth rate is soon re-established. Additional analytical study should be directed to this phenomenon and an attempt made to incorporate and evaluate the effect in a vehicle environmental design spectrum. (The crack extension or "creep crack" at the end of 11,000 cycles in Figure 30 is from 1.05" to 1.10").

5. Figure 32 illustrates the residual strength of cracked panels tested at different rupturing temperatures. The effect of post-straining that is

sometimes observed is shown by the results of the test panels in this figure.

6. Figures 33 and 34 report some additional crack growth data on panels of different thicknesses.

7. Figure 35 shows the test results of an experiment designed to purposely disrupt the growth of the crack. Center-punch mark indentations were purposely placed in the path of the advancing fatigue crack and have delayed the propagation rate somewhat. The overall effect appears to be slight. It may be plausible, however, that as the right-hand crack grows longer and the center-crack eccentricity increases that the right-hand crack could accelerate in its growth.

8. Figure 36 is a graph of the Anderson-Paris parameter, Reference 3 , plotted as a function of crack rate for the panels tested at 75° and 80°F. The crack rates $\Delta\ell/\Delta n$ were obtained by differentiating the data of Figures 28, 29, and 33. Figure 36 can be used as the basis for predicting crack-growth curves, since the rate of cracking is defined as a function of crack length and gross section stress. The fact that the crack rate is not considered to be a function of the critical crack length is believed to be a shortcoming of this approach. Refer to Section 14 for a further discussion of rate of crack propagation.

9. Figure 37 shows the agreement between observed crack growth and values calculated on the basis of the lower envelope of the data shown in Figure 36. Good agreement is indicated. Note however that Figure 36, plotted to a log scale, shows appreciable scatter, so that a prediction based on these data is subject to considerable interpretation. Compare Figure 36 with Figure 131, which compares test results with a new empirical approach on a graph plotted in ordinary coordinates.

10. Figure 38 similar to Figure 36 is an Anderson-Paris parametric plot (Reference 1) of crack-growth at elevated temperature. This diagram is used to predict the rate and accumulation of fatigue cracking in the tests shown by Figure 39. The construction of this diagram is similar to that described in summary 8 above.

11. Figure 39. This graph shows good agreement between actual and predicted fatigue crack growth. A spectrum of four different maximum cracking stresses and two levels of cracking temperatures were used. The calculations for the 80° F. condition were made by integrating the lower limit boundary curve of Figure 36. The 600° F. conditions were calculated from the curve of Figure 38.

    It is pointed out that fair agreement is attained between calculated and actual conditions only when the lower limit of the data is used. If averages or upper limits of the data-scatter were used, then the calculated method would not be conservative. It can be seen in Figure 39 that even with the lower limit data the calculated accumulative growth alternates from conservative to unconservative.

    Figure 40 is a typical load-strain curve for standard ASTM tensile coupons in the material AM355. The yield loads are noted on the curves

of specimens 2 and 3 and can be compared to the F_{ty} values in Table 3 if the stress-strain characteristics are desired.

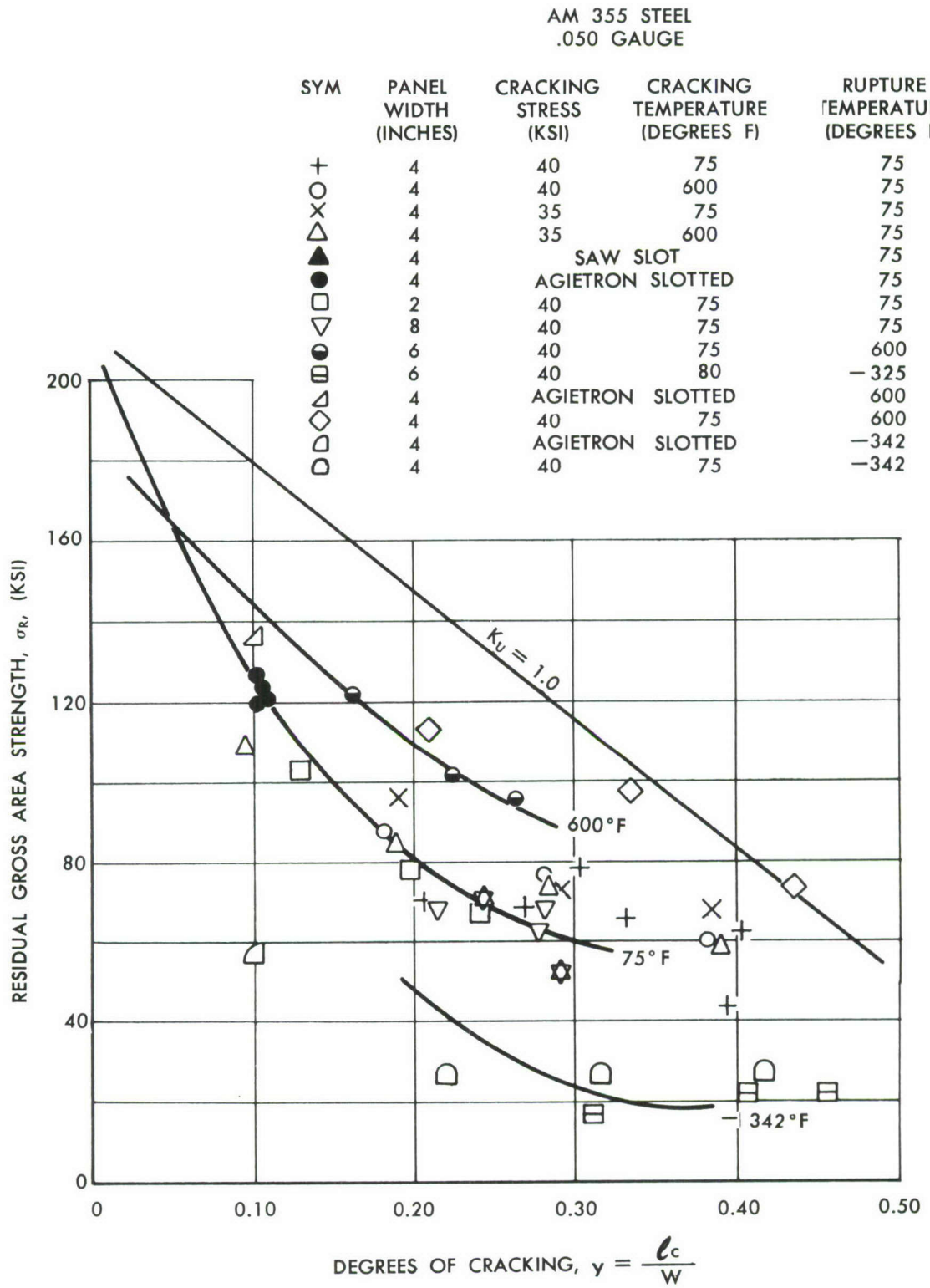


Figure 27. RESIDUAL STRENGTH vs DEGREE OF CRACKING

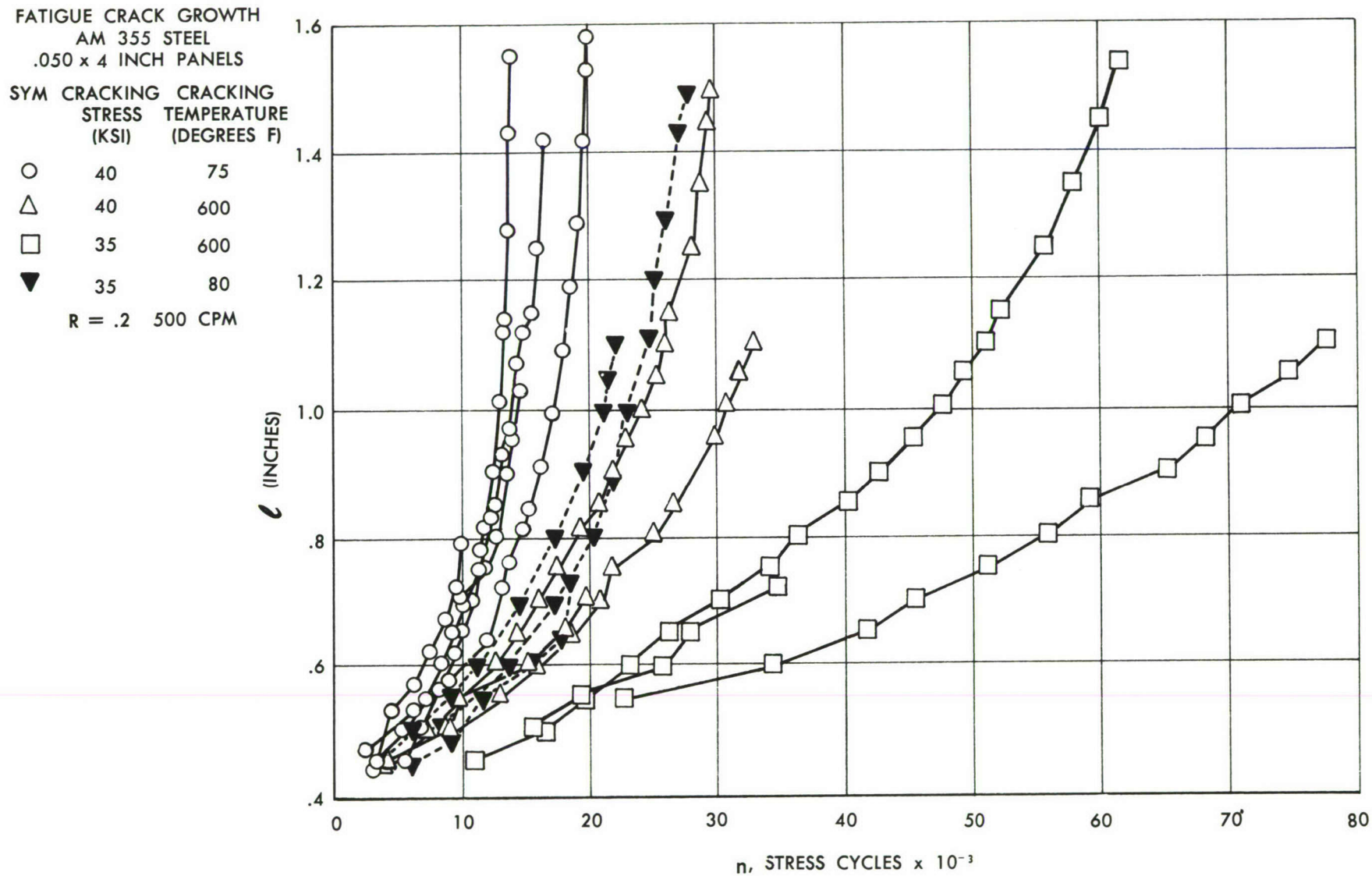


Figure 28. FATIGUE CRACK GROWTH

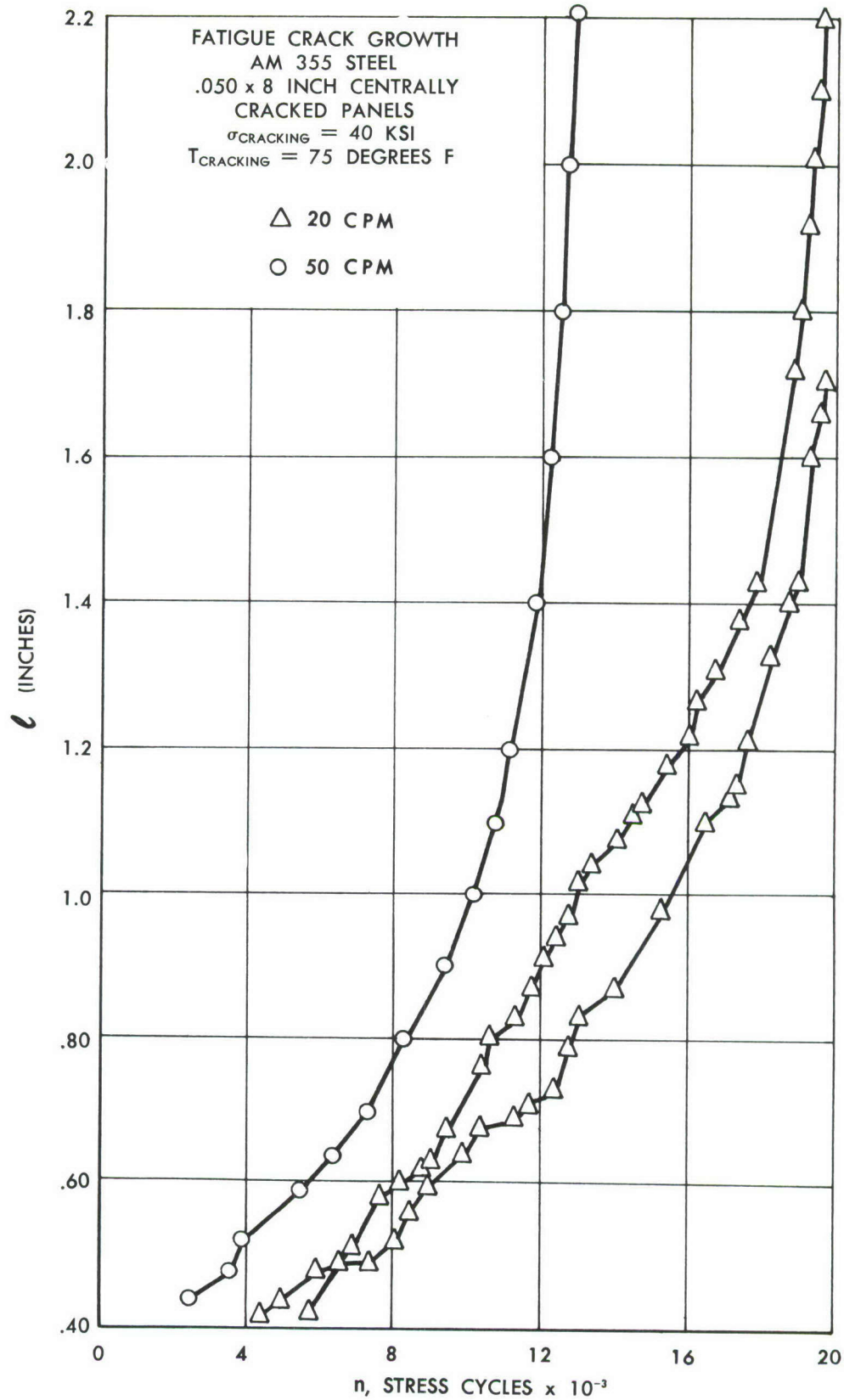


Figure 29. FATIGUE CRACK GROWTH

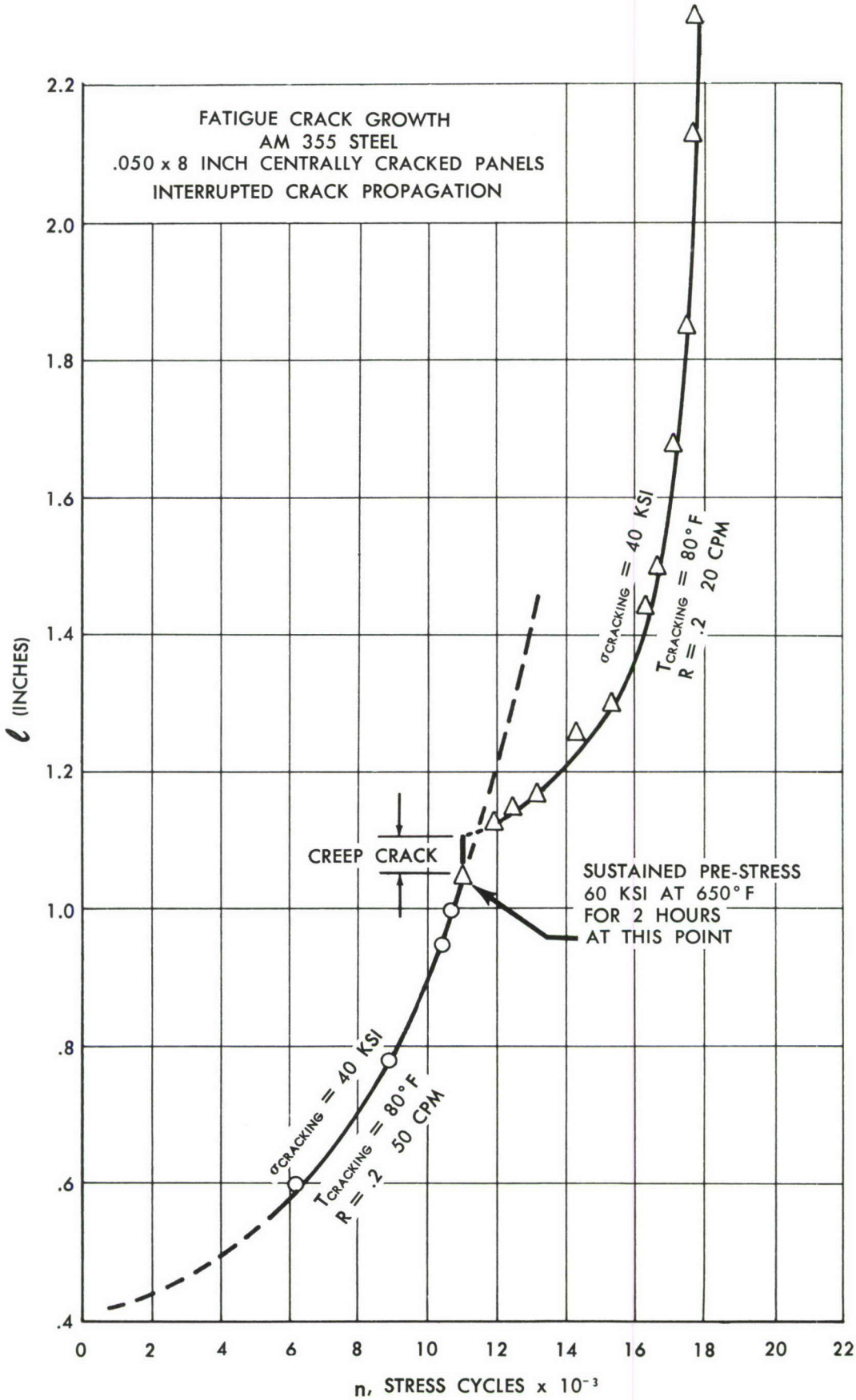


Figure 30. INTERRUPTED FATIGUE CRACK GROWTH

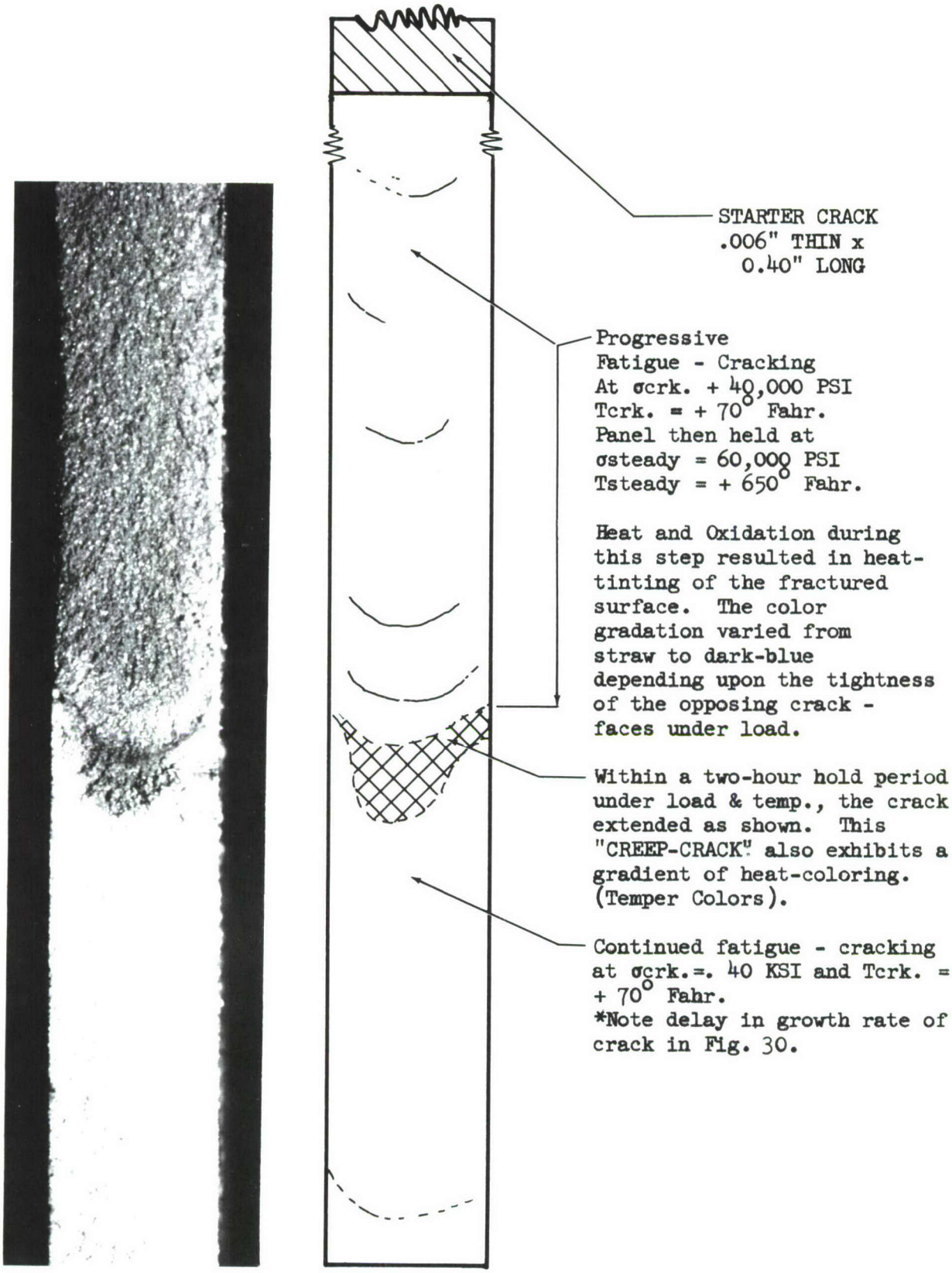


Figure 31. FATIGUE-CREEP CRACK

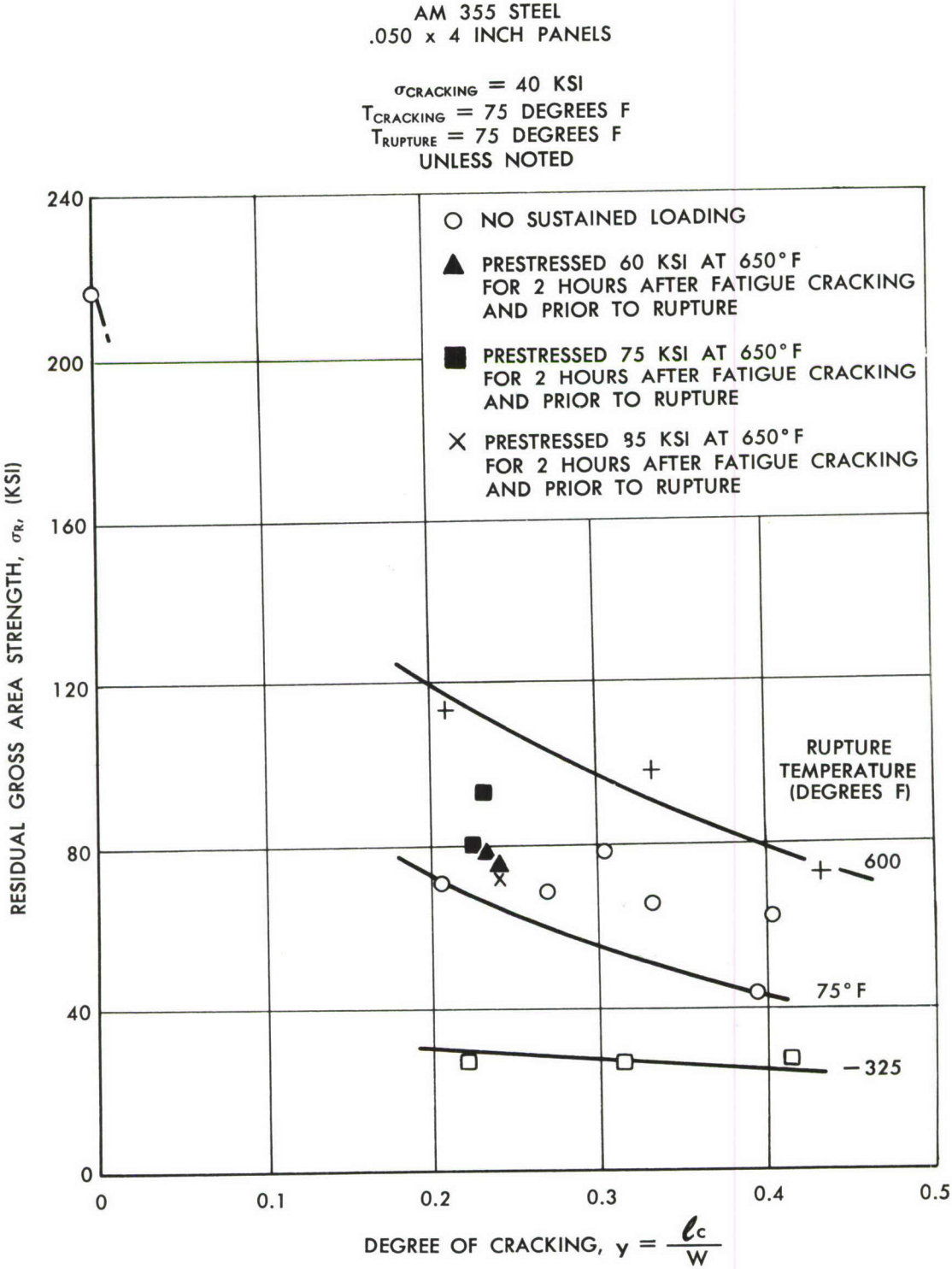


Figure 32. RESIDUAL STRENGTH vs DEGREE OF CRACKING

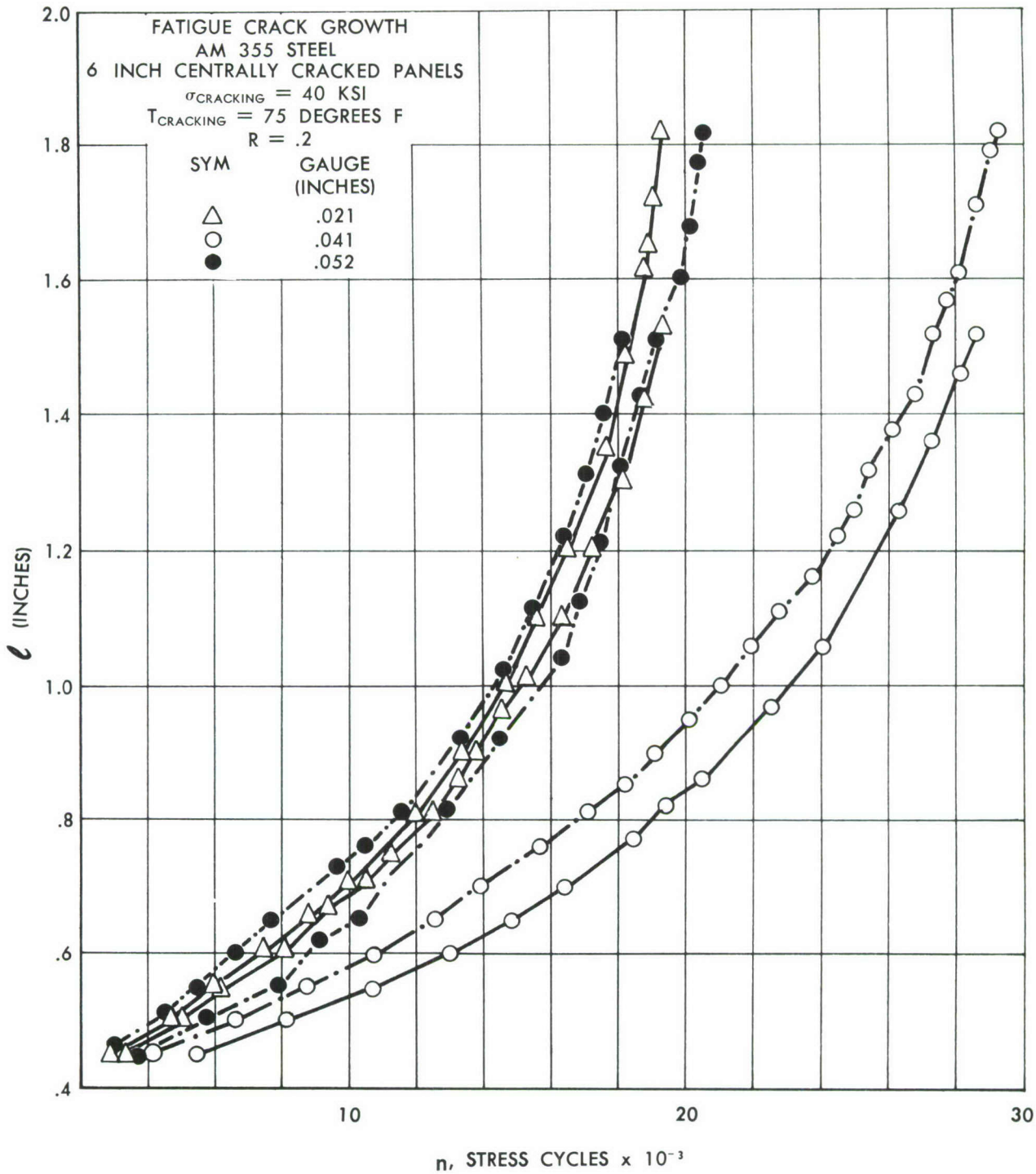


Figure 33. FATIGUE CRACK GROWTH

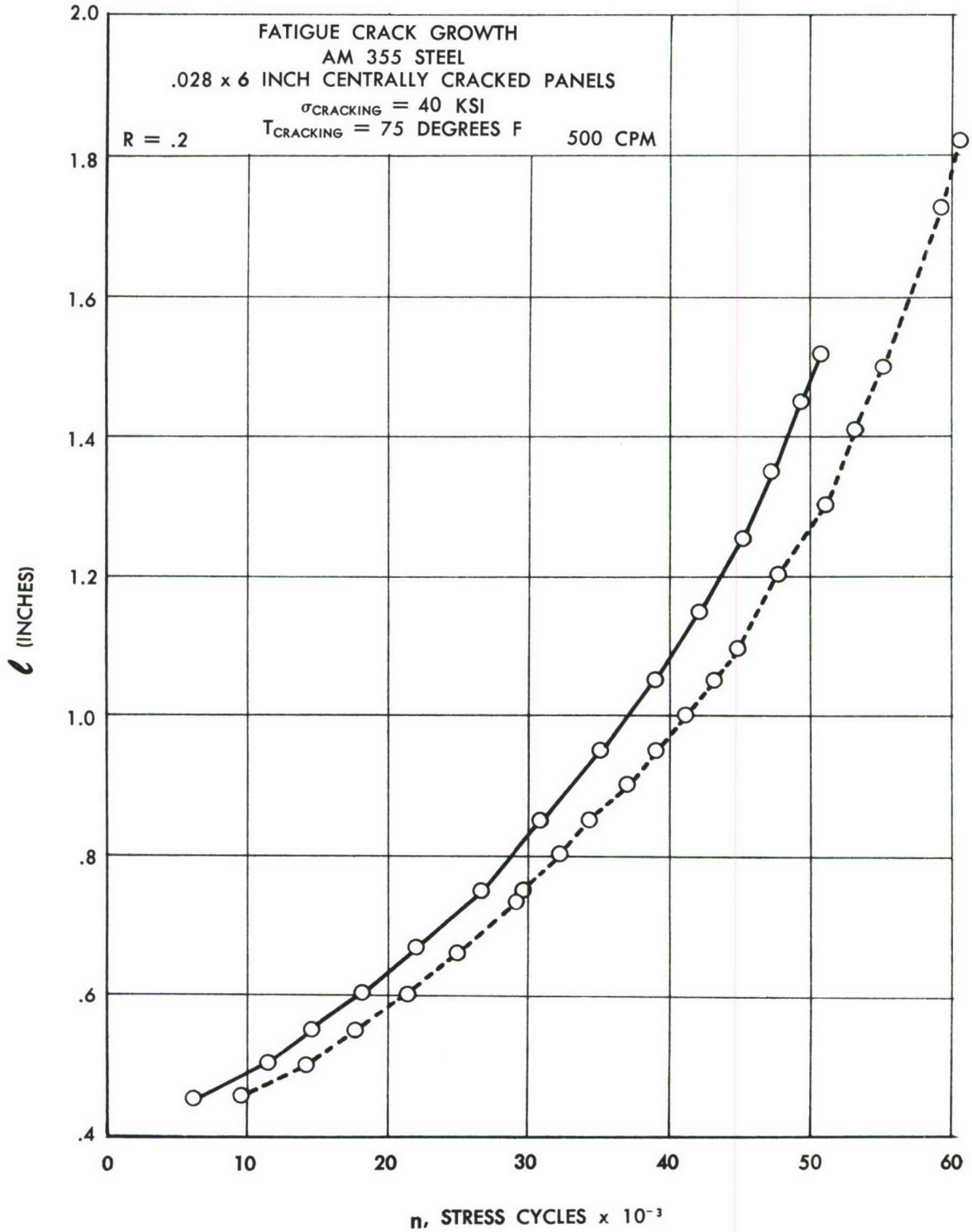


Figure 34. FATIGUE CRACK GROWTH

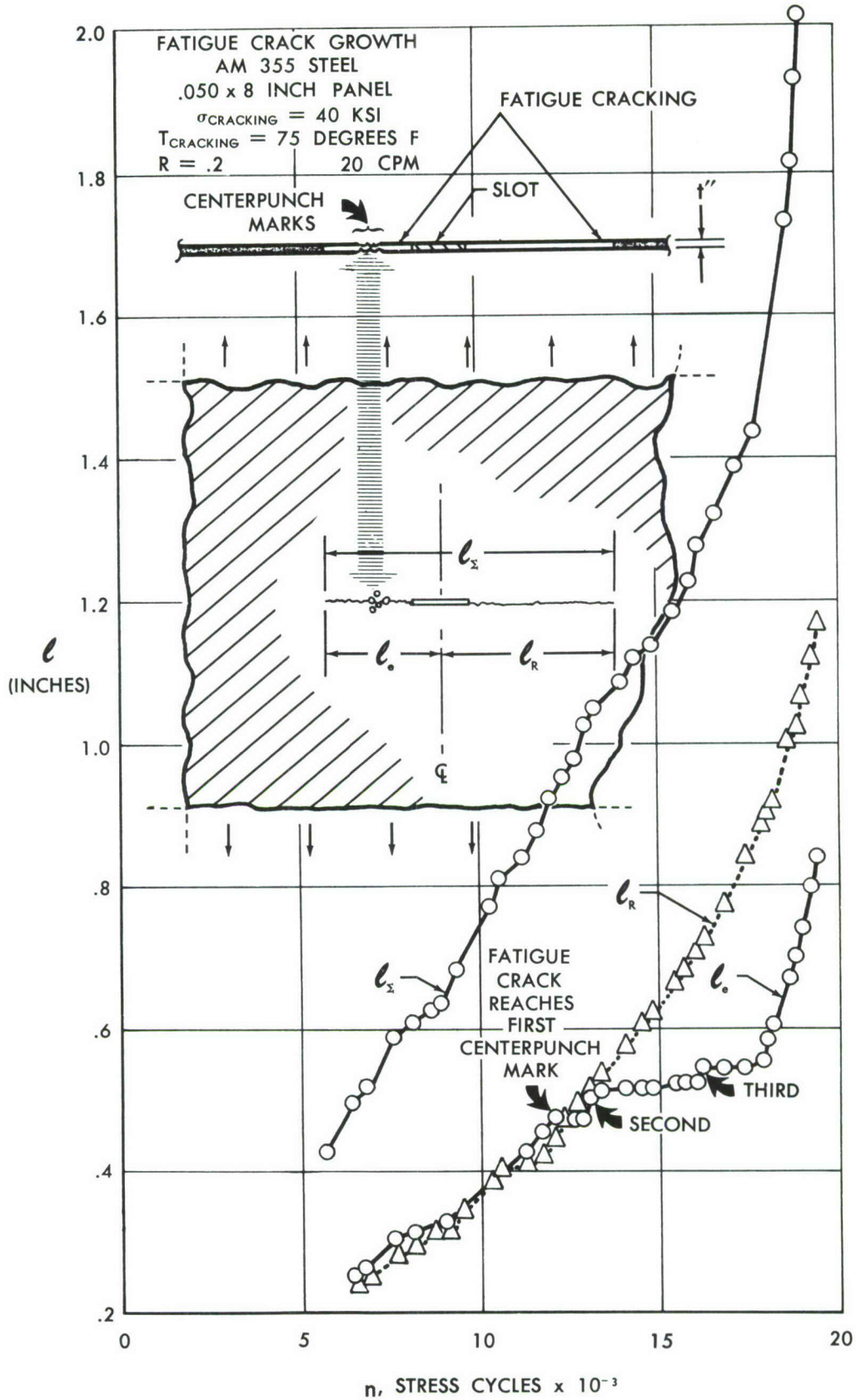


Figure 35. FATIGUE CRACK GROWTH

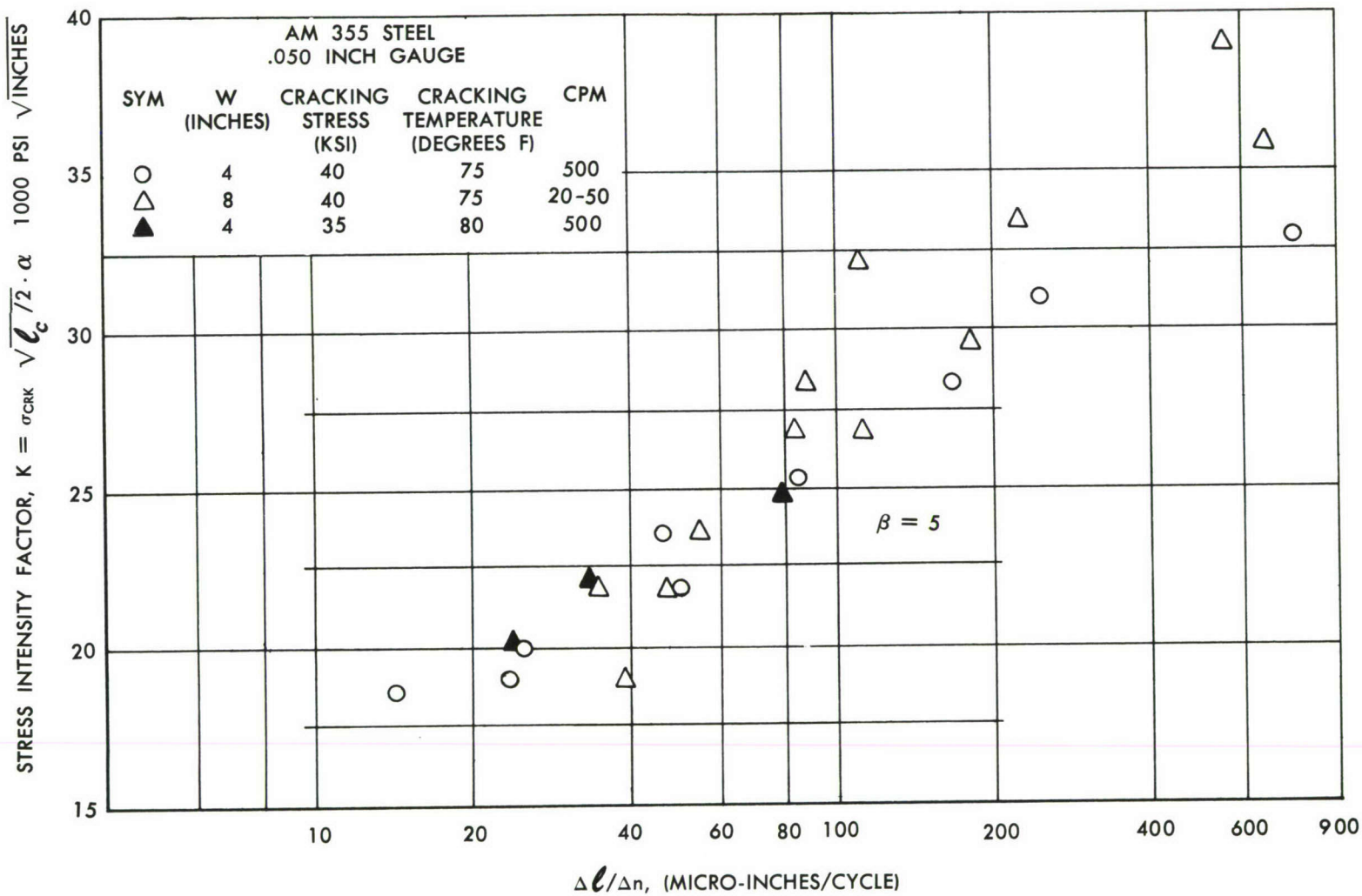


Figure 36. STRESS INTENSITY vs RATE OF CRACKING

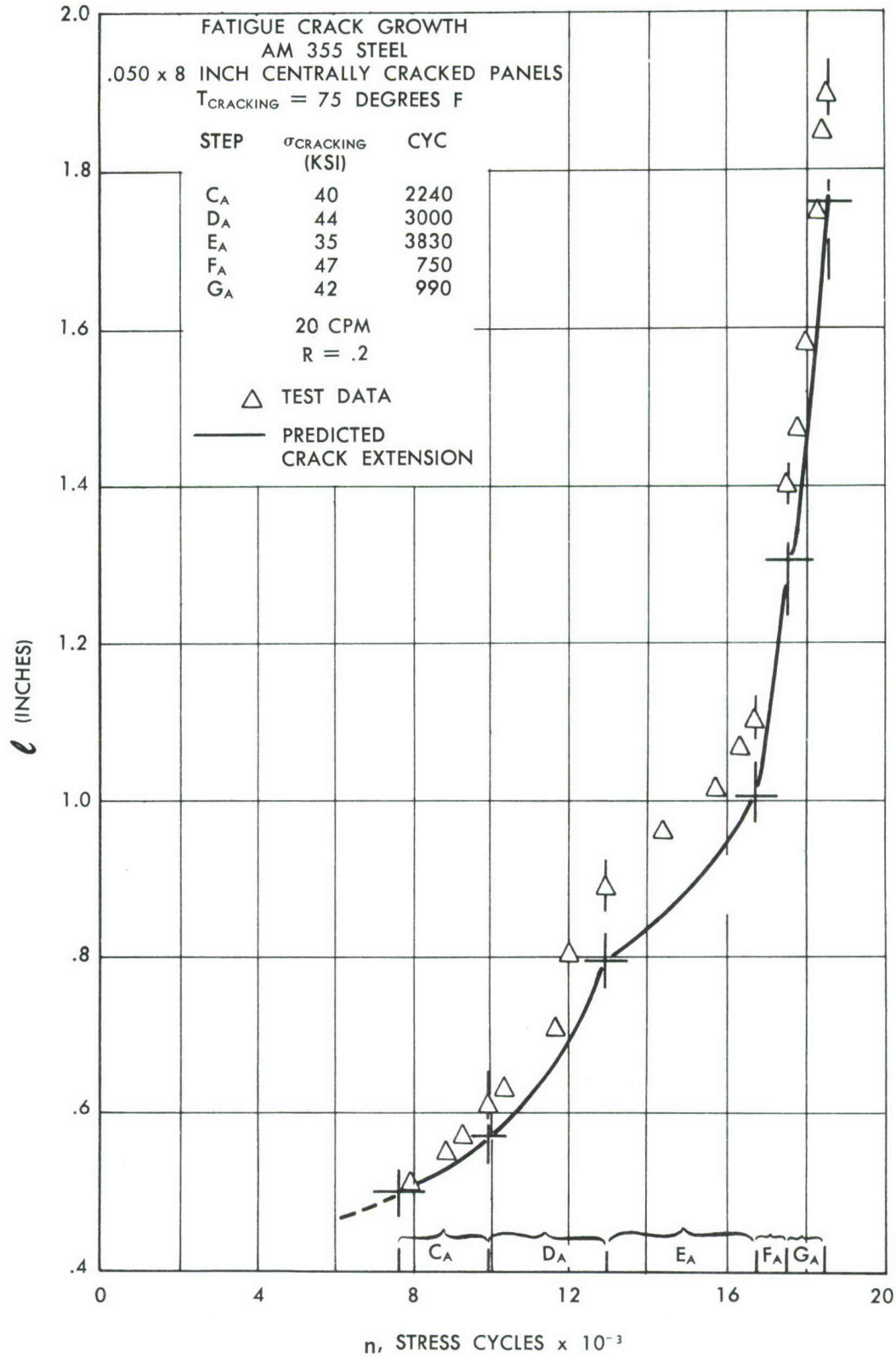


Figure 37. ACCUMULATIVE FATIGUE CRACK GROWTH

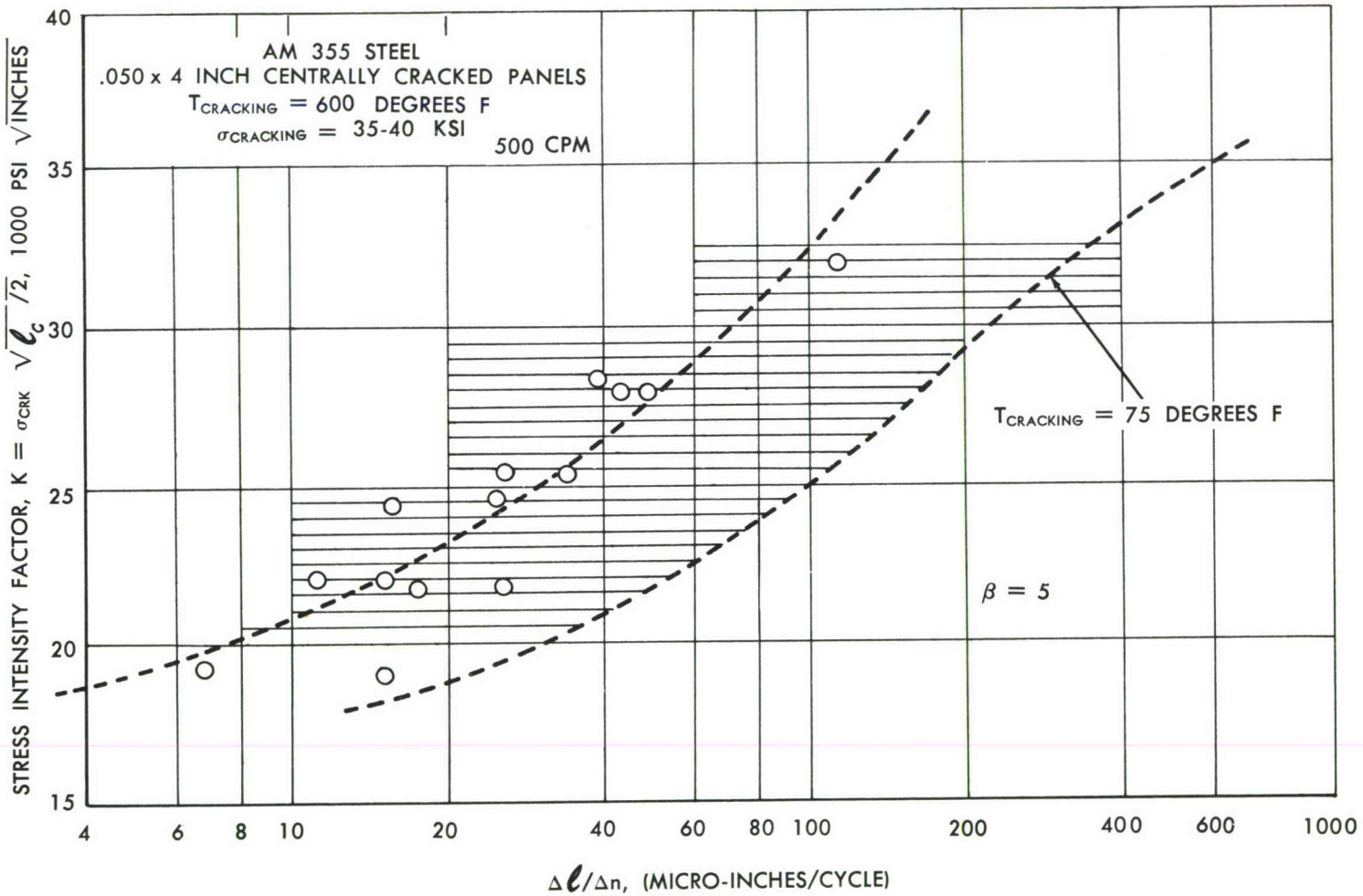


Figure 38. STRESS INTENSITY vs RATE OF CRACKING AT ELEVATED TEMPERATURES

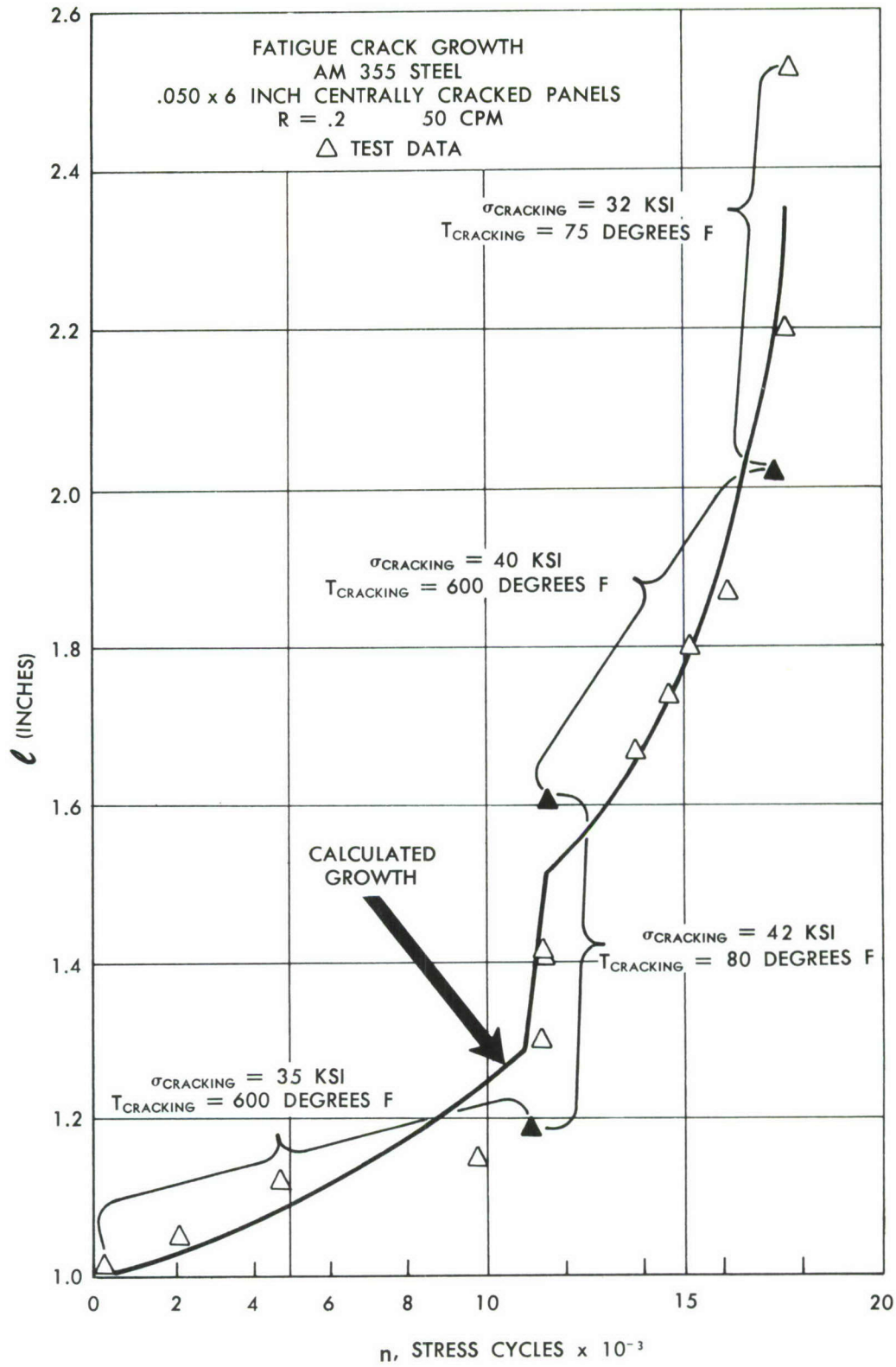


Figure 39. ACCUMULATIVE FATIGUE CRACK GROWTH

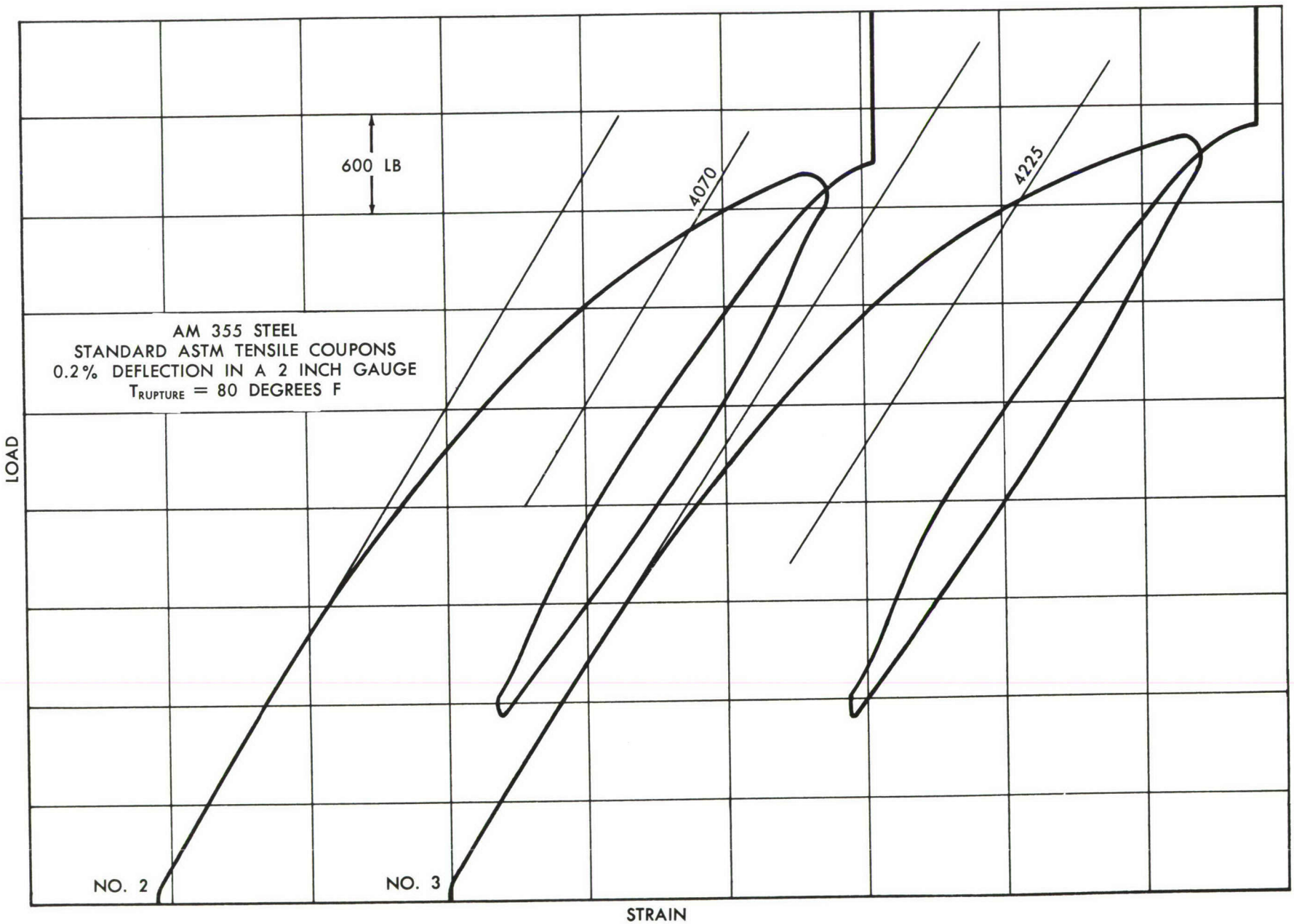


Figure 40. LOAD-STRAIN CURVE

MECHANICAL PROPERTIES OF AIR HARDENING

AM 355 STEEL

The test coupons and panels were made from Allegheny Ludlum's AM355 steel. The various gauge panels were received in the annealed condition and heat treated for test according to the following schedule.

Condition at +1710° F. for 10 minutes.

Air Cool.

Refrigerate at -100° F. for 3 hours.

Age at +850° F. for 3 hours.

Air Cool.

TABLE 3

ALLEGHENY LUDLUM

H 45474
J 0611

Spec.	Rolling Dir.	Ft_y	Ft_u	% Elong. (2" g.l.)
1	Longit.	157,480	210,830	7.5
2	Longit.	160,870	213,640	10.0
3	Longit.	162,205	216,730	11.0
4	Longit.	165,355	217,320	
5	Transverse	155,385	211,150	11.5
6	Transverse	163,035	211,280	11.5
7	Transverse	161,925	213,850	18.0
8	Transverse	165,040	211,110	10.3

TABLE 4

CHEMICAL ANALYSIS

Cr	Ti	Mn	Mo	Ni	Si	Al	Fe
15.70	--	0.75	2.52	4.07	0.31	--	Bal.

TABULATED TEST DATA

Spec No (AM355)	W (in)	T_{crk} °F	T_{rupt} °F	σ_{crk} (ksi)	ℓ_c (in)	$y=\frac{\ell_c}{W}$	σ_r (psi)	n (cyc)
-2 -1	2	+ 75	+ 75	40	.52	.260	102,000	6,800
-2 -2	2	+ 75		40				9,400
-2 -3	2	+ 75	75	40	.75	.375	79,000	15,400
-2 -4	2	+ 75		40				13,400
-2 -5	2	+ 75	75	40	.93	.465	68,500	9,700
-2 -6	2	+ 75		40				8,800
-6 -1	6	+ 75	+ 75	40	1.53	.255	71,200	19,400
-6 -2	6	+ 75	+ 75	40	1.82	.303	62,900	19,350
-6 -3	6	+ 75	+ 75	40	1.54	.257	109,000	51,000
-6 -4	6.02	+ 75	+ 75	40	1.83	.304	101,400	60,600
-6 -5	6.04	+ 75	+ 75	40	1.53	.254	82,300	28,600
-6 -6	6.04	+ 75	+ 75	40	1.84	.305	82,800	29,300
-6 -7	6	+ 75	+600	40	1.35	.225	102,000	19,700
-6 -8	6	+ 75	-325	40	1.85	.308	18,665	36,200
-6 -9	6	+ 75	-318	40	2.73	.455	20,165	34,000
-6-10	6	+ 75	+600	40	.98	.164	122,000	
-6-11	6	+ 75	+600	40	1.60	.267	95,000	
-6-12	6	+ 75	-319	40	2.45	.408	20,080	
-6-13	6	+ 75	+ 75	40	1.54	.257	77,700	18,200
-6-14	6	+ 75	+ 75	40				20,550
-6-15	6	+ 75	+ 75	40				54,673
-8 -1	8	+ 75	+ 75	40	1.73	.216	68,300	19,698
-8 -2	8	+ 75	+ 75	40	2.23	.280	67,500	19,717
-8 -3	8	+ 75	+ 75	40	2.22	.277	60,500	12,930

TABULATED TEST DATA

Spec No (AM355)	W (in)	T_{crk} °F	T_{rupt} °F	σ_{crk} (ksi)	ℓ_c (in)	$y=\frac{\ell_c}{w}$	σ_r (psi)	n (cyc)
-8 -4	8	+ 75	+ 75	40	1.93	.240	69,000	18,360
-8 -5	8	+ 75	+ 75	40	2.35	.293	50,500	17,800
-8 -6	8	+ 75		40	3.07			13,483
-4 -1	4	+ 75	+ 75	slot	.408	.103	127,485	
-4 -2	4	+ 75	+ 75	slot	.405	.103	120,400	
-4 -3	4	+ 75	+ 75	slot	.402	.102	121,640	
-4 -4	4	+ 75	+ 75	40	.81	.207	69,750	10,950
-4 -5	4	+ 75	+ 75	40	1.19	.302	77,250	16,400
-4 -6	4	+ 75	+ 75	40	1.59	.403	61,000	19,950
-4 -7	4	+ 75	+ 75	40	1.07	.271	69,400	14,400
-4 -8	4	+ 75	+ 75	40	1.29	.327	65,800	16,500
-4 -9	4	+75	+ 75	40	1.55	.393	43,500	13,850
-4-10	4	+600	+ 75	40	.71	.180	89,600	19,550
-4-11	4	+600	+ 75	40	1.09	.276	77,200	32,950
-4-12	4	+600	+ 75	40	1.51	.382	60,000	29,700
-4-13	4	+ 75	+ 75	35	.75	.190	96,200	
-4-14	4	+ 75	+ 75	Saw slot	.38	.096	109,500	
-4-15	4	+ 75	+ 75	35	1.53	.388	67,900	
-4-16	4	+600	+ 75	35	.74	.187	84,700	34,850
-4-17	4	+600	+ 75	35	1.11	.281	72,200	77,850
-4-18	4	+ 75	+ 75	Ag slot	.43	.109	124,000	
-4-19	4	+600	+ 75	35	1.53	.387	59,000	61,550
-4-20	4	+ 75	+ 75	35	1.14	.289	71,700	
-4-21	4	+ 75	+600	40	.84	.210	113,000	11,200

* Ag = Agietron formed slit (.005" wide).

TABULATED TEST DATA

Spec No (AM355)	W (in)	T_{crk} °F	T_{rupt} °F	σ_{crk} (ksi)	ℓ_c (in)	$y=\frac{\ell_c}{w}$	σ_r (psi)	n (cyc)
-4-22	4	+ 75	-340	40	.88	.220	26,500	10,000
-4-23	4	+ 75	600	40	1.34	.335	97,200	13,750
-4-24	4	+ 75	-340	40	1.27	.317	26,550	15,600
-4-25	4	+ 75	600	40	1.74	.435	73,200	18,350
-4-26	4	+ 75	-340	40	1.67	.417	27,100	17,000
-4-27	4	+ 75	+ 75	40	.925	.234	77,900	13,000
-4-28	4	+ 75	+ 75	40	.95	.241	76,100	12,800
-4-29	4	+ 75	+900	40	.94	.235	102,250	12,450
-4-30	4	+ 75	+600	Ag slot	.41	.103	135,500	
-4-31	4	+ 75	-340	Ag slot	.41	.102	56,850	
-4-32	4	+ 75		40	.92	.230	93,000(a)	
-4-33	4	+ 75		40	.95	.237	74,500(c)	
-4-34	4	+ 75		40	.94	.235	79,500(b)	
-2 -6	2	+ 75	+ 75	40	.94	.470	71,000	
-2 -2	2	+ 75	+ 75	40	.53	.365	98,800	
-2 -4	2	+ 75	+ 75	40	.69	.345	91,000	
-6-15	6.02	+ 75	+ 75	40	2.61	.434	47,800	
-6-14	6.02	+ 75	+ 75	40	1.85	.308	64,800	
-8 -6	8.02	+ 75	+ 75	40	3.14	.392	40,850	

(a) Held at 75,000 psi at 650°F for 2 hours then ruptured at + 75.
(b) Held at 75,000 psi at 650°F for 2 hours then ruptured at + 75.
(c) Held at 85,000 psi at 650°F for 2 hours then ruptured at + 75.

SECTION 6

SUMMARY OF TEST RESULTS ON AISI 4340 STEEL SHEET

The 4340 steel panels in this section were oil-quenched and hardened to the 270-280,000 tensile strength range. Varying lengths of centrally oriented fatigue cracks were then generated in the test panels. The cracking temperature during the fatigue testing was between 75°F and 80°F.

The maximum fatigue cracking stress level used was either 37,500 or 40,000 psi. The stress ratio during the fatigue testing was held constant at a value of +.20 ($R = \sigma \text{ min}/\sigma \text{ max} = .2$). Panels from 1" to 8" in width and from .020 to 0.10 in thickness were tested.

1. Figure 41 shows the residual strength characteristics of 4" wide by .050 steel panels containing centrally located fatigue cracks. A few jewelers saw slotted panels are shown for comparison. It should be noted that this material as many others is far more sensitive to the natural fatigue crack than it is to a thin machined slot.

2. Figure 42 shows the fatigue test results on 2" to 8" panels tested in a variety of environments.

3. Figure 43 is an enlarged scale plot of micro-cracks that have been generated by fatigue action yet only go part way through the thickness of the sheet material. Data shown in Figure 41 and 43 have been taken from a Douglas Aircraft Company sponsored research program. The program is discussed in greater detail in reference 14. The specimen types discussed closely duplicate thick sections with minimum amounts of shear lip at fracture. The degree of micro-cracking most closely represents the degree of damage for test evaluation purposes that may be present in fabricated rocket motor cases. An interesting observation from the data can be seen by apparent insensitiveness of certain small cracks to the engineering material strength. The term "climactic cracking" has been selected to describe the highest strength that can be attained under these micro-cracked conditions.

4. Figure 44 shows one type specimen that can be used for evaluating micro-crack strengths. The schematic sketch also illustrates the manner in which the micro-cracks are formed. The photograph of Figure 45 is an 8x enlargement of test specimens with an .070" x 1.0" cross-section and shows the size of the initial fatigue cracks that may be generated by the device of Figure 44.

5. Figure 46 illustrates the time dependency of residual strength for part-way-through micro-cracks. (Low-cycle fatigue). The test data of figures 41 and 43 have been replotted as a function of the number of cycles of load to generate the micro-cracks. The greater exposure times will naturally develop larger crack sizes which in turn will result in larger decreases in strength.

6. Figure 47 shows fatigue crack growth characteristics of .050" x 6" wide panels.

7. Figure 48 is a typical stress-strain curve for the AISI 4340 steel of this program.

8. Some residual strength tests of AISI 4340 steel as a function of sheet thickness is given in Section 12.

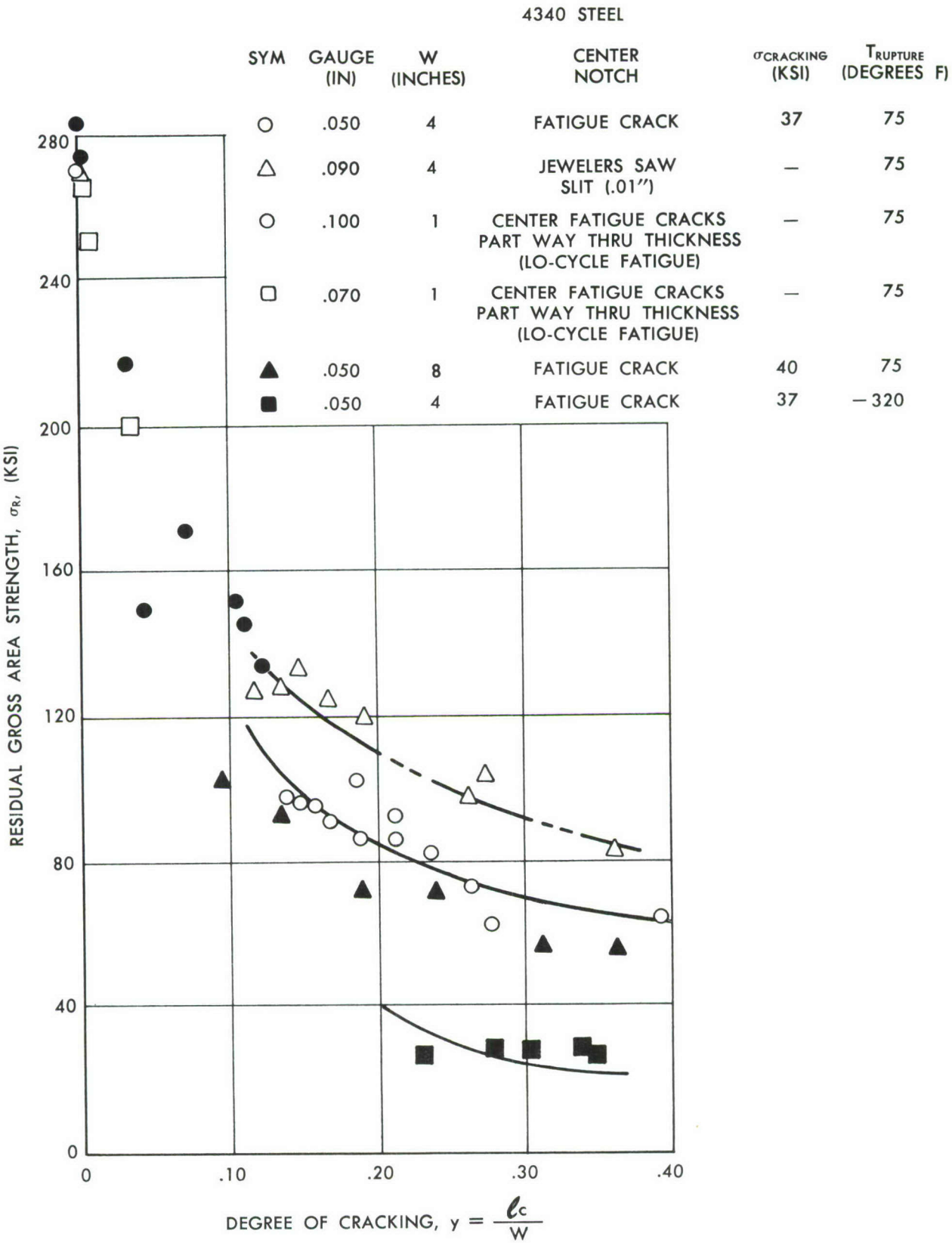


Figure 41. RESIDUAL STRENGTH vs DEGREE OF CRACKING

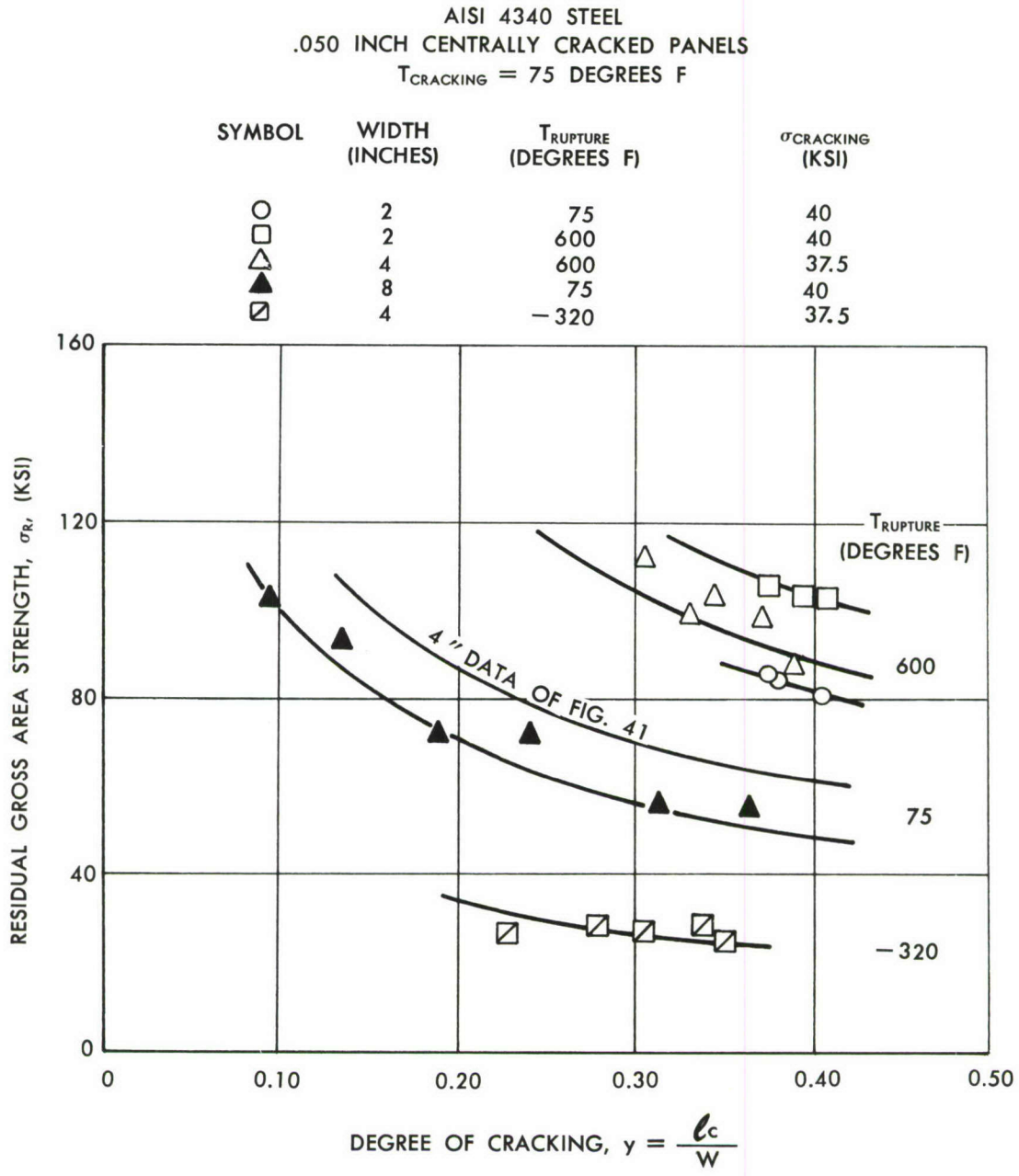


Figure 42. RESIDUAL STRENGTH vs DEGREE OF CRACKING

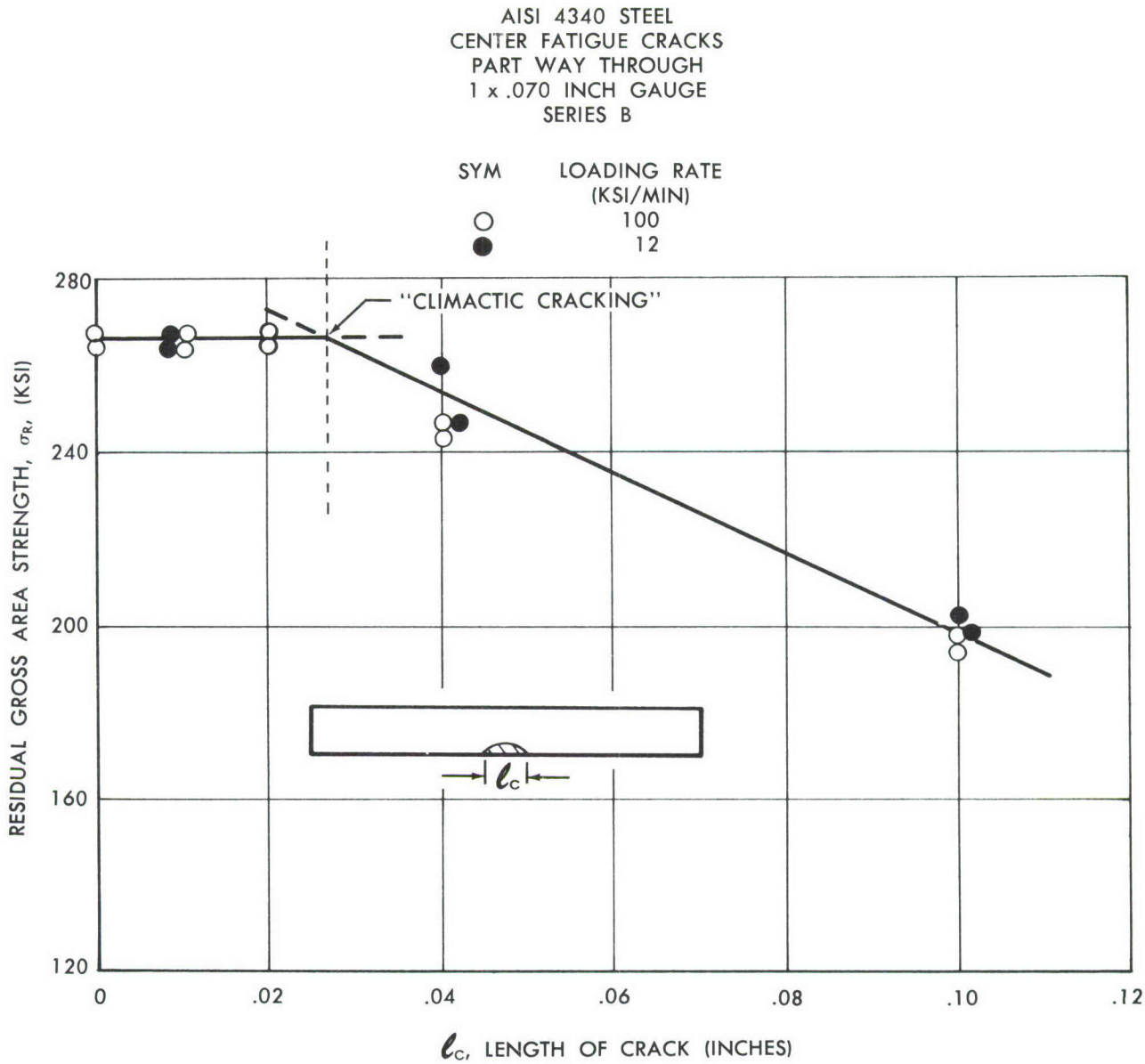


Figure 43. RESIDUAL STRENGTH vs LENGTH OF MICRO CRACKS

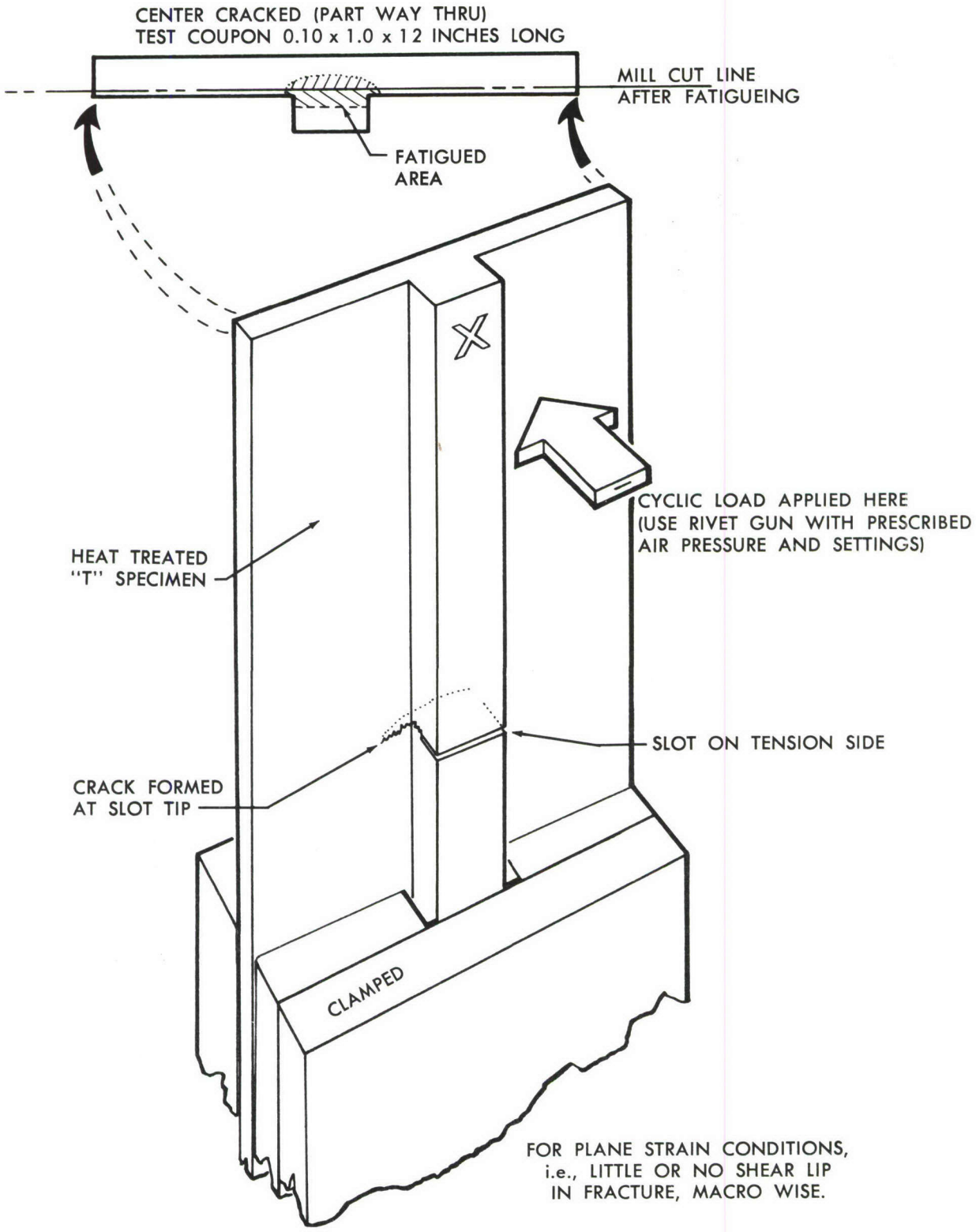
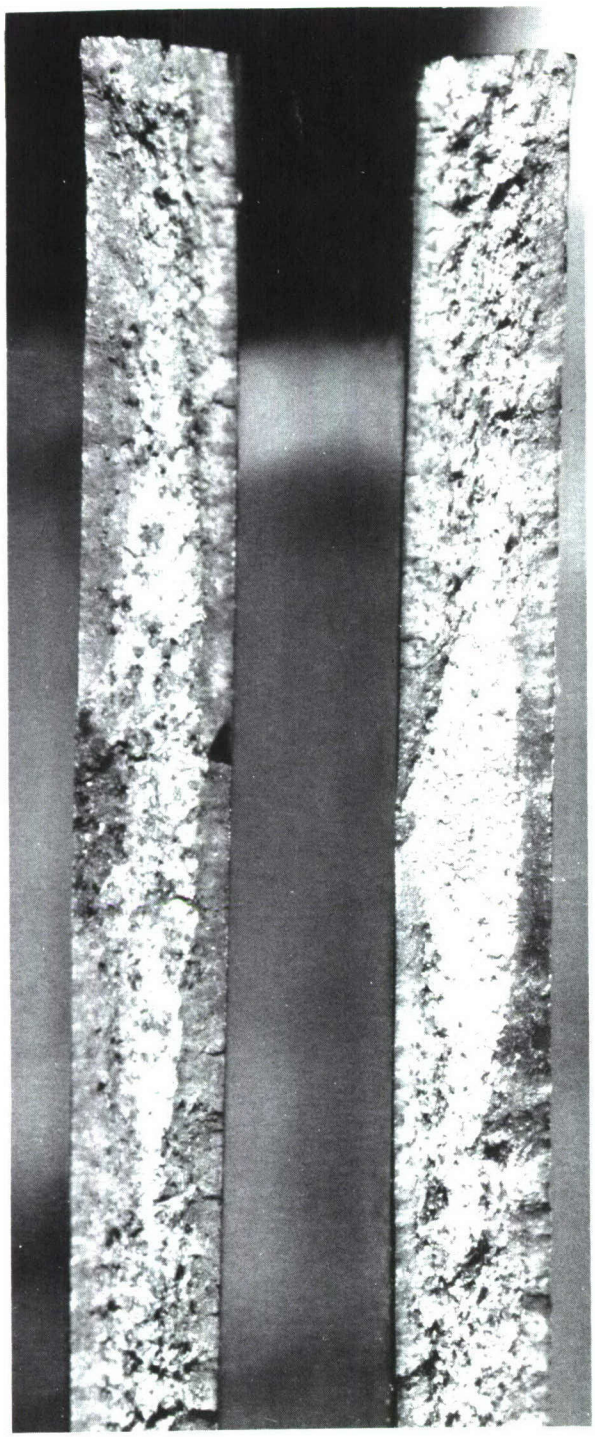
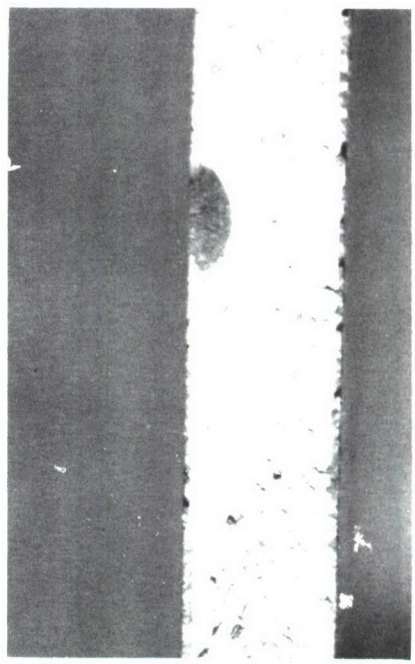


Figure 44. MICRO-CRACK SPECIMENS





Part-way Thru Center
Fatigue Cracks.
Magnification 8X

Above:

Cracks in Vasco Jet 1000

Left:

Micro surface cracks in
4340 steel.

Figure 45. FRACTURE SURFACES OF MICRO-CRACKED SPECIMENS

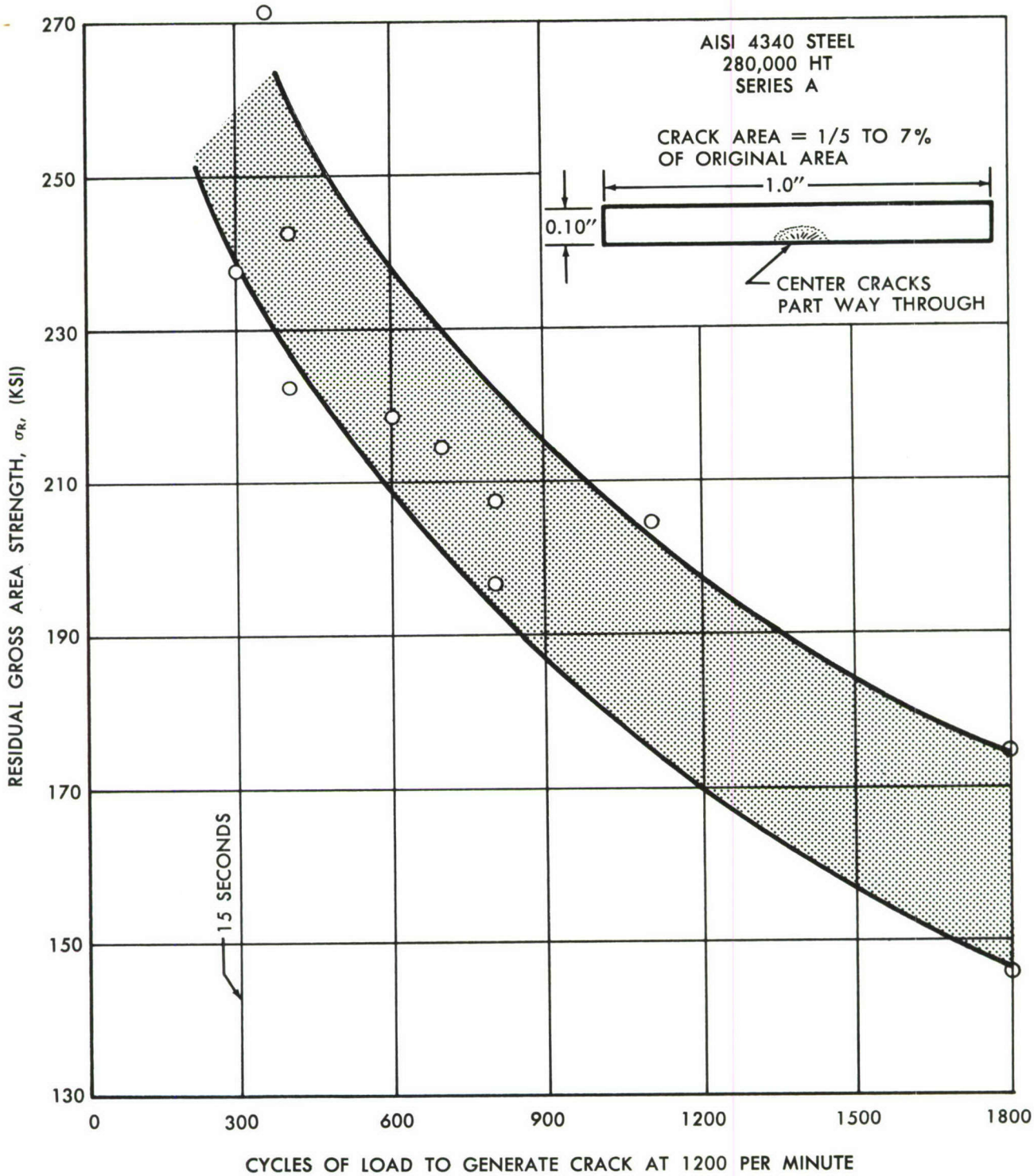


Figure 46. RESIDUAL STRENGTH AS A FUNCTION OF CYCLES OF LOADING

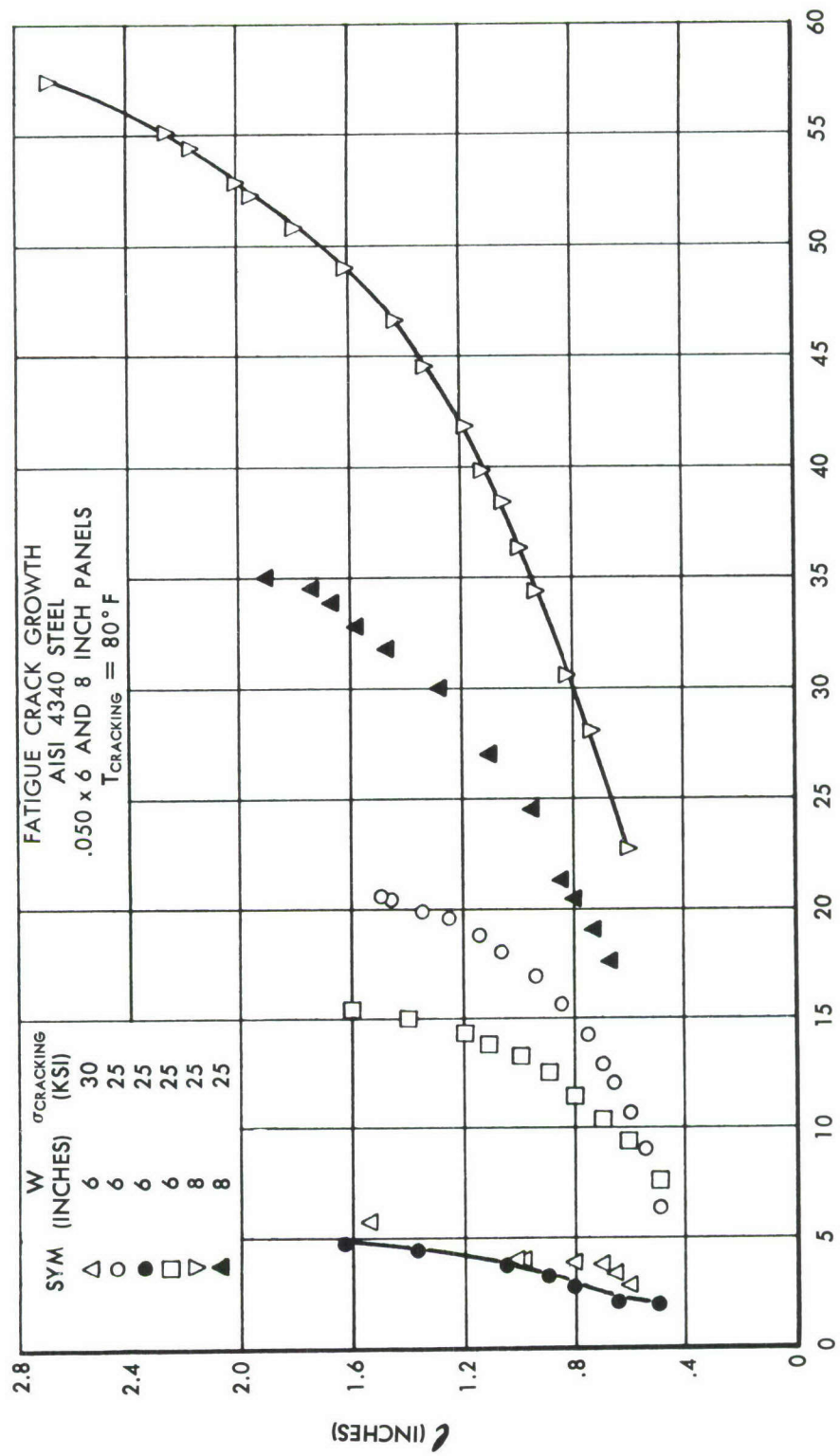


Figure 47. FATIGUE CRACK GROWTH

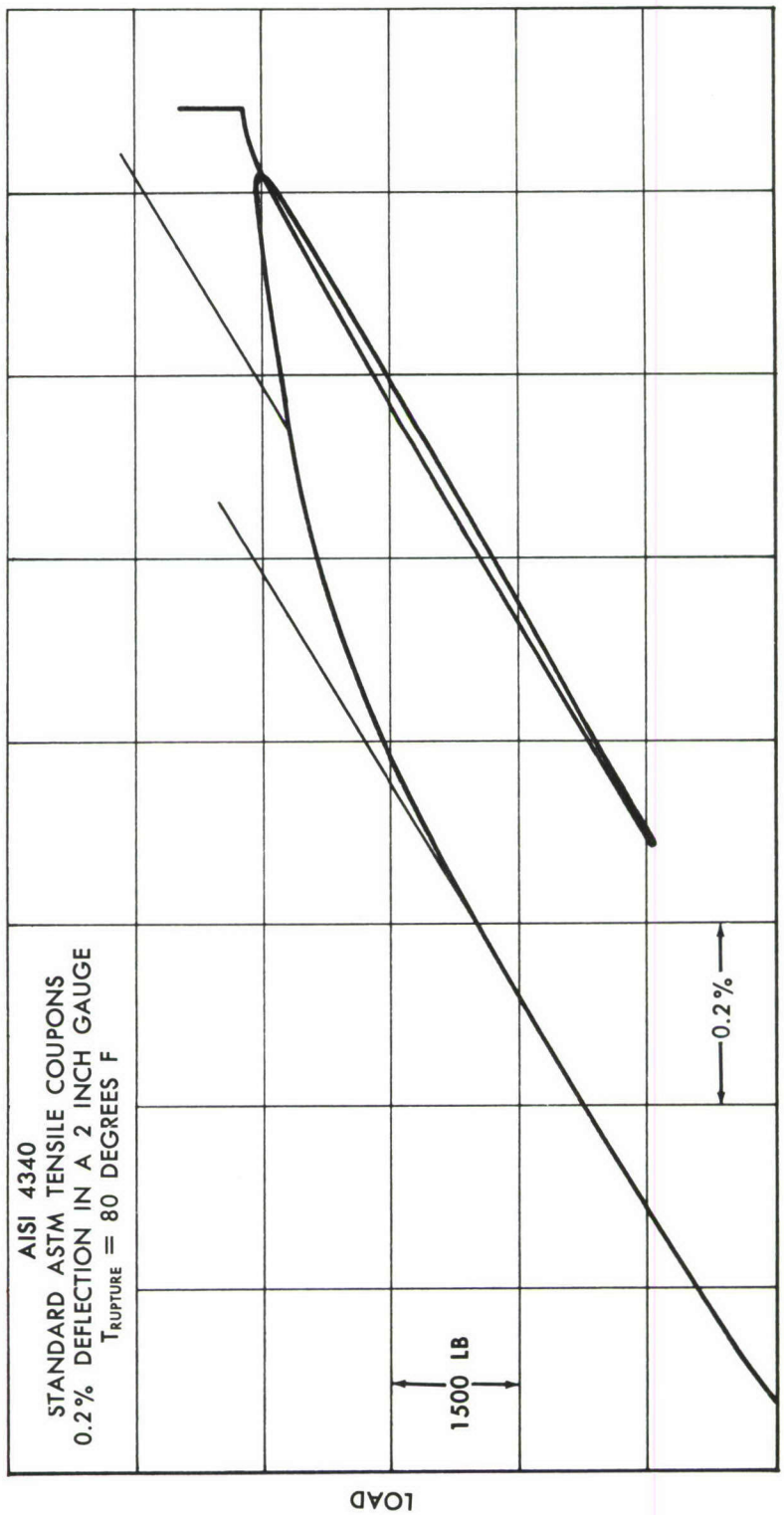


Figure 48. LOAD-STRAIN CURVE

MECHANICAL PROPERTIES

The test coupons and panels were made of AISI 4340 steel from Allegheny Ludlum Steel Company. The lot of steel sheet was from heat #38524. The material was received in the cold rolled and normalized condition. The .020 to .050 gauge test panels were sheared, milled, drilled and slotted prior to heat treatment. The heat treatment of the finished test panels was as follows:

Hardening at 1,525°F. for 45 minutes.

Oil quench to room temperature.

Draw at 410°F. for four hours.

Air cool.

Standard ASTM material tensile coupons from the lot of material gave the average properties listed below:

F_{ty}	F_{tu}	% Elongation (2"g.l.)
225,520	276,095	7.8

TABULATED DATA

Spec No	W (in)	T_{crk} °F	T_{rupt} °F	σ_{crk} (ski	ℓ_c (in)	$y=\frac{\ell_c}{w}$	σ_r (psi)	n (cyc)
ST-4-1	3.95	+ 80	+ 80	40	1.10	.279	60,800	4,700
ST-4-2	3.95	+ 80	+ 80	37.5	1.05	.266	73,500	7,900
ST-4-3	3.95	+ 80	+ 80	37.5	1.54	.390	63,800	10,800
ST-4-4	3.95	+ 80	+ 80	37.5	.58	.147	95,900	2,500
ST-4-5	3.95	+ 80	+ 80	37.5	.52	.132	97,800	2,750
ST-4-6	3.95	+ 80	+ 80	37.5	.62	.157	95,700	9,400
ST-4-7	3.95	+ 80	+ 80	37.5	.66	.167	90,200	8,100
ST-4-8	3.95	+ 80	+ 80	37.5	.72	.182	102,500	13,800
ST-4-9	3.95	+ 80	+ 80	37.5	.74	.187	86,600	7,100
ST-4-10	3.95	+ 80	+ 80	37.5	.84	.212	86,600	11,550
ST-4-11	3.95	+ 80	+ 80	37.5	.84	.212	92,800	10,700
ST-4-12	3.95	+ 80	+ 80	37.5	.93	.236	81,100	8,900
ST-6-15	6.0	+ 75	+ 75		1.59	.265	66,500	21,900
ST-6-2	6.0	+ 75	+ 75	40	1.61	.269	49,700	10,400
ST-6-14	6.0	+ 75	+ 75		1.59	.265	74,500	28,750
ST-6-10	6.0	+ 75	+ 75	40	1.65	.275	57,700	15,500
ST-6-8	6.0	+ 75	+ 75	40	1.62	.270	70,000	33,650
ST-6-6	6.0	+ 75	+ 75		1.62	.270	64,700	10,600
ST-6-5	6.0	+ 75	+ 75	40	1.62	.270	60,300	4,850
ST-6-4	6.0	+ 75	+ 75		1.33	.221	63,000	3,200
ST-6-3	6.0	+ 75	+ 75		1.59	.265	63,500	17,400
ST-6-1	6.0	+ 75	+ 75	29	1.63	.271	69,300	26,650

TABULATED TEST DATA

Specimen	W (in)	T_{crk}	T_{rupt}	σ_{crk} (ksi)	ℓ_c (in)	ℓ_c/w	σ_r (psi)	n (cyc)
ST-8-4	8		+ 75	40	1.92	.240	70,918	35,010
ST-8-6	8		+ 75	40	2.93	.366	55,102	58,380
ST-8-1	8		+ 75	40	.76	.095	100,957	27,380
ST-8-5	8		+ 75	40	1.07	.134	93,367	28,340
ST-8-2	8		+ 75	40	2.50	.313	57,653	18,730
ST-8-3	8		+ 75	40	1.52	.190	70,153	16,500
ST-4-13	3.96		-320		.92	.230	26,186	16,200
ST-4-14	3.96		-320		1.12	.280	28,350	20,550
ST-4-16	3.96		-320		1.22	.305	28,144	12,700
ST-4-21	3.96	+ 80	-320	37.5	1.40	.350	27,577	13,700
ST-4-20	3.96	+ 80	-320	37.5	1.36	.340	29,897	10,700
ST-2-1	2	75	+ 75	40	.75	.375	85,714	11,900
ST-2-4	2	75	+ 75	40	.76	.380	84,183	13,500
ST-2-2	2	75	+ 75	40	.81	.405	80,102	21,650
ST-2-3	2	75	+600	40	.82	.410	102,551	13,550
ST-2-5	2	75	+600	40	.78	.390	102,551	12,700
ST-2-6	2	75	+600	40	.75	.375	104,590	12,200
ST-4-15	3.96		+600		1.20	.303	111,082	18,900
ST-4-17	3.96	80	+600	37.5	1.30	.328	98,454	14,550
ST-4-18	3.96	80	+600	37.5	1.35	.341	103,350	10,000
ST-4-22	3.96	80	+600	37.5	1.47	.371	98,196	17,700
ST-4-23	3.96	80	+600	37.5	1.53	.386	87,113	18,300
ST-6-11	5.92	75	+ 75	40	1.71	.288	51,271	10,500
ST-6-9	5.92	75	+ 75	40	1.71	.288	63,771	12,500

TABULATED TEST DATA

Specimen	W (in)	T_{crk} °F	T_{rupt} °F	σ_{crk} (ski)	ℓ_c (in)	$\ell_{c/w}$ y=	σ_r (psi)	n (cyc)
ST-6-16	5.92	75	+ 75	40	1.70	.287	67,733	20,700
ST-6-18	5.92	75	+ 75	40	1.74	.293	55,233	7,900
ST-6-17	5.92	75	+ 75	40	1.73	.292	73,377	15,000
ST-6-7	5.92	75	+ 75	40	1.69	.285	67,100	13,550
ST-6-12	5.92	75	+ 75	30	1.55	.261	51,207	Var. σ
ST-6-13	5.92	75	+ 75	25	1.51	.255	57,586	Var. σ

SECTION 7

SUMMARY OF TEST RESULTS ON UNITEMP (RENE' 41) NICKEL ALLOY SHEET

This section reports the test data on the material UNITEMP (RENE' 41). The 52+% nickel (Cr.-Mo.-Co.) alloy sheet panel specimens, from Universal Cyclops Steel Co., were heat-treated to the 195-200,000 tensile strength range. The 2", 4", 6" and 8" wide panels were, in general, prepared in the same manner as those reported in previous sections of this report.

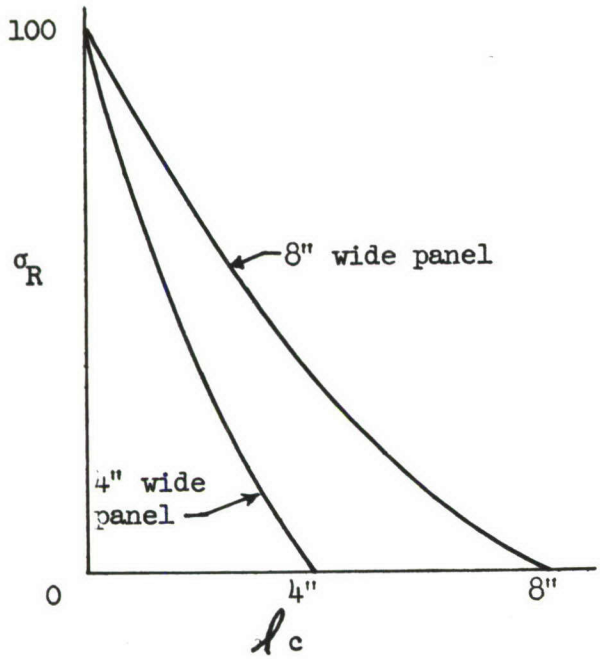
Over seventy panels have been fatigue cracked and tested in this material. Panel fatigue tests have been conducted through constant amplitude as well as multiple stress ranges. Some additional tests have been conducted wherein the fatigue cracking temperature has been varied. All of the prior fatigue cracked panels (varying crack lengths) were then ruptured at various tensile testing temperatures.

Unlike the behavior of the steel alloys, at various temperatures, this high nickel base alloy appears to be very notch insensitive over quite a range of rupturing temperatures. Test temperatures from -330°F. to 1,800°F. have been investigated with extremely promising results for this material.

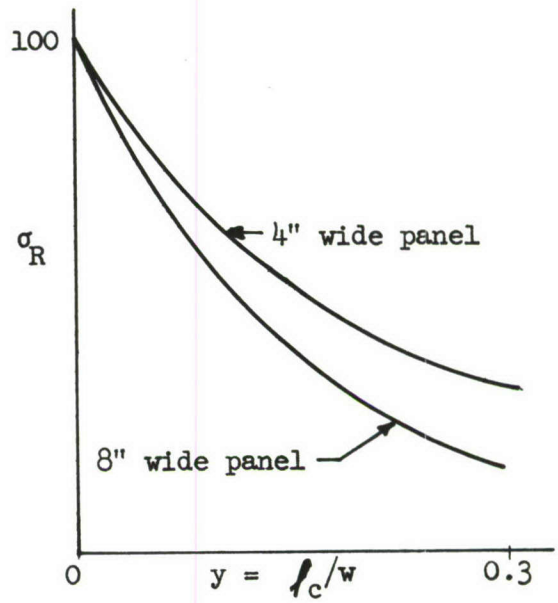
1. Figures 49 and 50 show a variety of panel widths tested over a great range of temperature. It is interesting as well as encouraging to note that there are some materials that appear to be fairly notch insensitive over such a wide useful range of environmental temperatures. The fracture toughness (K_{c1}) for the panels has been calculated and the results are plotted in Figure 51. A comparison of the RENE' 41 material to the air-hardening PH15-7 Mo is shown on this graph.

   One of the most consistent observations made is the reciprocal behavior characteristics of this material as compared to many of the steels. For example, in the material PH15-7 Mo large differences are observed in residual strengths at the various rupture temperatures. This is also true for the varying panel widths. In the material RENE' 41 there appears to be a very slight difference in residual strength as a function of panel width and it could then be surmised that this could also be the case for residual strength at various rupturing temperatures. The test results bear out this information.

2. A review of the literature has revealed that an alternate method, often used in plotting residual strength data as a function of crack length, is as shown in Sketch A on the following page. The same data, however, can be replotted as shown in Sketch B. There is a seeming discrepancy here, although physically both types of plots can be obtained and yield reliable data.



Sketch A



Sketch B

For a given degree of physical damage or percent of crack length, the residual (σ_R) strengths will be greater for the smaller panel widths. It is therefore believed that the type of plot as shown in Sketch B has the greatest physical significance. The reasons for the apparent greater allowable strengths for the smaller panels is discussed in Section 14.

3. Figure 52 shows arithmetic average crack-growth curves for many of the 4" wide panels tested at various maximum cracking stresses.

4. Figures 53 to 58 show fatigue crack growth curves at constant stress ranges and cracking temperatures for panels from 2" to 8" in width.

5. Figures 59 through 63 show the accumulative crack growth curves versus number of stress cycles for panels tested under a variety of programmed spectra.

6. Figure 64 shows a comparison between theoretical fatigue crack-growth and actual test data. The derivation of these curves is given and explained in Section 14. By the use of this method the cumulative crack growth under programmed loading has been calculated by the Douglas Method and is shown in Table 5. Good agreement is obtained between actual and calculated values.

7. Additional calculations for the theoretical growth of a crack under programmed loading are given in Table 6. By using the lower limit of the Anderson-Paris curve (Figure 65 -also see Section 5 for initial discussion), it was found that good agreement was obtained between actual and theoretical results. The method also resulted in 11% conservatism. Although these results appear to be promising, at least for the material RENE' 41, it is realized that much additional work remains to be done. Some preliminary work on the aluminum alloys for example has shown that crack growth rates can be extremely discontinuous when programming from one stress level to another. However, as long as there is a delay period (affine-macro isomotive period) during the crack propagation under random loading, then the calculated methods will always be conservative for design, even if not accurate. A brief discussion of these effects is given in Appendix A and in the Analysis Section 14.

8. Figure 66 shows a typical stress-strain curve for the RENE' 41 material tested in this program.

9. Figure 67 shows the ultimate tensile and yield strengths of the nickel base alloy as a function of testing temperature. This plot is a composite of the allowables obtained in this program as well as in WADD TR 60-410 Part II and ARDC TR 59-66.

10. The tabulated test results, panel geometries, testing temperatures and cracking stresses are given in the tables at the end of this section.

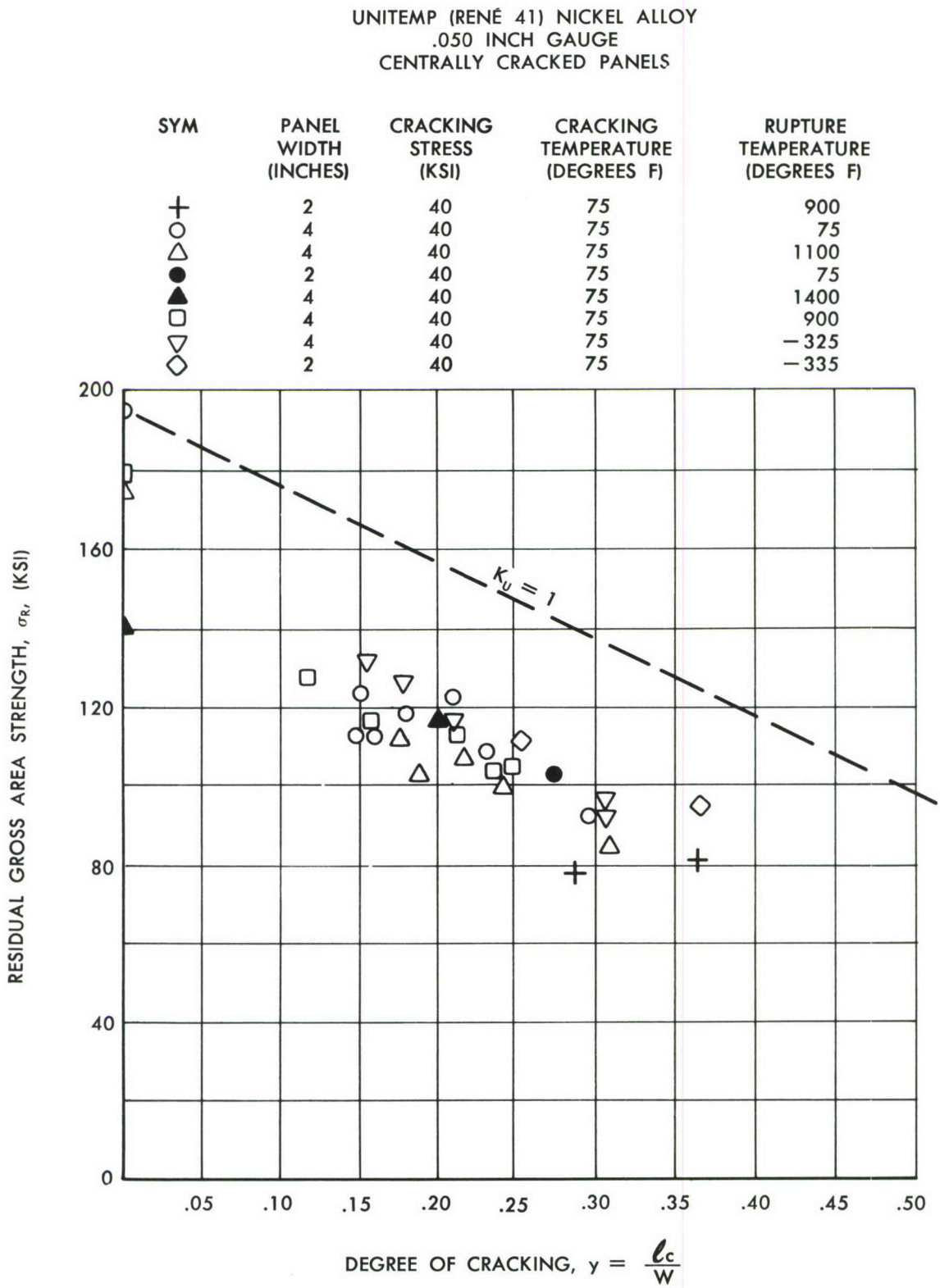


Figure 49. RESIDUAL STRENGTH vs DEGREE OF CRACKING

UNITEMP (RENÉ 41) NICKEL ALLOY
.050 INCH GAUGE
CENTRALLY CRACKED PANELS

SYM	W (INCHES)	$T_{RUPTURE}$ (DEGREES F)	$T_{CRACKING}$ (DEGREES F)	$\sigma_{CRACKING}$ (KSI)
○	6	80	80	40
✠	6	1620	80	40
✚	6	1810	80	40
●	4	80	80	37-45
△	4	1420	80	37
⊗	4	1000	80	45
◑	4	1220	900	45
▼	6	−303	80	40
+	8	810	80	40
┼	8	600	80	40
▲	8	1000	80	40
×	8	1200	80	40

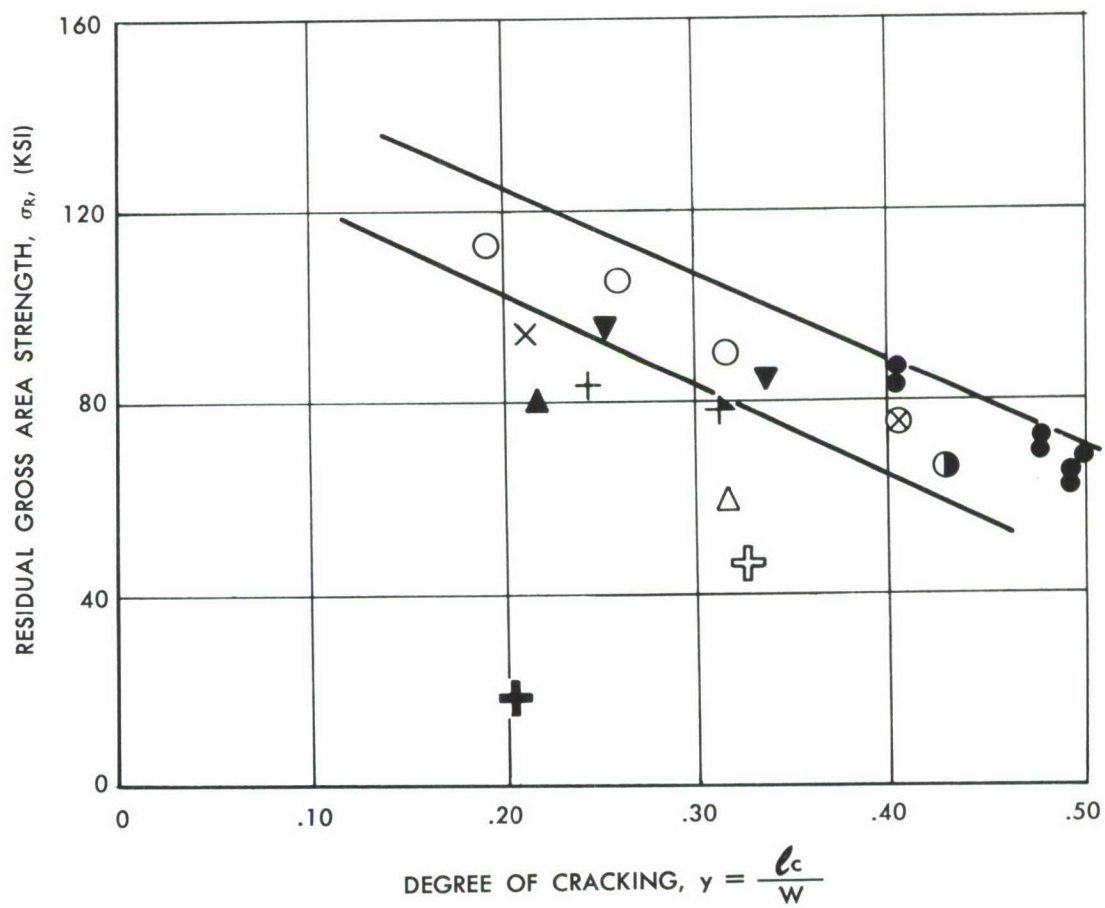


Figure 50. RESIDUAL STRENGTH vs DEGREE OF CRACKING

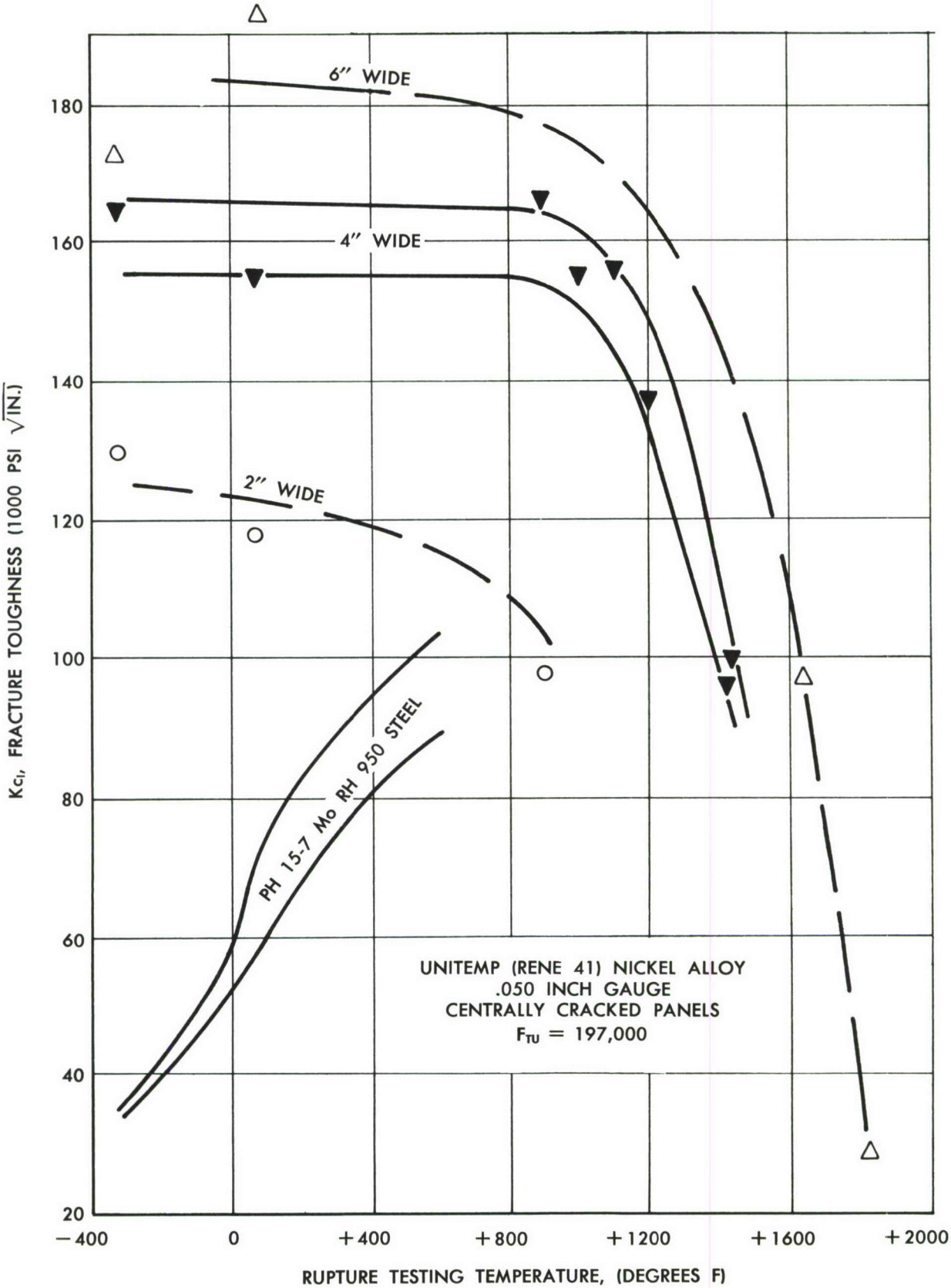


Figure 51. FRACTURE TOUGHNESS vs TEST TEMPERATURE

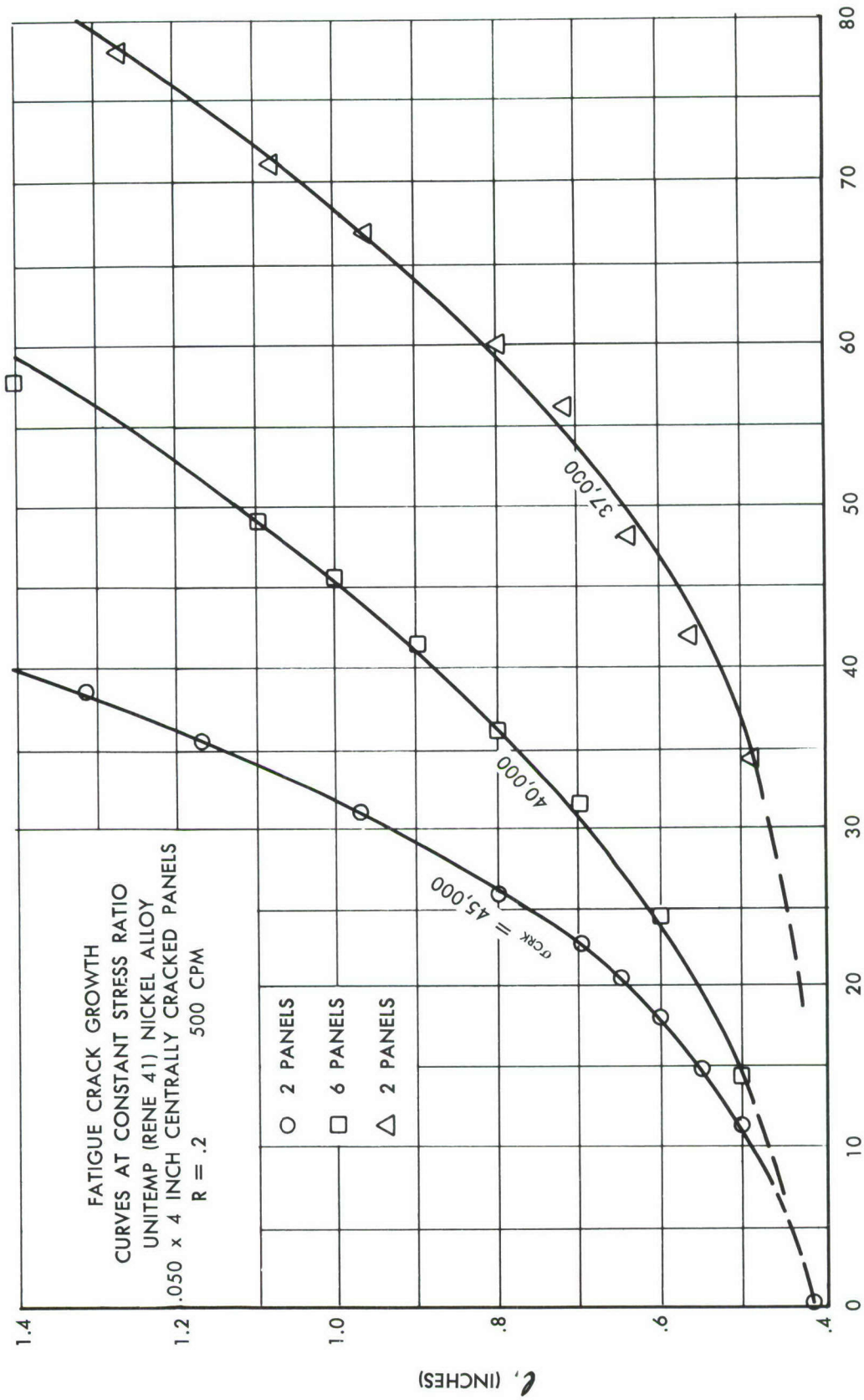


Figure 52. FATIGUE CRACK GROWTH

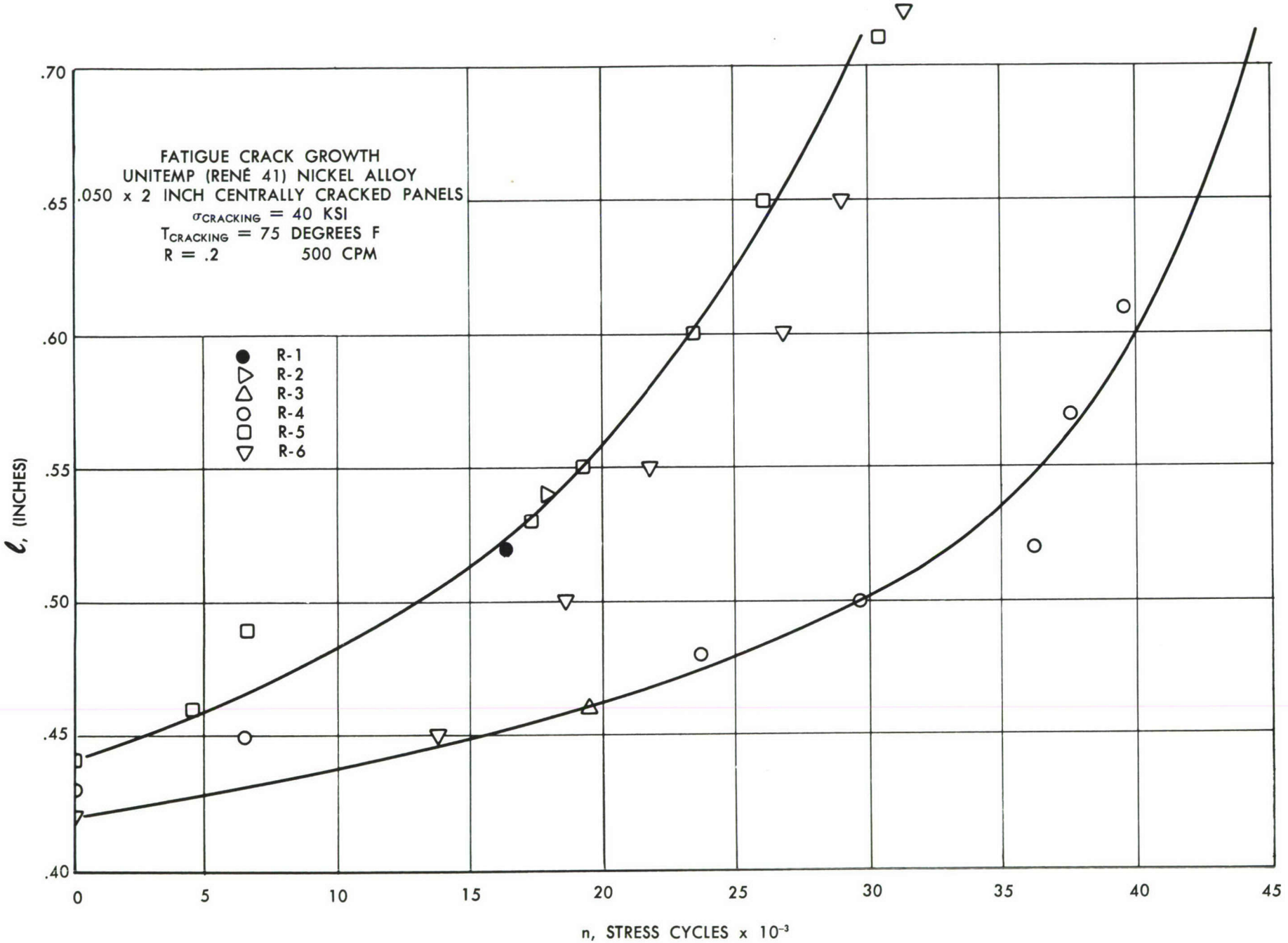


Figure 53. FATIGUE CRACK GROWTH

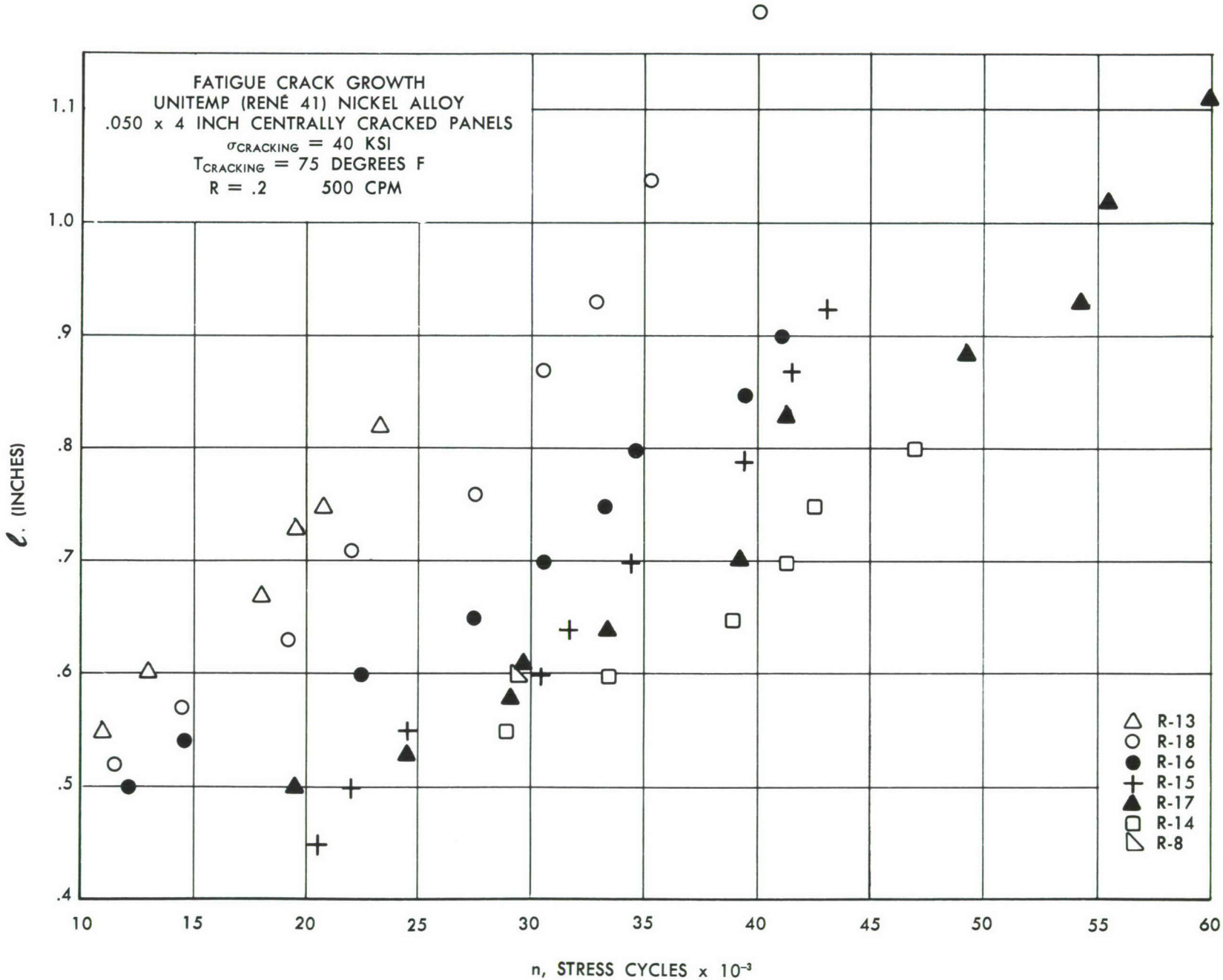


Figure 54. FATIGUE CRACK GROWTH

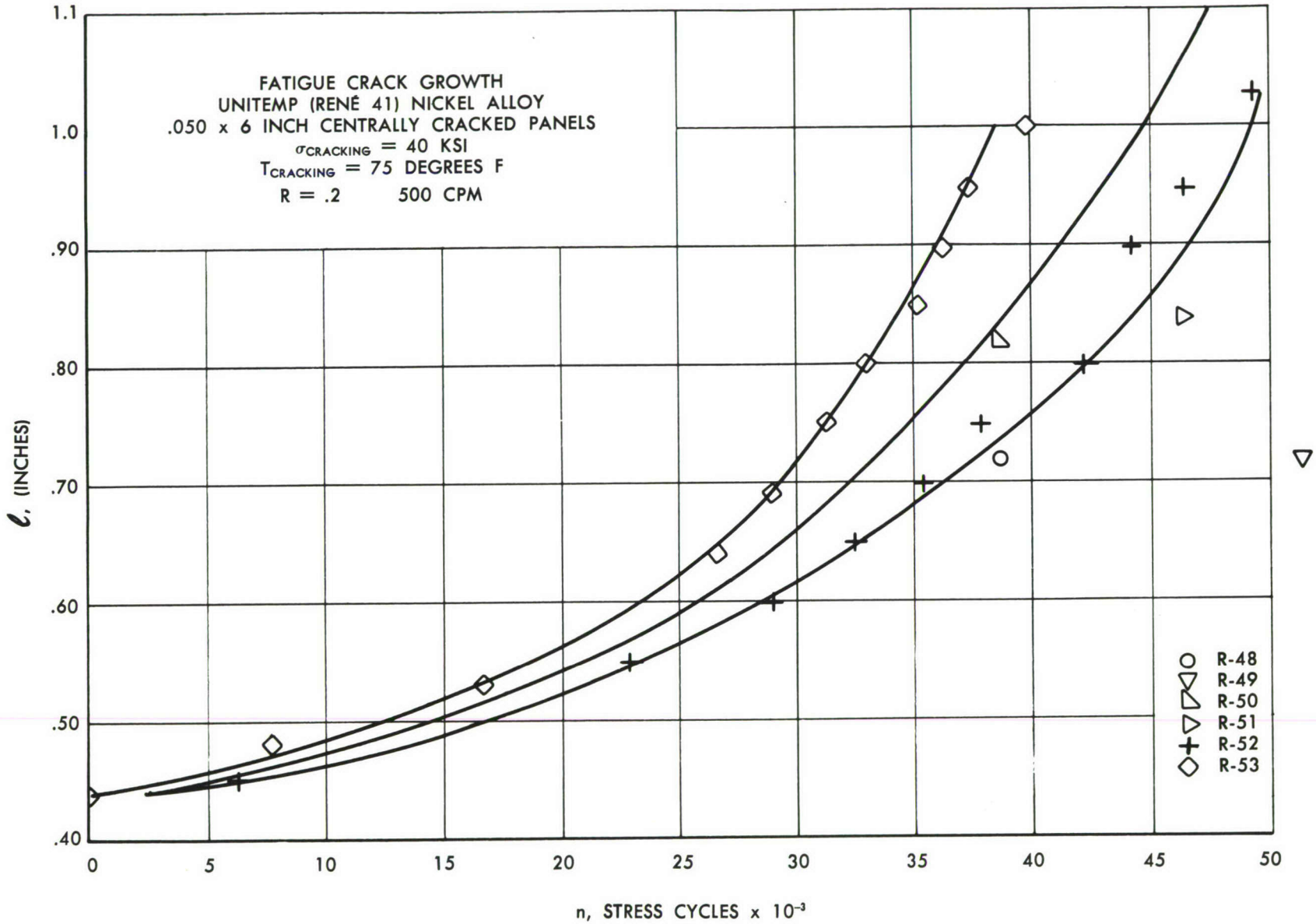


Figure 55. FATIGUE CRACK GROWTH

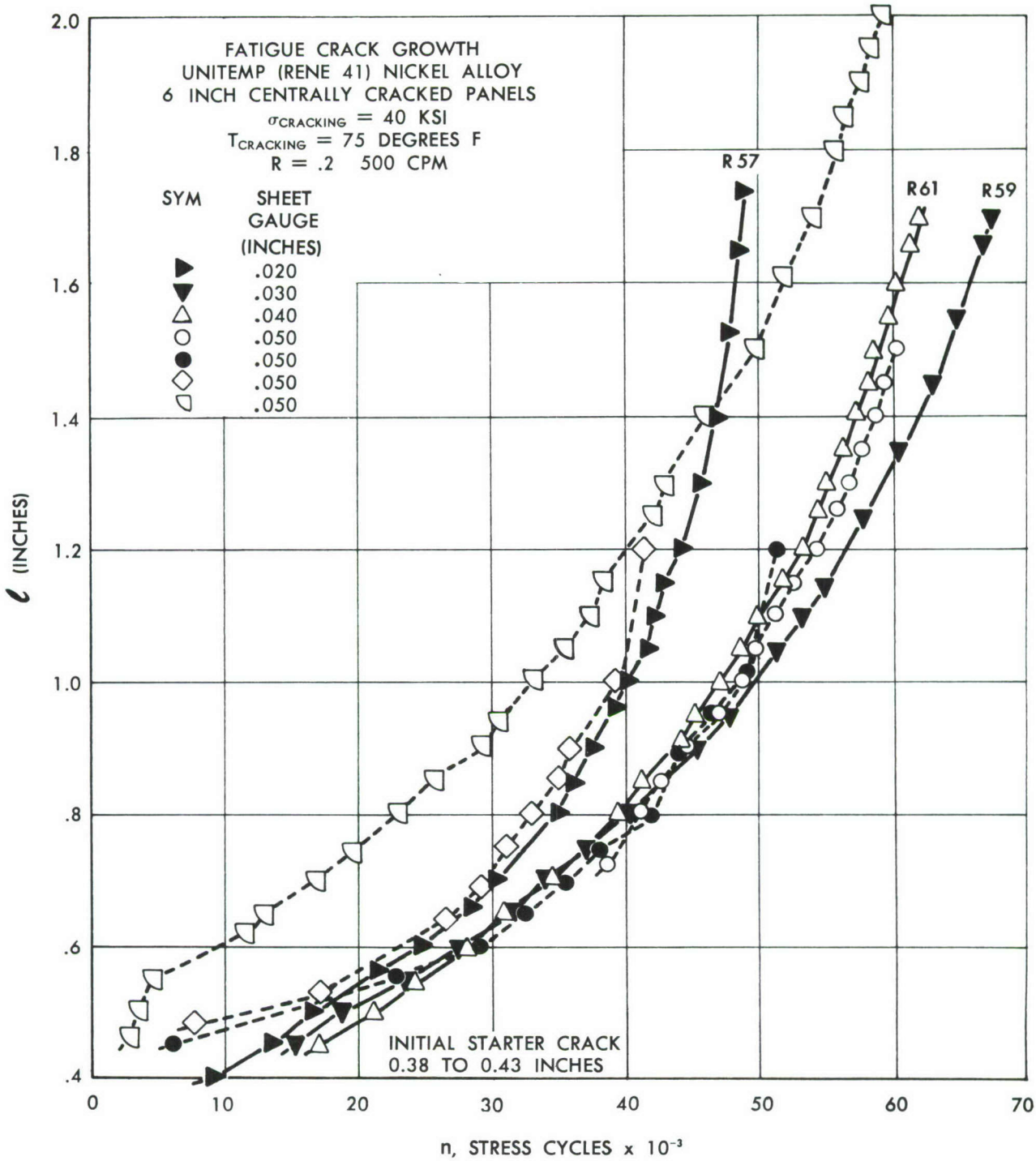


Figure 56. FATIGUE CRACK GROWTH

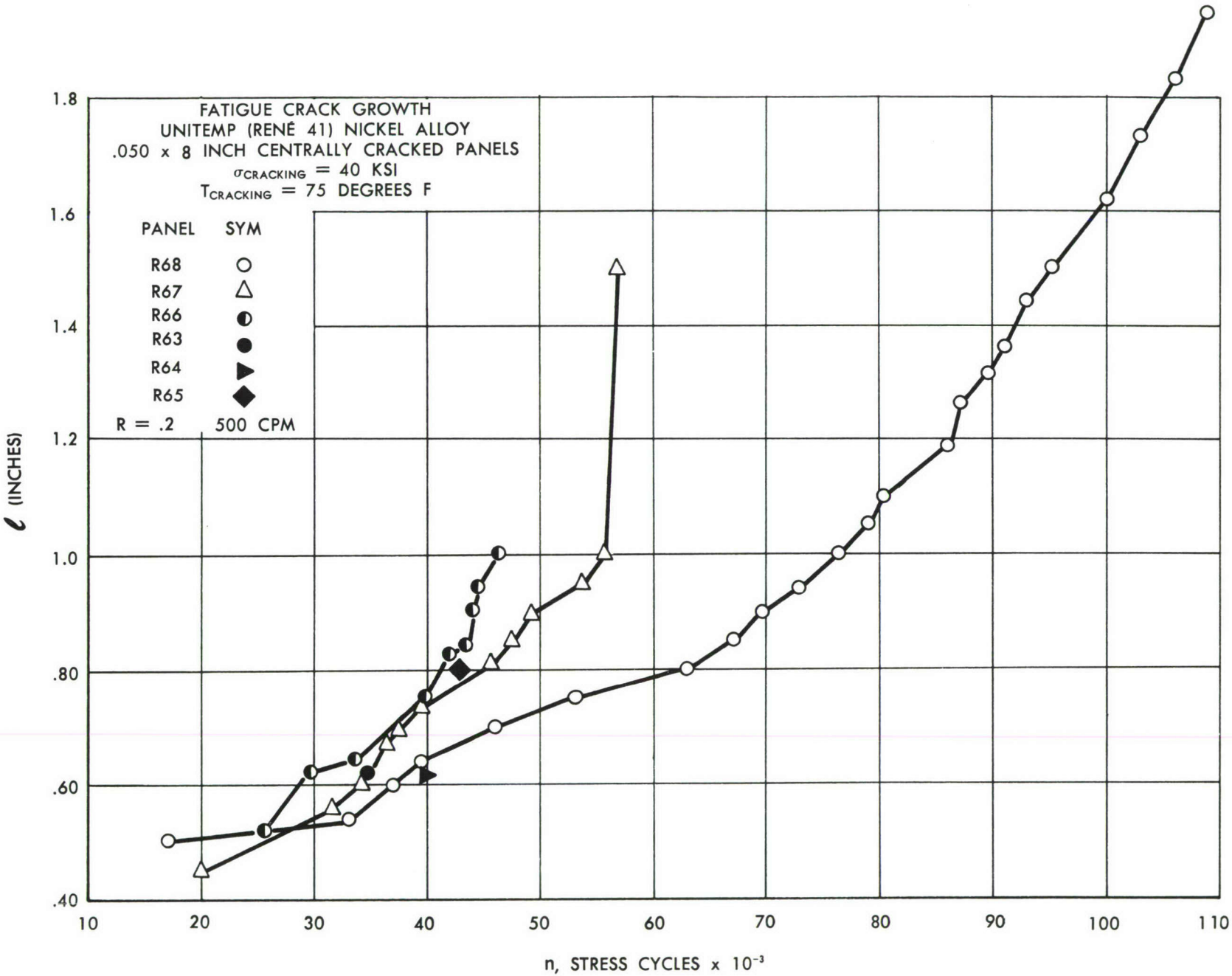


Figure 57. FATIGUE CRACK GROWTH

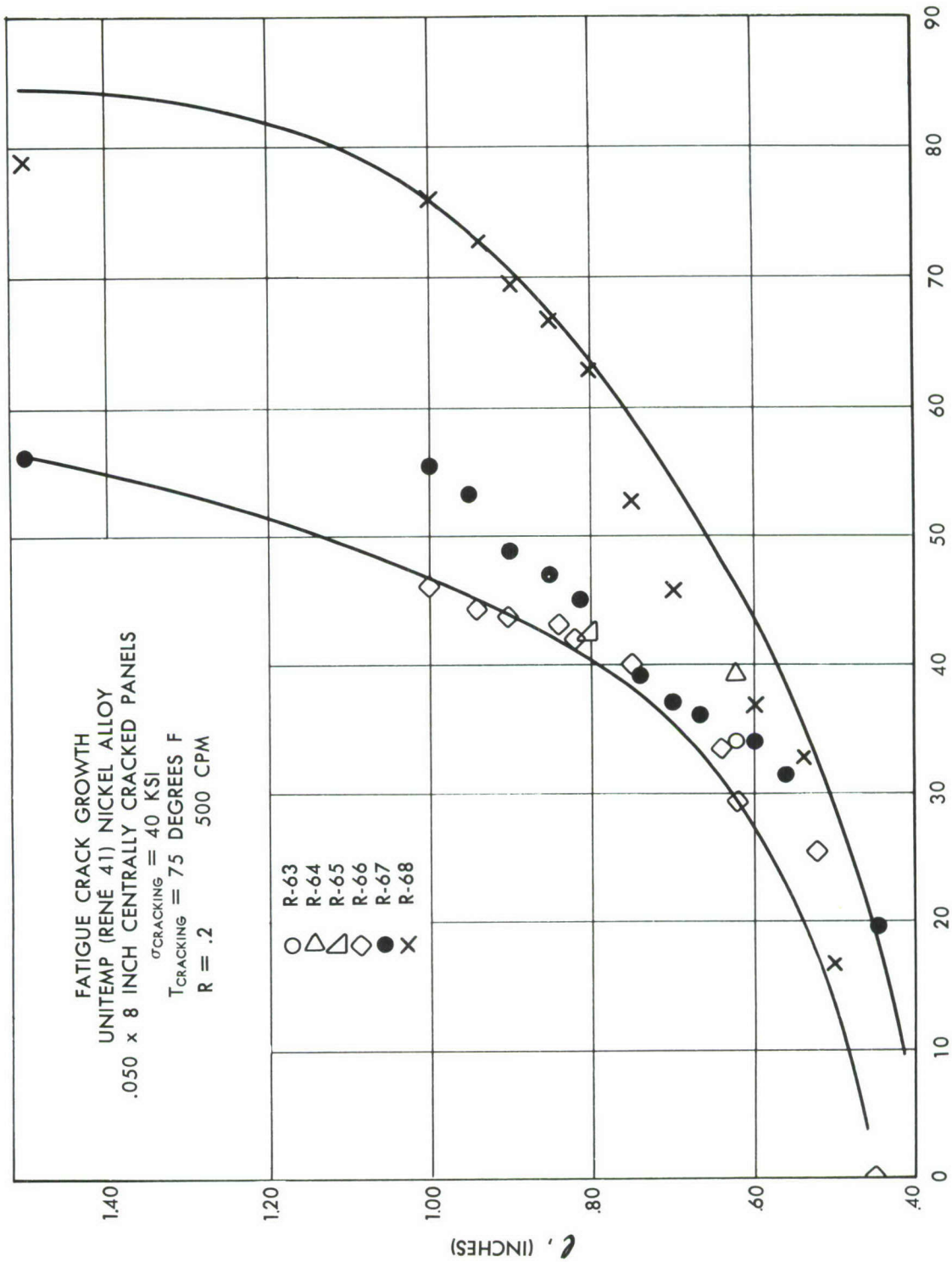


Figure 58. FATIGUE CRACK GROWTH

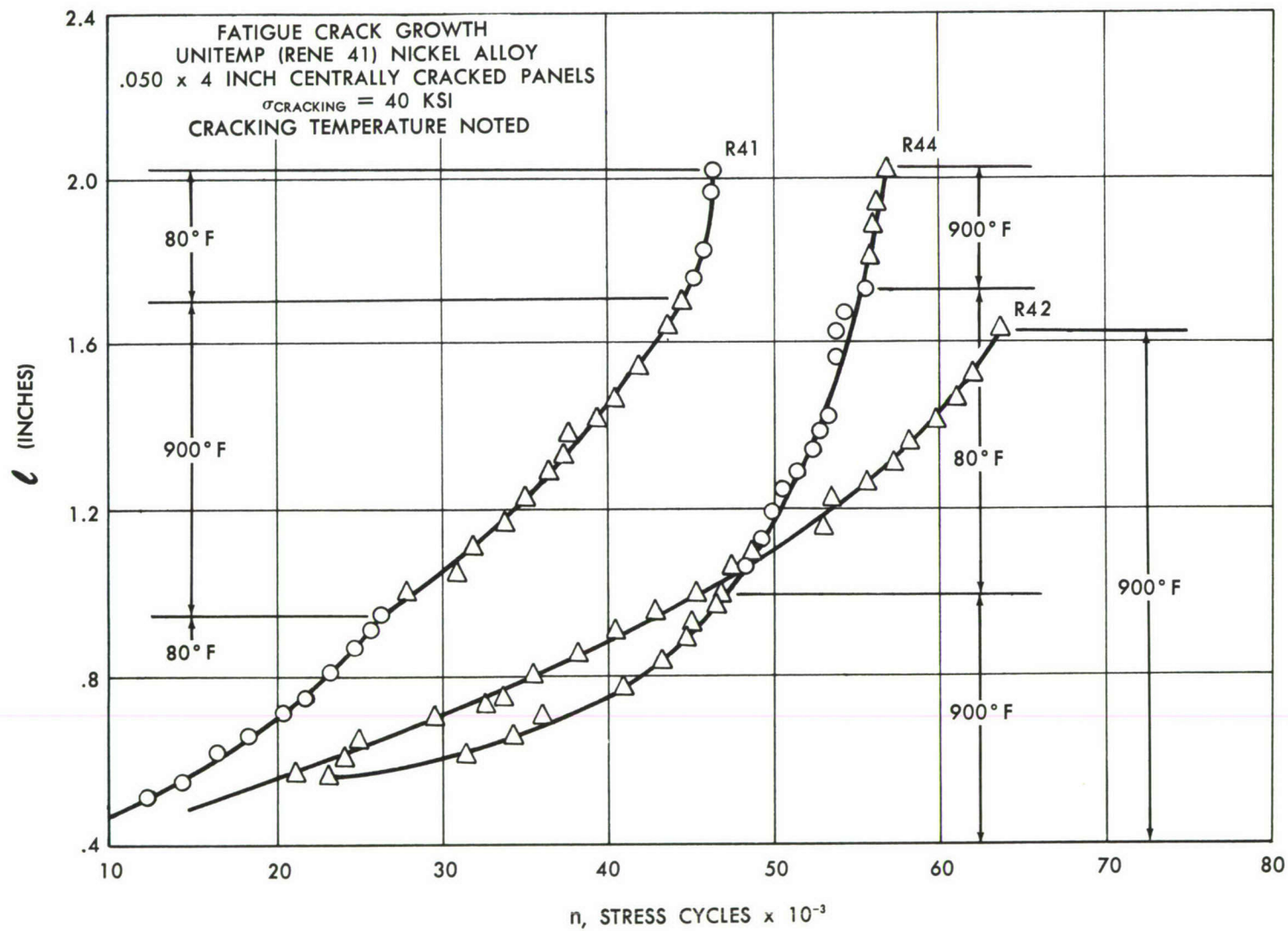


Figure 59. PROGRAMMED FATIGUE CRACK GROWTH

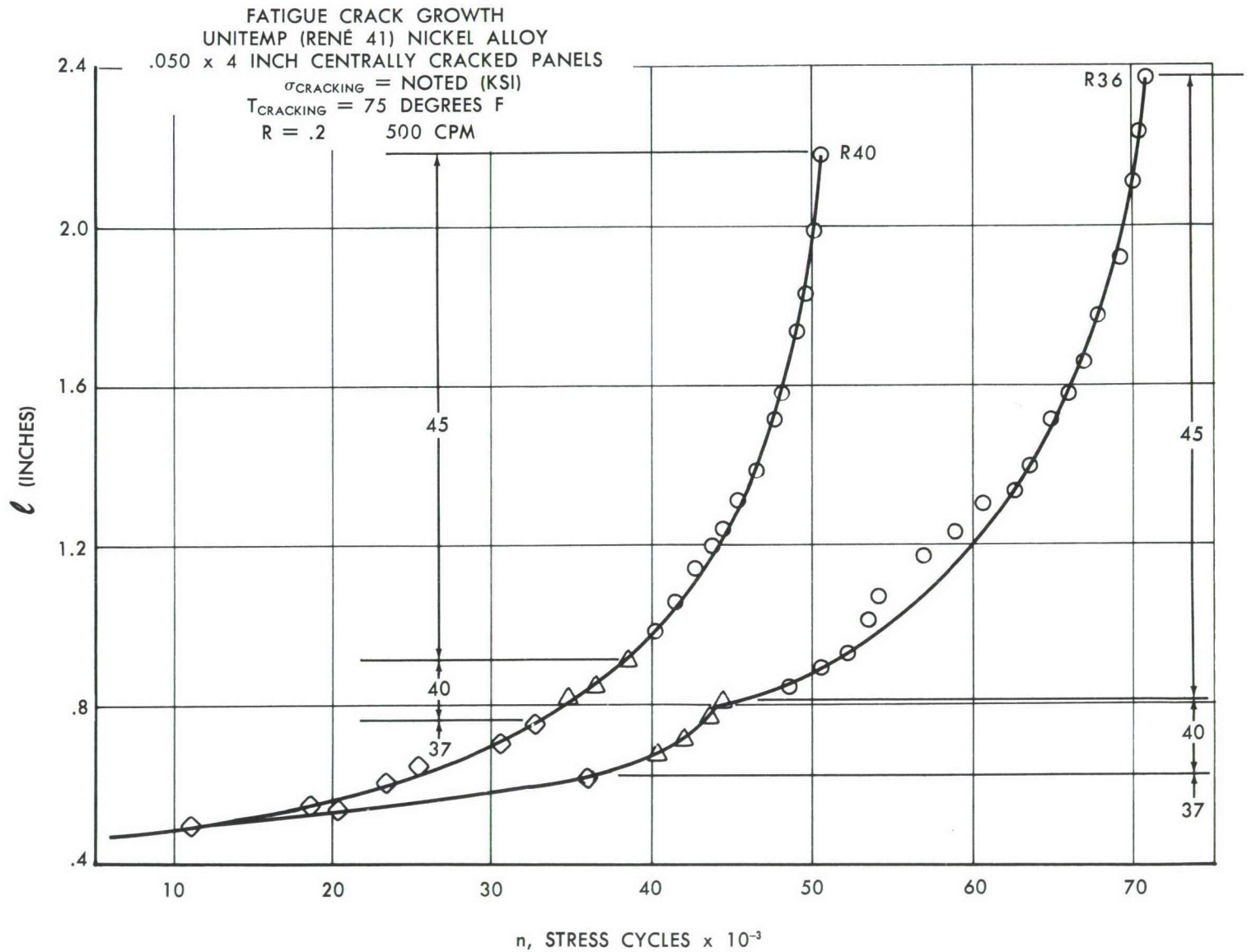


Figure 60. PROGRAMMED FATIGUE CRACK GROWTH

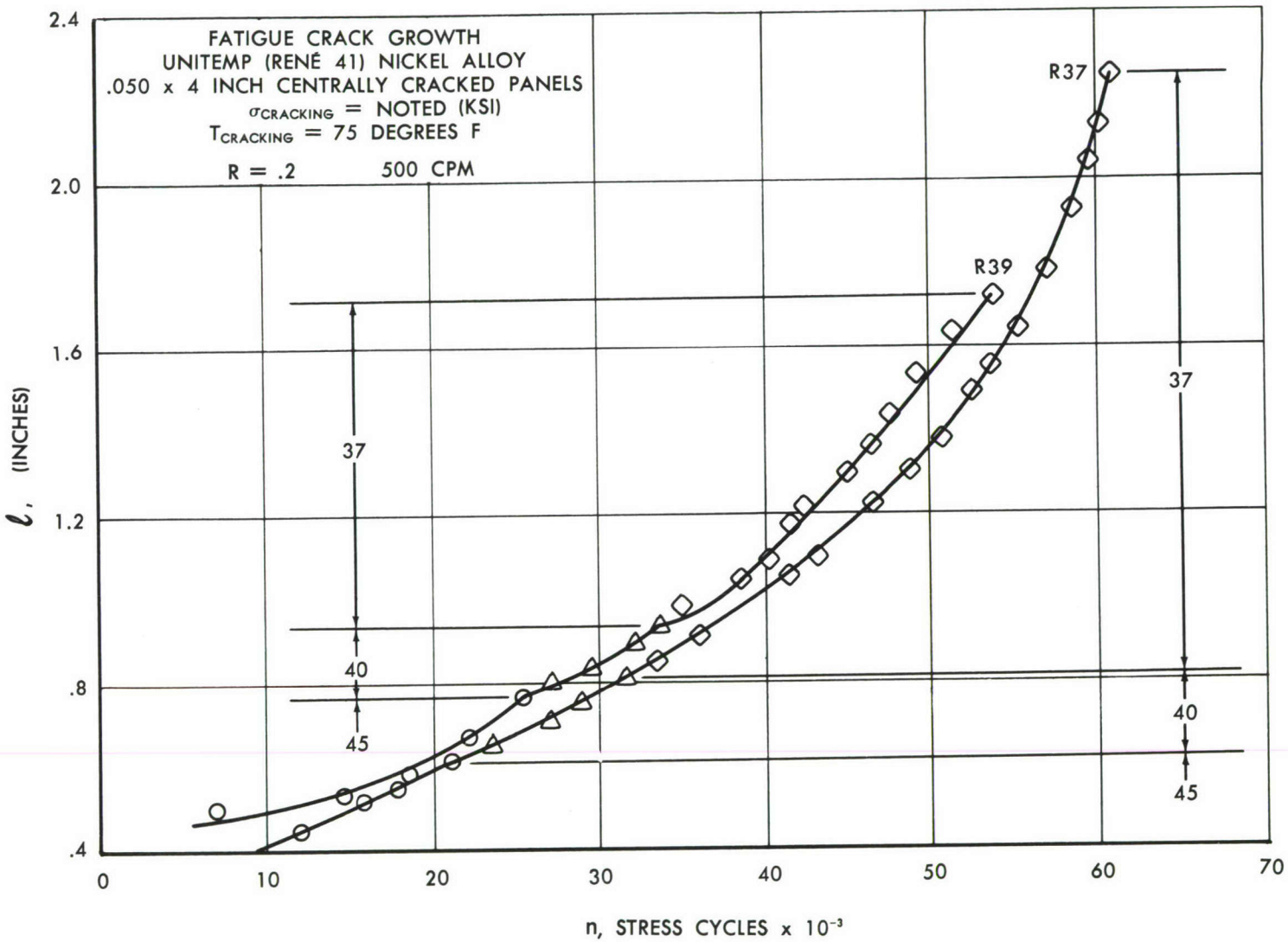


Figure 61. PROGRAMMED FATIGUE CRACK GROWTH

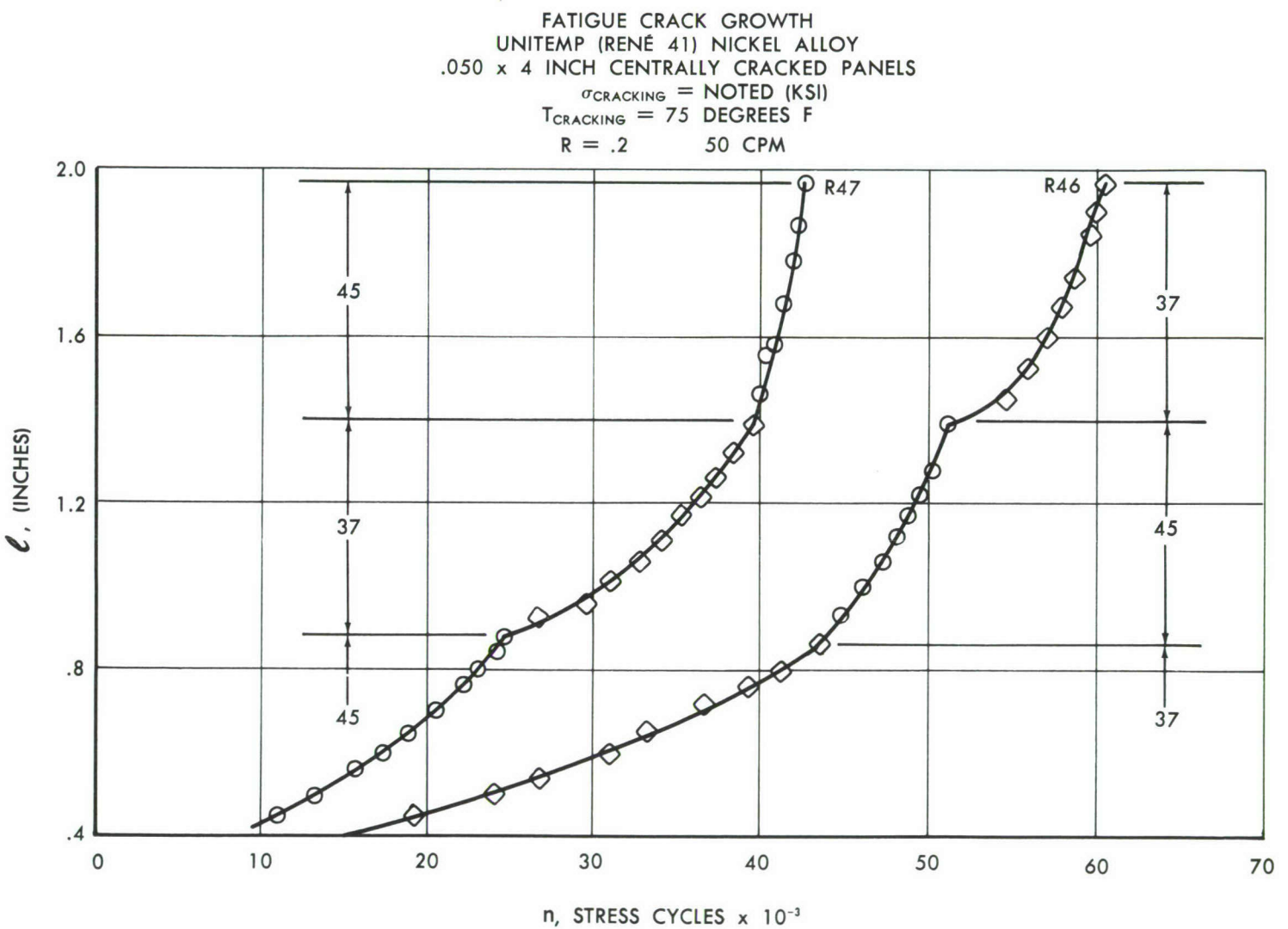


Figure 62. PROGRAMMED FATIGUE CRACK GROWTH

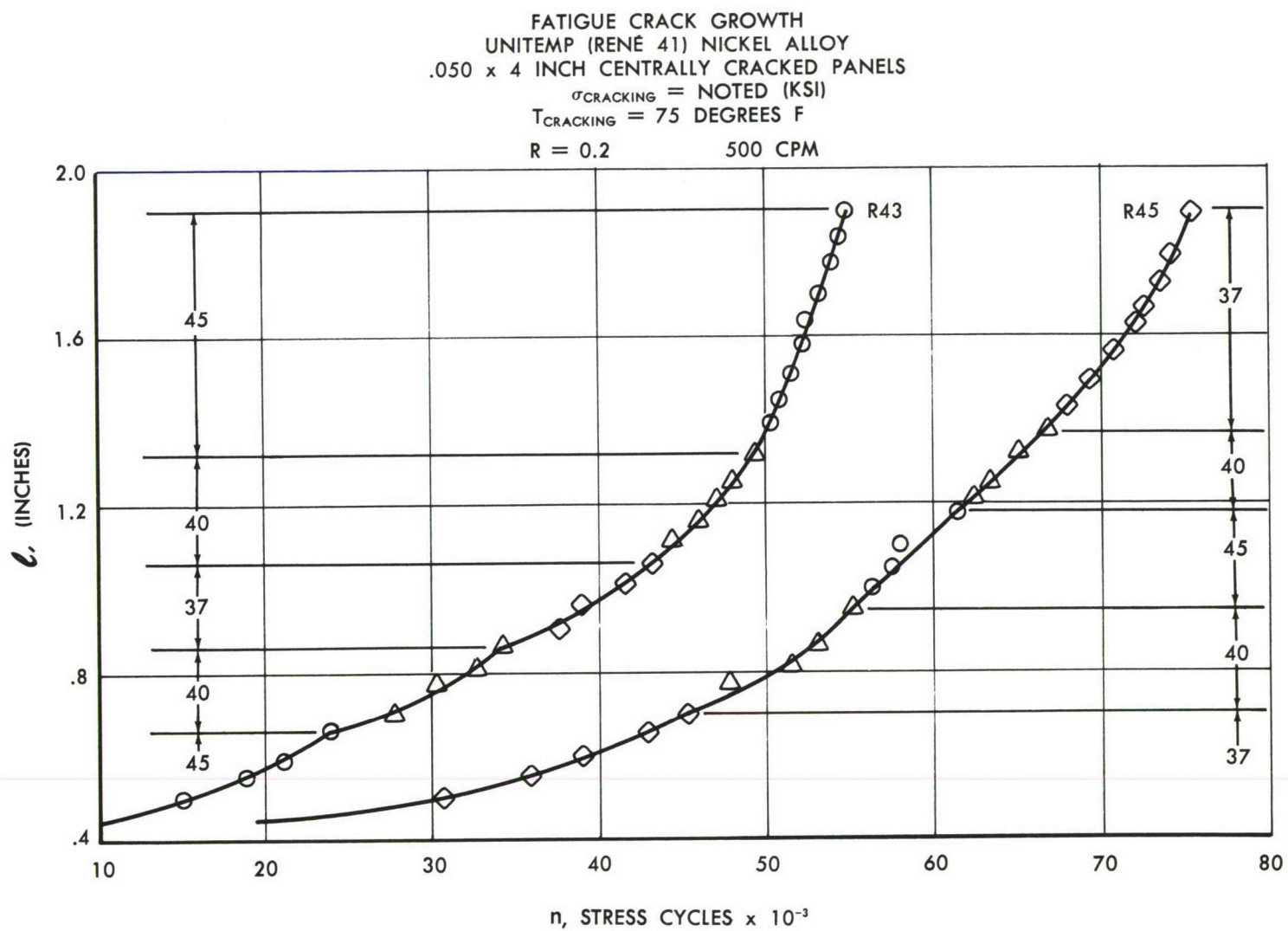


Figure 63. PROGRAMMED FATIGUE CRACK GROWTH

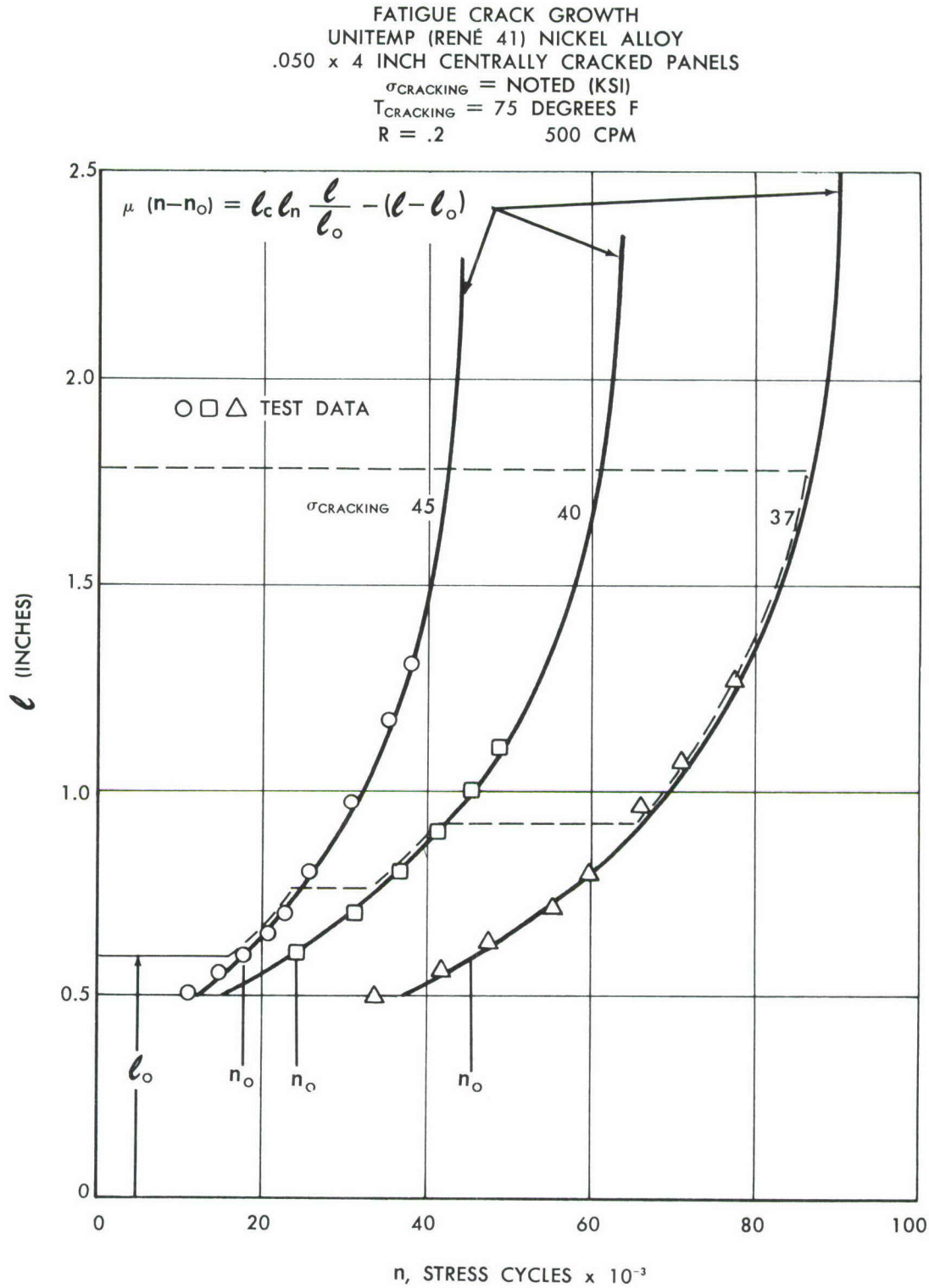


Figure 64. THEORETICAL CRACK GROWTH CURVES

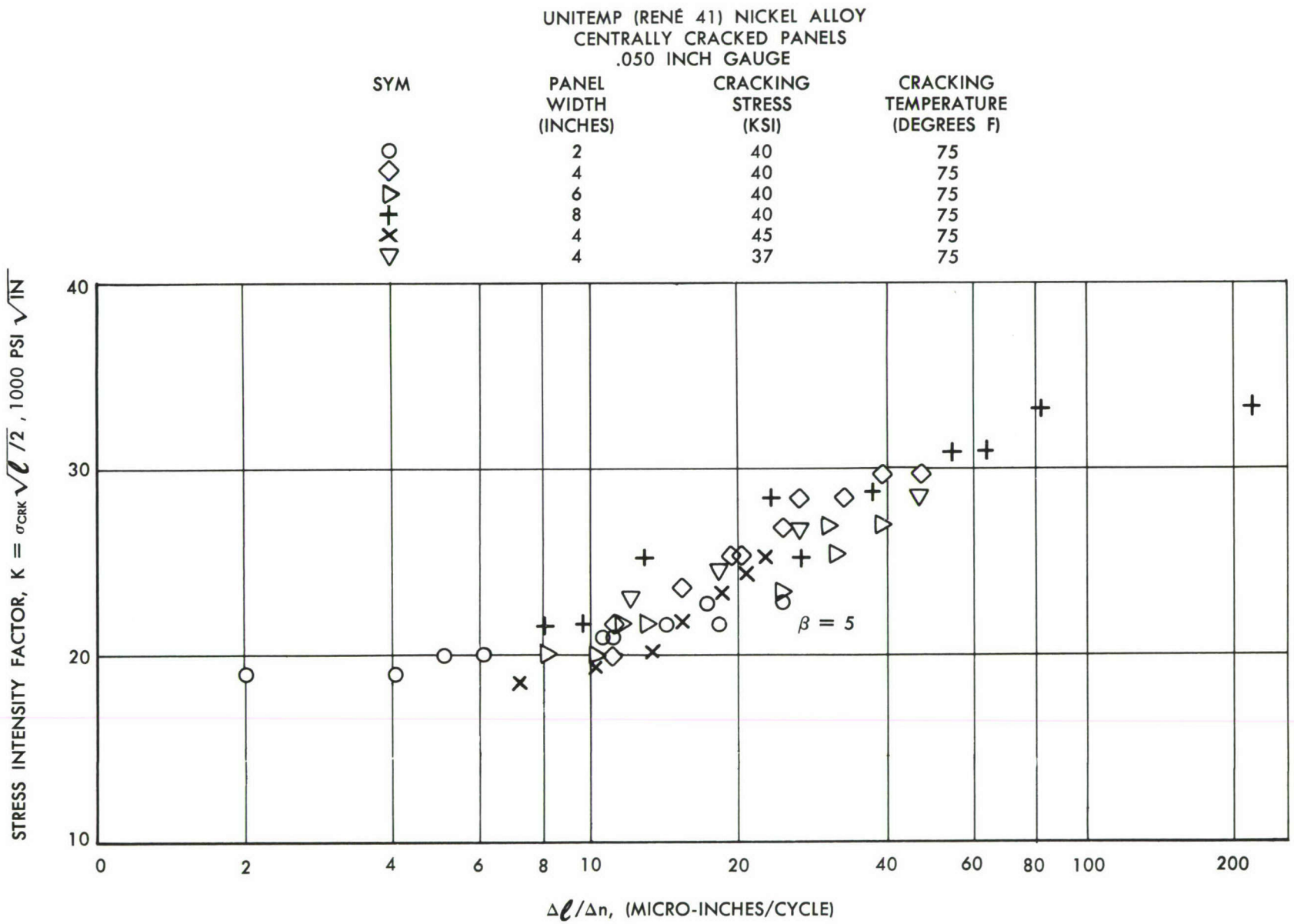


Figure 65. STRESS INTENSITY vs RATE OF CRACKING

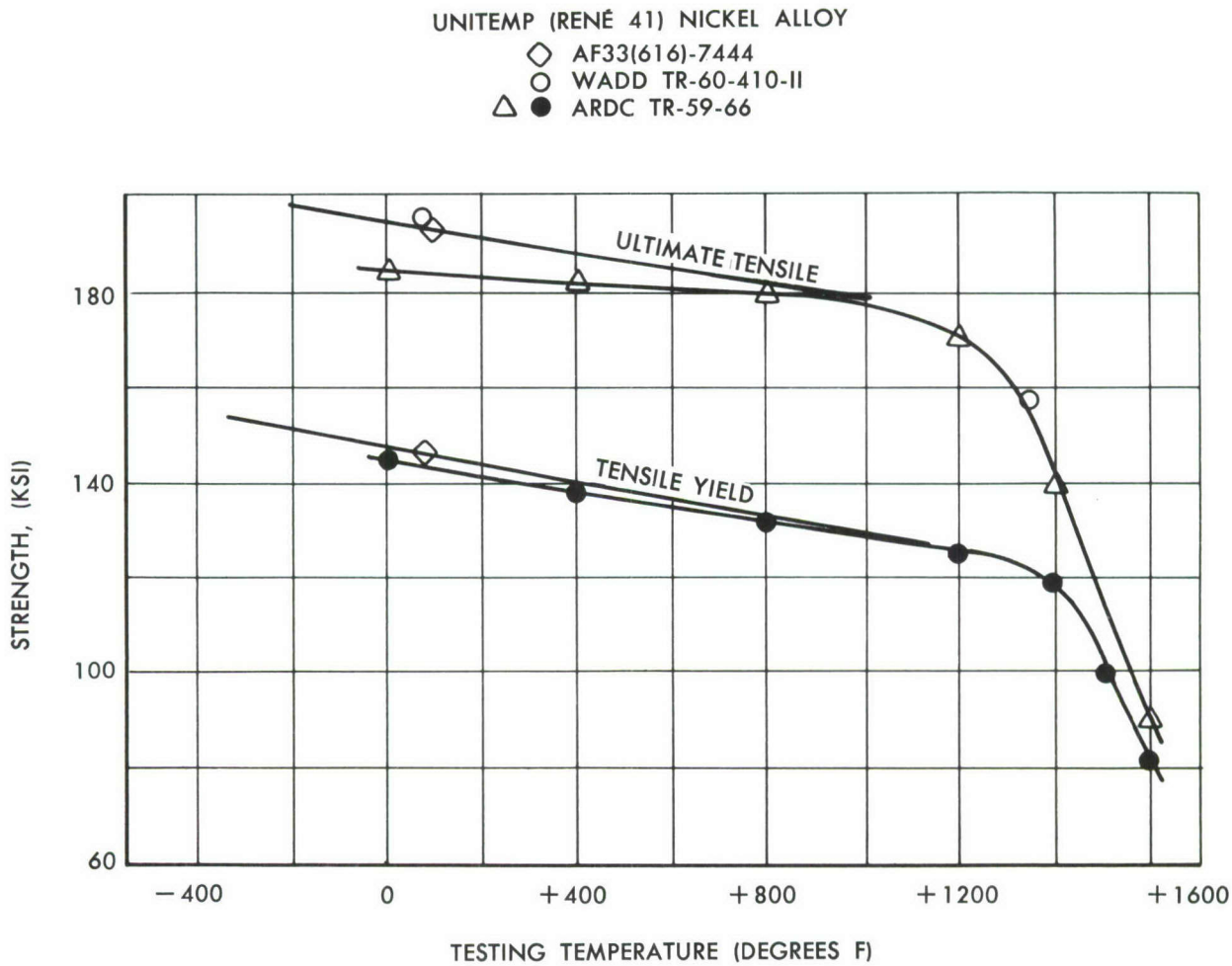


Figure 66. UNNOTCHED TENSILE STRENGTH AS A FUNCTION OF TEST TEMPERATURE

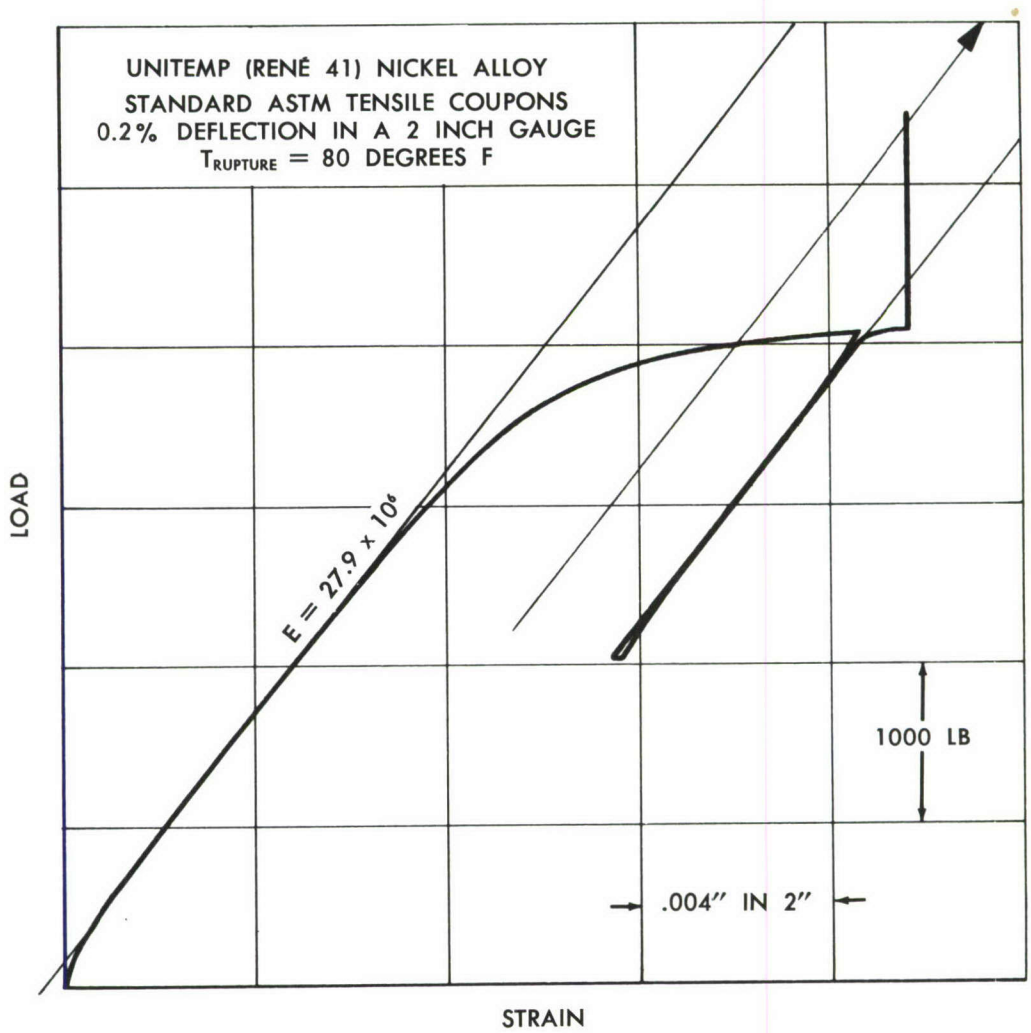


Figure 67. LOAD-STRAIN CURVE

TABLE 5

CUMULATIVE CRACK GROWTH UNDER PROGRAMMED LOADS AND TEMPERATURES BEYOND AN INITIAL AND VISIBLE CRACK LENGTH OF .6" (RENE' 41) .050" x 4" PANELS

Test Panel	Step (Order)	Spectrum Max. Stress (ksi)	Spectrum Max. Temp. (°F)	Cycles or Stress (n)	Calculated Growth (in) From Fig. 64 $\Sigma\Delta l$ - .6	Act. Growth Fm. Applied Spectrum Σl - .6 (Figs 59-63)	Theo. Calc. / Actual
	1	45	+ 80	7,400			
R47	2	37	+ 80	14,850			
	3	45	+ 80	3,000	.66	1.37	.48
	1	37	+ 80	12,500			
R46	2	45	+ 80	7,600		1.37	.53
	3	37	+ 80	9,500	.73		
	1	37	+ 80	3,000			
R36	2	40	+ 80	8,400			
	3	45	+ 80	19,100	1.69	.80	2.12
	1	37	+ 80	9,450			
R40	2	40	+ 80	5,850			
	3	45	+ 80	11,600	.77	1.40	.55
	1	45	+ 80	2,800			
	2	40	+ 80	10,200			
R43	3	37	+ 80	9,000			
	4	40	+ 80	6,300			
	5	45	+ 80	5,500	1.18	1.30	.91
	1	37	+ 80	6,000			
	2	40	+ 80	9,850			
R45	3	45	+ 80	6,400			
	4	40	+ 80	5,250			
	5	37	+ 80	8,750	1.22	1.30	.94
	1	45	+ 80	7,000			
R37	2	37	+ 80	8,000			
	3	37	+ 80	20,500	1.18	1.12	1.05
	1	45	+ 80	900			
R39	2	40	+ 80	10,500			
	3	37	+ 80	27,600	1.37	1.40	1.03
							Avg. .95

TABLE 6

CUMULATIVE CRACK GROWTH $\ell_n = \sum_{i=1}^{b} \left(\frac{\Delta \ell}{\Delta n}\right)_i \cdot \Delta n_i$ UNDER PROGRAMMED LOADING BEYOND AN INITIAL CRACK LENGTH OF 0.6" (MATERIAL RENE'41) .050" x 4" PANELS

Spec	$\sigma_{max.}$ @ R=+.2 (ksi)	Δn (cyc)	T_{crk} (°F)	ℓ_c (in.)	$K=\sigma_{max}\sqrt{\ell_c/2}$ 1000 psi in	$\frac{\Delta \ell}{\Delta n}$ (Fig 65)	$\Delta \ell_i = \frac{\Delta \ell}{\Delta n} \cdot \Delta n$	Calc. Theo. Crk. Length (in.) $\Sigma \ell_i = \ell_c + \Delta \ell_i$	Actual Crack Length Under Lds. in Spect. (Figs 59-63)	Theo. Calc. / Actual
	45	7,400	+ 80	.600	24.7	33	.244	.844	.88	.96
R47	37	14,850	+ 80	.844	24.0	30	.445	1.289	1.39	.92
	45	3,000	+ 80	1.289	36.2	180	.540	1.829	1.97	.93
	37	12,500	+ 80	.60	20.3	11.8	.147	.747	.86	.87
R46	45	7,600	+ 80	.747	27.4	56.0	.425	1.172	1.39	.84
	37	9,500	+ 80	1.170	28.3	66.0	.627	1.799	1.97	.91
	37	3,000	+ 80	.600	20.3	11.8	.035	.635	.62	1.02
R36	40	8,400	+ 80	.635	22.5	21.3	.179	.814	.81	1.01
	45	19,100	+ 80	.814	28.7	69.0	1.320	2.134	2.37	.90
	37	9,450	+ 80	.600	20.3	11.8	.111	.711	.76	.93
R40	40	5,850	+ 80	.711	23.9	29.5	.172	.883	.91	.97
	45	11,600	+ 80	.883	29.9	84.0	.975	1.858	2.18	.85
	45	2,800	+ 80	.600	24.7	33.0	.092	.692	.66	1.05
	40	10,200	+ 80	.692	21.9	19.0	.194	.886	.86	1.03
R43	37	9,000	+ 80	.886	24.6	32.0	.288	1.174	1.06	1.11
	40	6,300	+ 80	1.174	30.6	90.0	.566	1.740	1.32	1.32
	45	5,500	+ 80	1.740	42.0	300.0	1.650	3.39	1.90	1.78
	37	6,000	+ 80	.60	20.3	11.8	.071	.671	.70	.96
	40	9,850	+ 80	.671	23.2	25.0	.246	.917	.95	.96
R45	45	6,400	+ 80	.917	30.4	88.0	.563	1.480	1.18	1.25
	40	5,250	+ 80	1.48	34.4	148.0	.775	2.255	1.37	1.64
	37	8,750	+ 80	2.25	39.2	240.0	2.10	4.35	1.90	2.29

TABLE 6 (Cont'd)

CUMULATIVE CRACK GROWTH LENGTH OF 0.6" $\ell_n = \sum_{i=1}^{b} \frac{\Delta \ell}{\Delta n}_i \cdot \Delta n_i$ UNDER PROGRAMMED LOADING BEYOND AN INITIAL CRACK (MATERIAL RENE'41) .050" x 4" PANELS

Spec	σ_{max} @ R=+.2 (ksi)	Δn (cyc)	T_{crk} (°F)	ℓ_c (in.)	$K=\sigma_{max}\sqrt{\ell_c/2}$ 1000 psi in	$\frac{\Delta \ell}{\Delta n}$ (Fig 65)	$\Delta \ell_i = \frac{\Delta \ell}{\Delta n} \cdot \Delta n$	Calc. Theo. Crk. Length (in.) $\Sigma \ell_i = \ell_c + \Delta \ell_i$	Actual Crack Length Under Lds. in Spect. (Figs 59-63)	Theo. Calc. / Actual
	45	7,000	+ 80	.600	24.7	33.0	.231	.831	.62	1.34
R37	40	8,000	+ 80	.830	25.8	43.0	.344	1.175	.81	1.45
	37	20,500	+ 80	1.175	28.4	66.0	1.35	2.525	2.25	1.12
	45	900	+ 80	.600	24.7	33.0	.029	.629	.77	.82
R39	40	10,500	+ 80	.629	22.4	21.0	.220	.849	.93	.91
	39	27,600	+ 80	.849	24.1	30.0	.827	1.676	1.72	.97
									Avg	1.11

MECHANICAL PROPERTIES

The tested coupons and panels presented in this section of the report were made from Universal Cyclops Steel Corp., UNITEMP (RENE') 41. All panels tested were .050 sheet stock and were milled, slotted, and drilled in the cold formed condition. The panels were then heat treated as follows:

Solution Treat at + 1,950° F. for 30 minutes.
Air cool.
Age at + 1,400° F. for 16 hours
Air cool

TABLE 7
UNITEMP (RENE')41
UNIVERSAL CYCLOPS
HEAT NO. KH 363

Specimen	Grain	F_{ty}	F_{tu}	% Elong. (2")
1	Trans.	146,265	199,290	17.5
2	Trans.	142,775	197,175	16.5
3	Trans.	146,070	197,500	17.0
4	Trans.	144,285	197,850	15.5
5	Longit.	144,565	196,740	18.0
6	Longit.	137,680	195,290	18.0
7	Longit.	144,565	198,915	17.0
8	Longit.	142,240	197,110	19.0

TABULATION OF TEST DATA

Spec	W (in)	T_{crk} °F	T_{rupt} °F	σ_{crk} (ksi)	ℓ_c (in)	ℓ_c/w	σ_r (psi)	n (cyc)	$\sigma_{y.s.}$ (psi) **	$\left(\frac{\sigma_r}{\sigma_{y.s.}}\right)^2$	$\frac{\pi \ell_c}{2w}$	Q_1*	$\sqrt{Q_1 W}$	K_{c_1}
R 1	1.97	75	75		0.54	.274	102,000	16,250	147,000	.482	.43	.675	1.15	117
R 3	1.97	Low Rockwell rdg.			.46			19,400	147,000					
R20	4.0	75		40	.50			15,900	147,000					
R31	4.0	75		45	1.60			45,300	147,000					
R32	4.0	75	1,000	45	1.63	.407	75,500	40,100	130,000	.335	.64	1.06	2.06	155
R33	4.0	75	75	37	1.62	.405	88,200	89,100	147,000	.360	.638	1.09	2.09	184
R34	4.0	75	75	37	1.62	.405	82,200	88,100	147,000	.313	.638	1.02	2.02	165
R36	4.0	75	75	37-45		fract.		63,800	147,000					
37	4.0	75	75	45-37	2.60	fract.		61,950	147,000					
38	4.0	75	75	37-45	2.48	fract.		71,400	147,000					
R39	4.0	75	75	45-37	1.74	fract.		61,950	147,000					
40	4.0	75	75	37-45	2.20	fract.		51,350	147,000					
41	4.0	var.	75	45	1.94	.48	71,800	46,400	147,000	.238	.753	1.27	2.25	162
42	4.0	900	1,222	45	1.71	.427	67,100	63,800	127,000	.279	.670	1.05	2.05	137
43	4.0	75	75	var.	1.91	.48	70,600	54,700	147,000	.232	.753	1.26	2.25	159

* Values of Q extrapolated slightly outside of ASTM recommended region.
** Extrapolated from ASTM data, see Figure 66.

TABULATION OF TEST DATA

Spec	W (in)	T_{crk} °F	T_{rupt} °F	σ_{crk} (ksi)	ℓ_c (in)	ℓ_c/W	σ_r (psi)	n (cyc)	$\sigma_{y.s.}$ (psi) **	$\left(\frac{\sigma_r}{\sigma_{y.s.}}\right)^2$	$\frac{\pi \ell_c}{2W}$	Q_1 *	$\sqrt{Q_1 W}$	K_{c1}
44	4.0	75	75	40	1.98	.495	67,500	56,600	147,000	.211	.776	1.29	2.27	154
45	4.0	75	1,417	var.	1.91	.318	59,700	75,500	120,000	.247	.499	.65	1.61	96
46	4.0	75	75	var.	1.99	.49	64,700	60,550	147,000	.193	.768	1.21	2.20	142
47	4.0	75	75	var.	1.99	.49	64,300	42,550	147,000	.192	.768	1.21	2.20	142
48	6.0	75	- 303	40	1.50	.25	95,500	60,400	152,000	.394	.392	.54	1.80	172
49	6.0	75	75	40	1.57	.26	105,300	76,050	147,000	.515	.408	.65*	1.97	202
50	6.0	75	1,619	40	1.96	.327	46,200	58,400	80,000	.332	.513	.73	2.10	97
51	6.0	75	75	40	1.90	.317	91,000	65,100	147,000	.382	.498	.74	2.11	192
R52	6.0	75	1,810	40	1.22	.203	18,200	51,600	30,000	.367	.319	.42*	1.59	29
R53	6.0	75	75	40	1.15	.19	111,600	41,400	147,000	.578	.298	.46*	1.66	185
R54	6.0	75	- 330	45	2.02	.337	84,500	59,100	153,000	.304	.529	.75	2.12	179
R55	6.0	75		45										
R56	6.0	75		37										
R35	4	75		45	.62			31,000						
R35	4	75		40	.81			44,300	Replicated - See Section A , Fig. 137					
R35	4	75		37	2.5	failure		81,600						

* Values of Q extrapolated slightly outside of ASTM recommended region.
** Extrapolated from ASTM data, see Figure 66.

TABULATION OF TEST DATA

Spec	W (in)	T_{crk} °F	T_{rupt} °F	σ_{crk} (ksi)	ℓ_c (in)	$y = \ell_c/w$	σ_r (psi)	n (cyc)	$\sigma_{y.s.}$ (psi) **	$\left(\frac{\sigma_r}{\sigma_{y.s.}}\right)^2$	$\frac{\pi \ell_c}{2w}$	Q_1 *	$\sqrt{Q_1 W}$	K_{c_1}
R 7	4	75	75	40	.60	.15	122,500		147,000	.694	.236	1.60	1.265	155
R 8	4	75	75	40	.59	.149	112,000	29,450	147,000	.581	.234	1.44	1.20	134
R10	4	75	75	40	.64	.160	112,500	32,450	147,000	.585	.251	1.56	1.249	141
12	4	75	75	40	.71	.178	119,500	34,900	147,000	.661	.280	1.48	1.216	145
13	4	75	75	40	.84	.21	122,500	23,750	147,000	.694	.330	2.40	1.548	189
15	4	75	75	40	.92	.23	109,500	43,850	147,000	.555	.361	2.30	1.516	166
117	4	75	75	40	1.18	.295	92,000	61,750	147,000	.392	.463	2.71	1.646	151
9	4	75	1,100	40	.70	.175	112,500	29,500	128,000	.773	.275	2.08	1.443	162
11	4	75	1,100	40	.75	.1875	102,000	42,300	128,000	.635	.294	1.92	1.386	141
14	4	75	1,100	40	.87	.217	108,250	47,000	128,000	.716	.341	2.60	1.613	175
16	4	75	1,100	40	.96	.24	100,000	41,500	128,000	.610	.377	2.59	1.612	161
R18	4	75	1,100	40	1.22	.305	84,000	40,850	128,000	.430	.479	2.96	1.720	144
R23	4	75	1,390	40	.80	.200	116,250	33,100	121,000	.941	.314			
25	4	75	900	40	.85	.212	112,725	42,150	131,000	.740	.333	2.37	1.540	174
R27	4	75	900	40	.99	.247	104,750	29,600	131,000	.640	.388	2.80	1.674	175

* Values of Q extrapolated slightly outside of ASTM recommended region.
** Extrapolated from ASTM data, see Figure 66.

TABULATION OF TEST DATA

Spec	W (in)	T_{crk} °F	T_{rupt} °F	σ_{crk} (ksi)	ℓ_c (in)	$y = \ell_c/w$	σ_r (psi)	n (cyc)	$\sigma_{y.s.}$ (psi) **	$\left(\frac{\sigma_r}{\sigma_{y.s.}}\right)^2$	$\frac{\pi}{2w}$	Q_1*	$\sqrt{Q_1 W}$	K_{c_1}
R26	4	75	- 320	40	.83	.21	118,375	36,900	153,000	.599	.330	2.16	1.470	174
R22	4	75	- 330	40	.594	.148	131,500	21,700	153,000	.738	.232	1.64	1.280	168
R30	4	75	- 327	40	1.22	.305	92,250	38,300	153,000	.364	.479	2.76	1.600	148
R29	4	75	- 320	40	1.24	.31	96,350	41,600	153,000	.397	.487	2.92	1.710	165
R24	4	75	- 317	40	.69	.172	126,700	30,900	153,000	.685	.270	1.84	1.358	172
R 5	2	75	- 340	40	.73	.365	95,800	30,275	153,000	.392	.573	1.94	1.395	134
R 2	2	75	- 334	40	.50	.25	112,000	17,800	153,000	.536	.393	1.26	1.125	126
R 4	2	75	900	40	.58	.29	79,000	39,500	131,000	.364	.455	1.29	1.137	89
R 6	2	75	900	40	.73	.36	80,000	31,300	131,000	.373	.573	1.83	1.355	108
R19	4	75	900	40	.47	.117	127,500	20,000	131,000	.947	.184			
R28	4	75	900	40	.96	.24	101,625	38,600	131,000	.602	.377	2.56	1.60	163
R21	4	75	900	40	.62	.155	115,000	23,600	131,000	.771	.243	1.84	1.358	156

* Values of Q extrapolated slightly outside of ASTM recommended region.
** Extrapolated from ASTM data, see Figure 66.

TABULATED TEST DATA

Spec No	W (in)	T_{crk} °F	T_{rupt} °F	σ_{crk} (ksi)	ℓ_c (in)	$y=\frac{\ell_c}{w}$	σ_r (psi)	n (cyc)
R56	6	75	75	37	1.34	.224	106,500	76,200
R59	6	75	75	40	1.69	.281	85,500	67,400
R57	6	75	75	40	1.89	.316	42,700	48,900
R61	6	75	75	40	1.71	.286	85,500	62,000
R58	6	75	75	40	1.39	.233	89,800	100,000
R60	6	75	75	40	1.28	.214	96,200	85,650
R62	6	75	75	40	1.30	.216	99,000	53,750
R66	8	75	810	40	1.97	.246	83,800	65,935
R68	8	75	598	40	2.50	.312	79,300	120,830
R65	8	75	1,000	40	1.77	.221	79,000	74,710
R63	8	75	1,200	40	1.70	.212	94,300	75,590
R67	8	75	80	bad specimen				

SECTION 8

SUMMARY OF TEST RESULTS ON B120VCA TITANIUM SHEET

This section reports the testing and results obtained on the material B120VCA, a beta-phase titanium of 11% chromium, 13% vanadium, and 4% aluminum composition.

Over seventy panels have been tested on the titanium alloy with strength characteristics very similar to the PH15-7 Mo steel. The titanium alloy, aged to the 207,000 tensile strength range, is extremely notch sensitive and exhibits very low crack strengths at cryogenic temperatures.

1. Figure 68 illustrates the residual strength characteristics of a few centrally fatigue cracked panels in the four-inch widths. The panel crack-strengths at an elevated rupturing temperature show the typical notch softening effect that previously has been reported and shown for the metals of this program.

   Additional prestrained panels have been tested and the results are shown on this graph. After post straining for three minutes at 600°F, the panels were ruptured near liquid nitrogen temperature (-320°F). The most pronounced difference in residual strengths, due to the effect of extending and disrupting the crack front (i.e.) by warm-prestressing, is shown by subsequent low rupturing temperature . For example, fracture at +75°F, following the prestraining of this material does not show great differences between preloaded and unpreloaded rupture tests.

2. Figure 69 shows the results of a few additional tests performed on the titanium alloy in the solution treated and cold rolled condition. Although the material is not necessarily used in this condition, the tests do demonstrate the wide variation in notch resistance for a given material as a function of its heat treatment and tensile strength range.

   Test panels at some intermediate strength range should therefore exhibit properties between the above extremes. Such strength characteristics may prove to be more useful from the designer's standpoint.

3. Figure 70 through 72 are graphs of fatigue crack growth versus number of stress cycles at three values of maximum cracking stress, (R = +.2). These types of curves and data may be used to obtain K vs $\Delta l / \Delta n$ plots similar to those shown in Section 5 and 7. This data may then be used to predict accumlative crack growth.

4. Residual strength tests on 6 inch wide titanium panels of various sheet thickness are given in Section 12.

5. Agreement between the actual fatigue crack growth ($\Delta l / \Delta n$) by test and by theoretical calculations is described and shown in the Analysis Section 14.

It is becoming more apparent that the design of a "small screening specimen" that will yield design data for large built-up structures may be lacking for some time. At present, a combination of the ASTM standard edge-notched specimen and the four-inch to six-inch wide center cracked fatigue panels appear to be good specimens for material behavior evaluations. It is emphasized that both of these types are needed. For some materials the ASTM edge-notch specimen (.0007 inches $\geq \rho$), Section 3 will provide significant notch strengths over the range of rupturing temperatures. For other materials, a natural fatigue crack indicates far greater reductions in strength than the ASTM specimen and for this reason yields the more conservative results.

It is believed that reliable design data pertaining to residual strengths of structure will only come from the testing of larger panels. It is suggested for the present, that future investigators test widths of panels from 18 inches to 36 inches for the most reliable design allowables. These sizes would pertain to the appropriate structures that are being considered for many of the hydrospace, aerospace, and space vehicles of the present.

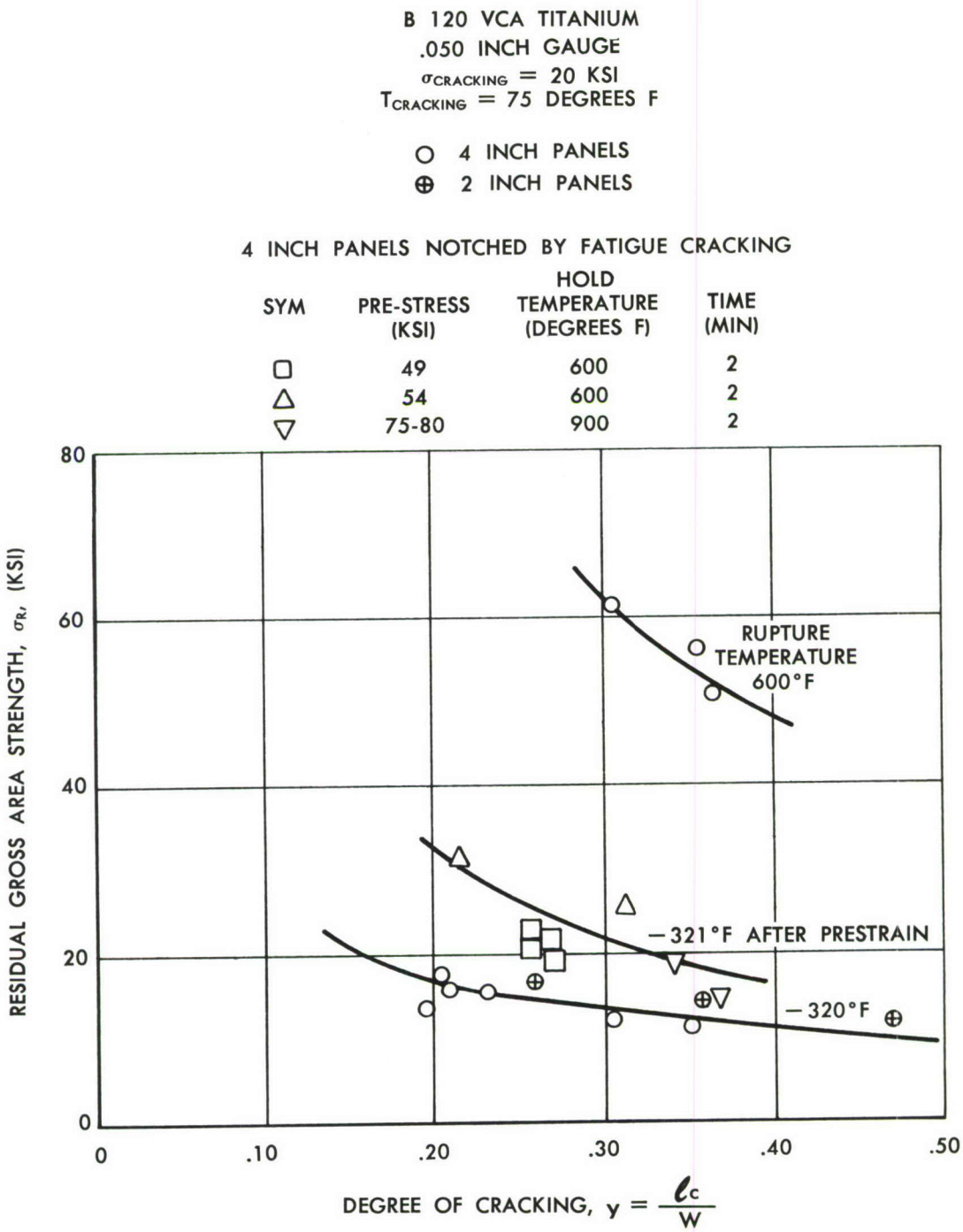


Figure 68. RESIDUAL STRENGTH vs DEGREE OF CRACKING

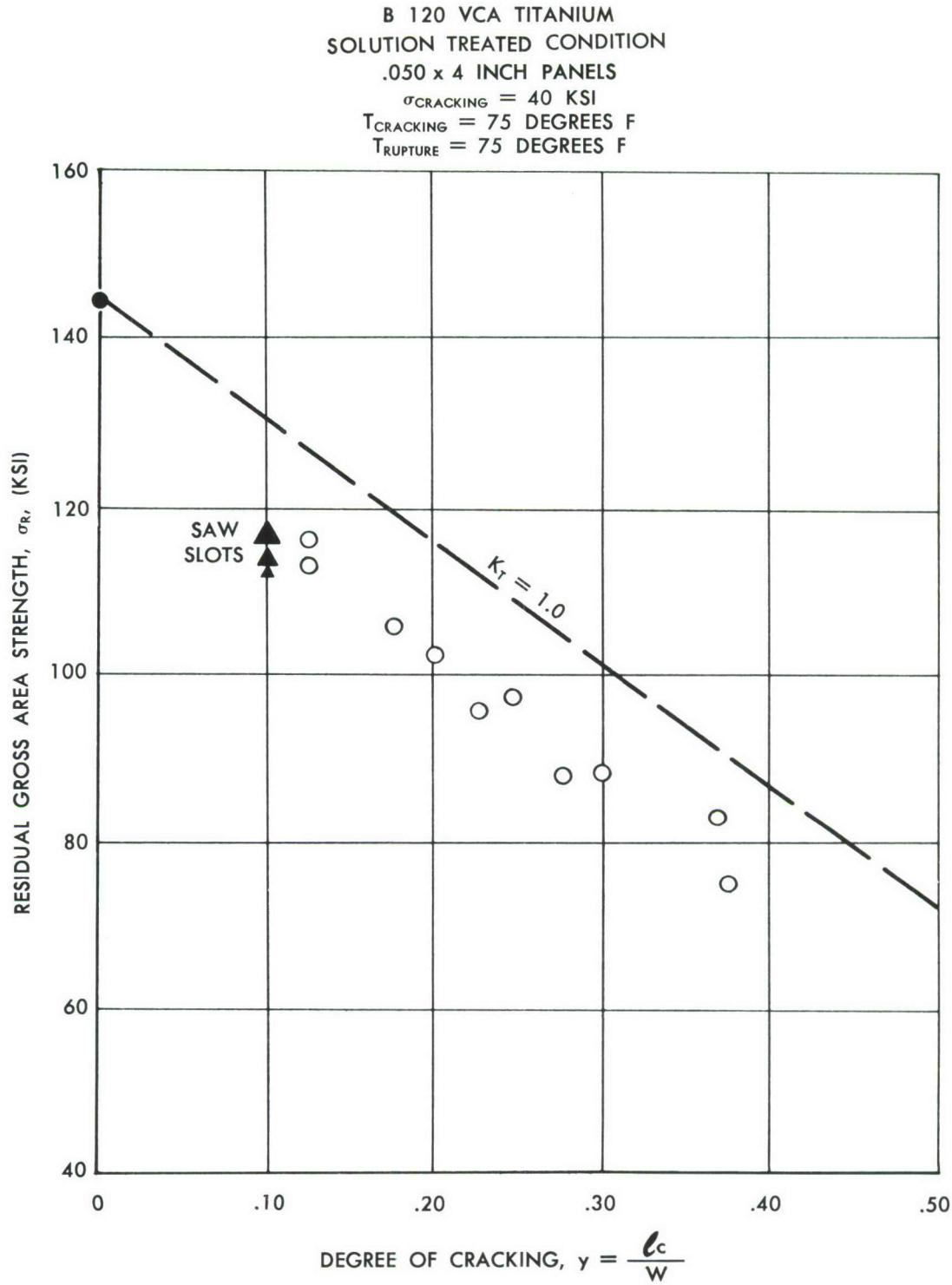


Figure 69. RESIDUAL STRENGTH vs DEGREE OF CRACKING

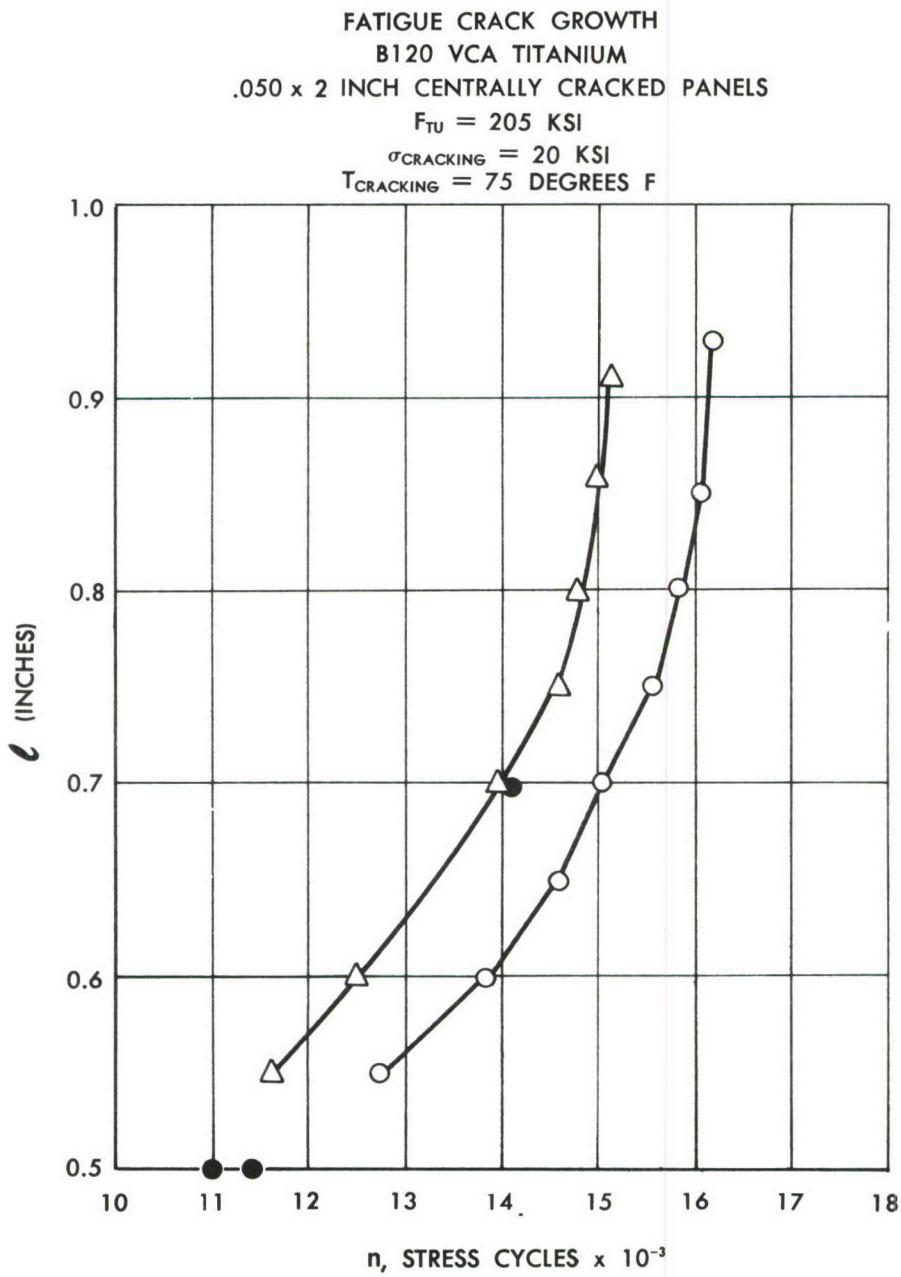


Figure 70. FATIGUE CRACK GROWTH

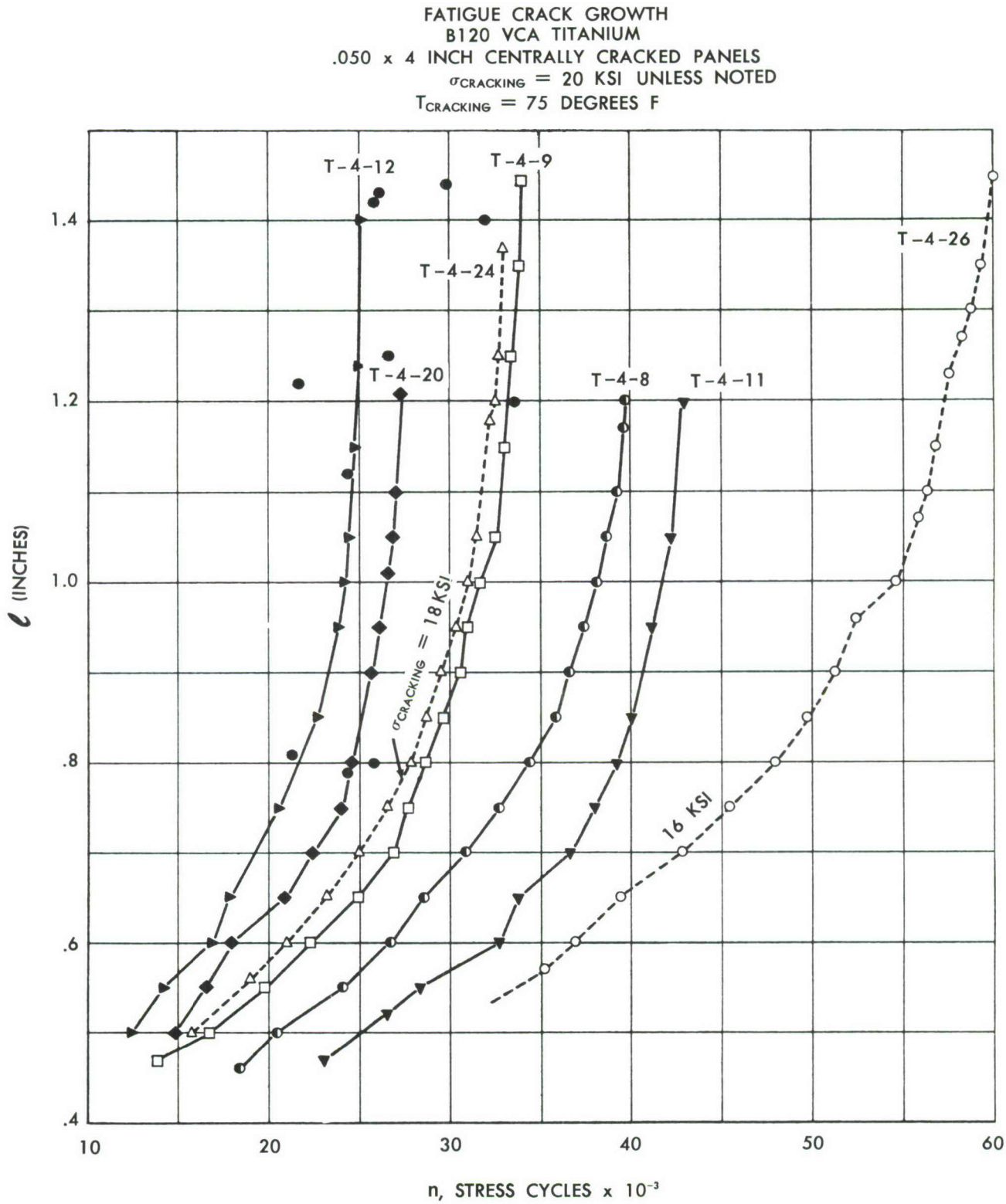


Figure 71. FATIGUE CRACK GROWTH

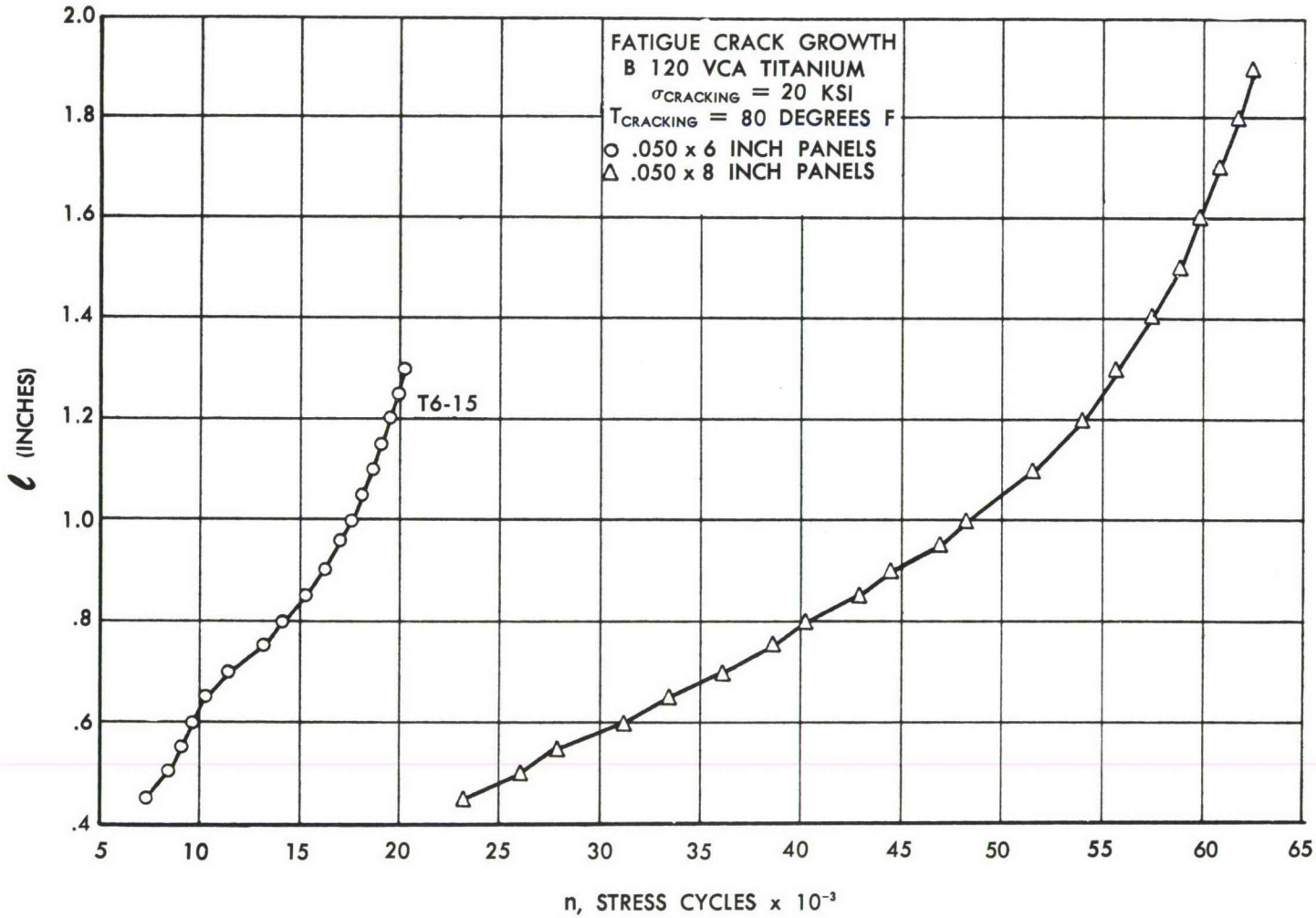


Figure 72. FATIGUE CRACK GROWTH

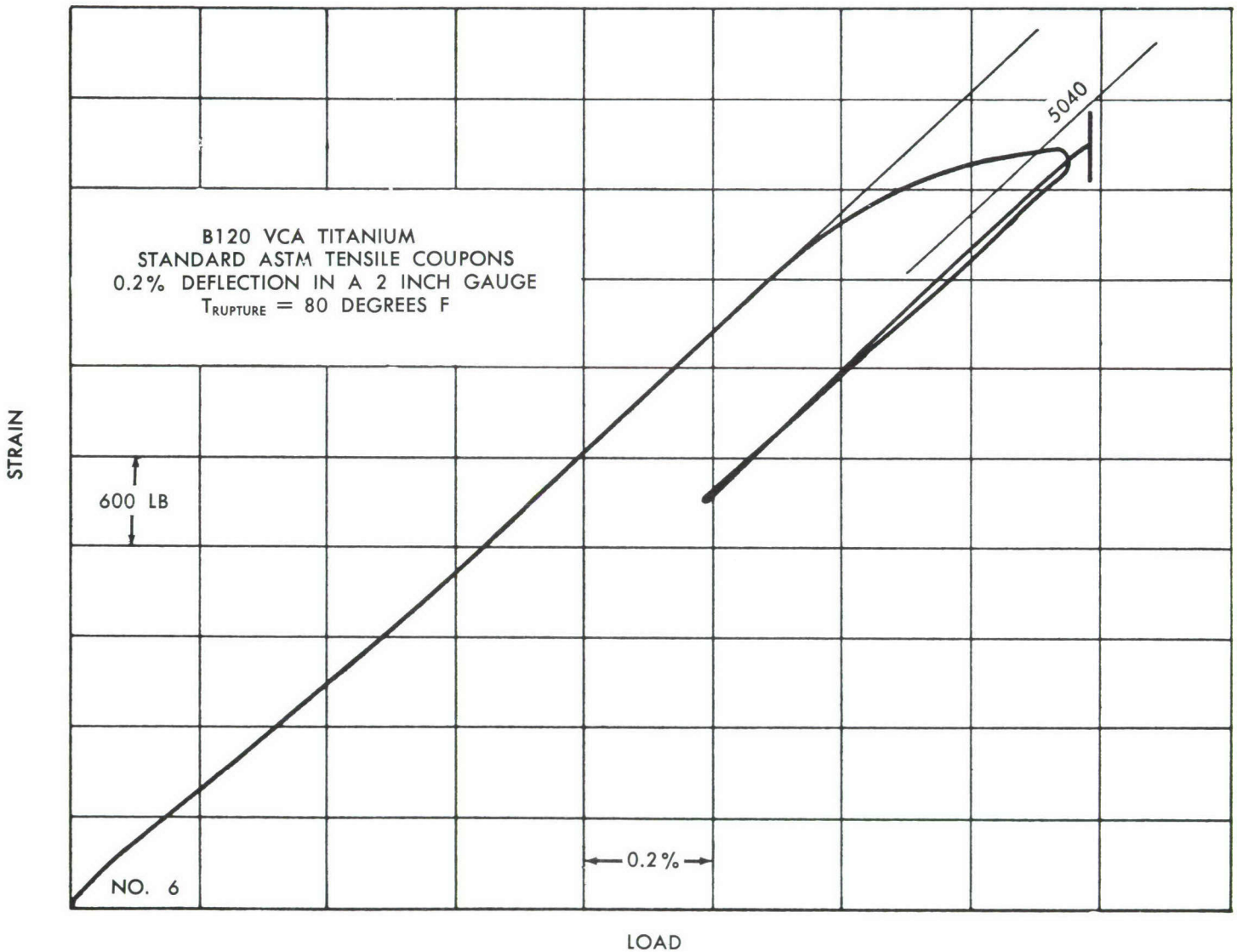


Figure 73. LOAD-STRAIN CURVE

MECHANICAL PROPERTIES OF B120VCA TITANIUM

The test coupons and panels were made from Crucible Steel Company's titanium. The various gage sheet panels were received in the solution treated condition. All milling, machining, and drilling was performed before the heat treatment. After degreasing and cleaning, the specimens were aged at +900°F. for 60 hours.

Crucible Steel Co.

Heat No.	F 91 - 76	050 gauge
Heat No.	F 96 - 60	040 gauge
Heat No.	F 94 - 60	030 gauge
Heat No.	F 96 - 74	020 gauge

TABLE 8

Spec. (.050 Ga.)	Rolling Dir.	F_{ty}	F_{tu}	% Elong. (2" g.l.)	Time (sec.)
1	Transverse	191,730	200,750	1.0	37
2	Transverse	190,910	205,490	1.0	77
3	Transverse	193,100	205,745	1.0	80
4	Transverse	191,635	201,900	1.0	69
5	Transverse	193,155	207,415	1.0	85
6	Transverse	193,960	205,285	1.0	70

A typical stress-strain curve for specimen number four is shown in Figure 73. The technique used in obtaining the mechanical property data was as follows:

1. The initial loading of the standard ASTM tensile coupons is performed and paced at a rate of 0.2 of an inch per inch per minute.

2. A back-modulus is taken beyond the 0.2% permanent strain region.

3. On reloading the coupons to the value of load reached before taking the back-modulus in 2. above the loading is again paced. From this point an attempt is made to fail the coupon within a period of 60 to 90 seconds. The time taken on each of the specimens is given in the above table.

TABULATED TEST DATA

Spec No	W (in)	T_{crk} °F	T_{rupt} °F	σ_{crk} (ksi)	ℓ_c (in)	$y=\frac{\ell_c}{w}$	σ_r (psi)	n (cyc)
T-6-4	6	75		20				29,350
T-6-5	6	75		20				16,750
T-6-6	6	75		20				25,600
T-4-16	4	75 - 319		20	.84	.21	15,800	19,200
T-4-8	4	75 - 319		20	1.21	.302	12,400	39,700
T-4-17	4	75	75	19	1.46	.365	20,200	29,900
T-4-7	4	75 - 319		20	.82	.205	17,150	18,400
T-4-10	4	75	75	20	.81	.202	29,600	21,300
T-4-9	4	75	600	20	1.47	.367	50,200	33,950
T-4-11	4	75	600	20	1.22	.305	61,500	42,950
T-4-12	4	75 - 319		20	1.40	.350	11,050	25,100
T-4-30	4	75 - 319		20	.86	.215	31,000	29,750
T-4-31	4	75	75	20	1.20	.300	25,400	33,400
T-4-23	4	600	70	20	1.20	.300	20,750	74,350
T-4-25	4	70	70	16	0.83	.207	26,100	49,850
T-4-40	4	600	70	20	1.03	.257	22,100	86,100
T-4-41	4	600	70	20	1.00	.250	24,500	75,500
T-4-36	4			Prestrained at				
T-4-37	4			49,000 psi and				
T-4-38	4			600° Fahr.				
T-4-39	4							
T-4-36	4	75 - 319		20	1.08	.270	22,200	19,900
T-4-37	4	75 - 319		20	1.06	.265	20,900	21,400
T-4-38	4	75 - 319		20	1.09	.272	19,800	28,300
T-4-39	4	75 - 319		20	1.04	.260	21,900	27,400

TABULATED TEST DATA

Spec No	W (in)	T_{crk} °F	T_{rupt} °F	σ_{crk} (ksi)	ℓ_c (in)	$y=\frac{\ell_c}{w}$	σ_r (psi)	n (cyc)
T-4-24	4			Prestrained 73,500 psi at 900° Fahr.				
T-4-26	4			Prestrained 82,500 psi at 900° Fahr.				
T-4-24	4	75	- 319	18	1.39	.347	19,100	32,950
T-4-26	4	75	- 319	16	1.46	.365	13,800	60,200
T-4-20	4	Prestrained 54,000 psi at 600° Fahr.						
T-4-20	4	75	- 319	20	1.25	.312	26,300	
T-4-27	4	600	- 319	20	0.78	.195	13,360	53,500
T-4-28	4	600	- 319	saw	slot	.100	13,200	
T-4-29	4	600	- 319	saw	slot	.100	12,700	
T-6-9	6.01	75	75	20	0.72	.120	29,600	17,200
T-6-7	6.01	75	75	20	0.88	.146	31,100	20,800
T-6-3	6.00	75	75	20	1.27	.212	22,700	39,950
T-6-2	6.00	75	75	20	1.53	.255	20,400	50,900
T-6-1	5.99	75	75	20	0.95	.159	23,600	35,000
T-6-8	6.01	75	75	20	1.49	.248	25,100	16,100
R55	5.99	75	75	45	1.80	.301	90,000	
T-6-10	5.99	75	75	20	1.33	.222	21,400	12,800
T-6-11	5.99	75	75	20	1.04	.174	22,100	27,450
T-6-12	5.99	20	75	20	1.38	.230	18,100	17,100
T-6-18	4	75	75	20	1.25	.312	22,100	26,750
T-6-19	4	75	75	20	.79	.197	29,400	24,350
T-6-20	4	75		20				27,350
T-6-33	4	75	- 319	20	.92	.23	15,570	21,050
T-6-34	4	75	75	20	1.12	.28	24,900	24,500

TABULATED TEST DATA

Spec No	W (in)	T_{crk} °F	T_{rupt} °F	σ_{crk} (ksi)	ℓ_c (in)	$y=\frac{\ell_c}{w}$	σ_r (psi)	n (cyc)
T-6-35	4	75	600	20	1.43	.357	56,400	25,600
T-6-24	4	75	- 319	18				32,950
T-4-21	4	600	600	20	1.60		20,000	75,300
T-4-22	4	600	bad spec.		.8			18,500
T-4-32	4	75	75	20	1.40	.35	20,000	32,000
T-4-14	4	75	75	35			35,000	150
T-4-13	4	75	75	40			40,000	250
T-4-15	4	75	75	20	1.45	.362	20,000	26,200
T-4-1	4	75	75	9	.4	.10	42,600	slot
T-4-2	4	75	75	0	.4	.10	43,300	slot
T-4-3	4	75	75	0	.4	.10	44,100	slot
T-4-4	4	75	75	20	.90	.200	28,400	25,800
T-4-5	4	75	75	20	1.22	.305	23,300	21,700
T-4-6	4	75	75	20	1.58	.395	19,850	20,600
T-2-1	2	75	75	20	0.50	.251	32,200	11,000
T-2-2	2	75	- 340	20	.72	.36	14,950	14,000
T-2-3	2	75	75	20	0.93	.466	21,350	16,200
T-2-4	2	75	340	20	0.52	.26	16,100	11,400
T-2-5	2	75	75	20	0.74	.371	25,200	17,350
T-2-6	2	75	- 340	20	.94	.47	12,360	15,150

TABULATED TEST DATA

Spec No	W (in)	T_{crk} °F	T_{rupt} °F	σ_{crk} (ksi)	ℓ_c (in)	$y=\frac{\ell_c}{w}$	σ_r (psi)	n (cyc)
T-6-4	5.99	75	75	20	0.92	.154	27,200	
T-6-5	5.99	75	75	20	1.27	.212	19,650	
T-6-6	5.99	75	75	20	1.30	.217	22,100	
T-6-5	5.99	75	75	20	0.52	.132	97,800	2,750
T-6-6	5.99	75	75	20	0.62	.157	95,700	9,400
T-6-7	5.99	75	75	20	0.66	.167	90,200	8,100
T-6-8	5.99	75	75	20	0.72	.182	102,500	13,800
T-6-9	5.99	75	75	20	0.74	.187	86,600	7,100
T-6-10	5.99	75	75	20	0.84	.212	86,600	11,550
T-6-11	5.99	75	75	20	0.84	.212	92,800	10,700
T-6-12	5.99	75	75	20	0.93	.236	81,100	8,900
T-6-14	6.0	75	75	20	1.46	.243	20,850	36,300
T-6-15	6.0	75	75	20	1.31	.219	32,400	20,100
T-6-13	6.0	75	75	20	1.51	.251	29,000	62,000
T-8-4	8.0	75	75	20	2.32	.290	19,400	64,100
T-8-3	8.0	75	75	20	2.57	.321	18,500	43,000
T-8-2	8.0	75	75	20	2.55	.319	18,200	51,900
T-8-1	8.0	75	75	20	2.90	.362	14,000	70,200
T-4-101	4	75	75	40	.99	.247	97,500	
T-4-107	4	75	75	40	.70	.175	106,000	
T-4-108	4	75	75	40	.80	.200	102,750	
T-4-105	4	75	75	40	.50	.125	113,300	
T-4-103	4	75	75	40	1.50	.375	75,200	
T-4-111	4	75	75	40	1.20	.300	88,100	

TABULATED TEST DATA

Spec No	W (in)	T_{crk} °F	T_{rupt} °F	σ_{crk} (ksi)	ℓ_c (in)	$y=\frac{\ell_c}{w}$	σ_r (psi)	n (cyc)
T-4-109	4	75	75	40	.91	.227	95,400	
T-4-102	4	75	75	40	1.49	.372	83,300	
T-4-110	4	75	75	40	1.11	.277	87,400	
T-4-104	4	75	75	40	.50	.125	116,000	
T-4-128	4		75	saw	.40	.10	117,800	
T-4-129	4		75	slit	.40	.10	114,500	
T-4-130	4		75		.40	.10	113,200	

SECTION 9

SUMMARY OF TEST RESULTS ON WROUGHT-SINTERED (COATED) MOLYBDENUM SHEET

The molybdenum test panels tested in this section of the report were obtained from Fansteel Metallurgical Corporation, Chicago, Illinois. The 99.9% molybdenum, lot numbers 494-5 and 495-5, was wrought-sintered. The test panels were formed from one-inch fourteen-kilogram bars after hot to cold working in intermediate steps down to the .050 sheet thicknesses. A few finished panels were tested in the as-received and uncoated condition. The majority of the panels .050 x 6" wide were protected with the W-2 (molybdenum disilicide) coating. A few additional panels were protected with a DURAK-B coating. The high-temperature oxidation-prevention coatings (.001" thick) were applied by the Chromizing Corporation of Los Angeles, California.

The high temperature rupture tests were performed with new type ceramic-reflector radiant heat lamps. Temperatures as high as +2,500°F. were reached on the 6" wide molybdenum panels within 11 seconds.

The testing program for the molybdenum sheet panels included fatigue crack growth tests of coated molybdenum at +80°F. to +1,350°F. Residual strength tests on all intact fatigue cracked panels were then conducted at various rupture temperatures (-340°F to +2,500°F). The test observations and conclusions that have been drawn are itemized in the summary below. From the limited number of tests performed, there are some encouraging as well as discouraging results.

1. Although the pure wrought metal has been investigated in this report rather than the alloyed metal there does not appear to be much difference between the tensile strengths after the protective coatings have been applied.

2. The refractory metal molybdenum has good strength properties at high temperatures, however, it is well known that it oxidizes rapidly if not protected with special coatings.

3. The coated pure wrought molybdenum as well as the alloyed arc-cast molybdenum (not tested in this program) appear to be especially notch sensitive to impact loads at normal and low temperatures.

4. The coating process, which is very necessary for the protection of the molybdenum under loads at high temperature, has an adverse embrittling effect at low temperatures. Coated molybdenum sheet panels when either subjected to light impact loads or accidently struct in the process of structure fabrication will shatter. It is suggested that this material be seriously reconsidered if there is any thought concerning its use as a material for primary load-carrying members in aerospace vehicles.

5. Exposure to temperatures of 1,300°F to 1,400°F for two hours (oxidation tests) on both the W-2 and DURAK-B coated panels showed no adverse effects or attack upon the protective coat or substrate.

6. Exposure to 1,350°F with the conjoint action of cyclical loading for a testing period of two hours (500 cpm) had very pronounced effects on the coated panels:

a. The coating breaks down and the molybdenum substrate rapidly oxidizes (MoO_3) through the cracked coating.

b. The W-2 coating appears to be less protective than the DURAK-B coating.

c. It may be possible that not enough study has been placed on the protective coating programs under fatigue environments. Coatings that can pass oxidation tests, with unnotched samples, under no or steady state loads do not necessarily provide the required protection under elevated temperature fatigue action.

7. The coating process has decreased the yield and ultimate tensile strength of the material and increased the elongation characteristics (80°F. properties) as shown in the table on page 139.

8. The coating processes have altered the 80°F. fatigue strength characteristics of the molybdenum as follows:

   a. Increased notch sensitivity and embrittleness to such a degree that it was not practical to obtain crack growth data at as high a cracking stress as the as-received, uncoated molybdenum panels.

   b. At low cracking stresses, the scatter in crack growth data was far greater than in any other of the materials or conditions thus far investigated. See Figure 78.

   c. The coatings have accelerated the crack initiation period.

9. Residual strength tests of centrally fatigue cracked panels as a function of rupturing temperature are shown in Figure 74.

   Since this material has good strength properties at elevated and high temperatures only when coated, and the protective coat is dependent upon "time at temperature", it would appear that the useful and practical strength characteristics of this material are also very time dependent. Many of the coatings possess healing characteristics at some temperature however when cracked at lower temperatures no protection for the molybdenum is provided. It is in this period that rapid oxidation and deterioration attacks the fatigue cracked panels.

   The series of tests shown in Figure 74 indicate this effect.

10. Figure 75 shows the residual strength of center cracked panels at high temperaturees and the effect of "soak-time" at these rupturing temperatures on the strength characteristics.

11. Figure 76 shows residual strengths of coated molybdenum panels containing .012" wide machines slots in lieu of fatigue cracks.

12. Exploratory programmed load tests on two molybdenum panels are diagrammatically illustrated on pages 137 and 138.

13. The mechanical properties of the metal panels are given in the table on Page 139. Typical load-strain curves for the standard tensile coupons are shown in Figure 83.

14. Two tantalum panels were tested in this program as a matter of interest and the data is plotted in Figure 74. Central fatigue cracks were generated in the 4" wide tantalum panels at a maximum cracking stress of 27,500 psi.

    One panel was ruptured in liquid nitrogen (-310°F) and the other at +80°F. Unlike any other material investigated in this program the metal tantalum exhibited extremely high notch resistance at cryogenic temperatures.

15. The test data for all of the molybdenum panels is tabulated on pages 143 to 146.

99.9% WROUGHT SINTERED MOLYBDENUM
LOT NO. 494 AND 495
.050 x 6 x 12 INCH PANELS
$T_{CRACKING}$ = 80 DEGREES F
R = 0.2 500 CPM

SYM	CRACKING STRESS (KSI)	RUPTURE TEMPERATURE (DEGREES F)	COAT
○	40	80	UNCOATED
+	40	−340	UNCOATED
△	40	−320	UNCOATED
▽	25	1810	W 2
▼	25	1400	W 2
⊕	25	1780	W 2
●	35	1870	DURAK B
▼	25	75	W 2
⧗	27	75	TANTALUM
⧖	27	−310	TANTALUM
◕	25	2500	W 2

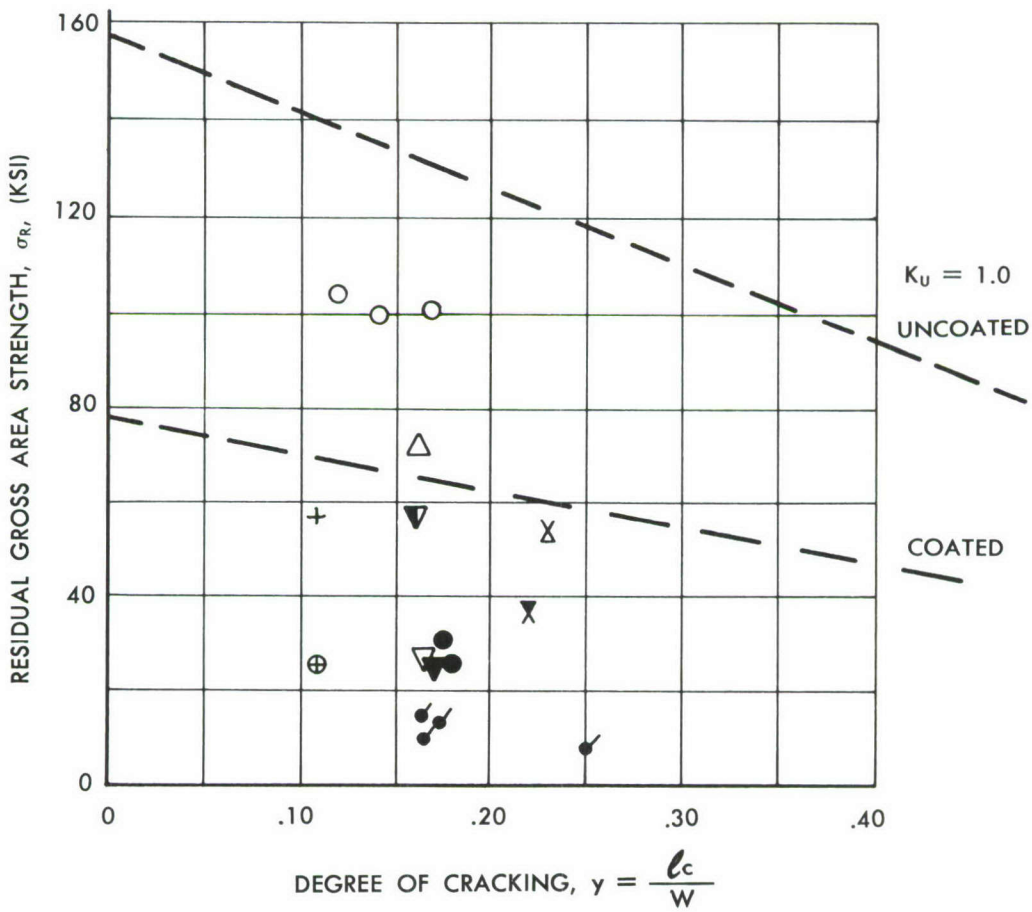


Figure 74. RESIDUAL STRENGTH vs DEGREE OF CRACKING

CENTER FATIGUE CRACKS
COATED MOLYBDENUM
.050 x 6 INCH WIDE PANELS
$\sigma_{CRACKING}$ = 25 TO 30 KSI
$T_{CRACKING}$ = 250 TO 300° F

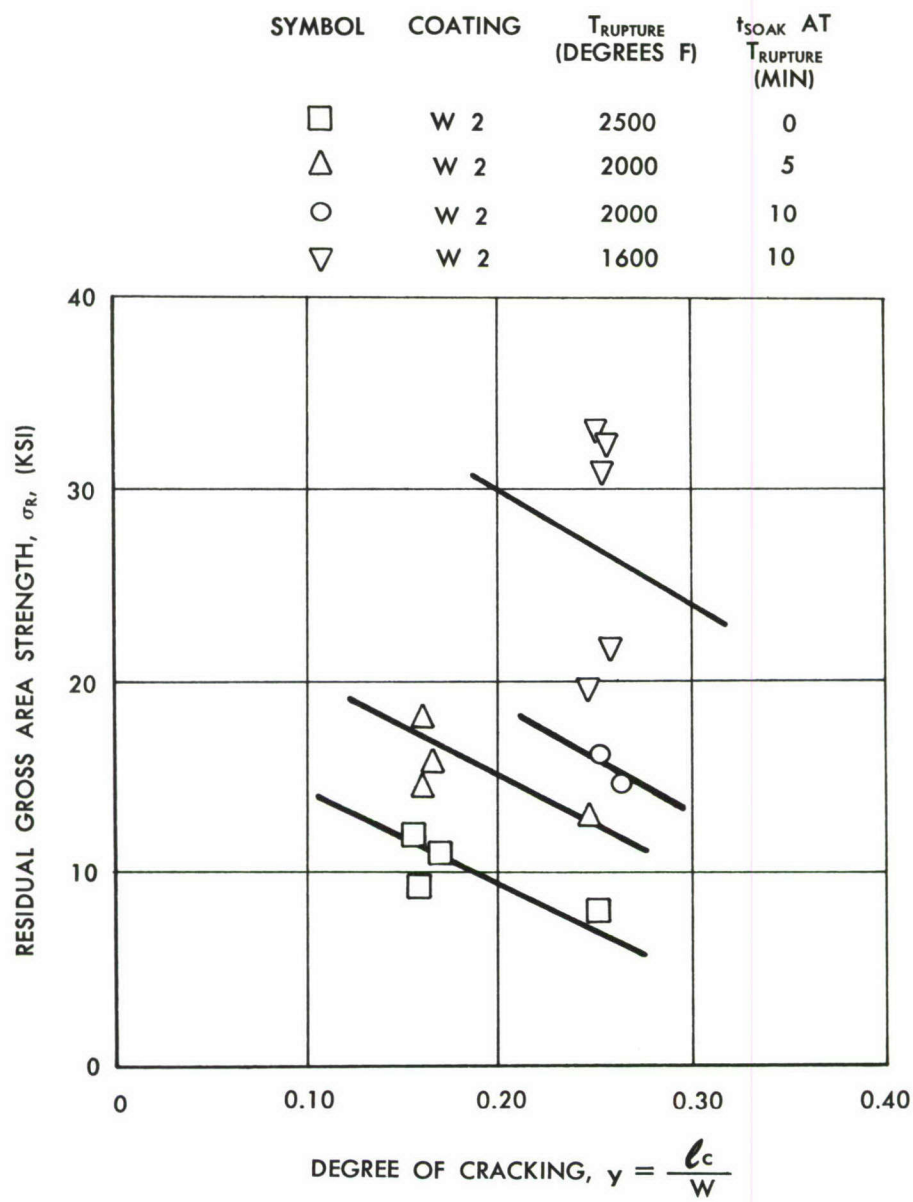


Figure 75. RESIDUAL STRENGTH vs DEGREE OF CRACKING

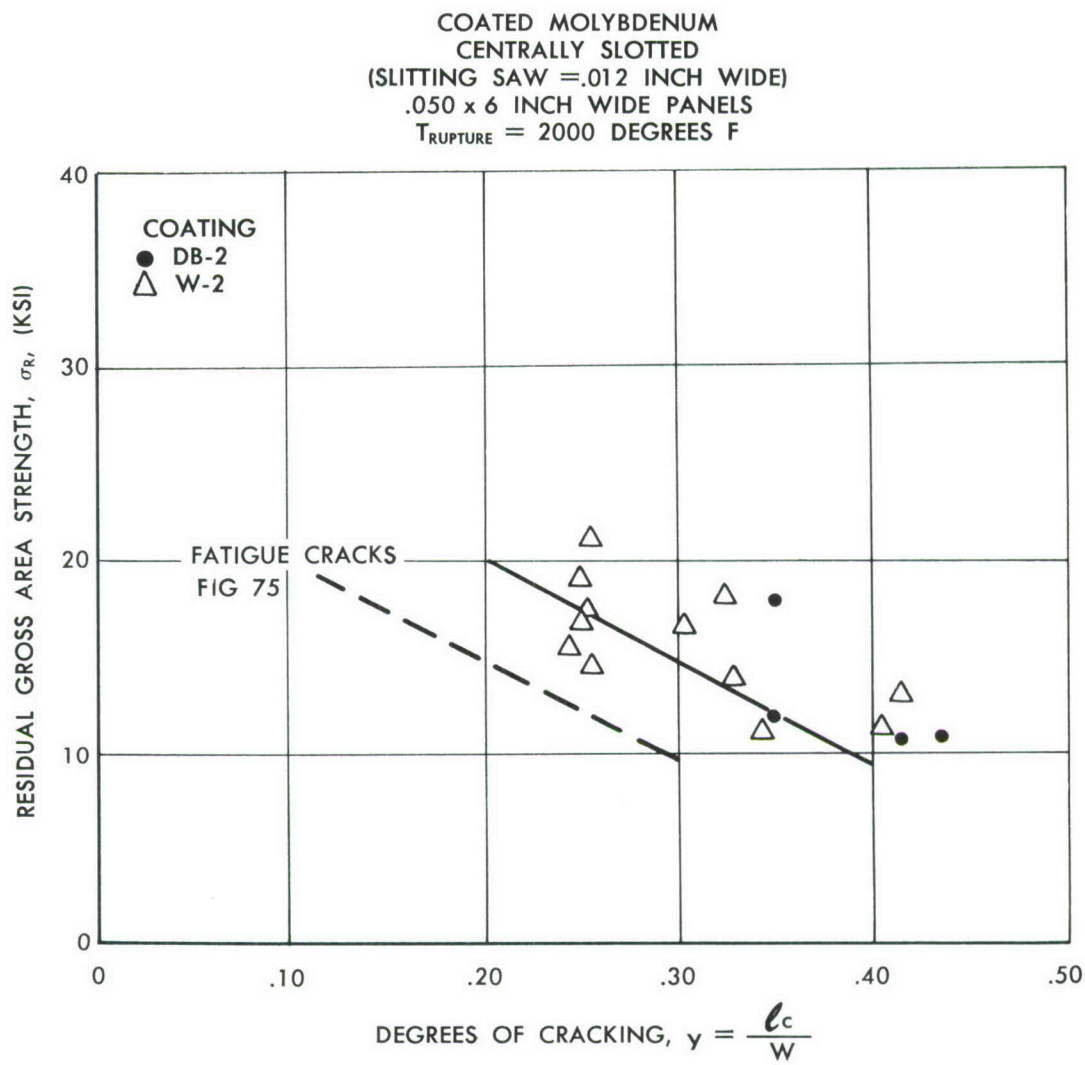


Figure 76. RESIDUAL STRENGTH vs DEGREE OF CRACKING

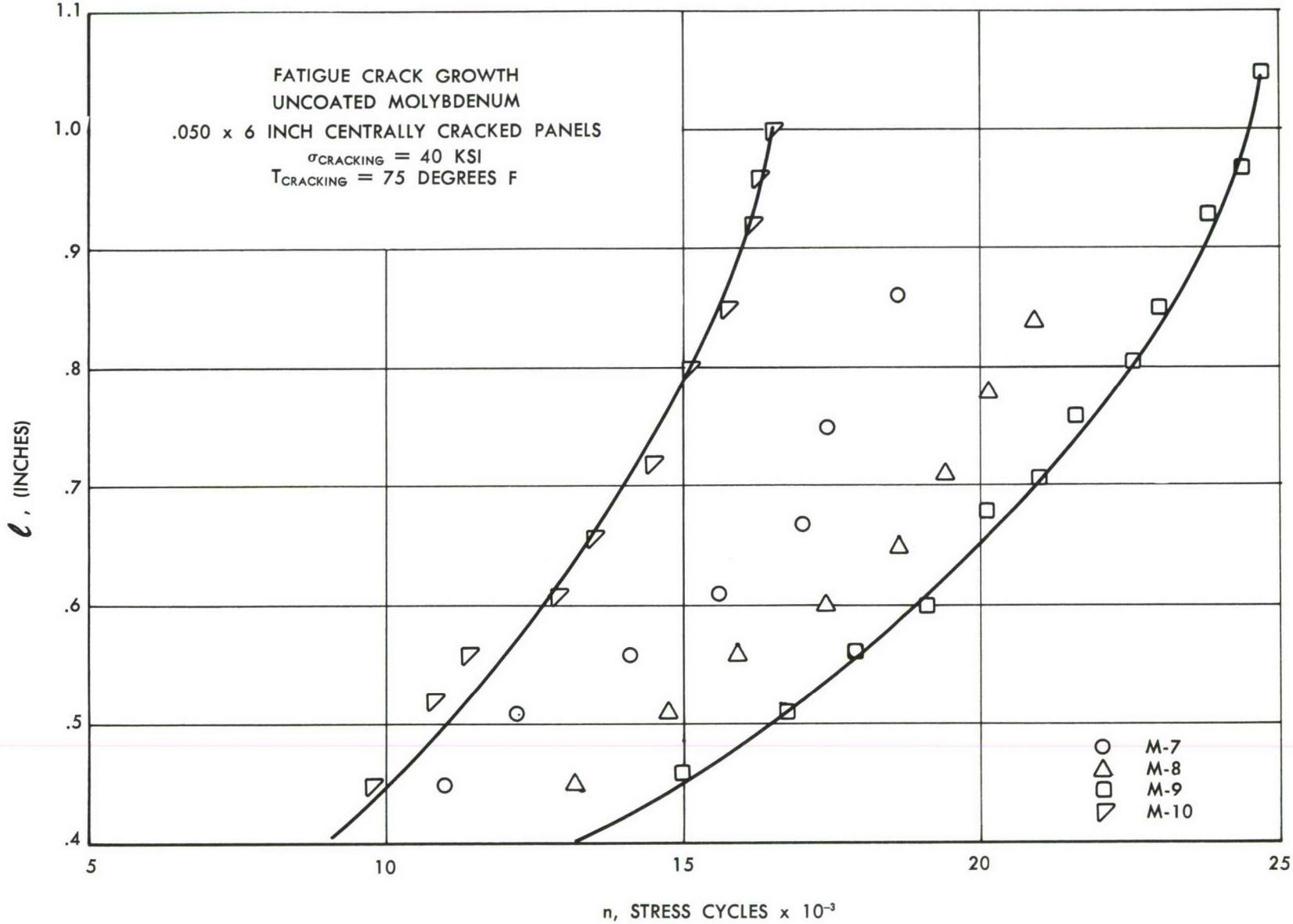


Figure 77. FATIGUE CRACK GROWTH

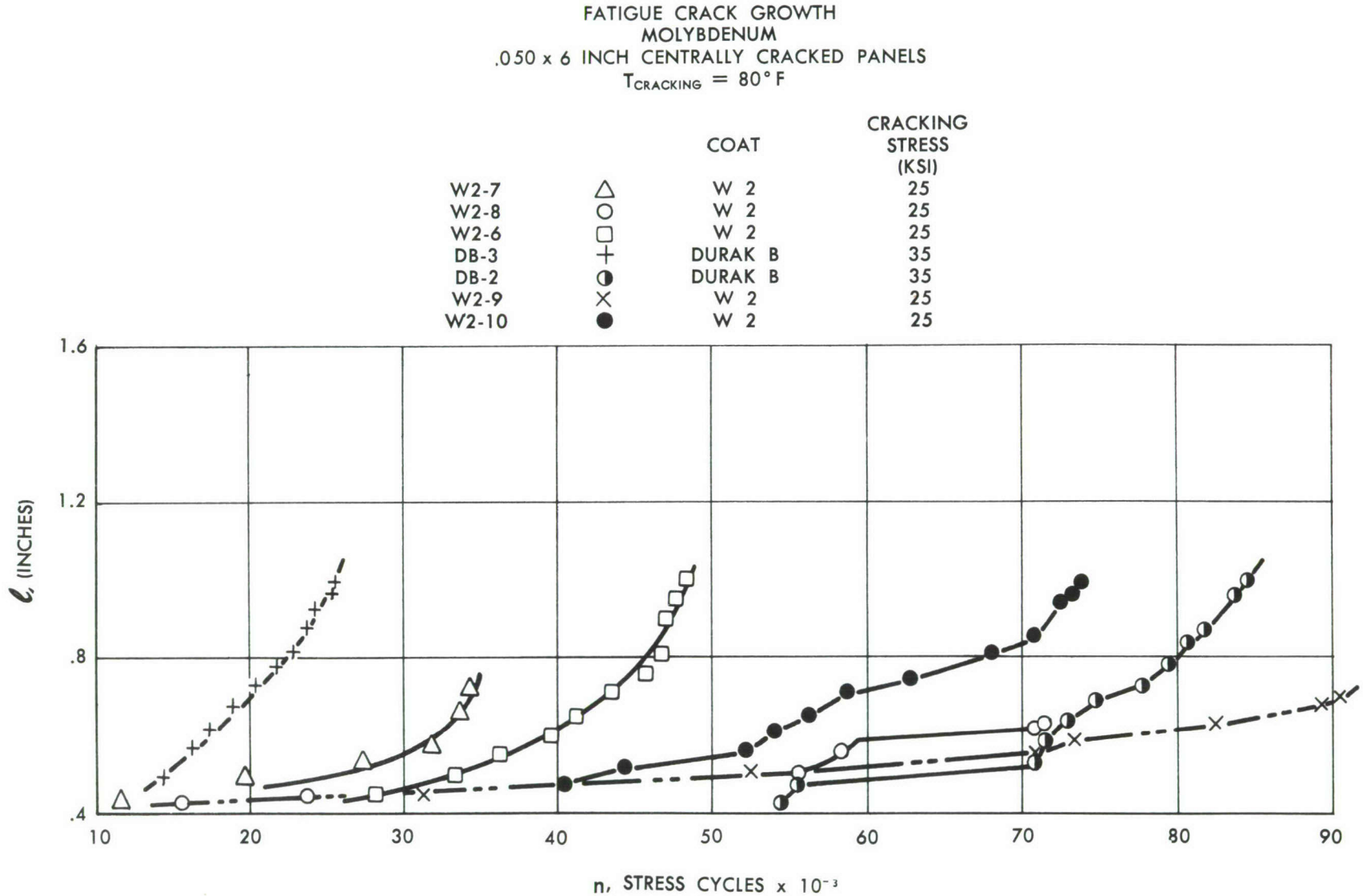


Figure 78. FATIGUE CRACK GROWTH

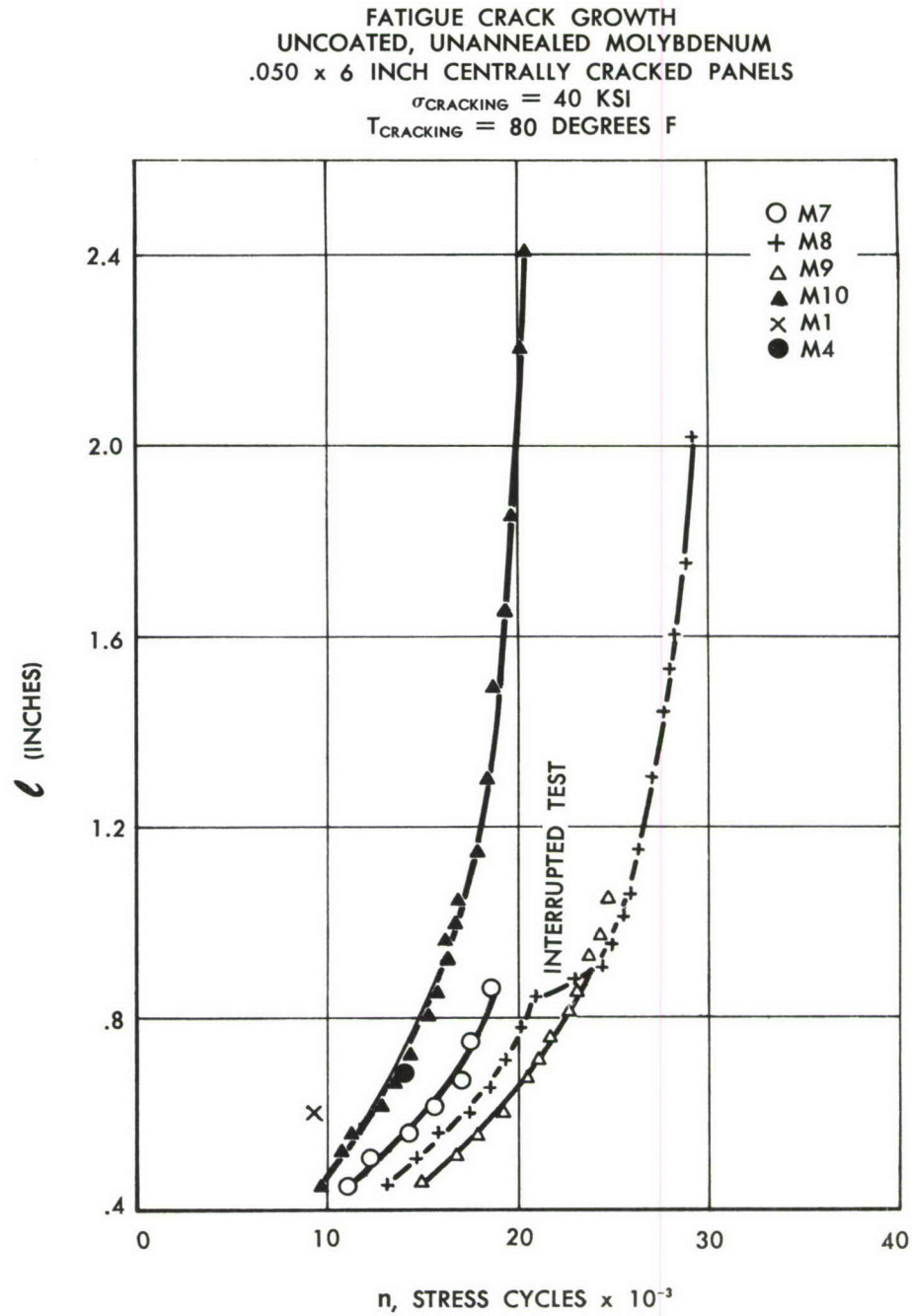


Figure 79. FATIGUE CRACK GROWTH

Figure 80. STRESS INTENSITY vs RATE OF CRACKING

PANEL DB-4

SEQUENTIAL TEST ENVIRONMENT (DEGREES F)	FATIGUE CRACKING STRESS (500 CPM)	STEADY STATE STRESS (KSI)	ACCUMULATIVE TIME OF EXPOSURE (MIN)	REMARKS
1358	11,670 PSI	—	120	SLIGHT OXIDATION
1350	0	5	195	SLIGHT OXIDATION
1352	25,000 PSI	—	202	GROSS TO COMPLETE OXIDATION
1350	0	0	262	VOIDS, HOLES THRU PANEL
1355	20,000 PSI	—	263	RUPTURE

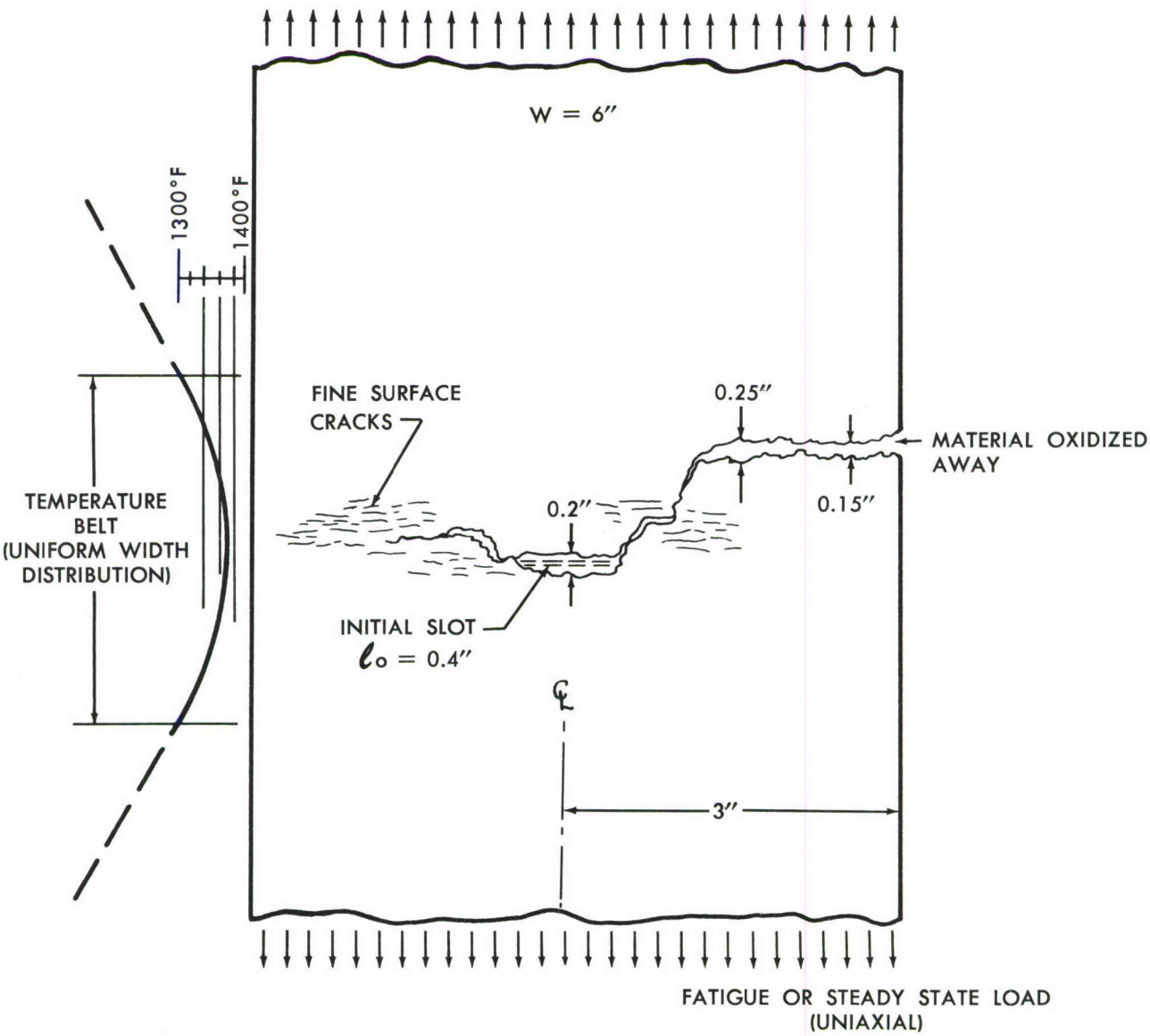


Figure 81. ENVIRONMENTAL BREAKDOWN OF MOLYBDENUM PANEL

PANEL W2 - 11

SEQUENTIAL TEST ENVIRONMENT (DEGREES F)	FATIGUE CRACKING STRESS (500 CPM)	STEADY STATE STRESS (KSI)	ACCUMULATIVE TIME OF EXPOSURE (MIN)	REMARKS
80	25,000 PSI	—	180	CRACK LENGTH ℓ_c = .6"
1350	25,000 PSI	—	217	FATIGUE FAILURE AS SHOWN BELOW

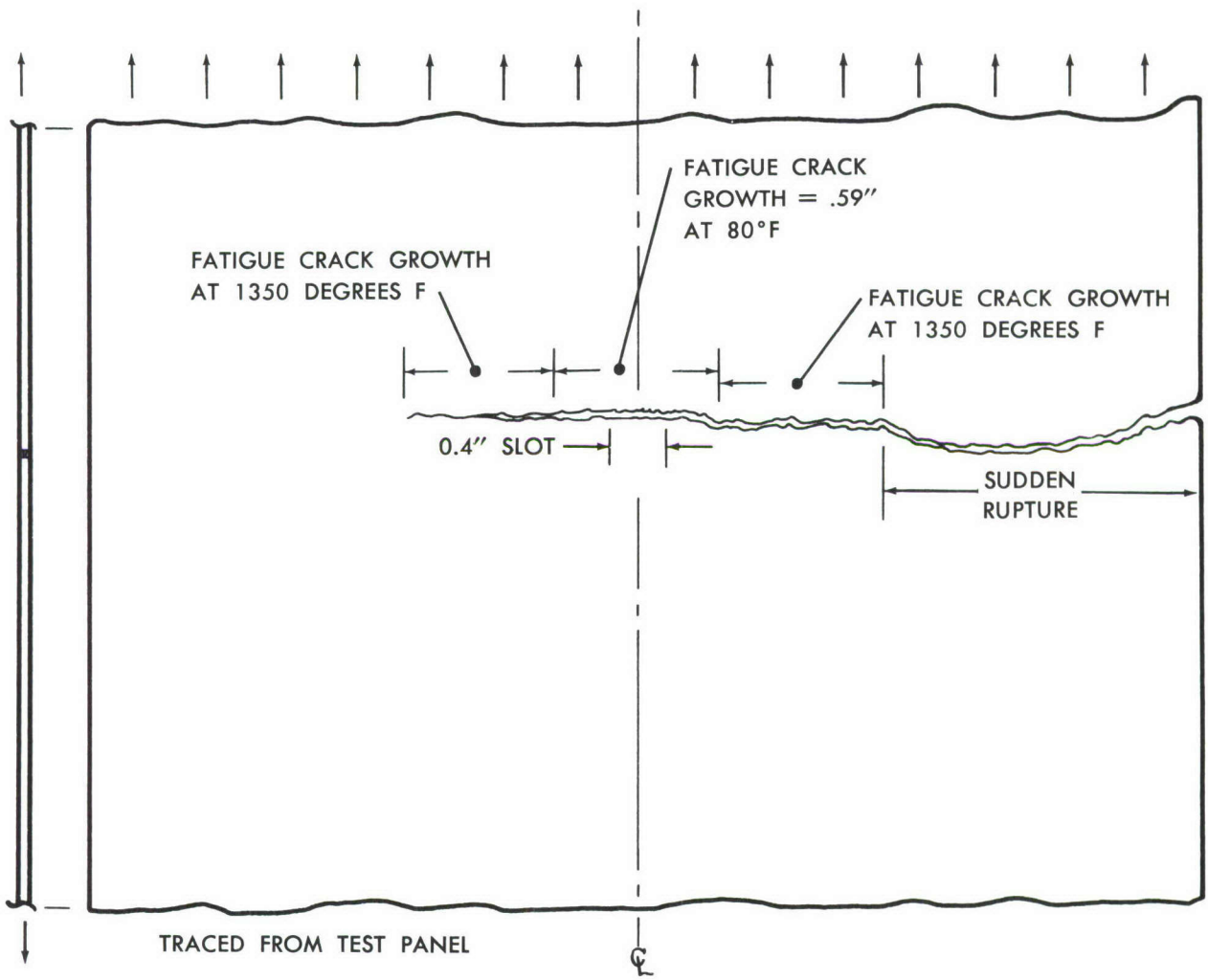


Figure 82. ENVIRONMENTAL BREAKDOWN OF MOLYBDENUM PANEL

MECHANICAL PROPERTIES AT + 80° F.

Condition of Material	Number Specimen Tested	(.2% Offset) F_{ty}	Ultimate Tensile F_{tu}	Elong. in 1" g.l. (%)
As-received (uncoated)	6	139,300	159,100	3.6
As-received	6*	136,400	160,400	6.1
W-2 coating	5	53,270	75,700	18.5
W-2 coating	6*	47,290	81,600	31.1

* Specimens marked (*) were in direction of panel width; all others longitudinal.

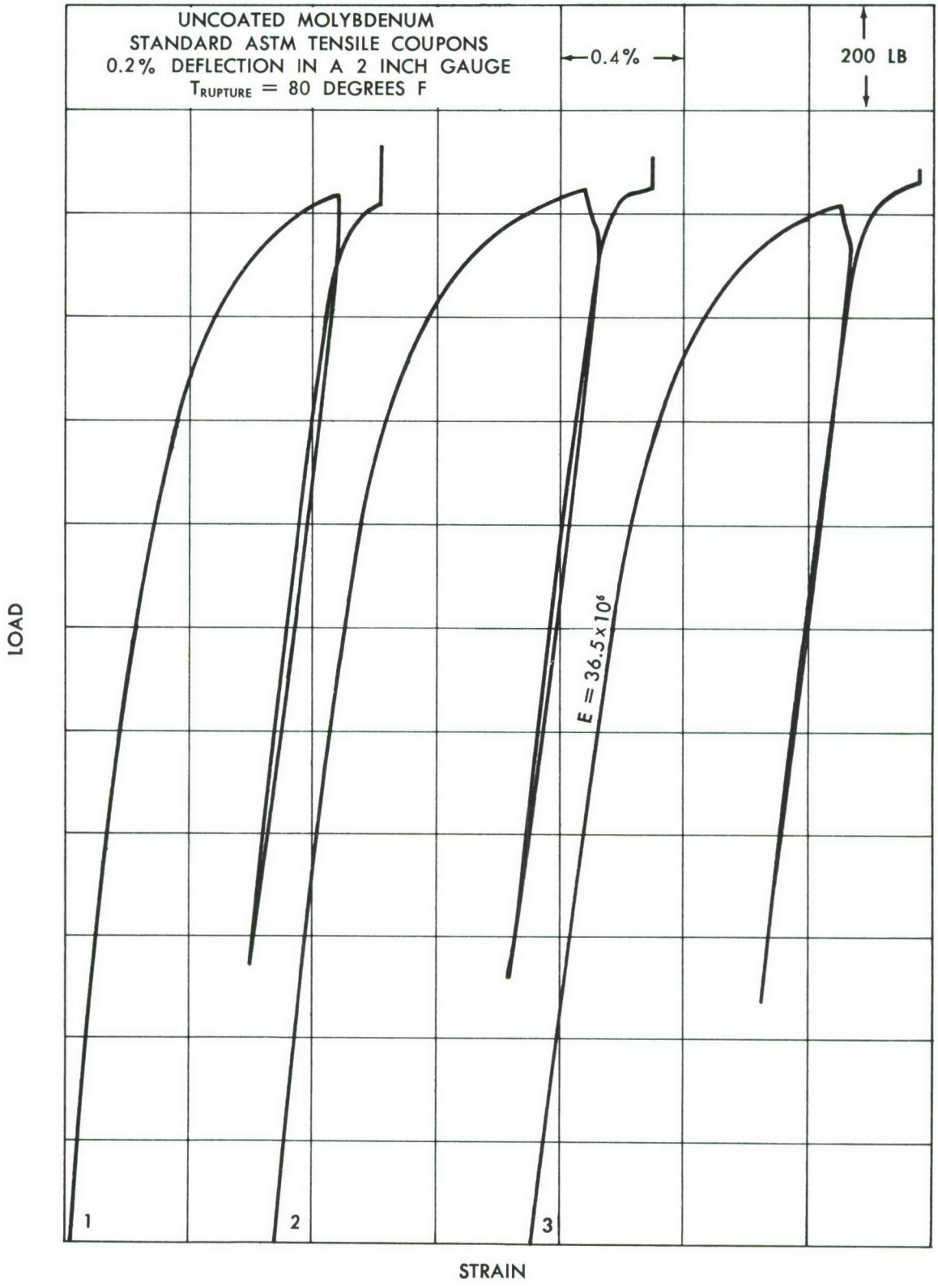


Figure 83. LOAD-STRAIN CURVE

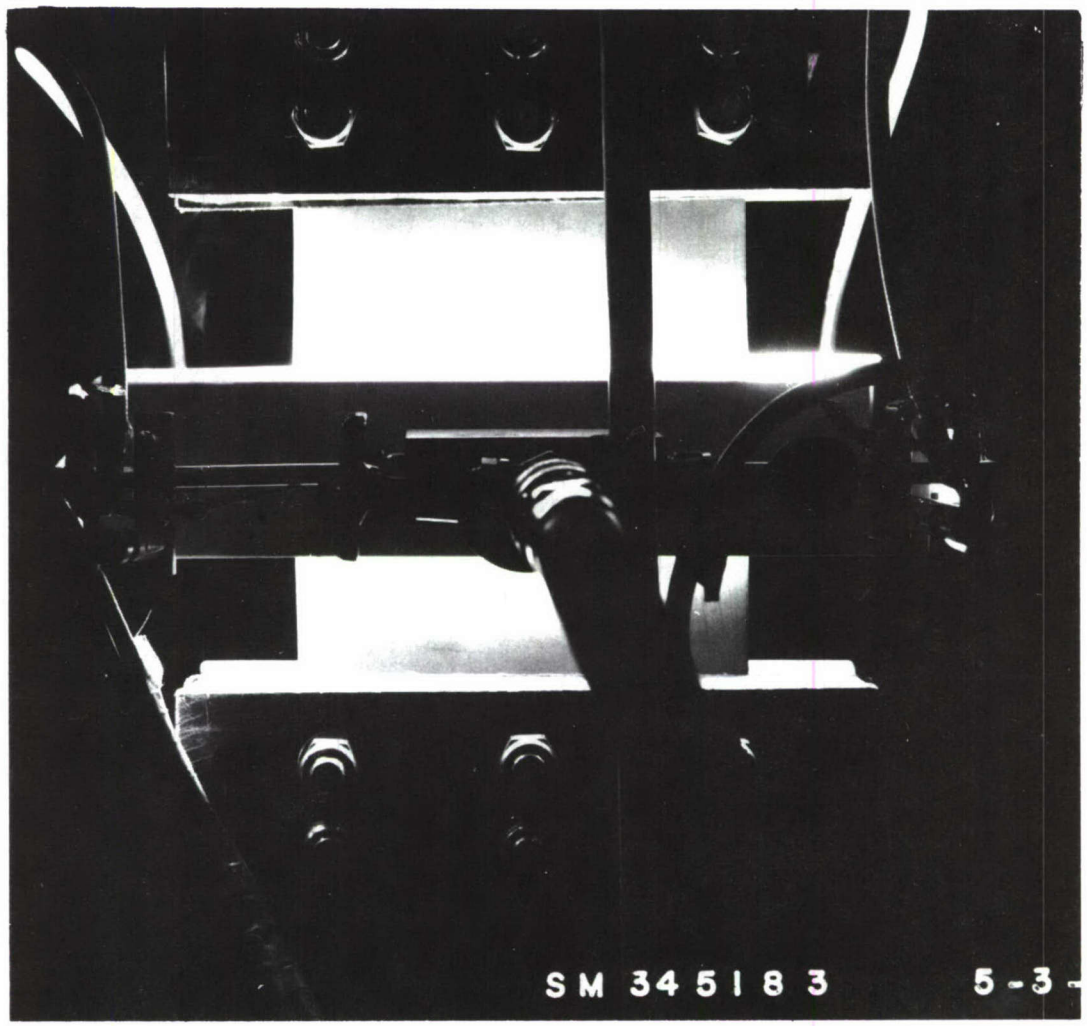


Figure 84. CENTER NOTCHED MOLYBDENUM TEST PANEL AT 2500°F

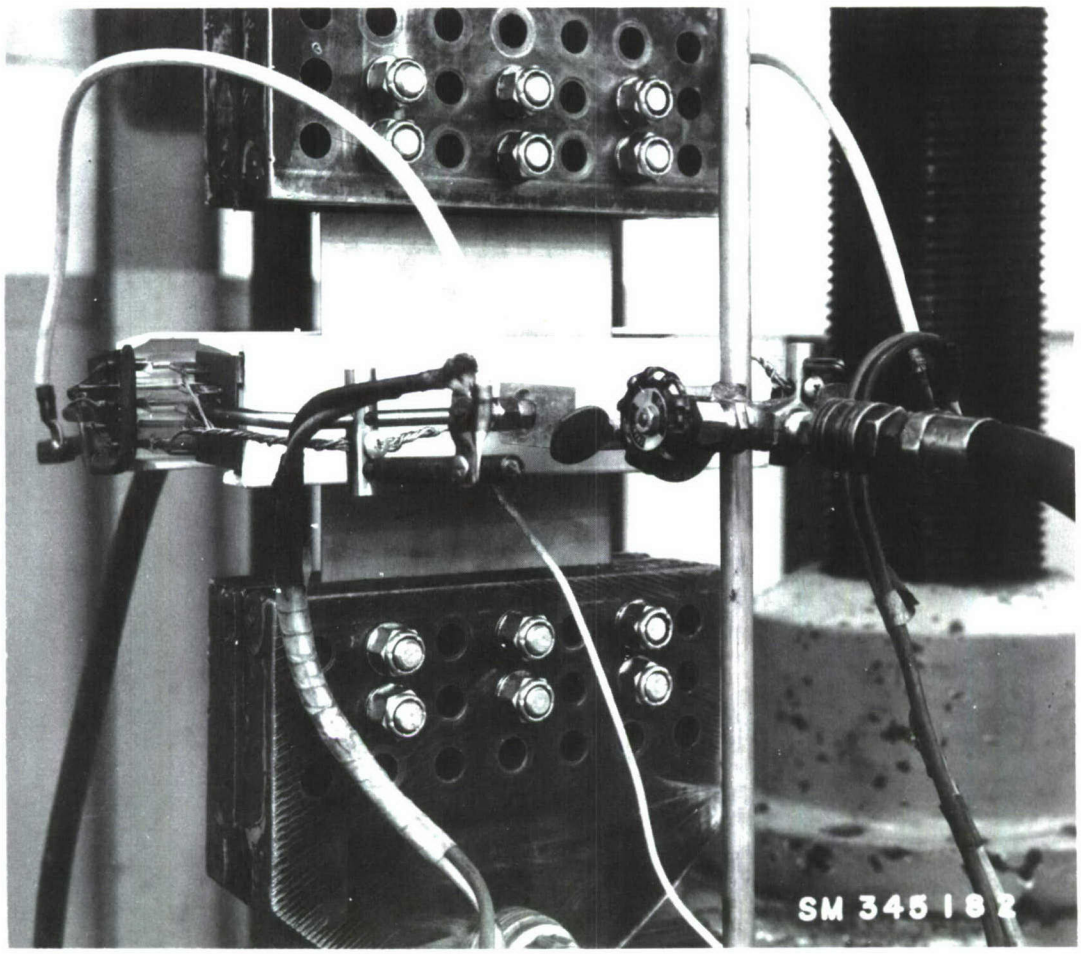


Figure 85. DETAIL OF HIGH TEMPERATURE TEST SET-UP

TABULATED TEST DATA

Spec No	W (in)	T_{crk} °F	T_{rupt} °F	σ_{crk} (ksi)	ℓ_c (in)	$y=\frac{\ell_c}{W}$	σ_r (psi)	n (cyc)
M 9	6	75	80	40	1.02	.170	100,600	24,700
M 7	6	75	80	40	.86	.143	100,000	18,600
M 3	6	75	- 340	40	.68	.113	57,670	17,200
M 6	6	75	- 320	40	.98	.163	72,670	16,950
M 1	6	75		40	.60			9,450
M 2	6	75		40	1.22			23,150
M 4	6	75		40	1.65			18,900
M 5	6	75	80	40	..73	.121	103,300	21,600
M 8	6	75		40	2.02			29,200
M10	6	75		40	2.41			20,500
Coated Molybdenum (W-2 and DB=DURAK-B)								
W2-1	6	80		40		-specimen broke-		100
W2-3	6	1,350		11.6 & var.		-badly oxidized-		95,000
W2-4	6	80	1,800	27.5	1.04	.174	26,300	132,000
W2-5	6	80		27.5		-specimen broke-		1,975
W2-6	6	80	1,398	25	1.00	.17	26,800	48,300
W2-7	6	80		25		-specimen broke-		34,350
W2-8	6	80		25	.67	.11	25,800	71,300
W2-9	6	80	80	25	.97	.16	57,600	90,300
DB-2	6	80	1,870	35	1.05	.175	30,250	var.
DB-3	6	80	1,867	35	1.06	.177	25,450	25,500
DB-4	6	1,350		11.6 & var.				

TABULATED TEST DATA

Spec No	W (in)	T_{crk} °F	T_{rupt} °F	σ_{crk} (ksi)	ℓ_c (in)	$y=\frac{\ell_c}{W}$	σ_r (psi)	n (cyc)
*Ta.-1	4	75	75	var. to 27	0.88	0.22	37,700	105,050
Ta.-2	4	75	- 310	var. to 27	0.92	0.23	53,000	81,600
W2-23	6	300	2,500	27.5	1.5	0.250	8,000	72,900
W2-10	6	250	2,500	25	1.03	0.172	11,333	75,550
W2-15	6	250	2,500	25	0.98	0.163	9,800	var.
Ww-16	6	250	2,500	25	0.97	0.162	12,166	77,700
W2-17	6	300	2,000	25	0.99	0.165	14,433	41,950
W2-18	6	300	2,000	27.5	0.98	0.163	18,633	var.
W2-19	6	300	2,000	27.5	1.00	0.166	15,533	61,000
W2-20	6	300	2,000	27.5	1.48	0.247	12,833	45,800
W2-21	6	300	2,000	27.5	1.50	0.250	16,666	103,700
W2-22	6	300	2,000	27.5	1.57	0.262	14,300	82,000
W2-24	6	300	1,600	27.5	1.51	0.252	32,333	115,250
W2-25	6	300	1,600	27.5	1.48	0.247	19,600	61,900
W2-26	6	300	1,600	30.0	1.52	0.253	21,466	66,800
W2-27	6	300	1,600	30.0	1.51	0.252	31,600	69,900
W2-28	6	300	1,600	30.0	1.50	0.250	32,666	101,900

* Tantalum panels.

TABULATED TEST DATA

Specimen	T_{rupt} °F	Lapse Time T_o-T_{max} (min.)	Soak Time At T_{max} (min)	Lapse Time P_o-P_{ult} (min.)
W2-23	2,500	5	0	2
W2-10	2,500	2	0	2
W2-15	2,500	4	0	1
W2-16	2,500	4	0	1 1/2
W2-17	+2,000	4	5	1
W2-18	+2,000	5	5	2
W2-19	+2,000	5	5	2 1/2
W2-20	+2,000	4	5	2 1/2
W2-21	+2,000	3	10	3 1/2
W2-22	+2,000	3 1/2	10	3
W2-24	1,600	4	10	4 1/2
W2-25	1,600	2	10	3 1/2
W2-26	1,600	4 1/2	10	3 1/2
W2-27	1,600	2	10	4 1/2
W2-28	1,600	3	10	5

All milled data.

TABULATED TEST DATA

Specimen (code)	W (in)	T_{crk} °F	T_{rupt} °F	σ_{crk} (ksi)	l_c (in)	y	σ_r (psi)
DB-10	6	*	2,000	*	2.50	Broke in set-up.	
DB-9	6	*	2,000	*	2.60	.433	10,690
DB-8	6	*	2,000	*	2.50	.416	10,320
DB-7	6	*	2,000	*	1.20	.200	
DB-6	6	*	2,000	*	2.10	.350	17,890
DB-5	6	*	2,000	*	2.10	.350	12,100
W2-42	6	*	2,000	*	2.50	.416	13,860
W2-41	6	*	2,000	*	2.45	.408	11,110
W2λ39	6	*	2,000	*	1.98	.330	14,100
W2-38	6	*	2,000	*	1.96	.326	18,100
W2-37	6	*	2,000	*	2.05	.341	11,760
W2-36	6	*	2,000	*	1.50	.250	19,620
W2-35	6	*	2,000	*	1.53	.255	14,290
W2-34	6	*	2,000	*	1.47	.245	15,170
W2-40	6	*	2,000	*	1.82	.303	17,090
W2-33	6	*	2,000	*	1.51	.251	17,410
W2-32	6	*	2,000	*	1.50	.250	17,170
W2-31	6	*	2,000	*	1.55	.258	21,400

* Saw slots.

SECTION 10

RESIDUAL STRENGTH OF CRACKED PANELS UNDER BIAXIAL STRESSING

The evaluation of the fracture strength of materials under biaxial-stressing conditions is rapidly becoming more important. The need for fracture strengths and residual strengths under only uniaxial conditions has a limited use in design.

It is realized that this is a far more complex problem to solve both experimentally as well as analytically, but it is believed that now is the time to put additional emphasis and effort into this case. Fracture testing under conditions of large stress gradients is an additional condition that has not received sufficient attention. The test data from the few biaxially stressed panels that have been tested in this program are centainly not sufficient for all of the design conditions that should be considered; however they do present some new data and possibly a new test technique. It is conceivable that the data and methods presented here may stimulate additional investigations as well as improved test techniques to obtain such allowables.

1. The test results of the biaxially stressed panels are shown in Figures 86 through 88. The data is for two materials, PH15-7 Mo RH950 steel and RENE' 41.

2. Figure 87 is a plot of the uniaxial and biaxial notched strength data on the material PH15-7 Mo RH950. The residual strength under biaxial conditions is lower than the uniaxial condition.

3. A threshold value of 92,000 psi was noted as the level for the transition from curved to straight running fractures.

   The letters "c" and "s" as noted on the plotted test points in Figure 88 represent the type of instability fracture in the biaxially stressed panels. The "c" denotes a curving fracture path and the "s" is straight running fracture. It can be seen from the plot that the curved fractures occurred at the higher stress levels. With the data available at this time, it has been shown that unstable fractures in a biaxial stress field will curve and have higher propagation velocities above 92,000 psi = σ_x = σ_y = σ_R. The significance of curving fracture paths in safe design is briefly discussed below.

4. On pages 153 through 155, photographs are shown of typical curved and straight fracture paths in the two materials under biaxial stressing.

5. The tabulated results for all of the biaxial tests are given in the table on page 156.

6. The procedure, technique and analytical methods used in conducting the biaxial (bulge panel) tests are given at the end of this section of the report.

Fracture Paths in Nonuniform Stress Fields

Figure 8, on page 78 of Reference 13 recalled the branching and curving fracture paths that have been observed in many full-scale fail-safe type structural tests. A review of the analysis and summary in Reference 13 suggested the possible need for additional study along these lines. The statement is made in the above reference that "a conservative estimate of the type of stiffener required for fracture arrest is obtained by assuming all cracks to propagate in a straight line." This statement is true. However the occurrence of curved fractures is also very important in the fail-safe behavior of structures. The path of a running fracture may curve because of a nonuniformity in the stress field resulting from various causes including, for example, rivet holes.

Figure 89 shows the results of an impromptu study on paper sheets containing initial cuts, representing cracks; and holes, representing rivet holes. The sheets were pulled apart under tension stress as indicated. When the propagating tear curved, entered a rivet hole and stopped, the fracture was classified as "safe". When the tear extended straight to the edge of the sheet, the fracture was said to be unsafe. The test was made for a number of sheets identical in every way except for variations in the crack length and rivet pitch.

The figure shows how the nature of the fracture depends on these parameters. When the tip of the crack is sufficiently far away from the rivet row, and the rivets are close enough together, the fracture curves, enters a rivet hole, and stops. When the crack tip is close to the rivet row and the rivets are far apart, the fracture extends clear across the sheet.

The data of Figure 89 were not collected for high strength metals; however, it is probable that the characteristics for these materials will be similar to those shown in this figure. The safe region was arbitrarily chosen as that region for which all fractures ran into holes. On this basis, optimum design arrangements may be conceived. At first glance, multiple rows with staggered pitch spacing seem most efficient in this respect.

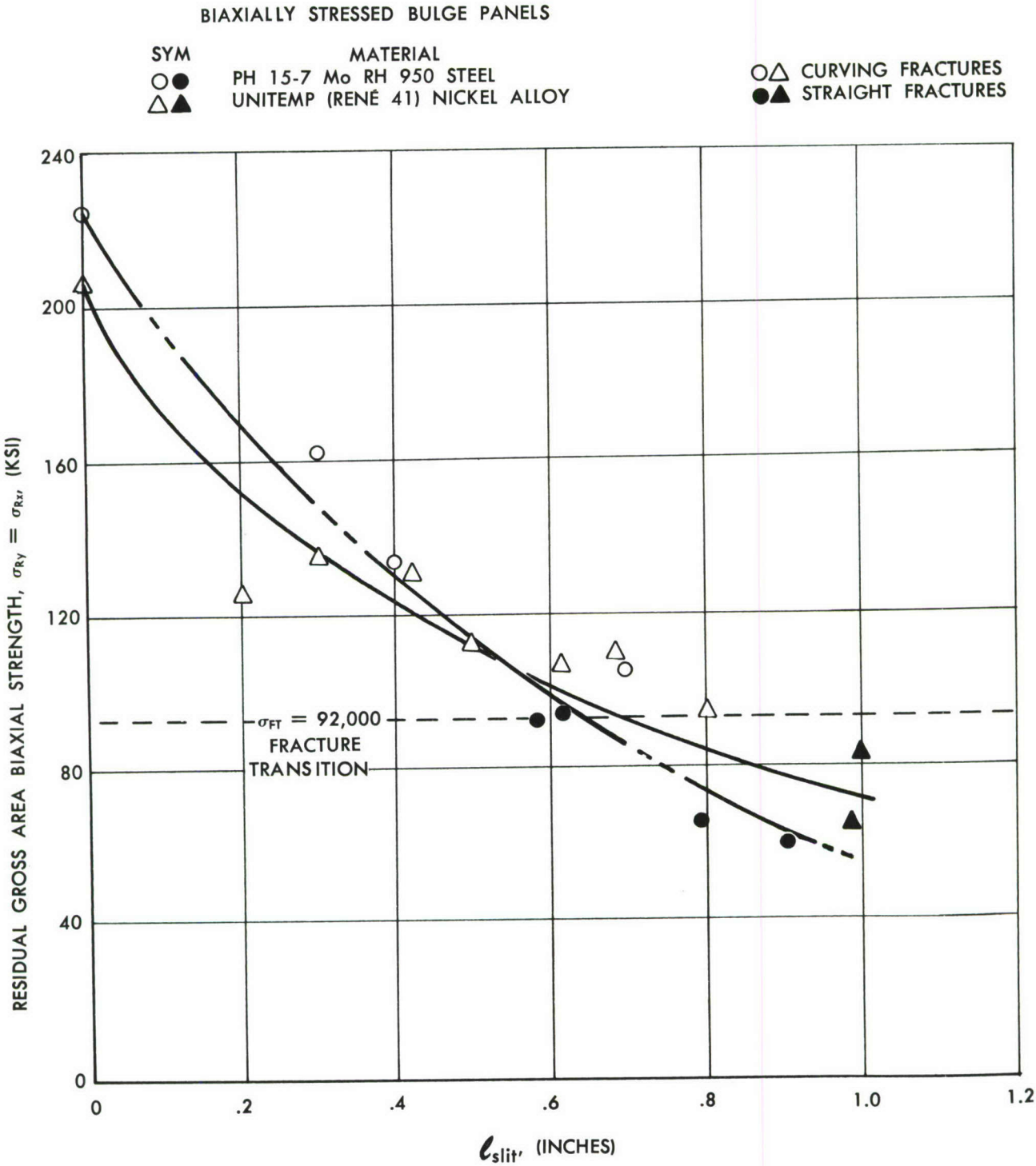


Figure 86. RESIDUAL STRENGTH vs CRACK LENGTH UNDER BIAXIAL LOADING

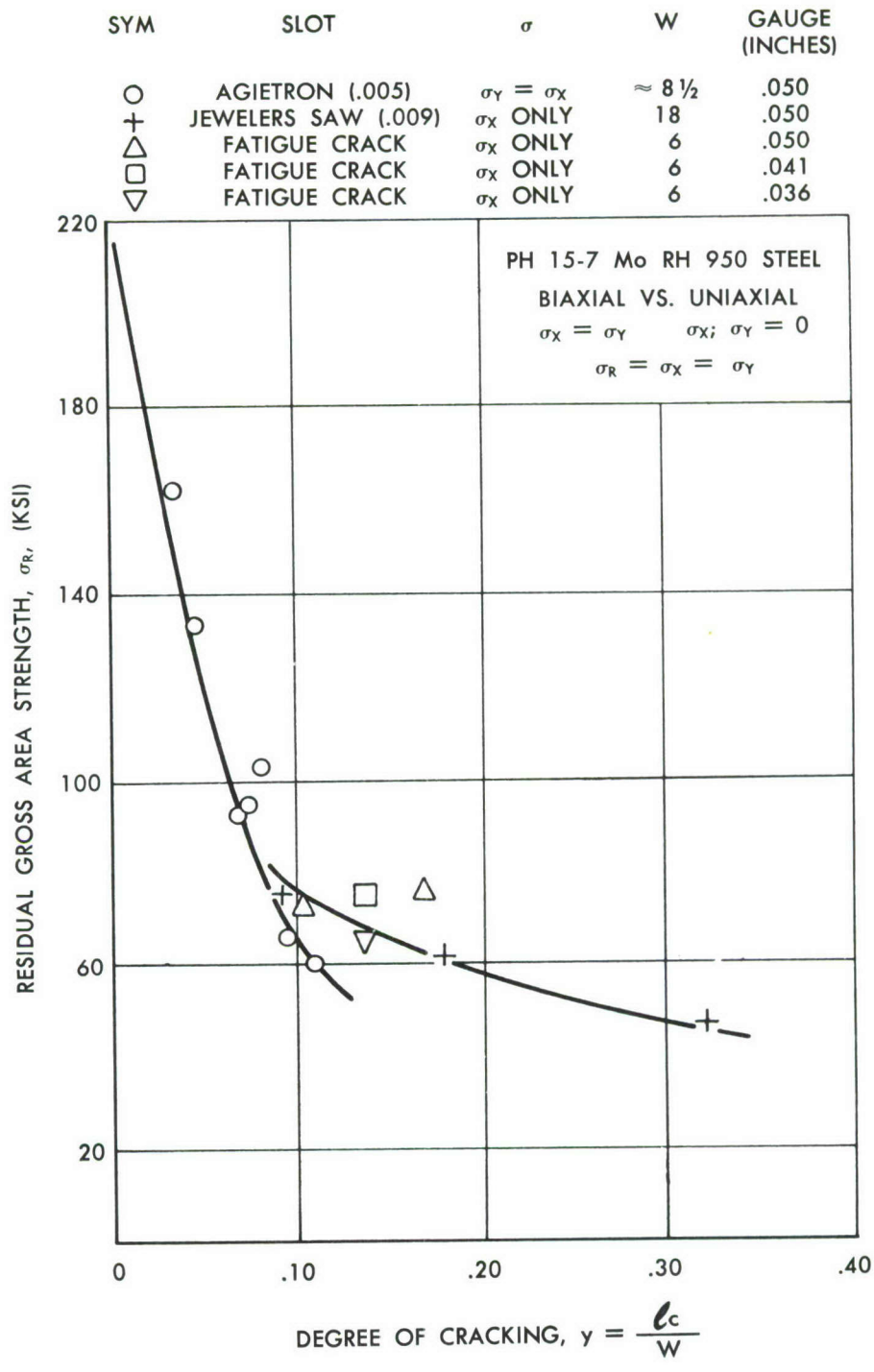


Figure 87. RESIDUAL STRENGTH vs CRACK LENGTH UNDER BIAXIAL LOADING

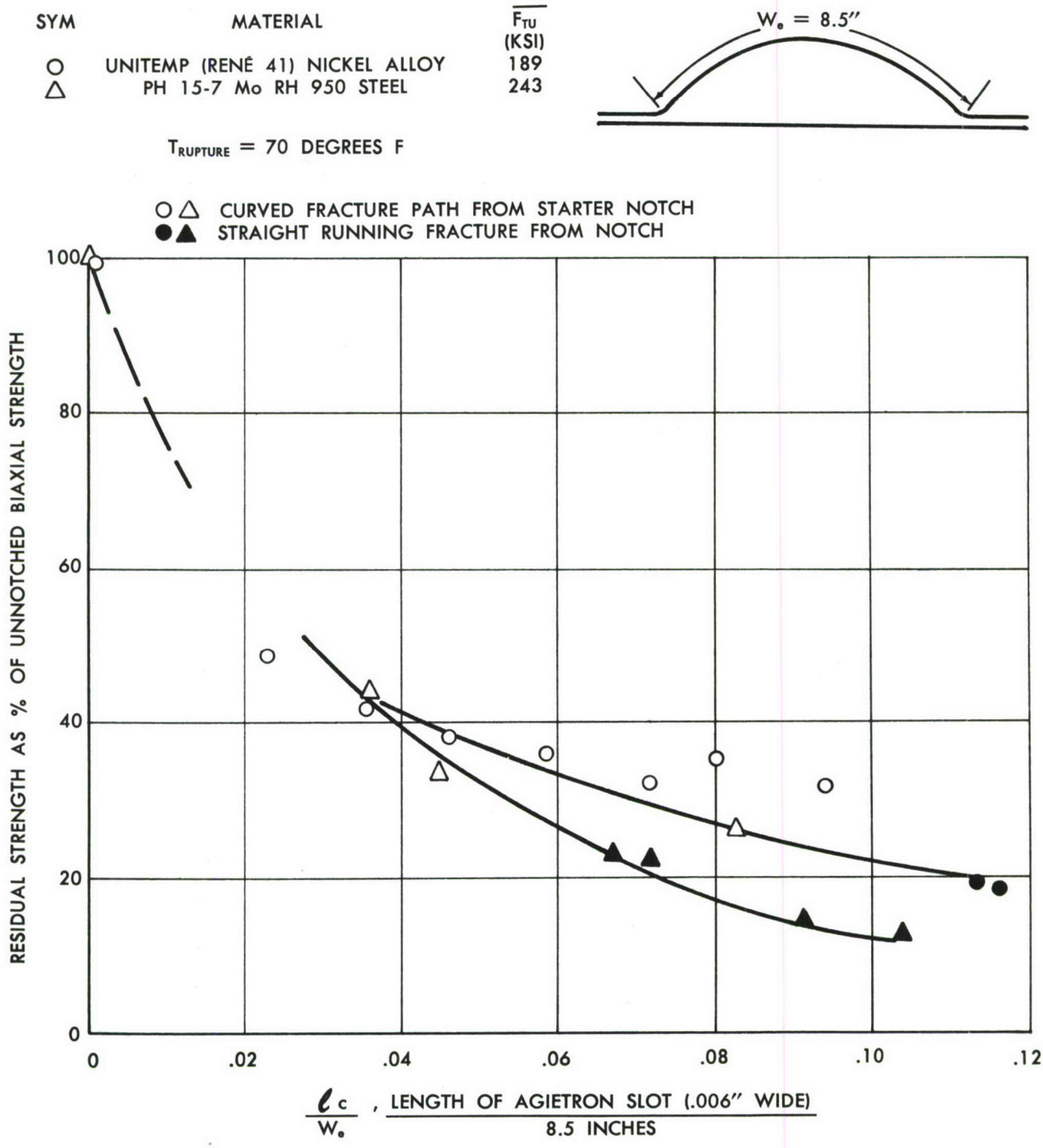
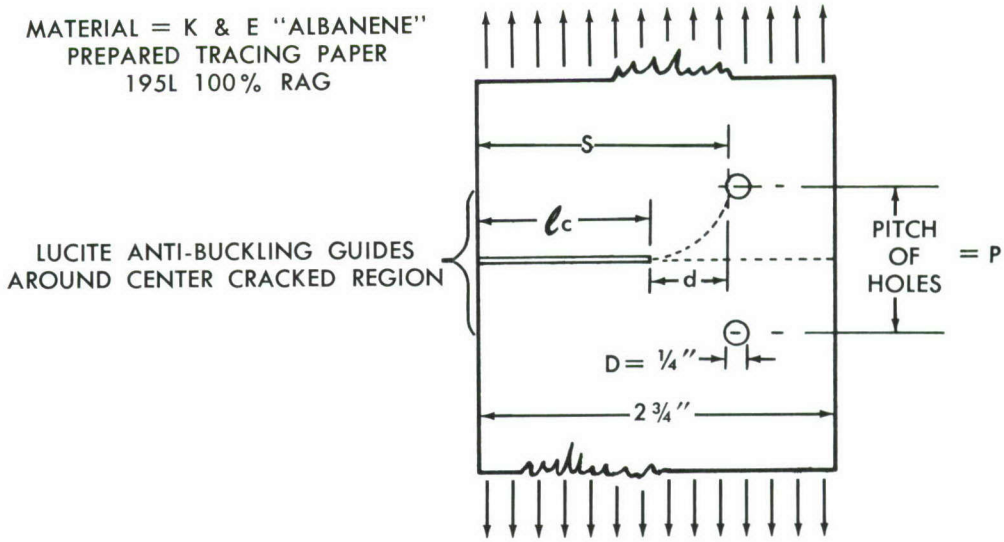


Figure 88. RESIDUAL STRENGTH vs CRACK LENGTH UNDER BIAXIAL LOADING



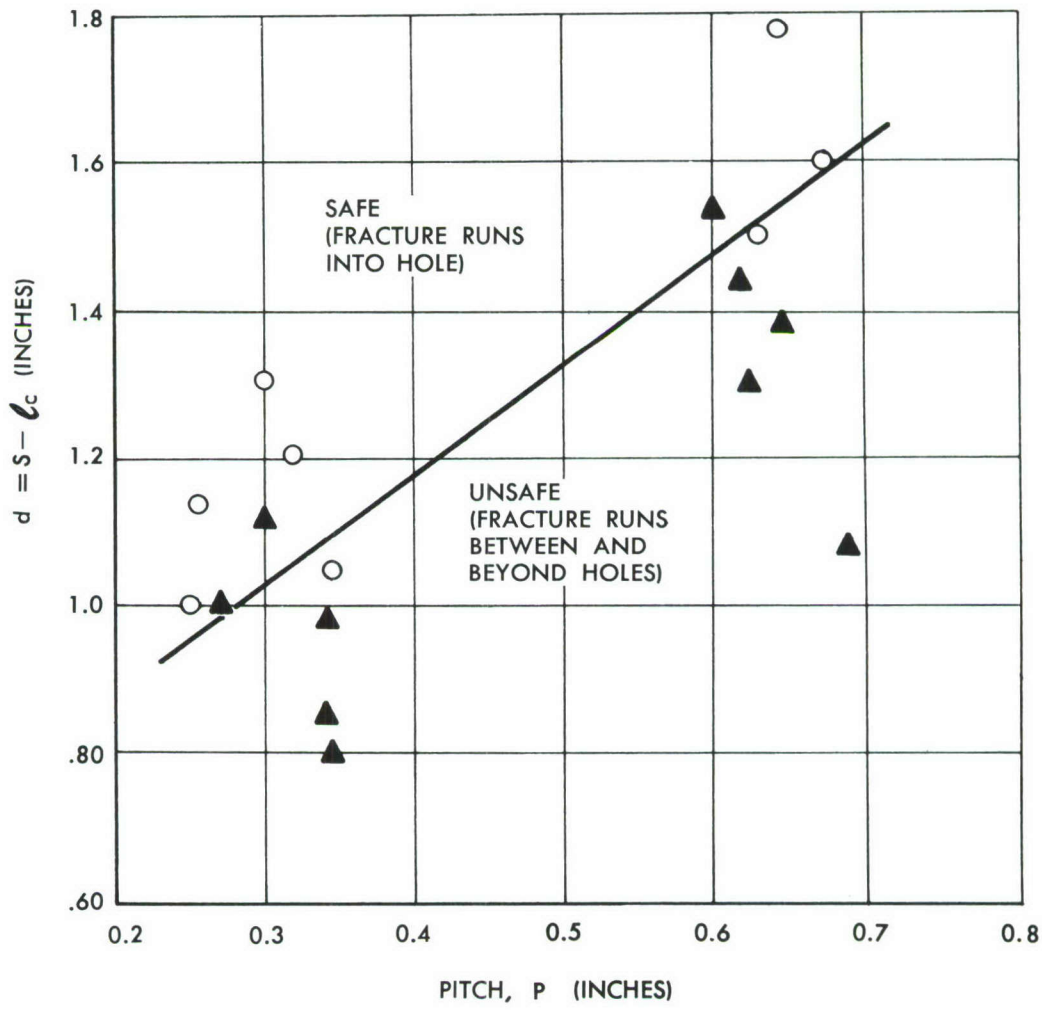


Figure 89. SAFE TO UNSAFE FRACTURE

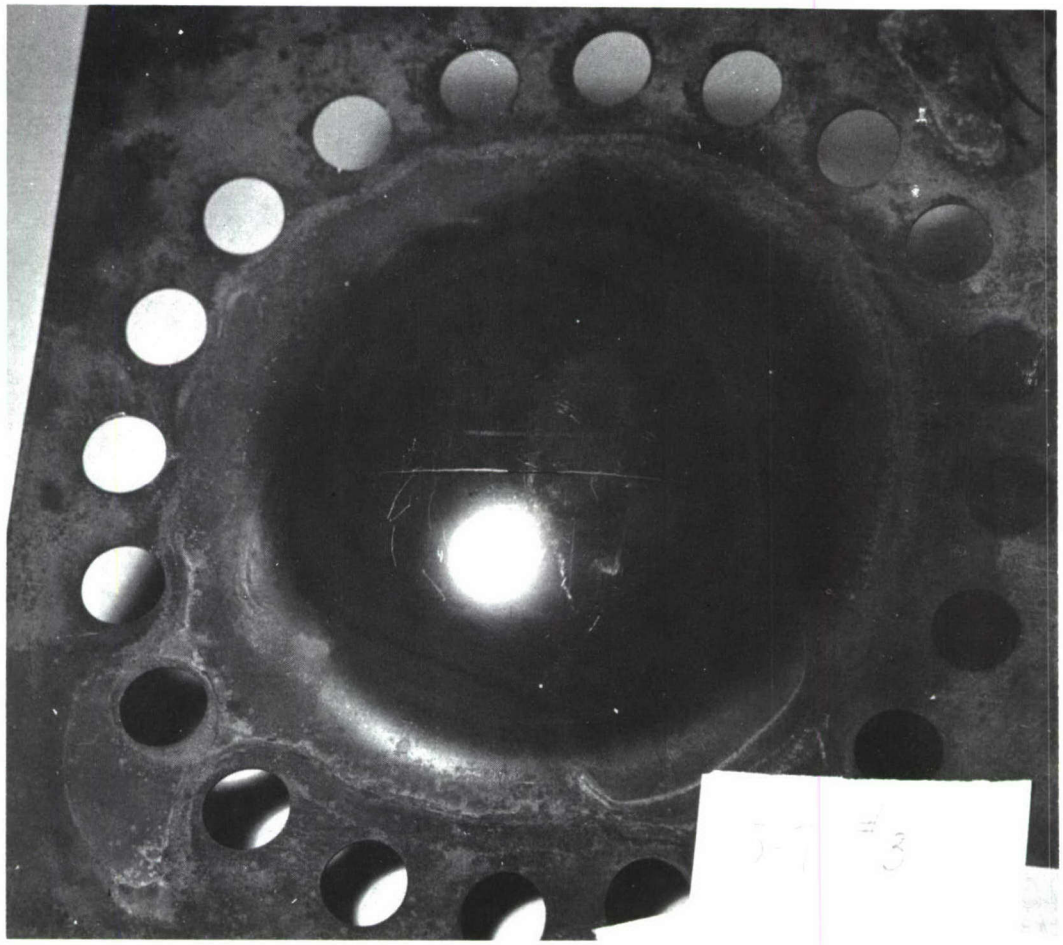


Figure 90. STRAIGHT RUNNING FRACTURE

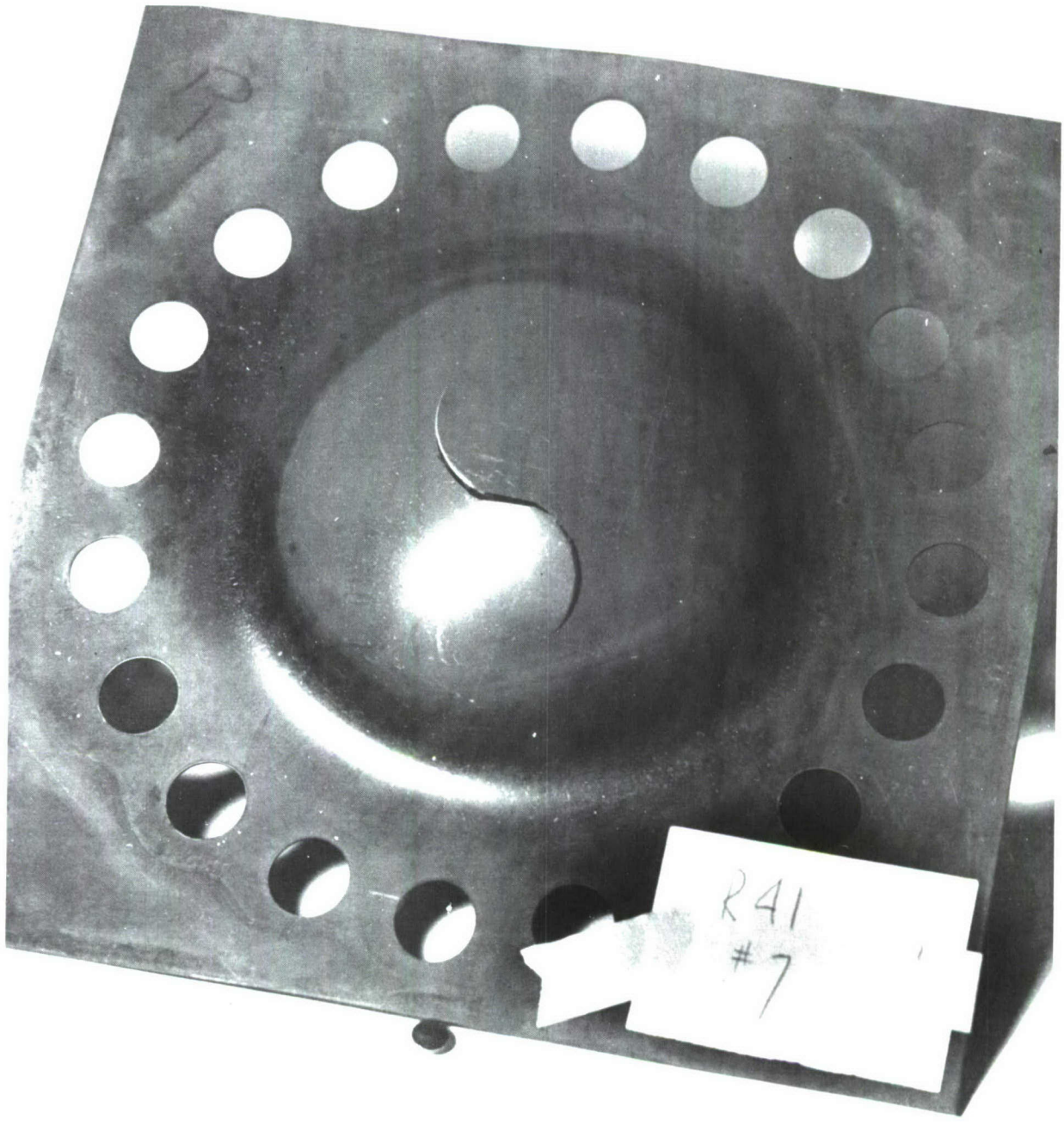


Figure 91. CURVED RUNNING FRACTURE

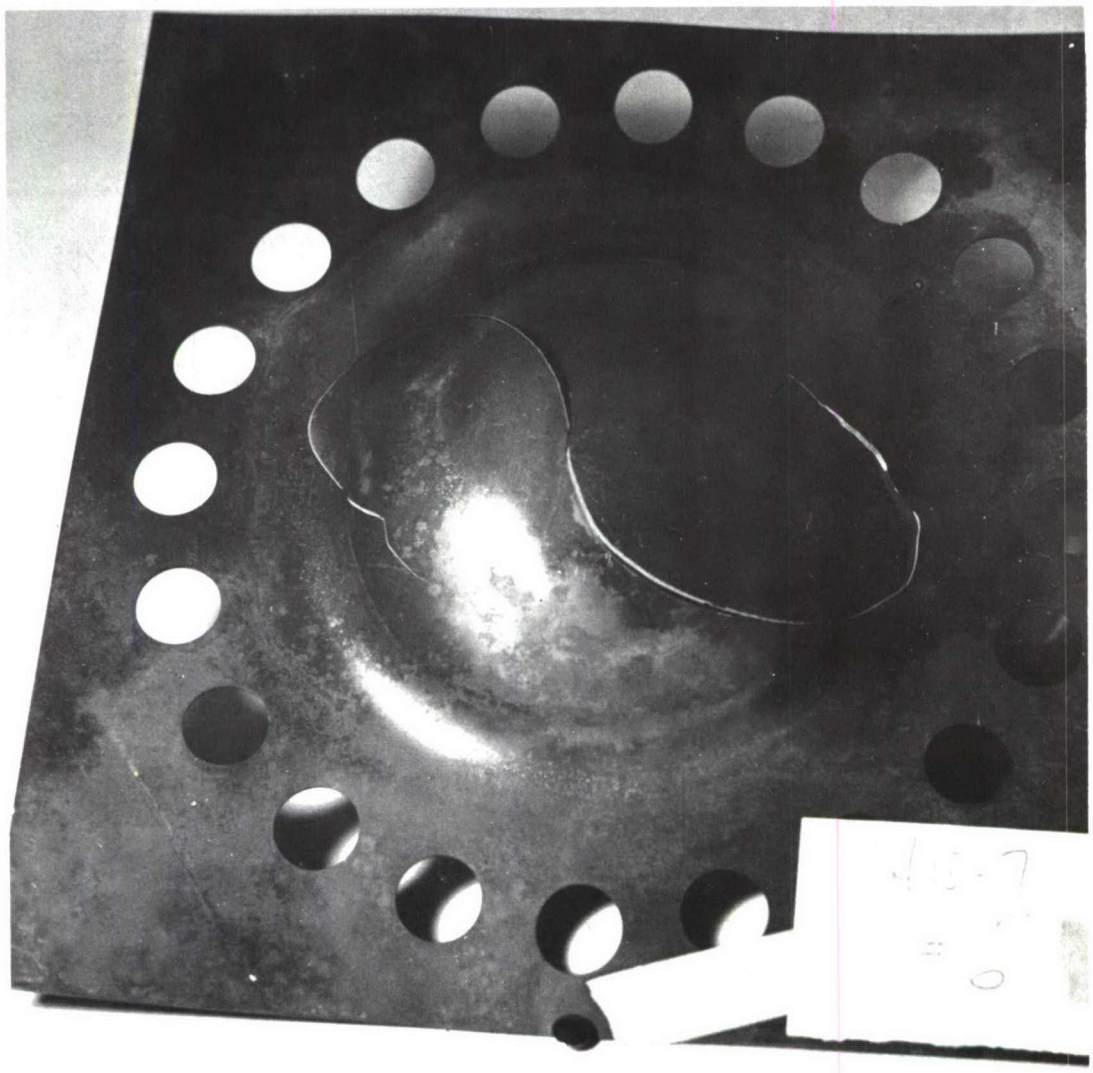


Figure 92. CURVED RUNNING FRACTURE

TABULATED DATA

BIAXIAL TESTS

Panel	Material	ℓ_c (in.)	$\sigma_r=\sigma_x=\sigma_y$	(a) y	(b) Fracture Path	$\frac{\ell_c}{2r_i}$	r_i, (in.)
1	PH15-7Mo	0.58	92,844	.0682	S	.0435	6.68
2	RH 950	0.40	134,161	.0470	C	.0298	6.71
3	RH 950	0.62	95,387	.0730	S	.0452	6.86
4	RH 950	0	222,548	0	X	0	4.32
5	RH 950	0.79	66,541	.0930	S - C	.0575	6.88
6	RH 950	0.30	161,961	.0353	C	.0227	6.62
7	RH 950	0.90	60,194	.1060	S	.0670	6.71
8	RH 950	0.70	104,958	.0824	C	.0520	6.74
1	Rene' 41	1.00	81,681	.1180	S	.0855	5.85
2	Rene' 41	0	205,997	0	X	0	4.21
3	Rene' 41	0.30	136,478	.0353	C	.0255	5.87
4	Rene' 41	0.40	132,051	.0470	C	.0334	5.99
5	Rene' 41	0.20	127,046	.026	C	.0185	5.41
6	Rene' 41	0.50	111,057	.0588	C	.0437	5.71
7	Rene' 41	0.68	109,873	.0800	C	.0585	5.82
8	Rene' 41	0.98	65,470	.1150	S	.0915	5.36
9	Rene' 41	0.61	106,248	.0720	C	.0521	5.85
10	Rene' 41	0.80	93,828	.0940	C	.0745	5.38

( ) Length of Agietron formed slit (Appendix C).

(a) y in these tests has been taken as $\ell_c \frac{\circ}{t}$ an effective width of 8.5 inch. The 8-1/2 inch dimension is the circumferential distance of the panel across the jig-bolt-ring.

(b) S = straight, C = curved, X = explosive rupture.

Procedure For Conducting Biaxial-Stress Bulge Panel Tests

The following discussion describes the development of a measuring technique and the measurements that are necessary in the analysis of bulge panel test data.

The evaluation of materials under the biaxial conditions described here (bulge pressure testing) requires that the arc-height of the test panels be continuously measured during the test. It is necessary that the arc-height of a segment of the partially hemisperical panels be measured and recorded as a function of pressure throughout the hydrostatic test period. Such a measuring device has been developed by the Douglas Company and can be used with the bulge panel test apparatus shown in the diagrammatic sketch of Figure 93.

One type of arc-height measuring device developed is shown in Figure 94. The center (floating) stem-plunger point actuates a dial gage and subsequently a microformer, providing both visual readout and recording capabilities. This type of test set-up is satisfactory in the elastic range of stressing and calibration but should not be used for fracture or burst testing. Rupture of the test panel would damage the dial gauge and microformer. A second type of set-up eliminates the dial gauge and with a rigid base support protects the microformer so that it can be used both up to and during fracture of the test panels.

Figure 95 shows the test recording arrangement with a dial gage attached to the microformer and recording head for calibration. The operation of this system is somewhat involved since the microformer sensing unit operates on AC and the recording unit (X-Y recorder) operates from a DC signal input. The input to the microformer is supplied by an oscillator, 600 cycles per second, three volts AC, and is checked with a vacuum tube voltmeter. The motion of the core of the microformer, i.e., the motion of the center stem-plunger of the head, varies the output in proportion to the distance traveled. This output signal is rectified by the demodulator and hence fed to the X axis of the recorder. It is found that the output of the microformer was not linear except over a central 0.100 inch range. As the core passed through the microformer, the output voltage decreased to a null point and then increased. This null point is the center of the linear range of the microformer and may be determined with the aid of the vacuum tube voltmeter to monitor the output voltage.

When a test is to be conducted, the initial arc-height of the bulge specimen must first be determined. The head with a dial gage attached (Figure 94) is used to accomplish this. The dial gage is read first with a flat piece of steel across all three points. The dial gage is then read while the device rests on the bulge specimen in position for test. The difference of the two readings is the original arc-height of the bulge before test. With the dial gage still in position, the recorder is calibrated in such a manner that the core of the microformer starts the test within the first 0.010 inch of the linear range. Since the relationship between the two fixed points and the center moving point is determined by the bulge specimen to be tested, the microformer itself may be moved in its mount (Figure 95) to establish the relationship between microformer and core that produces linear output signal.

A block diagram of the instrumentation system, including the pressure sensing system, is shown in Figure 97. A 20,000 psi pressure transducer is hooked to a balance panel powered by two power supplies. The output from the balance panel is fed to the Y axis of the X-Y recorder. The small DC voltmeter is used to monitor the power supplies. Only one channel of the balance panel and one of the power supplies were used during these tests. This device, with the use of the microformer, thus provides a continuous measurement of arc-height during the bulge pressure testing. The arc-height is automatically plotted as a function of test pressure on an X-Y recorder (Figures 96 and 98).

Analysis of a bulge panel test is then accomplished by manually extracting values of pressure in (psi) and values of arc-height (h) in inches from the X-Y graph. A rather simple program incorporating the following equations and measurements is then carried out in an LGP 30 computer. The resulting analysis provides a table of stress levels as a function of hydrostatic test pressures. The fracture stress, burst stress, or residual strength, in this case, is taken as the highest value of stress attained.

Bulge panel characteristics measured:

t_n =	nominal thickness	reflectoscope measurement (inches)
h =	arc-height (inches)	X axis on recorder
p =	hydrostatic pressure (psi)	Y axis on recorder
s =	arc-length (inches)	Constant

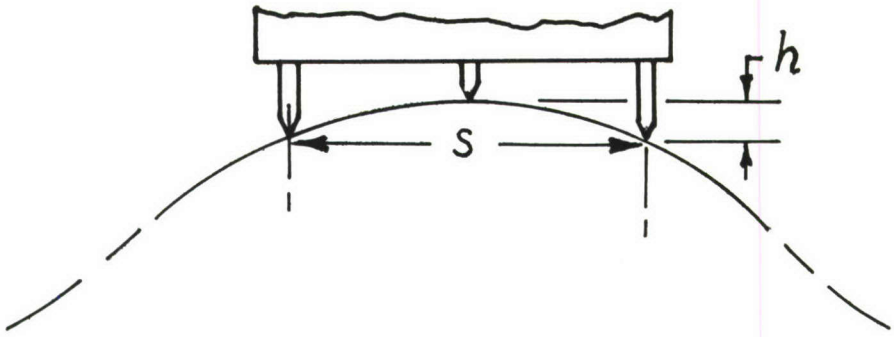
From these measurements the outside and inside radii of the bulge test panel are calculated with the aid of the following equations:

$$r_o = \frac{s^2}{8h} + \frac{h}{2} \tag{1}$$

$$r_i = r_o - t_n \tag{2}$$

The stress is then calculated from:

$$\sigma_y = \sigma_x = \sigma_r = \frac{p \cdot r_i}{2\, t_m} \tag{3}$$



The notches in the bulge panels were performed by the electric-arc discharge method. See Appendix C. Varying lengths of slits .006" in width were formed 1/2" from the center line and crown of the panels. The various lengths of notches (slits) are listed in the tabulated data on page 156.

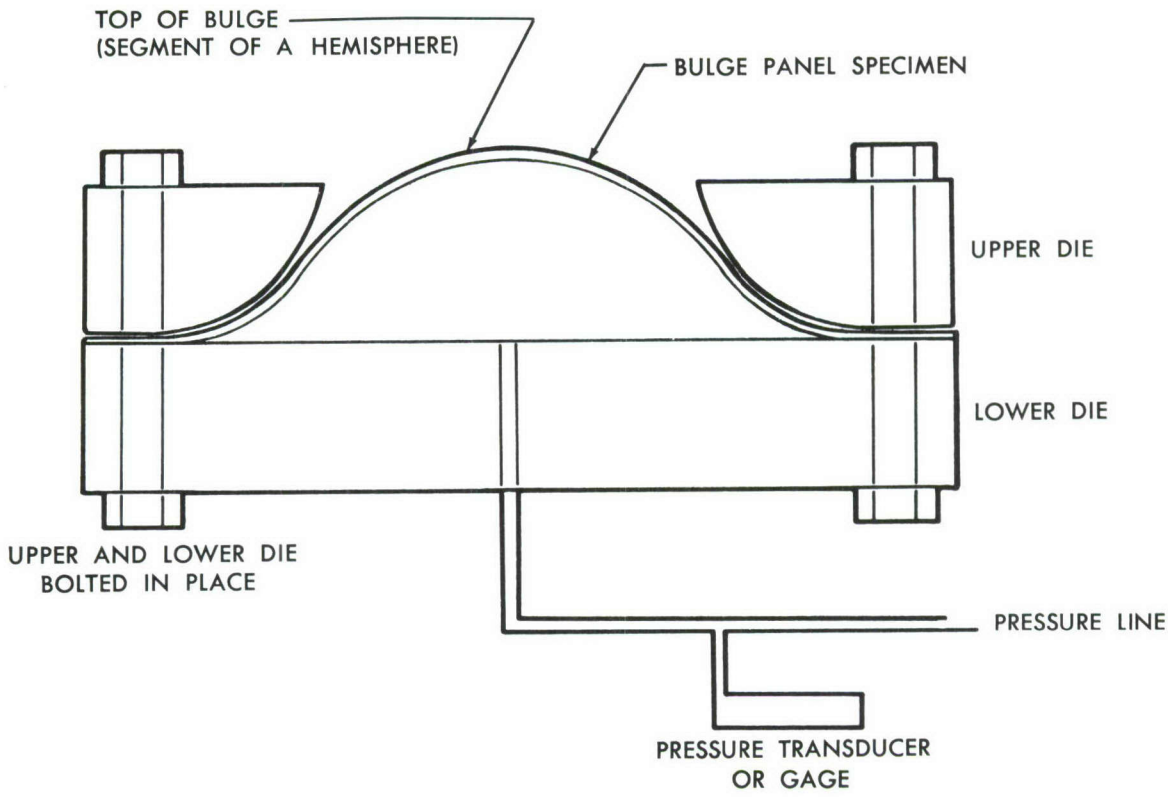


Figure 93. CROSS-SECTION OF BULGE SPECIMEN TEST APPARATUS

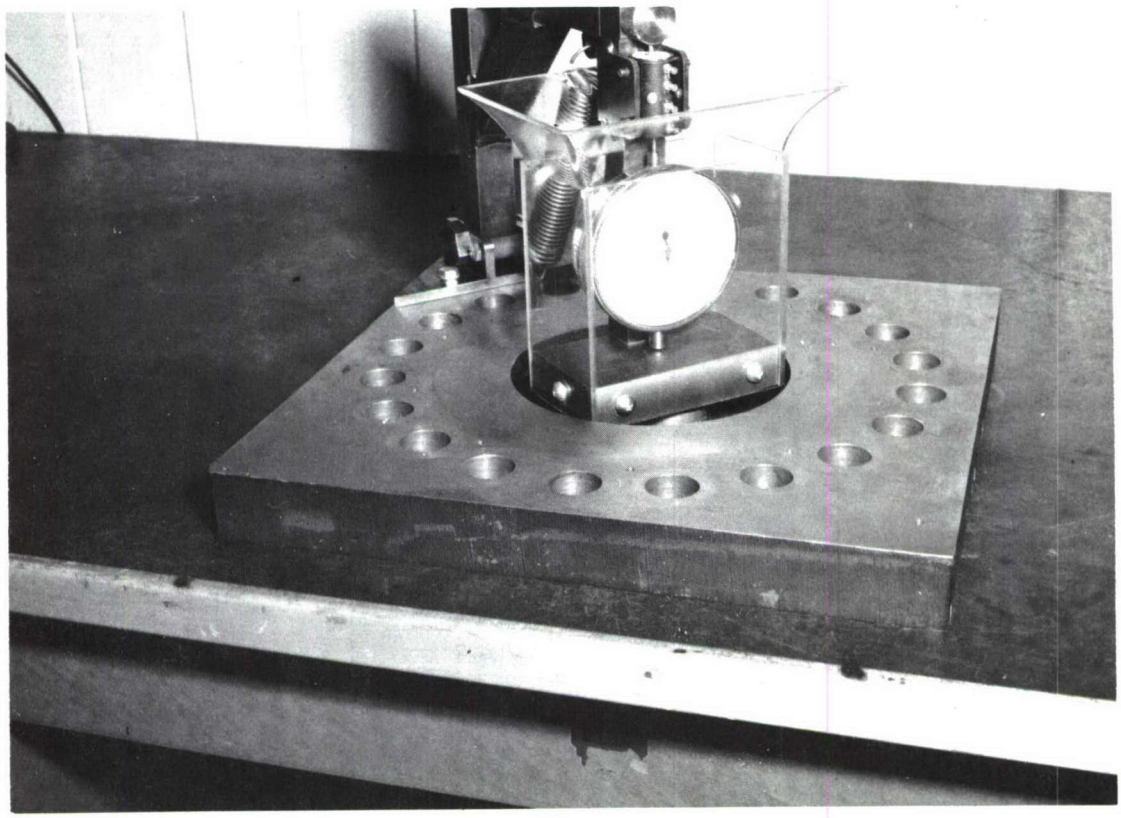
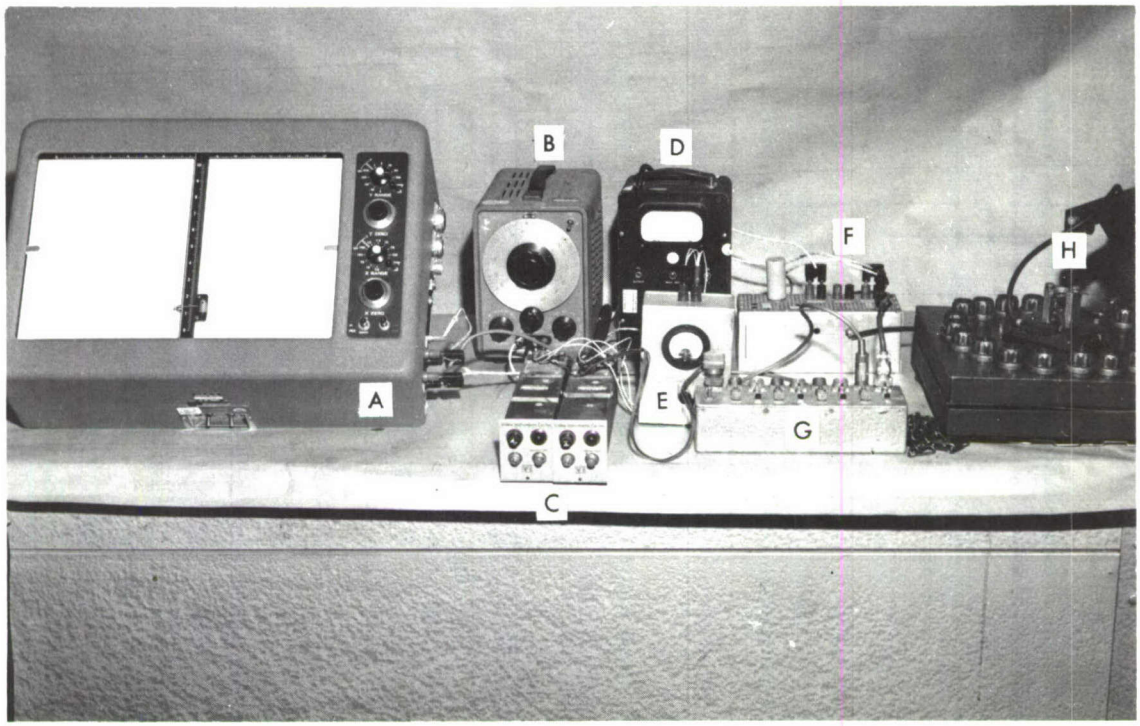


Figure 94. BULGE ARC-HEIGHT MEASURING DEVICE — TYPE 1



Figure 95. BULGE ARC-HEIGHT MEASURING DEVICE — TYPE 2



A. X-Y RECORDER

B. OSCILLATOR

C. D. C. POWER SUPPLY

D. VACUUM TUBE VOLTMETER

E. D.C. VOLTMETER

F. DEMODULATOR

G. BALANCE PANEL

H. RECORDER HEAD

Figure 96. TEST RECORDING AND PRELIMINARY CALIBRATION EQUIPMENT

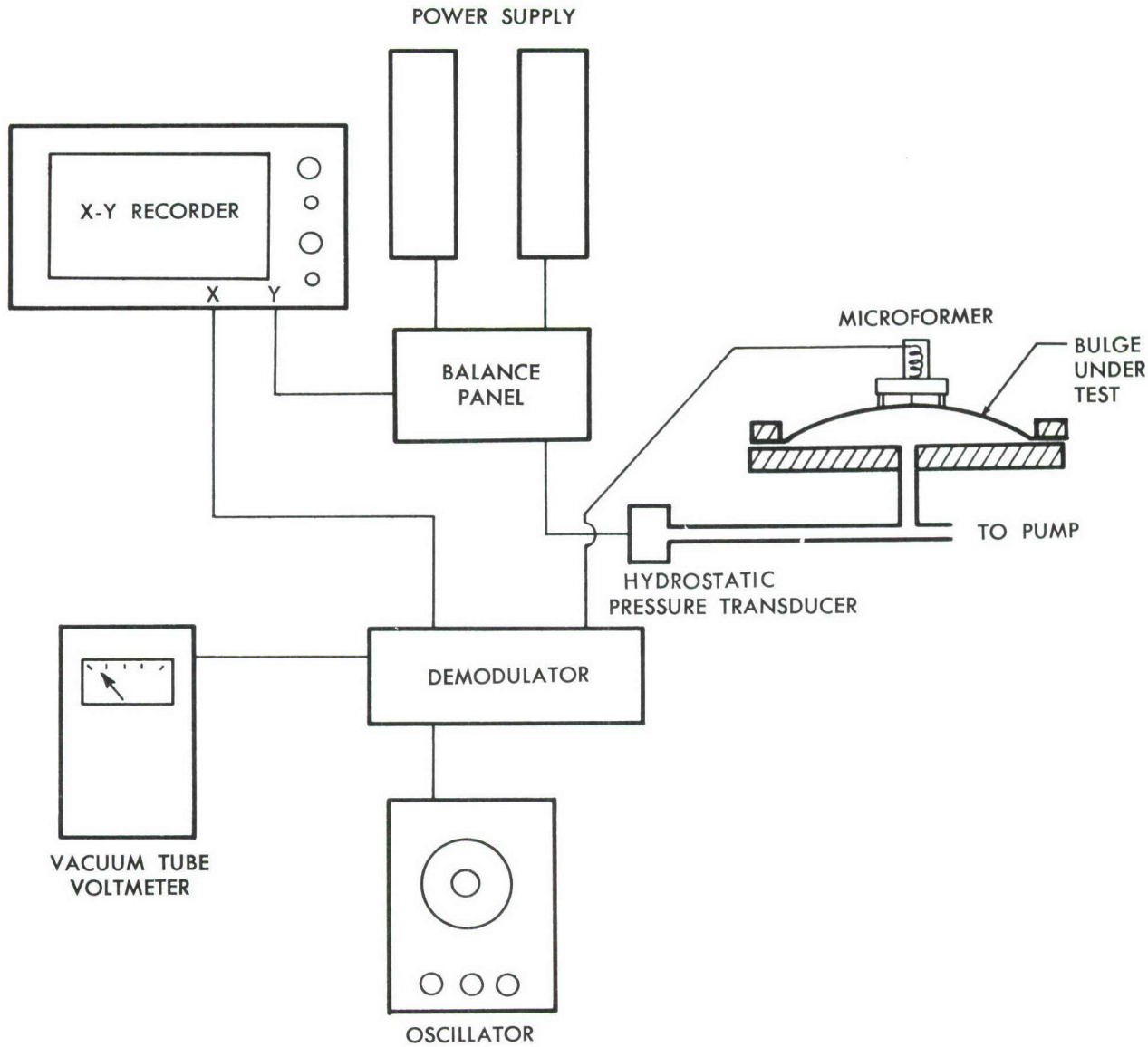


Figure 97. BLOCK DIAGRAM OF BULGE PANEL ARC-HEIGHT vs PRESSURE RECORDING SYSTEM

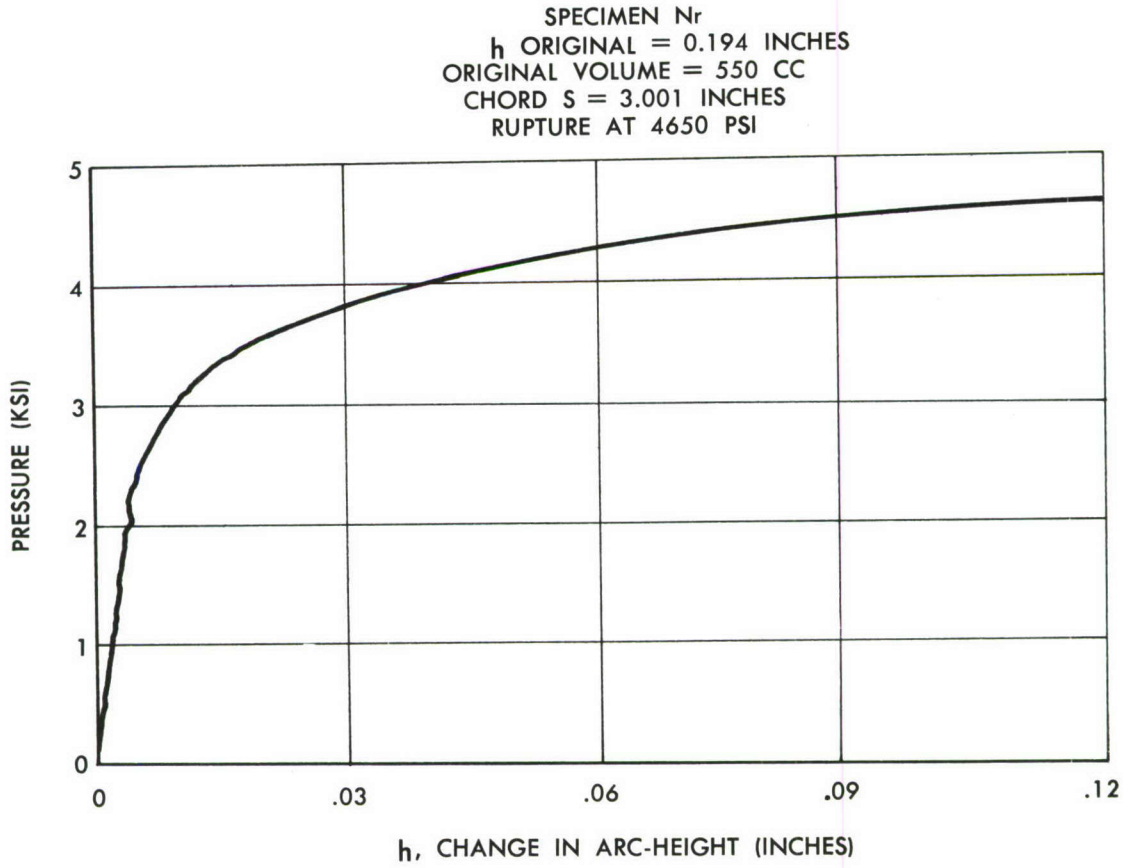


Figure 98. TYPICAL XY RECORDING OF BULGE ARC-HEIGHT CHANGE vs PRESSURE INCREASE

SECTION 11

RESIDUAL STRENGTH TESTS OF STRUCTURALLY STIFFENED STEEL PANELS CONTAINING CRACKS

Panel Description

Two structurally stiffened steel panels were fabricated and tested. These panels were 20 inches wide by 40 inches long. The panel skin was .050 PH15-7 Mo. RH950 sheet which was rolled in the 40-inch direction. Four stringers and crack arresting strips were riveted to the sheet, providing three 6-inch bays, with 1 inch edge distance on each side of the panel. The stringers were brake-formed in the shape of zee sections 1-1/4 inches high with 7/8 inch wide legs using .050 PH15-7 Mo. steel sheet stock. Crack arresting strips consisting of 2 inch x .020 1/2 H stainless steel were added in order to arrest the running fracture as it entered the reinforced regions and reduced stress fields. The stringers and arresting strips were fastened to the skin with 1/8 inch diameter 17-7 PH steel rivets. The panel is shown in Figure 100.

Method of Testing

End plates were fabricated, spaced with doublers and attached to the specimen such that the applied tensile load was at the neutral axis of the panel. An initial crack was then introduced into the panel by the following method: In the desired section of the panel center bay a rivet was removed from the row nearest to the neutral axis and attaching the crack arresting strip to the panel skin. A rotary file was then used to cut the panel transversely across the center bay to within 1/32 inch of the desired length. The starter crack was then completed at the end of the slot with a jewelers model hand saw which was .009 inches thick.

The panel specimens were tested in a 400,000 pound Capacity Southwark Emery testing machine. A loading rate of approximately 50,000 pounds per minute was applied to each specimen.

After completion of each test, a skin splice was accomplished so that additional tests could be conducted. It is believed that the location of the saw cuts and failures were such that the skin splices (patches) had no direct effect on the subsequent test results:

Summary of Test Results

1. The residual strengths of the stiffened cracked panels are shown in Figure 99.

2. The prediction of the stiffened panel strengths from the 4" and 18" wide unstiffened panels is shown by the analytically calculated curve. The calculated curve is based on the formula for unstiffened panels. Use of the formula in this application is "stretching a point."

3. The unstable fractures in all of the stiffened panel tests were arrested by the crack arrest structure.

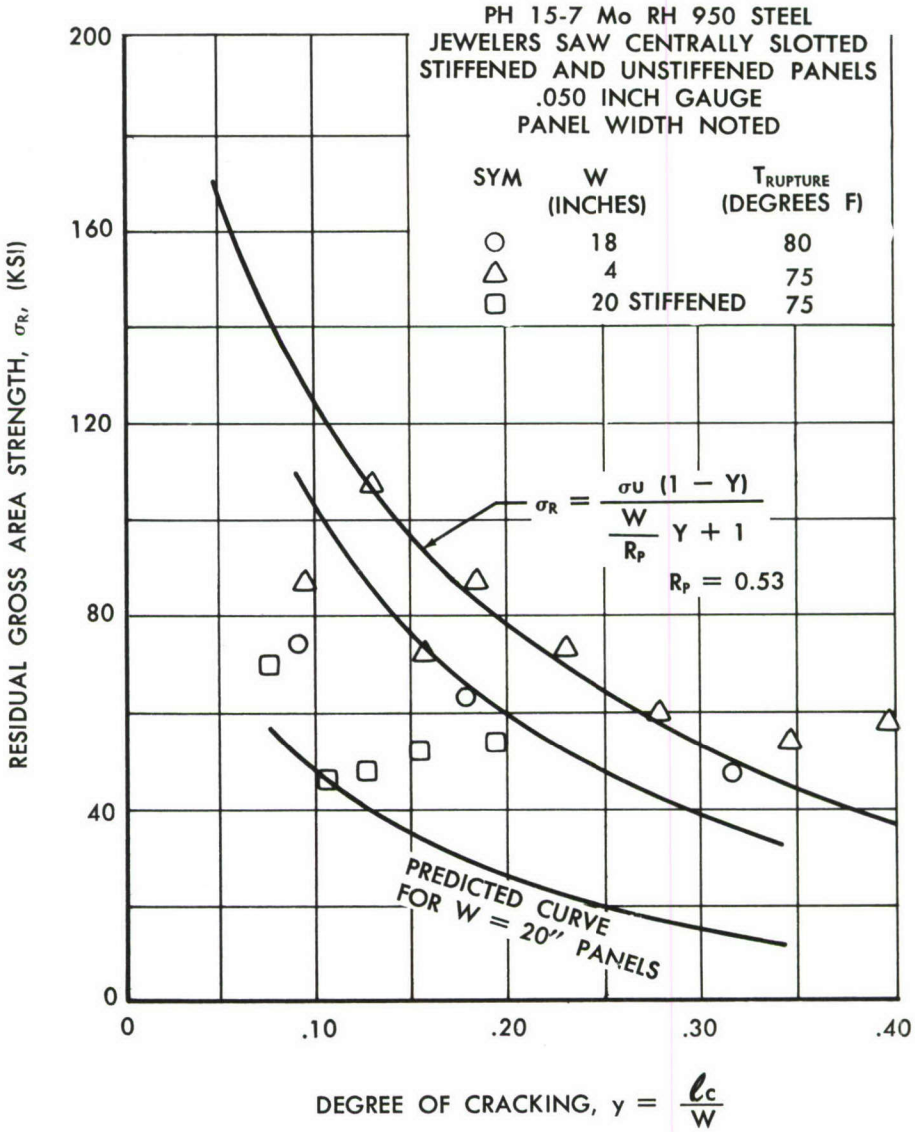


Figure 99. RESIDUAL STRENGTH vs DEGREE OF CRACKING

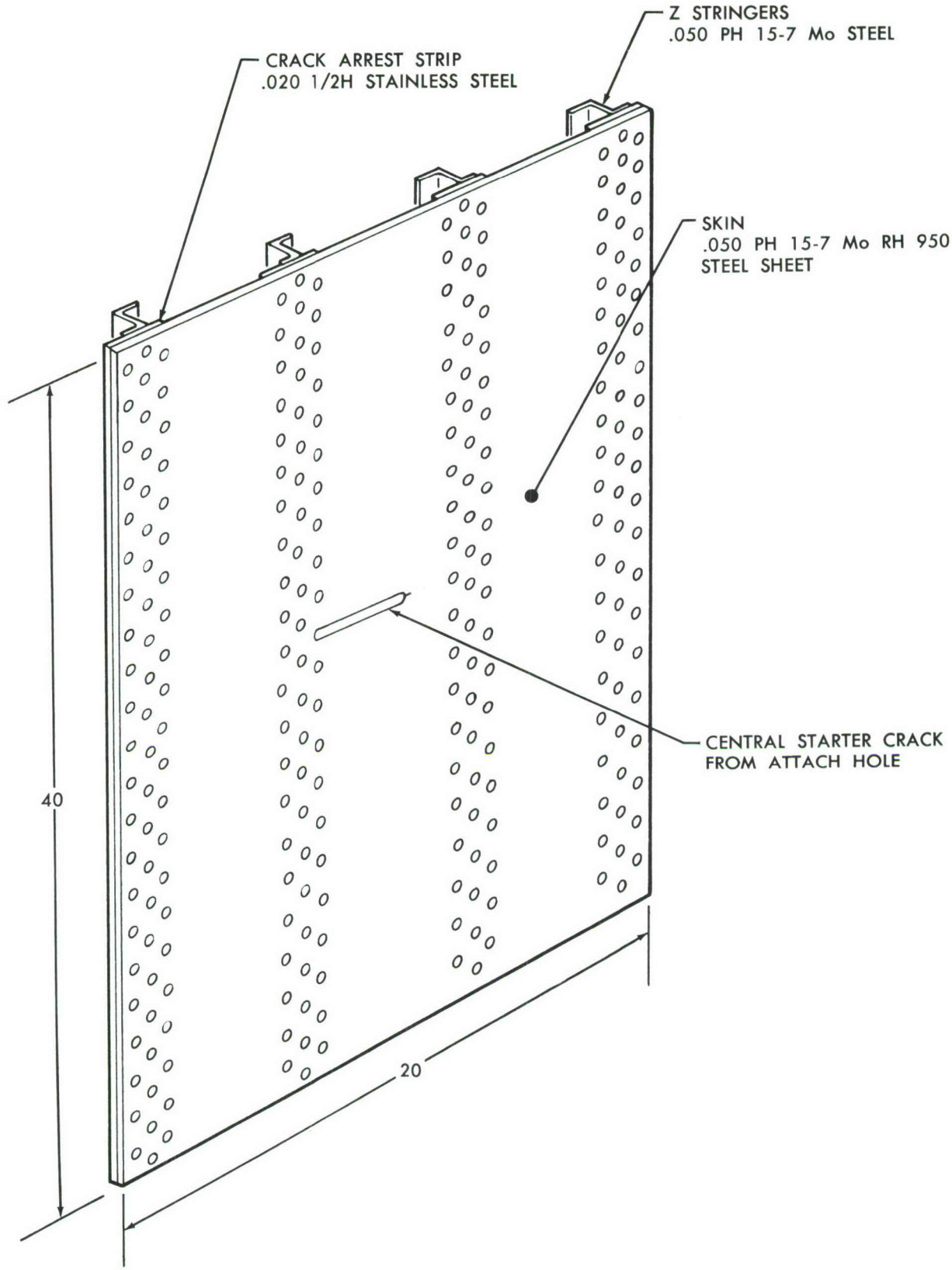
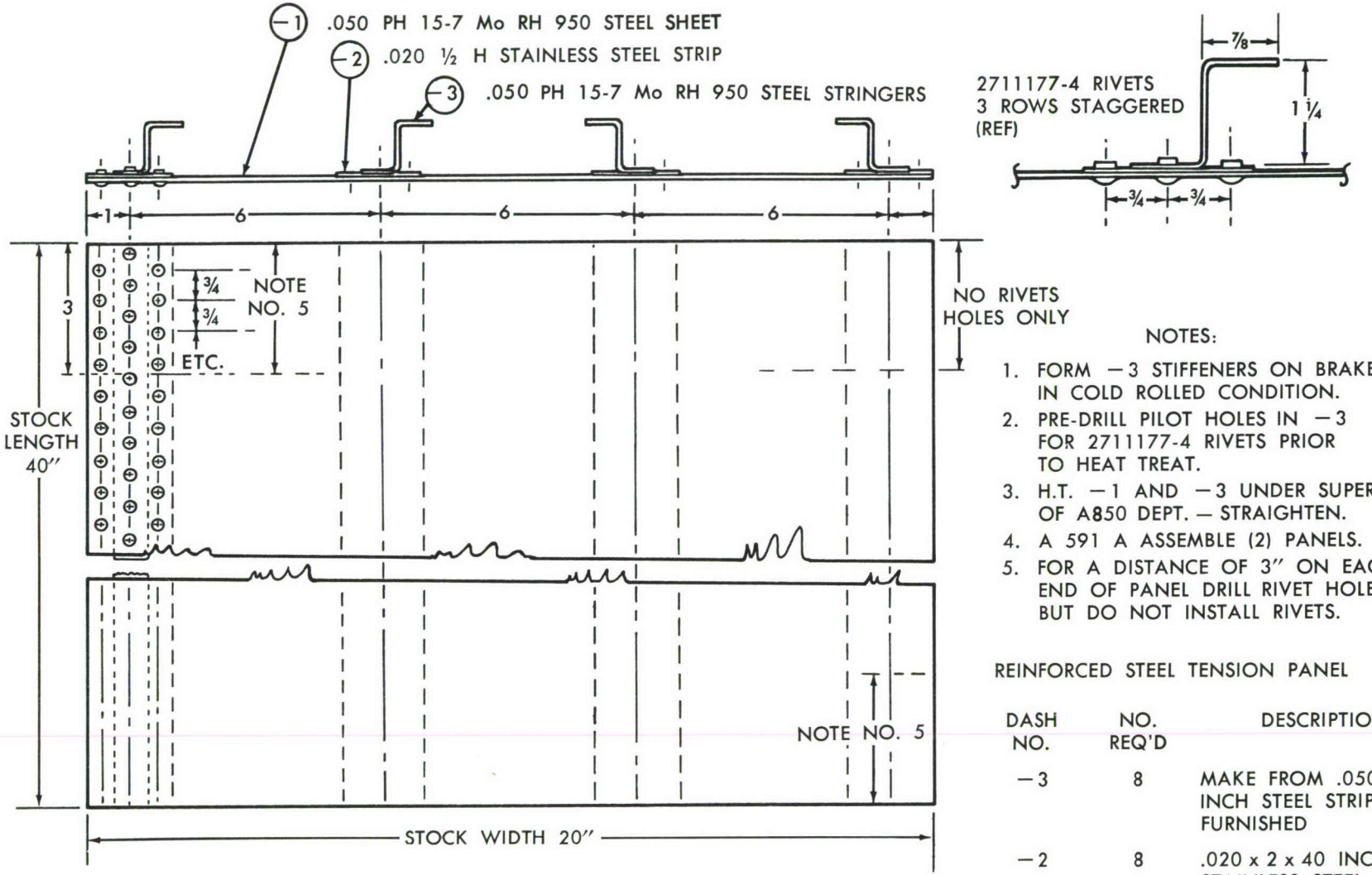


Figure 100. STIFFENED STEEL PANEL — UNIAXIAL LOADING



NOTES:

1. FORM −3 STIFFENERS ON BRAKE IN COLD ROLLED CONDITION.
2. PRE-DRILL PILOT HOLES IN −3 FOR 2711177-4 RIVETS PRIOR TO HEAT TREAT.
3. H.T. −1 AND −3 UNDER SUPERVISION OF A850 DEPT. — STRAIGHTEN.
4. A 591 A ASSEMBLE (2) PANELS.
5. FOR A DISTANCE OF 3″ ON EACH END OF PANEL DRILL RIVET HOLES BUT DO NOT INSTALL RIVETS.

REINFORCED STEEL TENSION PANEL

DASH NO.	NO. REQ'D	DESCRIPTION
−3	8	MAKE FROM .050 x 3 x 40 INCH STEEL STRIP TO BE FURNISHED
−2	8	.020 x 2 x 40 INCH ½ H STAINLESS STEEL SHEET
−1	2	FURNISHED STEEL SHEET .050 x 20 x 40 INCHES

Figure 101. PANEL FABRICATION DETAILS

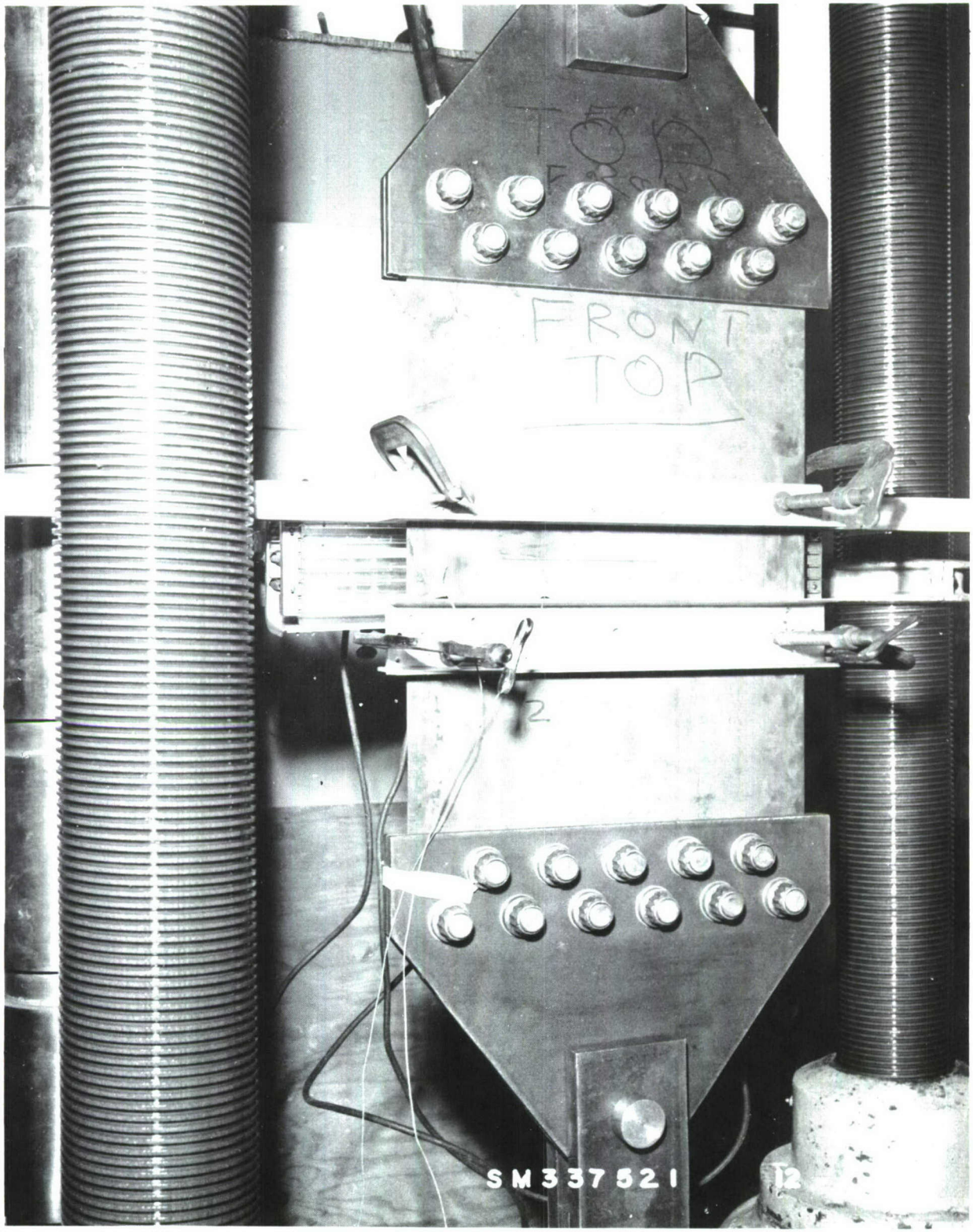


Figure 102. 18 INCH WIDE UNSTIFFENED PANEL IN TESTING MACHINE (HEAT LAMPS SHOWN ON ONE SIDE ONLY)

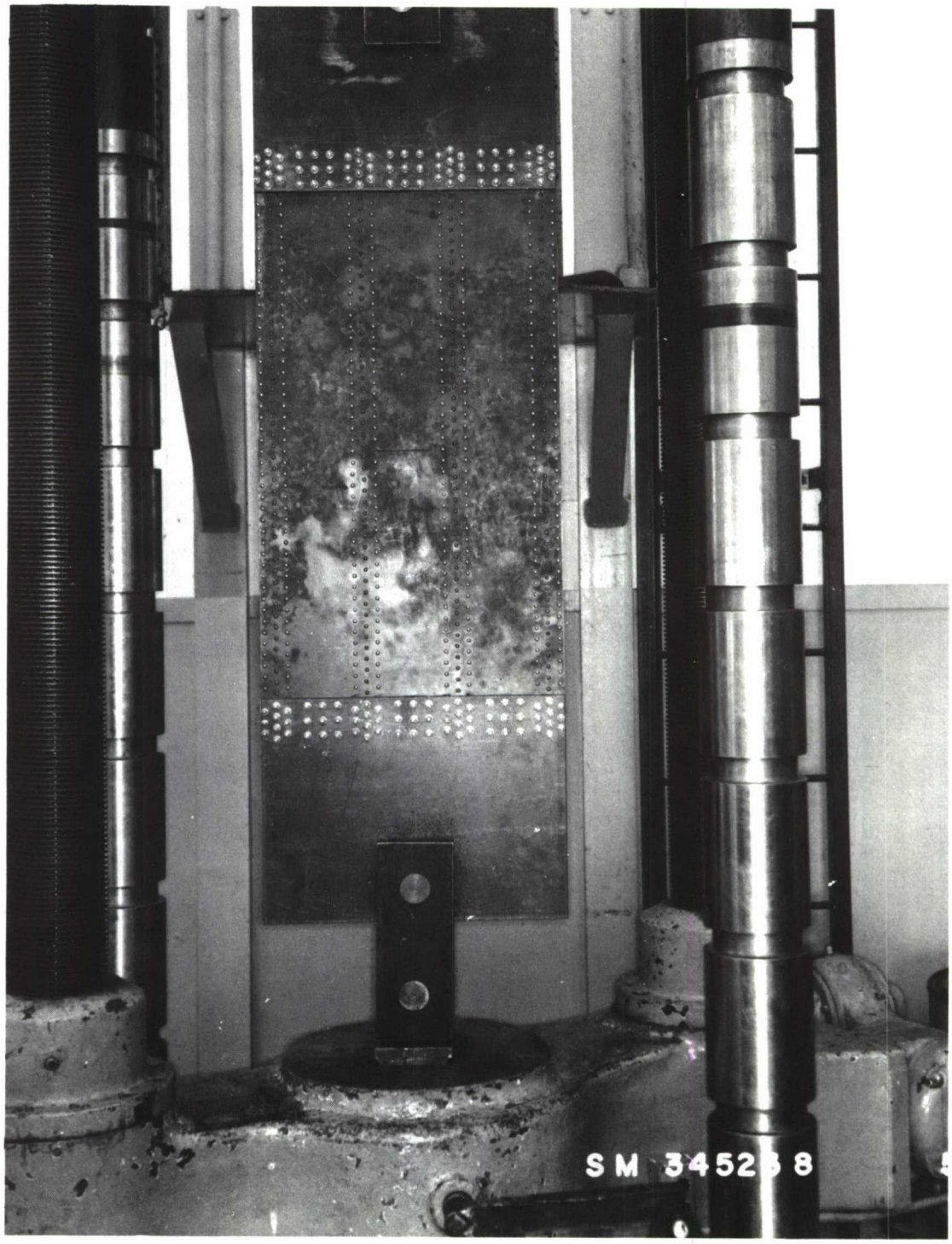


Figure 103. TEST SET-UP OF CENTER SLOTTED 20 INCH PANEL

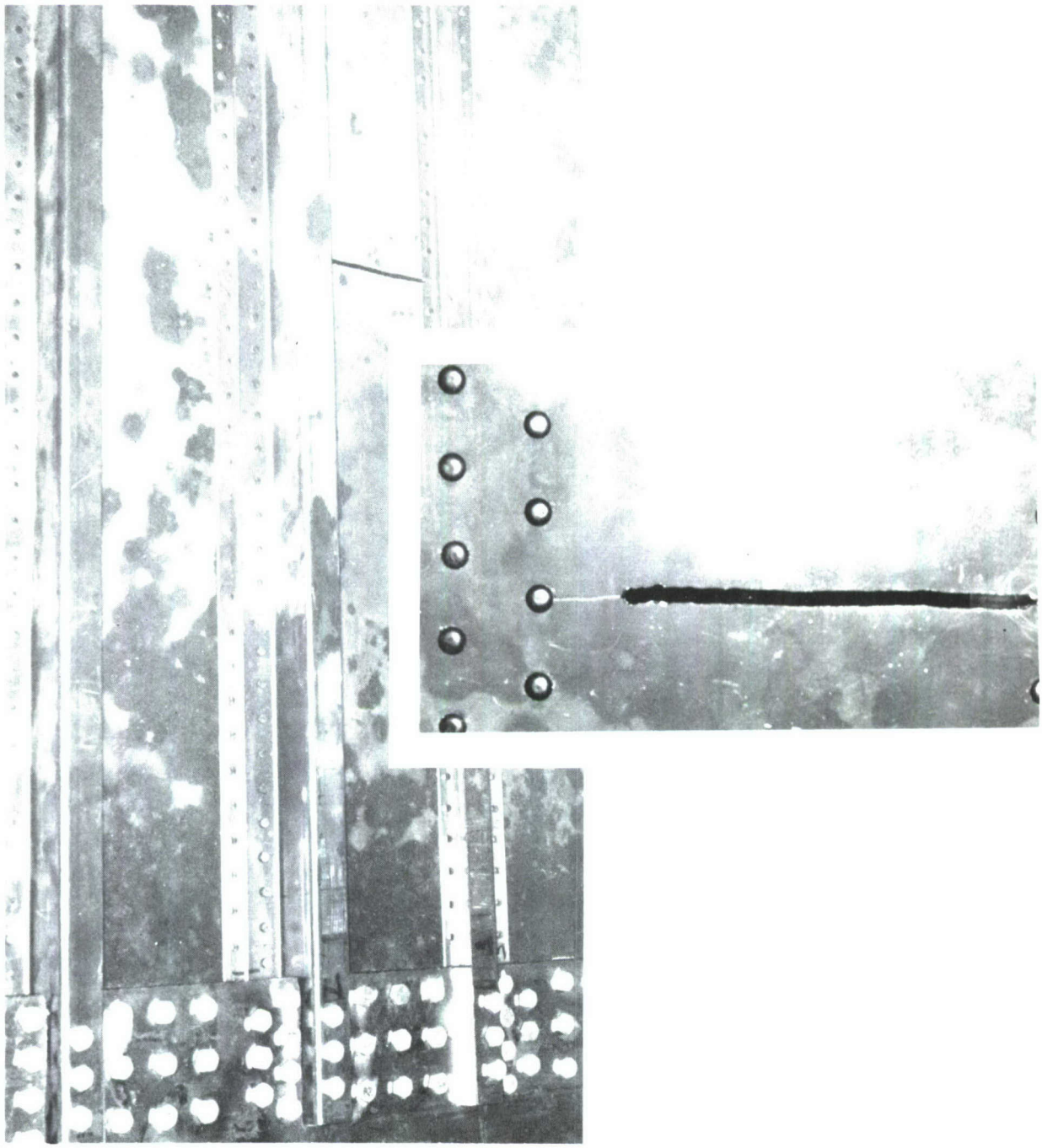


Figure 104. Enlarged View of Stiffened Panel. Insert of Unstable Crack

TABULATED DATA

Panel No.	Test No.	ℓ_c	ℓ_c/W	Ult Load (lbs)	Failing Stress (KSI), σ_R
1	1	3.82	.191	*93,500	52,800
	2	3.04	.152	92,000	51,977
	3	1.48	.074	125,800	71,073
2	1	2.53	.126	87,050	49,180
	2	2.11	.105	85,750	48,446

* Failure occurred 92,000 - 95,000 pounds. Exact load in doubt

SECTION 12

RESIDUAL STRENGTH OF FATIGUE CRACKED PANELS AS A FUNCTION OF SHEET THICKNESS

1. This section reports the fracture tests conducted on a variety of panels in various sheet thicknesses. Four different sheet gauges in five different metals have been investigated. The results are presented as residual crack strengths and shown on the accompanying figures. No K_c or c values have been determined from the data although their relative c values are roughly in the same relationship as the order of their residual strengths. The results from these tests are believed to be reasonably accurate and representative of the particular materials tested. There are indications from these tests that the relationship of crack strength to sheet thickness is not the same for all materials. It is unfortunate that more tests were not planned for this variable. The investigations that have been conducted are all for cross grain properties; i.e., the crack and sheet rolling are in the same (perpendicular to the loading) direction.

2. The general conclusions that can be drawn from these tests, within the range of sheet thickness investigated, (.020" - .051"), are as follows:

   a. For materials of low ductility the fracture strength decreases with an increase in sheet thickness (Figure 107).

   b. For materials with a high percent of elongation the fracture strength decreases with a decrease in sheet thickness (Figure 105).

   c. For some materials the strength characteristics may exhibit such a degree of scatter that it may not be possible to classify the strength characteristics as a function of thickness (within a small range of gauges).

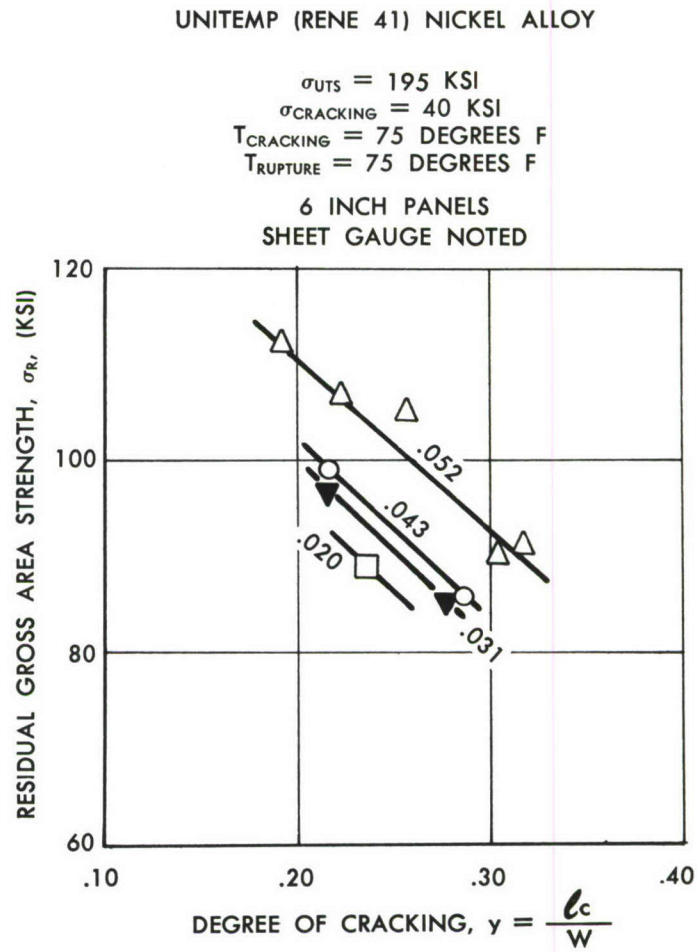


Figure 105. RESIDUAL STRENGTH vs DEGREE OF CRACKING

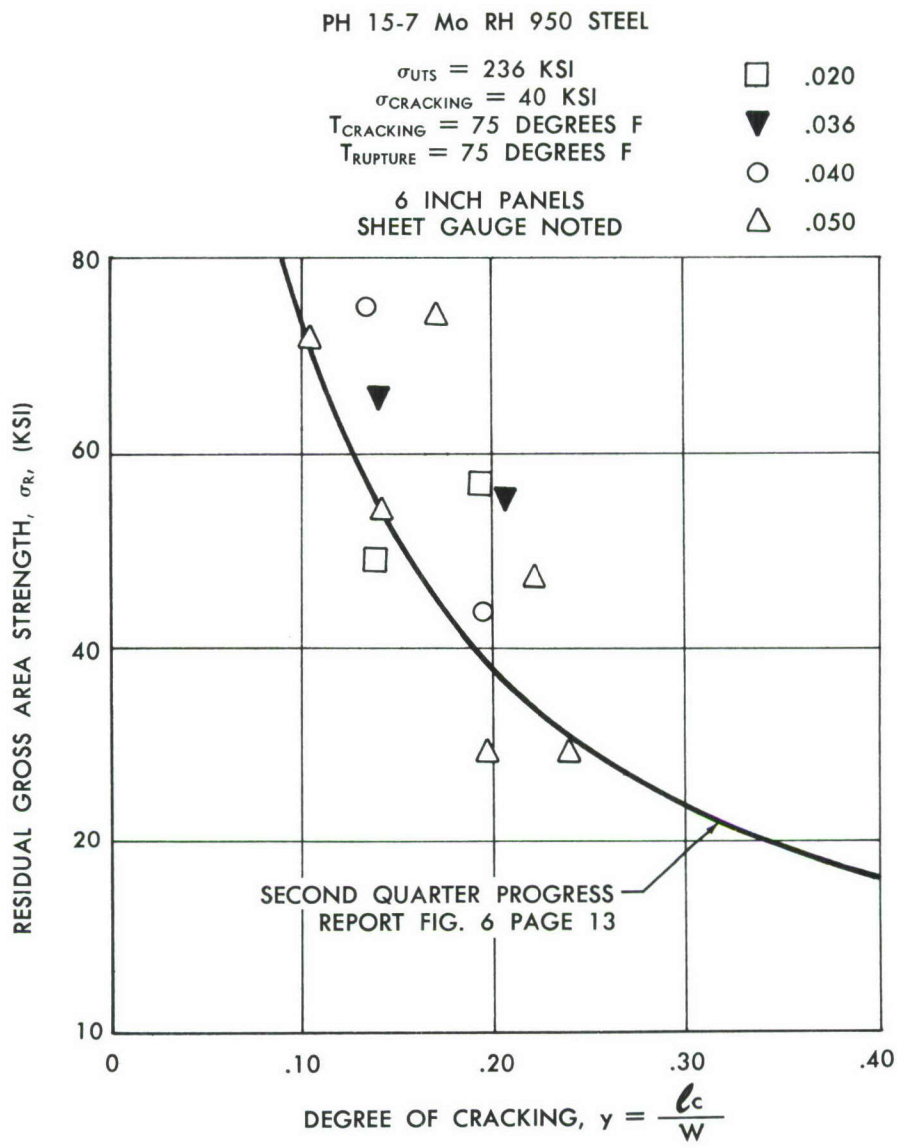


Figure 106. RESIDUAL STRENGTH vs DEGREE OF CRACKING

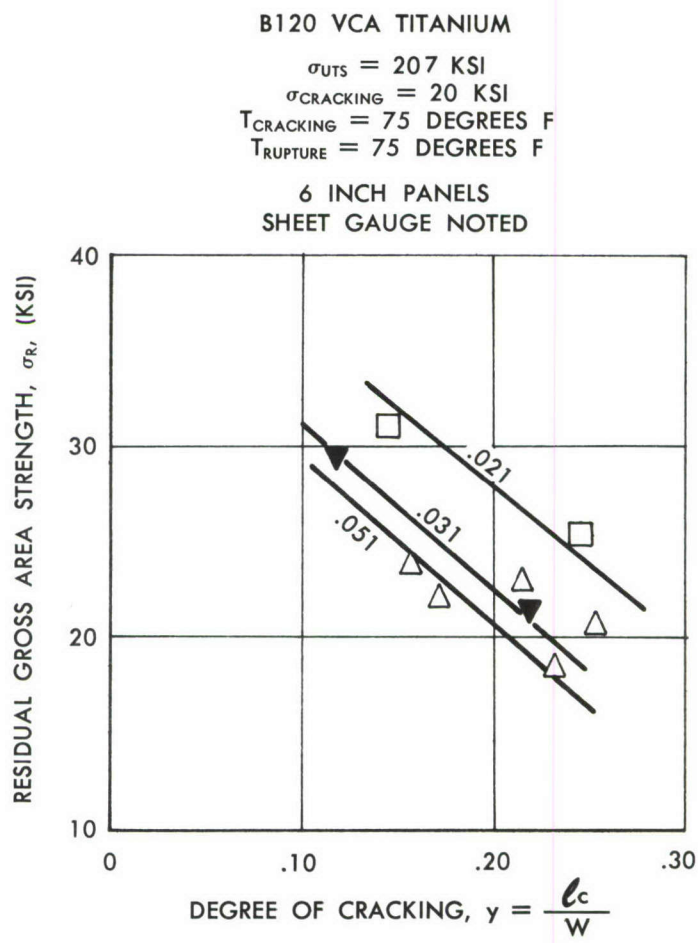


Figure 107. RESIDUAL STRENGTH vs DEGREE OF CRACKING

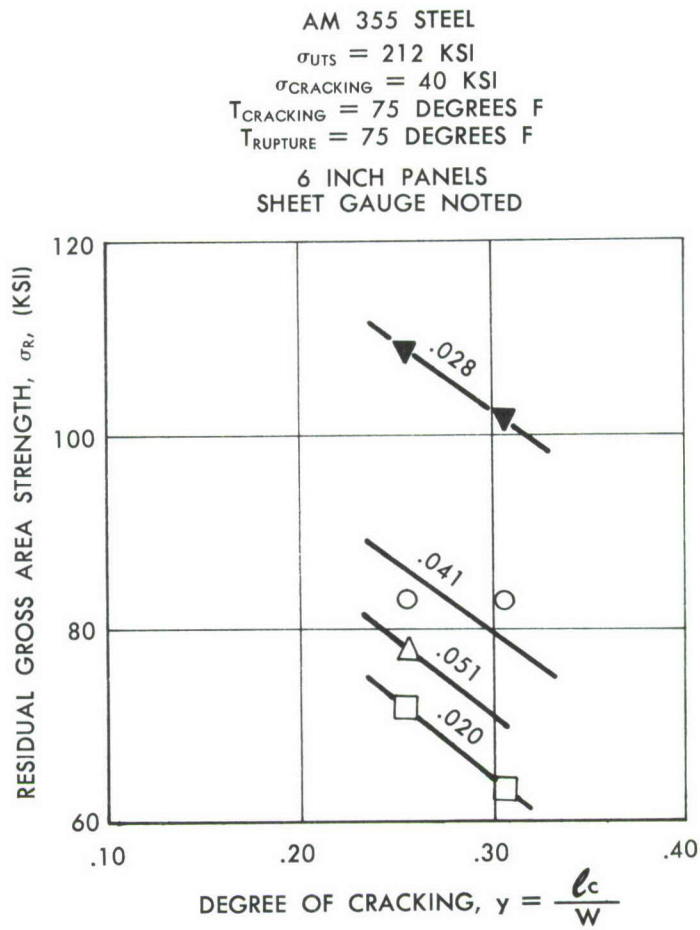


Figure 108. RESIDUAL STRENGTH vs DEGREE OF CRACKING

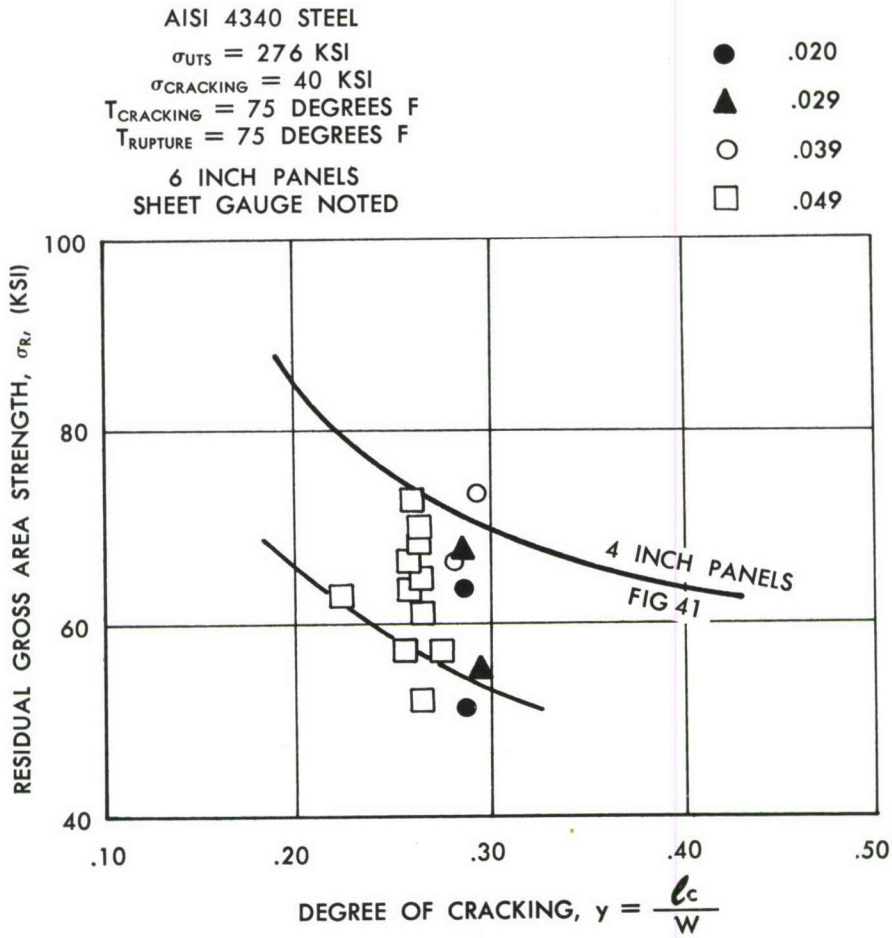


Figure 109. RESIDUAL STRENGTH vs DEGREE OF CRACKING

SECTION 13

PROGRESSIVE FORMATION OF CRACKS LEADING TO FRACTURE

This section has been divided into three parts and includes general discussions on (a) fatigue cracking, (b) creep cracking and (c) the slow extension of the crack in microsteps leading to critical lengths for catastrophic rupture.

Fatigue Cracking

Until very recently the growth of fatigue cracks in metals has been thought to occur in a continuous accelerated manner. Evidence now indicates that the crack extension occurs in well defined "spurts" or "jumps" and that it makes little difference if the crack growing environment is constant or erratic. In this respect, a similarity can be drawn between the interrupted or spurting growth of a propagating crack in a metal and the natural growth of many things.

Figure 110 on page 185 is constructed from a motion picture recording of the fatigue fracturing of a metal plate. It shows, on a macro-scale, many apparent "hesitation periods" throughout the interrupted propagation of the crack. The Electron Microscope Appendix A, however, indicates that the cracking mechanism during these hesitation periods is not completely dormant, but continues on a much finer (micro) scale. Cracks that nucleate and grow both externally and internally ahead of the tip of the main fatigue crack front are also in evidence and extend during these "apparent dormant periods". These inchoate cracks can be used to explain the "arrest" of the spurts in crack growth as the newly generated crack fronts reach micro critical-lengths for temporary instability.

Figures 111 through 113 on pages 186 through 188 show, on a macro scale, such discontinuities between fine and coarse fracture mechanisms.

These observations now support the view that surface cracks as well as minute internal cracks can be formed on the single application of a load that is well below the load that would completely fracture a part. Repeated application of these lesser loads will extend the crack front and progressively nucleate new cracks and enlarge these new cracks ahead of the main crack.

It may, therefore, be theorized that the mechanism of fatigue damage during crack propagation is nothing other than a series of minute static ruptures. These minute ruptures occur suddenly and probably when the greatest tension value of the cyclically changing load has been reached. The growth "lines" or arrest "lines" (see Figure 111 and Illustrations in Appendix A) are thought to be due to the plastic deformation that occurs at the tip of the crack as it suddenly spurts forward. Continued load cycling advances the crack front in these micro-steps until it reaches a micro-critical length. At this stage a sudden macro fracture occurs. This fracture, however, only extends into the advanced and newly cracked regions (see Figure 113 on page 188) that have been generated from the prior loading. An important observation here is that slow progressive fatigue cracking advances further on the surface than it does internally. The sudden single load-cycle macro-fracture on the other hand generates a more pointed crack front and extends further internally than at the surface. This certainly suggests the dependency of the shape of the crack-front as to whether the progression is slow micro cracking or fast

macro fracturing. This is analogous to the case of a macro-crack which becomes unstable in a large plate. The crack can be temporarily arrested in its propagation by either running into low stress fields, discontinuities, holes and voids all of which, in effect, represent a less servere notch or stress riser than the tip of the running crack.

Micro-Crack Progression

The progressive growth of a fatigue crack in metal, beyond the nucleation stage, has been illustrated by its propagation on both macro and micro scales. Under a complex loading schedule it is now possible to observe micro and macro scale fracturing in random patterns Figure 114. The distance between the micro growth stages or "arrest lines" as shown in the electron microfractographs (Figure 115 on page 190) can be shown to vary directly with the value of the cyclical test load applied in progressively fracturing the metal. It can also be shown that for a given value of "cracking load" the distance between the arrest lines will gradually increase with time. In one aluminum alloy test part it has been calculated, from measurements, that at high load levels two applications of the load were required in order to advance the fracture "one" arrest line; at lower load levels from five to twelve load applications were required to propagate the crack to the next growth line. For some loads sufficiently small there would be no growth whatsoever. Appendix A gives some calculations on the metal RENE' 41 tested in this program. The hesitation periods within the micro-crack region discussed here are not observable during the fatigue loading of a part and are in addition to the macro pauses previously discussed which are visually observed in gathering external crack growth data.

It would be interesting, as well as useful, if the total or a fraction of the number of load cycles required to fail a part multiplied by the spacing between each growth line could be related to the total distance the part had fatigue cracked at the end of its life. At present, the difficulties in making and interpreting such measurements have prevented precise calculations from being made. For example, the growth spacing primarily would appear to be a function of material, microstructure, temperature, stress level and particularly prior load history.

Temperature Effects

Although the fatigue life of metals is generally decreased by an increase in testing temperature, it has been observed that the rate of growth of the fatigue crack is often less for some metals at an increase in cracking temperature. Typical growth curves such as given in Figures 28 and 59 indicate that a greater number of cycles are required to progressively propagate a crack at the higher temperatures. This seeming discrepancy, of a greater overall fatigue life at temperature, may partially be explained with the aid of Figure 116 on page 191. The crack growth phase can be longer in the elevated temperature environment but its crack nucleation period is much shorter than at lower temperatures. The overall effect, with no starter crack, is that a greater number of cycles are required at the lower temperatures to grow a critical size of crack for instability; although the absolute critical length of crack at the lower temperature is shorter than the higher temperatures.

Figure 117 shows an interesting observation made with the electron micro-

scope. Examination of the progressively fatigue fractured surfaces revealed that the crack growth lines cover almost the entire surface for the panel tested at a cracking temperature of +600°F. At the lower cracking temperatures there appear to be domains of static plastic rupture and then continued progressive cracking. For materials with high ductilities or percentage of elongation there appears to be a more uniform appearance to the fatigue fractured surfaces. An increase in testing temperature can produce this effect. The material RENE' 41 with 17+% elongation at room temperature shows this uniform density in "growth lines" even at lower temperatures. See example in Appendix A.

Creep Cracking

Figure 118 is another macro-fractograph, similar to the one shown in Figure 111. This figure shows the fracture texture resulting from more complex loading forms. From the starter notch this crack grew under repeated loading for a distance just short of the dark textured fracture region. The test panel was then held at load and temperature for two hours. During this period two phenomena occurred. The heat and atmosphere oxidized the newly fractured surface in degrees depending upon the tightness or openness of the crack along its length. The result is a gradiently color-tinted crack face which on closer examination has again brought out the spurts in crack-growth-fronts as shown in Figure 113. The most important phenomenon in this illustration is the presence of the slow-extension of the crack under the steady load conditions. The extension in cracking can be termed "creep-cracking". This step in any program adds analysis complications but is most important in that it adds realism to the test in providing a potential vehicle environment. Its significance is shown in Figure 30. The cracking beyond the creep-front in the figure is again progressive-fatigue-crack growth under repeated loading at a lower temperature.

Figure 30 shows the measured and recorded data from a previously discussed test panel. An extension of approximately .05" in crack-length was observed during the "creep period". Upon resuming oscillatory loading, a pronounced decrease in the rate of crack growth can be seen. This decrease is attributed to the disruption of the prior crack leading edge by the coarser creep growth. The crack front now had a blunter leading edge which therefore produced a lower stress concentration. The original crack growth rate was eventually resumed but not until after a small delay period during which time the leading edge of the crack had gradually returned to its original acuity. The creep effect, so far, appears to be beneficial, although there is still much to learn of the conjoint action of fatigue and creep cracking.

Slow Micro Extension of Crack Prior to Rupture

Measurements on a micro as well as a macro scale have been taken and it may be well to briefly discuss a few of these observations at this point. Although many of these observations have not yielded quantitative data they have revealed phenomenon that are helpful in explaining many observations.

Figure 119 shows the technique and setup for measuring micro-sounds that accompany micro-cracking in stressed metal. To date, these studies have indicated that micro-cracking can occur on the application of a load as low as 30% of the load that would normally fracture the material. This set-up is similar to one that has been devised by NRL (Bibliography 26) in which micro

cracks were recorded in less severely notched panels at 70% of the fracture load. With finer measuring techniques on panels with more severely formed fatigue crack fronts, it should be possible to record micro instability fracturing at much lower loads. The 30% level cited was for a fatigue cracked RENE' 41 panel which has proven to be a fairly notch insensitive material. The principle of the recording technique is as follows:

As the micro-crack occurs, it sets up a vibration wave that propagates through the metal. A crystal accelerometer, cemented to the test panel in a direction perpendicular to the loading, picks up this component of the wave motion in the same manner as a seismograph does in recording earthquakes. The magnitude of the early micro-cracks are in the order of .004 g's. These micro-metalquakes can be converted into sound pressures and made audible with the aid of conventional head-sets. It can be stated that a value of zero db is the threshold of unaided hearing and 80 db the level of normal conversation then this will represent a measurement latitude from 1 to 10,000. The micro-sounds recorded in these experiments are believed to be far below this threshold value and therefore the magnification has been many times more than 10,000. The physical significance of this observation is that the occurrence and generation of heretofore undetectable cracks were probably formed very early in the useful life of structures. The growth and extension of such cracks then will increase with the continued use of the vehicle.

The existence of "non-propagating" cracks should be considered as a laboratory oddity or for "one-amplitude-structures" but should not be counted upon in the presence of the spectrum of loads that are the environment for aerospace vehicle structure.

Additional cyclic load tests should be planned to determine, if possible, a crude rate at which the progressive micro-fatigue cracking occurs during the early stages. The crystal accelerometer could be bonded to the fatigue test panels. Rather than insulate or cool an accelerometer on a heated panel, it would be more practical to attach the accelerometer to an extension rod, welded to the test panel. In this manner it may be possible to cross-check some of the cracking at temperature effects discussed in "Temperature Effects". For example, micro-cracking at elevated temperatures should occur earlier than at low temperatures. This phenomenon can exist even though the rate of fatigue crack growth is slower at the elevated temperature.

Critical Length for Residual Strength Evaluation

Macro cracks or visible cracks, about which this report is more immediately concerned, have been evaluated as shown in Figure 120. The sketch in the figure should be self-explanatory and show the method used to evaluate the total crack length at the instant of rupture instability. The ink-stain method during loading was not used since it was not possible to apply in either the elevated or sub-zero temperature environment. The fracture appearance has shown one observation that two often has not been mentioned or observed; namely, the "flip-flop" nature of the traveling shear lip fracture and the extent of the cleavage fracture.

A possibility exists that many, if not most, fractures occur on shear planes and that the subtle difference between cleavage and shear lip is only a micro to macro scale distinction. For example, are the light colored cleavage

fractures in Figure 121, or in the photograph on page 74, the so-called slow-extensions of the crack or just the first area to rupture? In this example the latter case is believed to be true. Additional measurements and measuring techniques will be required to establish the chronology of these phenomena.

Some work in fracture mechanism has already been carried out in the field of Electron Microscope (Appendix A) which suggests that additional study may be very fruitful. For example, the transition from slow cracking to rapid crack propagation with the usual macro-visible "Chevron" markings has never been clearly defined. The illustration on page 197 with the electron microfractographs of regions of the fractured surface indicate the differences during the dynamics of fracturing. After the "slow" cleavage extension of the fracture has occurred beyond the fatigue crack tip furing the monotonic loading, the transition suddenly develops into complete rupture. This rapid fracture occurs incrementally on nearly parallel cleavage planes hinged plastically at the surface. As the fracture planes intersect, within the metal first, cross slip occurs thus forming the "chevrons" or arrows pointing back to the nucleus. The fracture planes are in a sense hinged at each surface and generate, similar to Frank-Read dislocation loops, fracture plane loops that cross connect near the center of the thickness in sheet materials.

Figure 123 shows an interesting fracture mechanism in a ruptured heavy-walled pressure vessel.

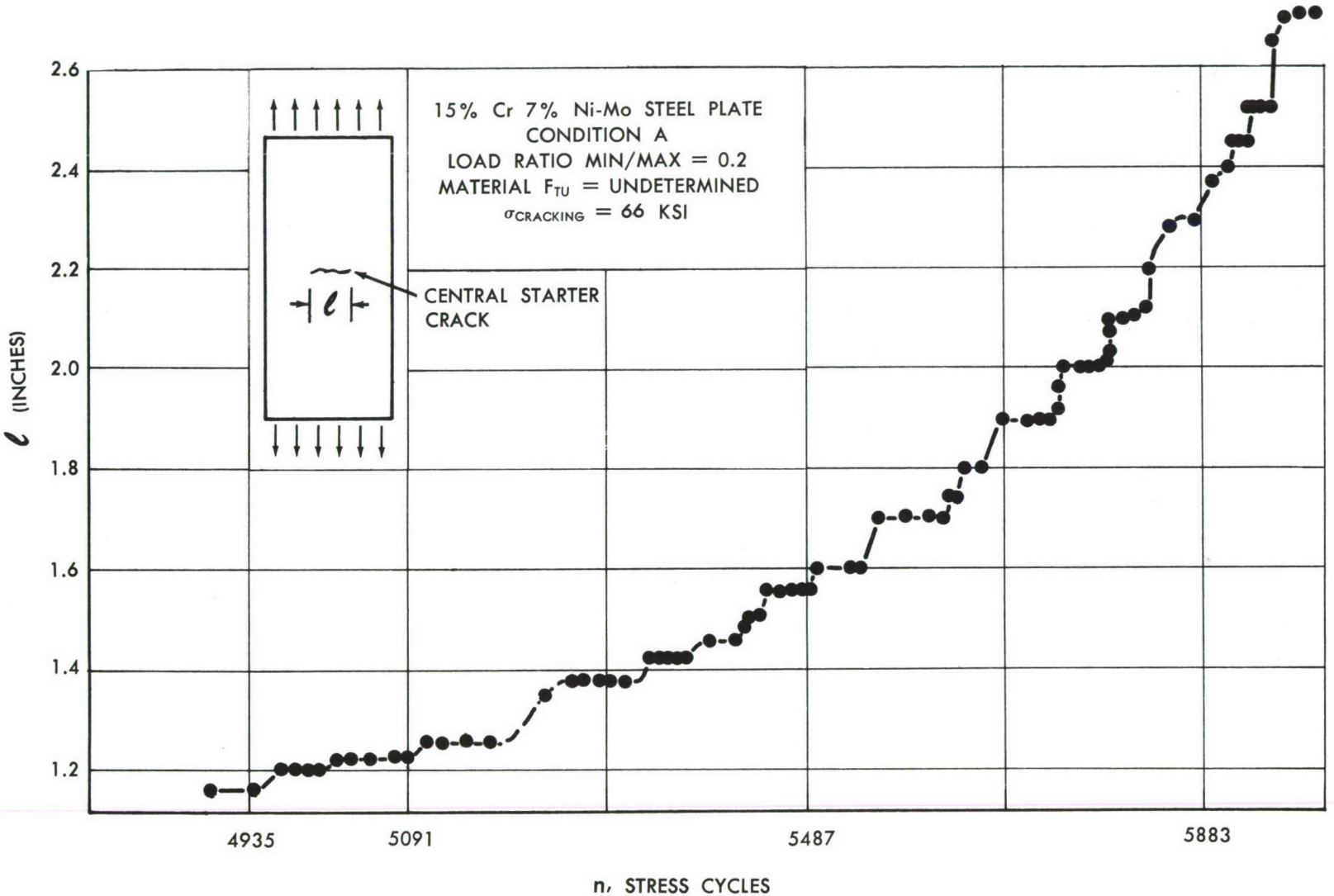


Figure 110. CRACK GROWTH vs NUMBER OF LOAD CYCLES

The "apparent" delayed-fractures are shown in this step-wise plot which has been obtained from a 16mm motion picture record of a metal specimen during the fatigue test. Exacting measurements now show that extremely fine fracturing is going on during these apparent delayed-fracture regions.

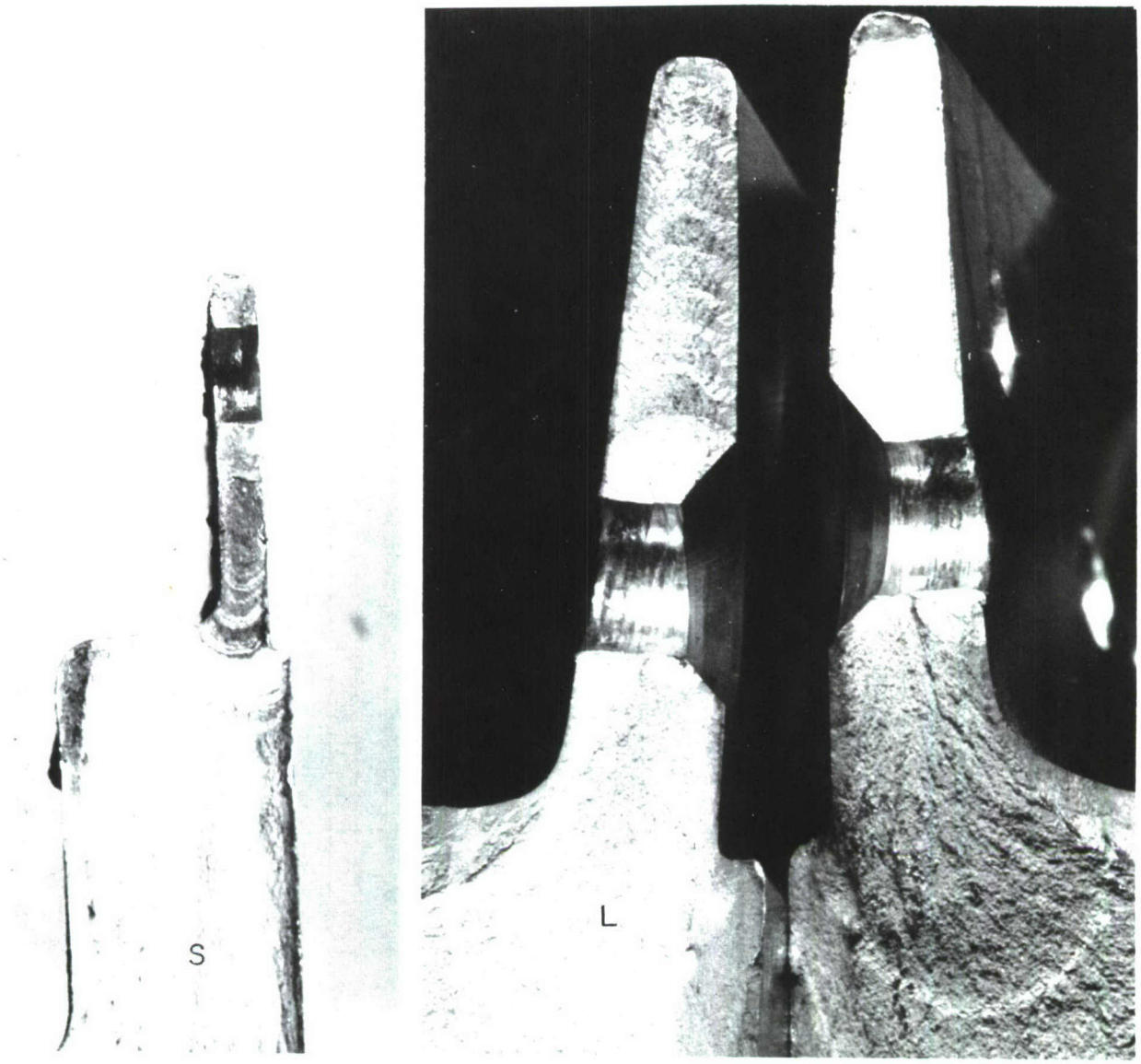


Figure 111. MICRO TO MACRO CRACKING

MICRO AND MACRO CRACKING during the fatigue crack progression in cyclically stressed aluminum alloy extrusions. These samples exaggerate the alternate cracking mechanisms, but vividly demonstrate the sequence of events. It is more difficult to see these regions on the finer grained steel alloys. The alternate light and dark textured surfaces represent the degree of fine and coarse crack growth. The fine growth lines cannot be resolved in these photographs and often not even with the light microscope; in these instances a "replica" is made of the fractured surface which, in turn, is resolved with an electron microscope. The fractograph marked "L" is of laboratory tested specimens; the one marked "S" is of a service "failure" and the sporadic growth of fracture has been due to the random service loading experience.

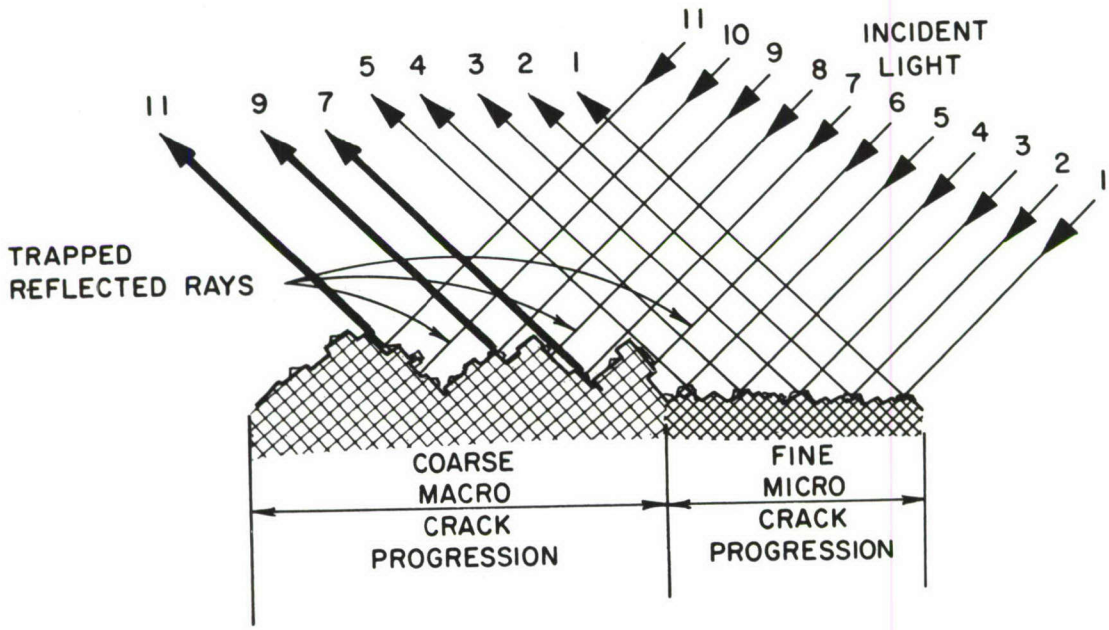


Figure 112. Coarse and Fine Fracture

Sketch shows manner in which the fracture face of the metal reflects incident light. The coarse fracture traps more of the incident light and results in a darker appearing texture than the finely fractured surfaces.

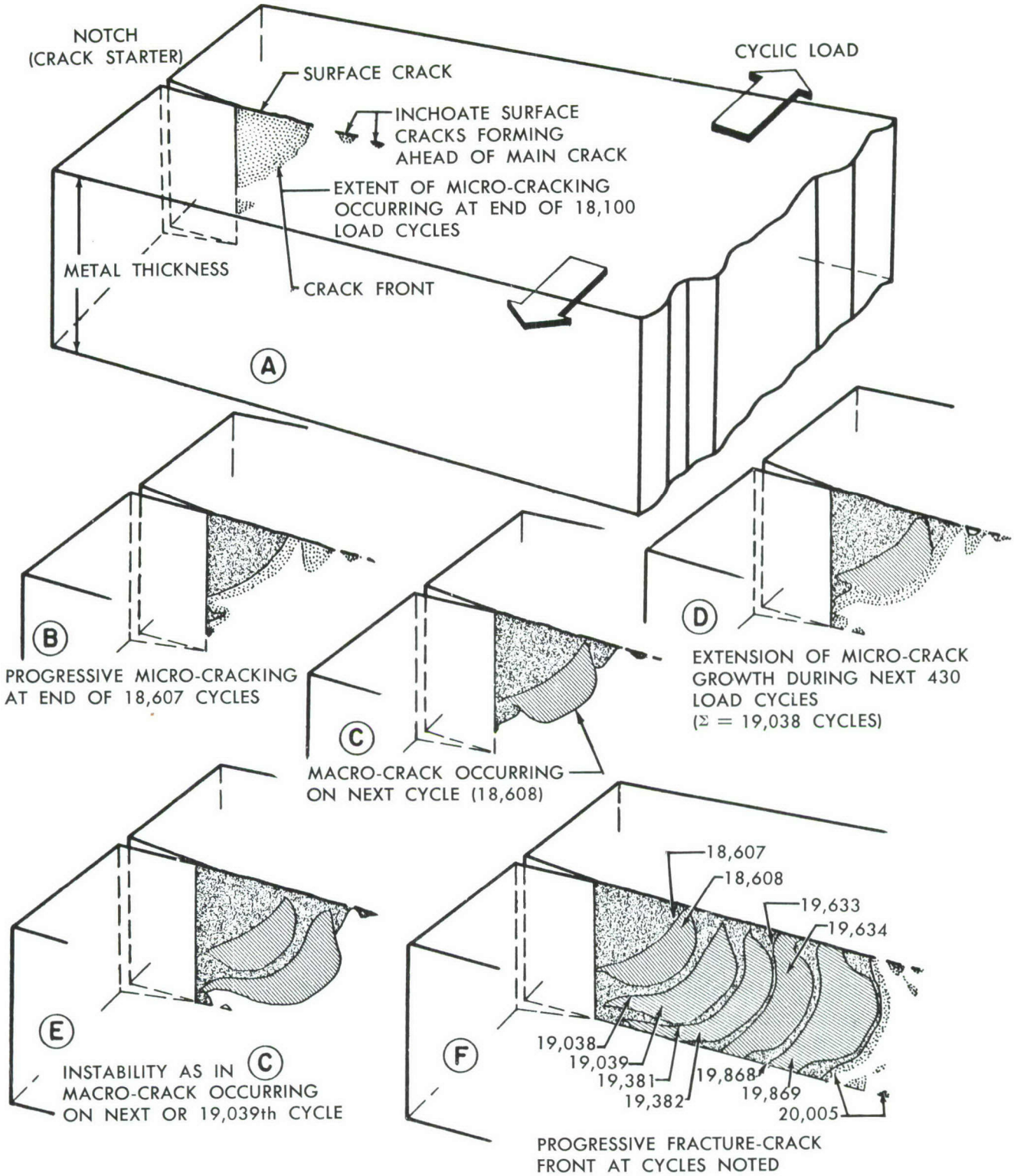
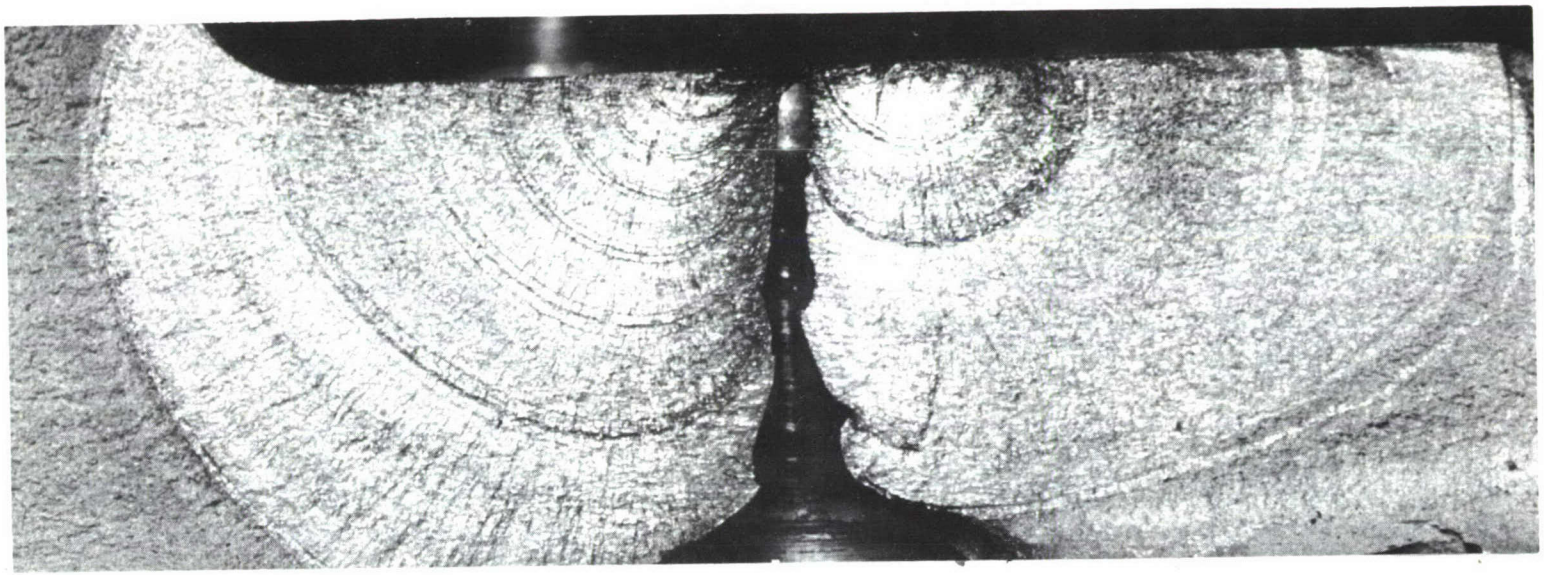


Figure 113. FATIGUE CRACK GROWTH IN LATER STAGES

Crack nucleation stage not illustrated. Note repetitive and alternate periods of micro and macro cracking which results in "jumps" or "spurts" during the progressive fracture. Dimensions of micro-crack growth are shown in the electron micrograph illustrations. Cycles of load are only approximate, but represent the progress of the micro and macro fracturing. SEE Figure 111.



Magnification: 4 1/3 times
Fatigue fracture progression of a test sample loaded sequentially through a programmed spectrum of loads made up of nineteen different load patterns repeated 16 1/2 times prior to final rupture (a total of 314 load steps and 629,035 load cycles). Zones marked on surface are locations in which replicas were made for examination at high magnification. Note the well-defined periodic arrest lines which suggest an alternating series of micro and macro progressive fracturing.

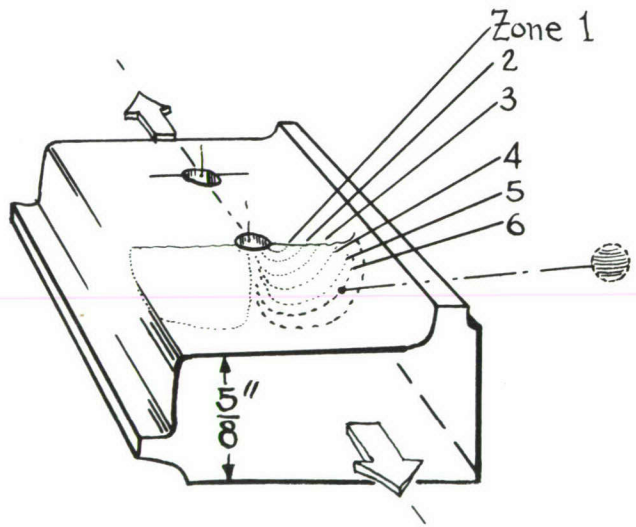
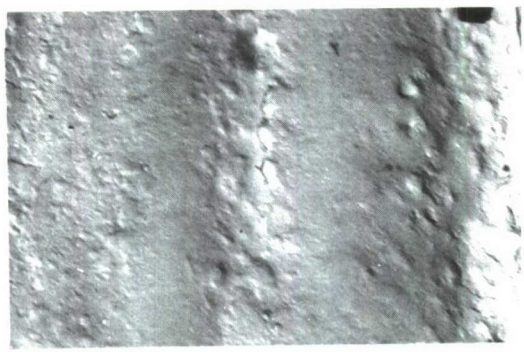


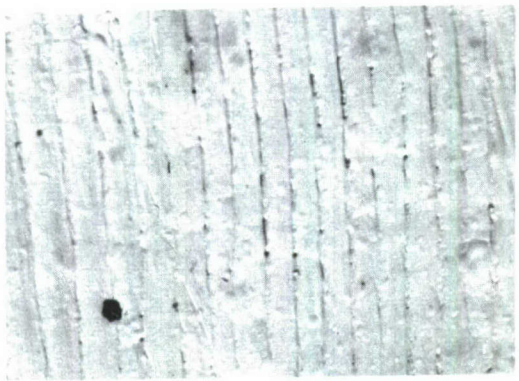
Figure 114. FATIGUE FRACTURE



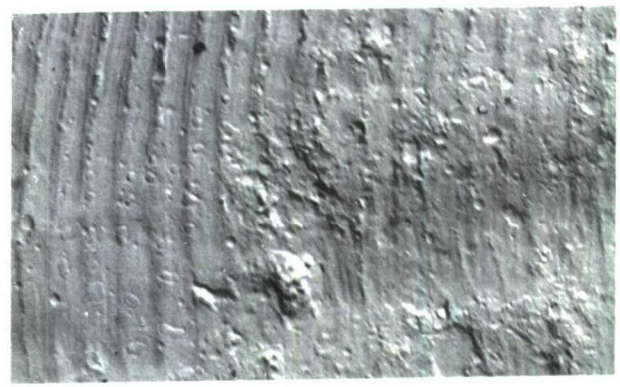
Zone 1: λ = 100 microinches during High-Loads.



Zone 1: λ = 55 microinches during Medium Loads



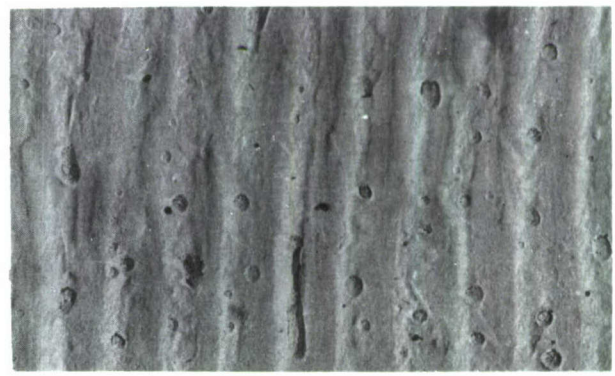
Zone 2: λ = 17 microinches during Low Loads



Zone 3: λ = 18 microinches during Low Loads



Zone 6: λ = 18 microinches during Low Loads



Zone 8: λ = 29 microinches during Low Loads at a later stage than Zone 6 at left.

Figure 115. PROGRESSIVE FRACTURE

Magnification: 10,260 times

Electron micrographs by the replica method of the fatigue fractured surface of a test sample. The replicas were made within the regions (zones) marked on the macro-photograph of illustration 114. Use of the electron microscope in examining fractured faces of fatigued metals is now yielding new information about progressive cracking-crack growth "spurts" between "arrest lines" (λ) 1/125,000 inches apart can be easily resolved.

n_T = END OF CRACK NUCLEATING PERIOD AND START OF OBSERVABLE GROWTH AT ELEVATED TEMPERATURE

n_o = END OF CRACK NUCLEATING PERIOD AND START OF OBSERVABLE GROWTH AT ROOM TEMPERATURE (75°F)

N_T = CYCLES TO FRACTURE IN REACHING ℓ_c AT ELEVATED TEMPERATURE

N_o = CYCLES TO FRACTURE IN REACHING ℓ_c

$(N_T - n_T) > (N_o - n_o)$ = OBSERVABLE CRACK PROPAGATION PERIOD. THIS PERIOD IS OFTEN GREATER AT ELEVATED TEMPERATURE THAN AT ROOM TEMPERATURE

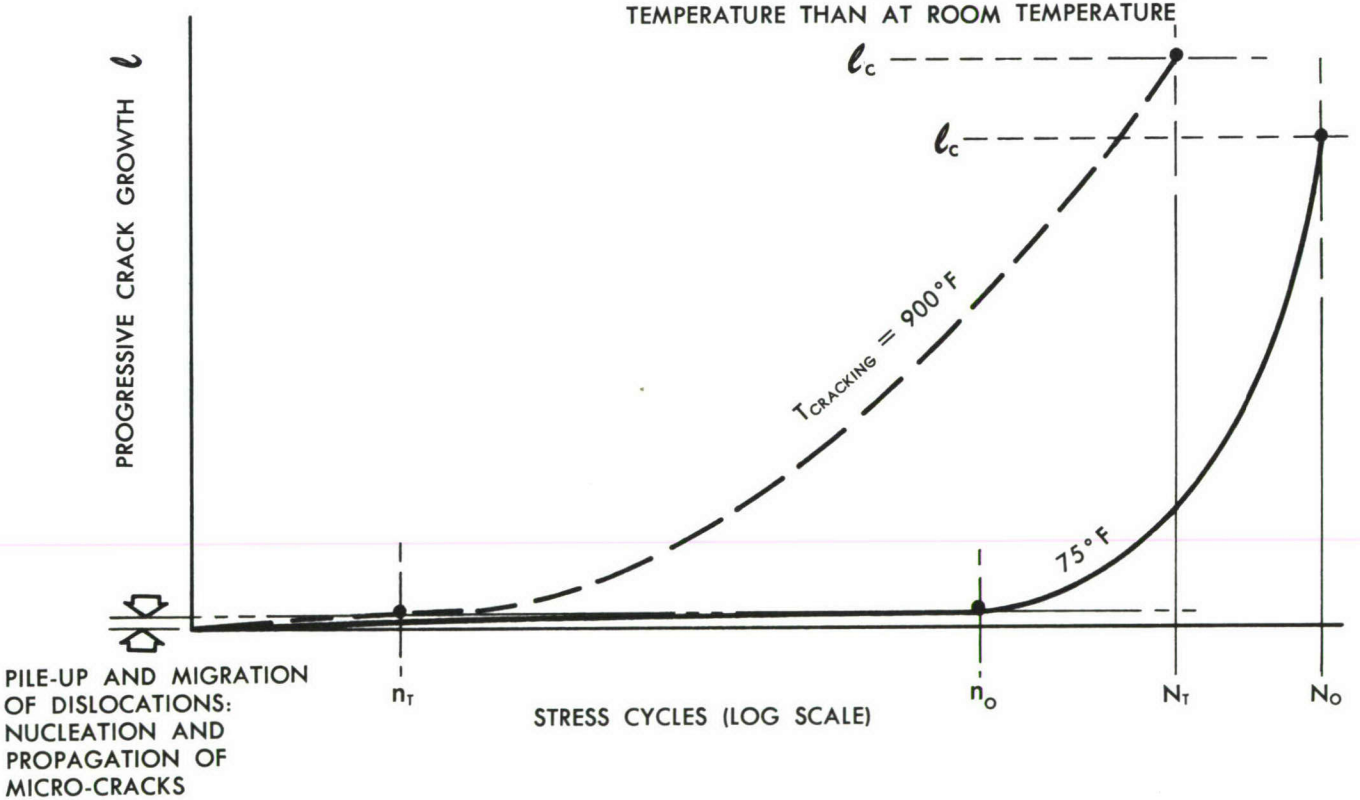


Figure 116. PROGRESSIVE CRACK GROWTH TEMPERATURE EFFECTS





ELECTRON MICROFRACTOGRAPHS at 18,500 X of the progressive fatigue cracking of PH 15-7 Mo RH 950 steel sheet. Test panel P 47, at top, was stressed at a maximum gross area stress of 40,000 psi and at a cracking temperature of +80° Fahr. Test panel P22, bottom, was stressed at 40,000 psi but at a maximum cracking temperature of + 600° Fahr.

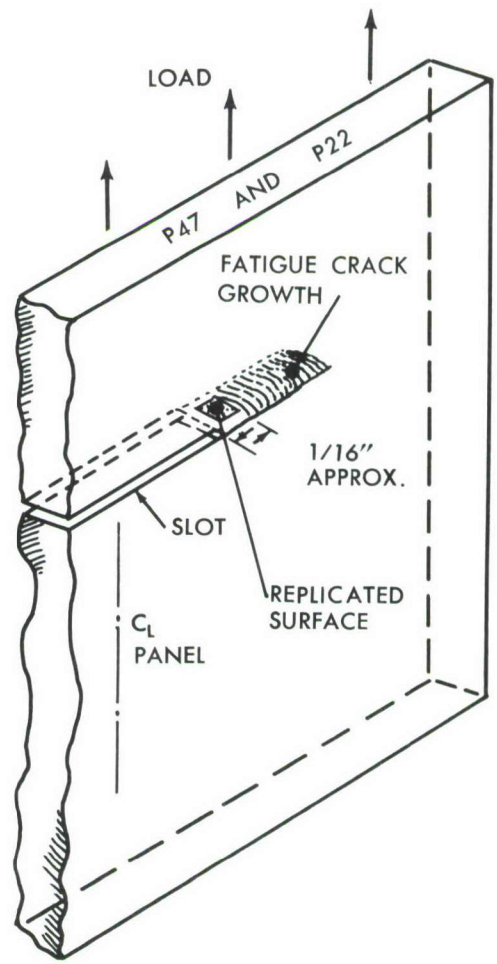


Figure 117. ELECTRON MICROFRACTOGRAPHS

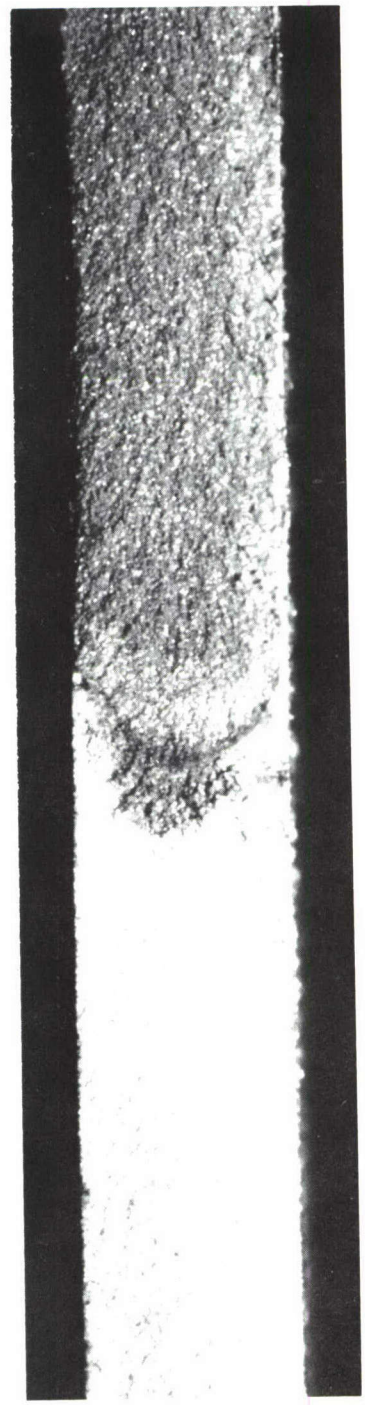
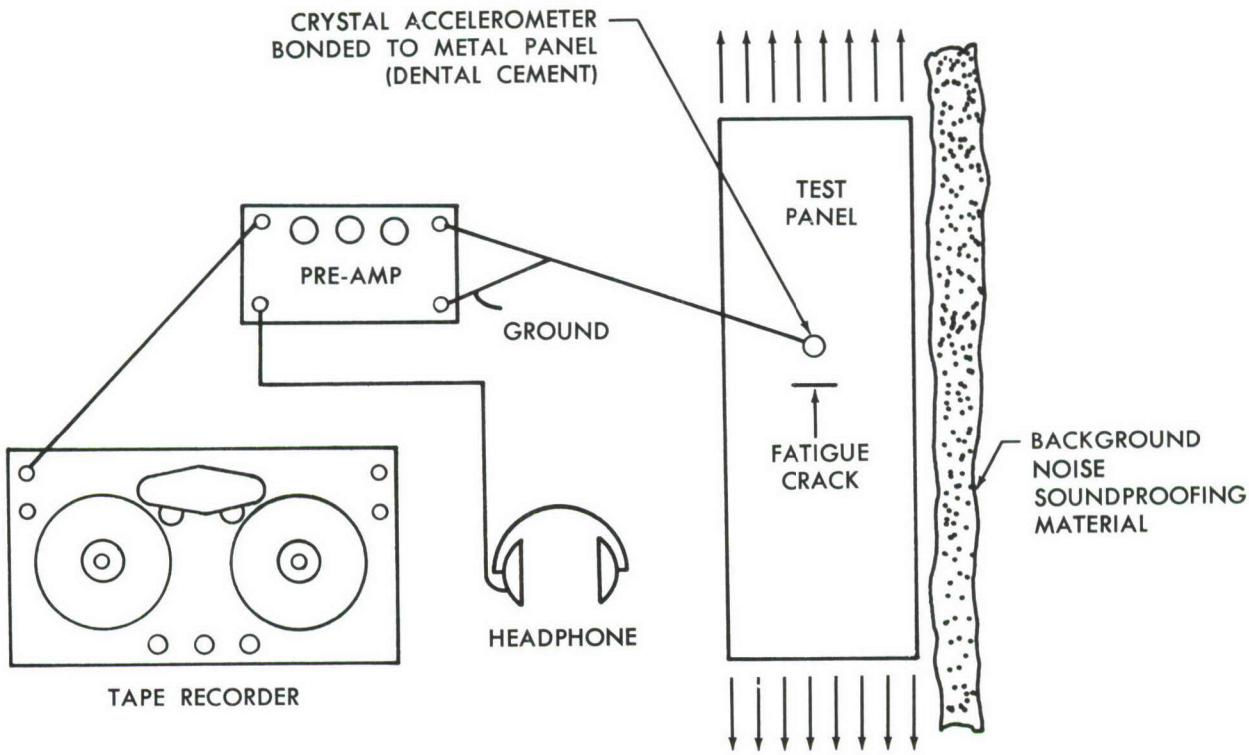
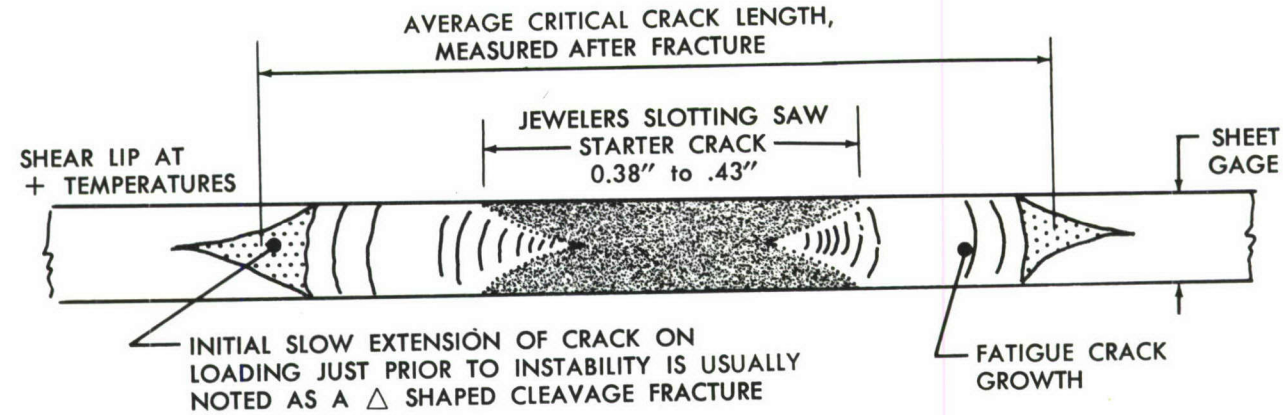


Figure 118. CREEP-FATIGUE CRACK

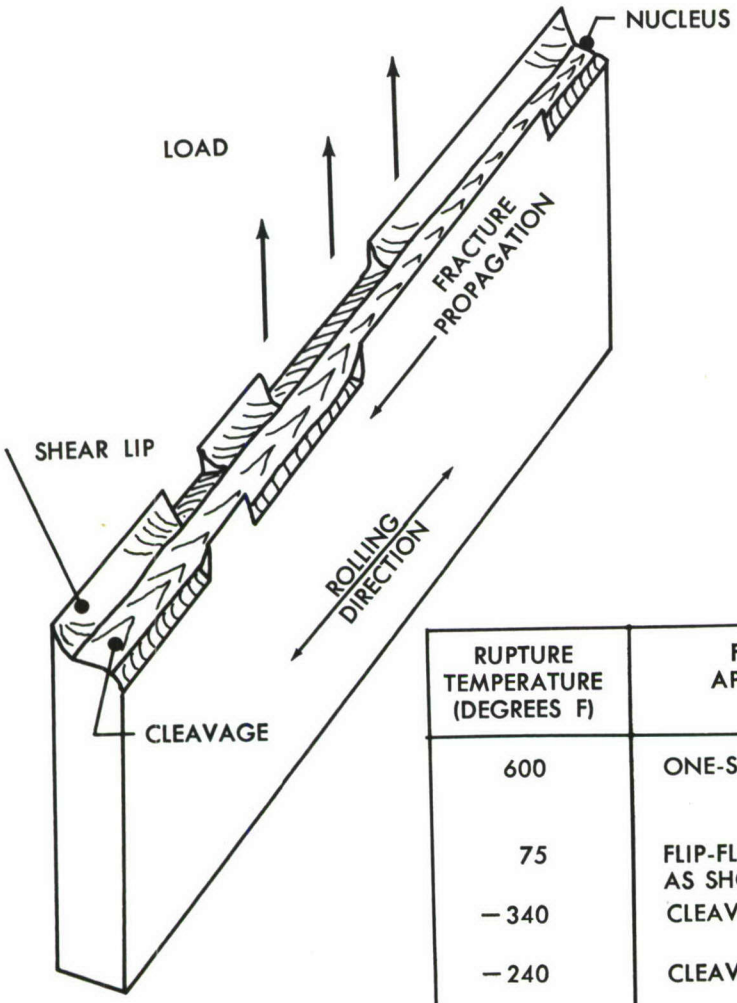


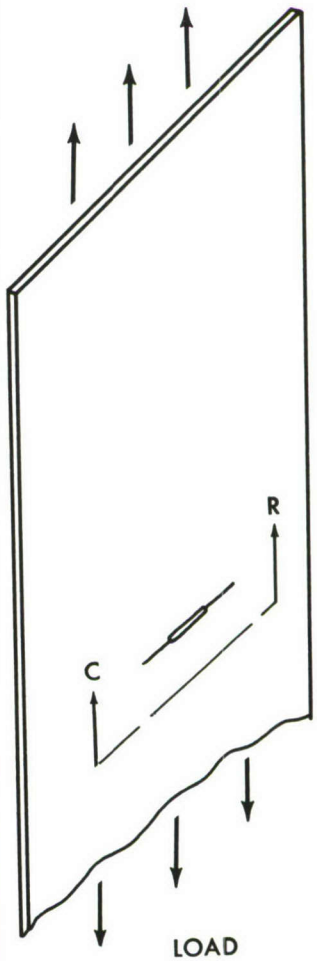
TEST SETUP FOR RECORDING MICROCRACK EXTENSION OF FATIGUE CRACK IN PANEL DURING STEADY STATE LOADING RATE OF 6000 LB PER MINUTE

Figure 119. MICRO-METAL QUAKES



THESE REGIONS ARE NOT VISIBLY
OBVIOUS AT FRACTURE TEMPERATURES
AS LOW AS −240 AND −340 DEGREES F





RUPTURE TEMPERATURE (DEGREES F)	FRACTURE APPEARANCE
600	ONE-SIDED SHEAR LIP
75	FLIP-FLOP SHEAR LIP AS SHOWN
−340	CLEAVAGE
−240	CLEAVAGE
−100	CLEAVAGE

Figure 120. FRACTURE APPEARANCE

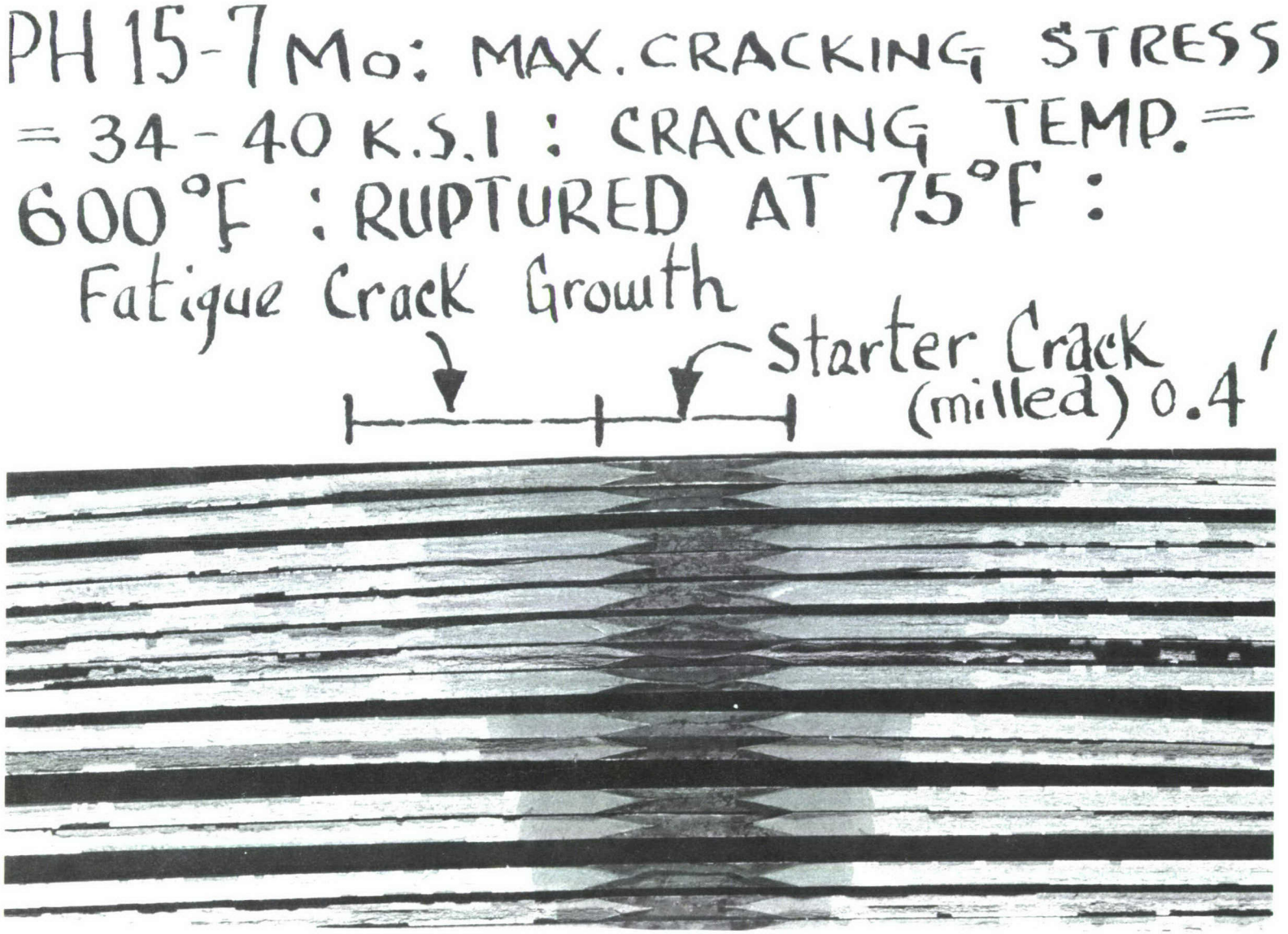


Figure 121. HEAT TINTED FATIGUE CRACKED SURFACES

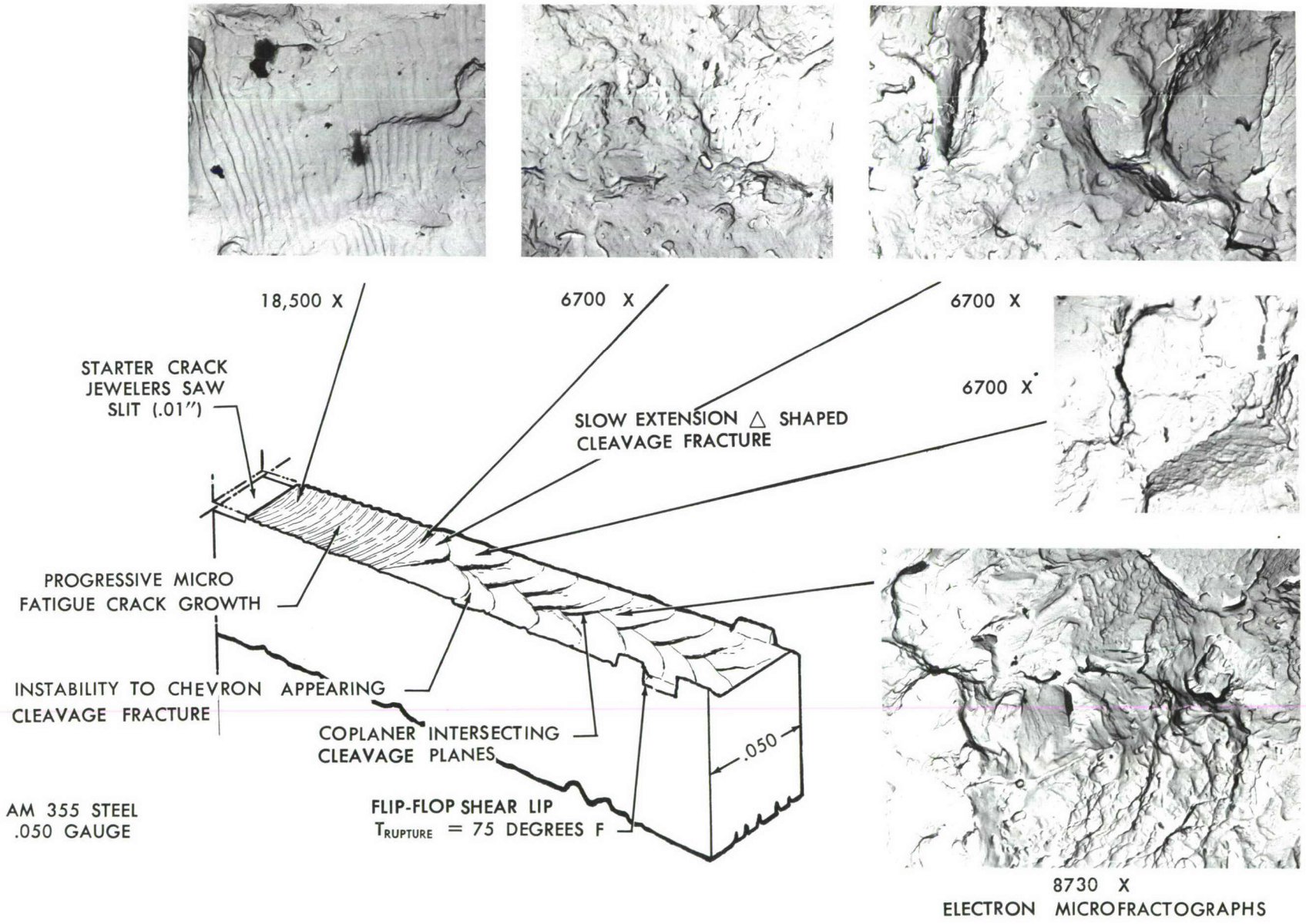


Figure 122. FRACTURE TRANSITION

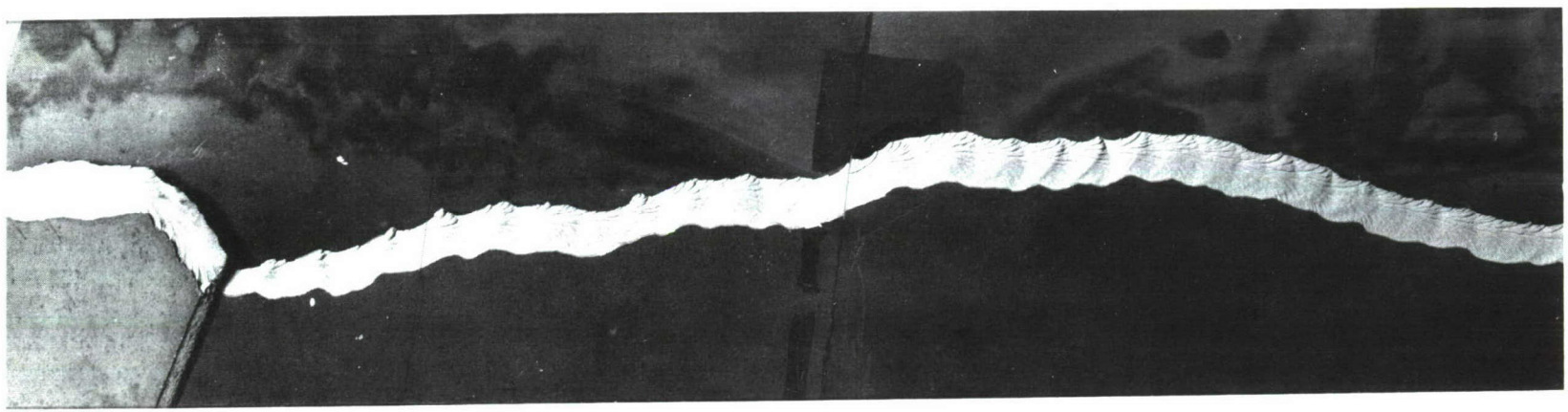


Figure 123. SINUSOIDAL FRACTURE PATH

Girthwise fracture in a 43 inch diameter pressure vessel of 0.250" - 4340 steel heat treated to 270,000 PSI tensile strength. Chevron markings pointing to the direction from which the crack propagated can be clearly seen. There are some additional interesting observations that are present on this fracture surface. The gross-curving of the fracture has coursed a crude sine-wave. Along the shear lip a finer sine-wave can also be seen. In the thickness direction of the shell another wave shape can be seen in a direction in and out of the plane of the photograph. This certainly suggests the three dimensional aspects of fracture dynamics (not counting time).

SECTION 14

ANALYSIS

The purpose of this section is to provide analytical methods of correlating, for design use, the test results of the previous sections. Two approaches are taken: one semi-empirical, and the other a more theoretical approach based on the use of the digital computer.

In the analytical study the significance of plastic deformation during the fracture of ductile metals is emphasized. For example, the empirical expression for residual strength of cracked plates is a modification of Crichlow's formula, Reference 6. This formula is based on the notion of an effective width of plastically strained material existing at the end of a crack.

The empirical expression for crack growth also is influenced by the idea of the width of the plastic zone. In addition, the expression accounts for the observed fact that the rate of cracking approaches infinity as the crack length approaches its critical value.

The digital solution is an analysis of the elastic and plastic stresses and strains existing in a cracked plate. The Redundant Force Method for statically indeterminate systems and the Reuss equations of triaxial plasticity are employed. The purpose of this study is to supply information about the shape and extent of the plastic region, and the stress and strain distributions existing in the region as functions of gross section stress. The results may remove some of the empiricism from the residual strength and crack propagation formulas, by allowing the correlation of the empirical constants with more fundamental material properties.

In the study of mechanical problems two basic methods are generally available: the energy method, and the approach through the solution of differential equations. When correctly applied with equivalent approximations the two methods give the same results. Both approaches have proved useful in fracture mechanics. In the present study, methods equivalent to the differential equation approach have been selected because of the emphasis on plasticity and the availability of the digital computer.

Residual Strength of Cracked Plates

A cracked plate of ductile material fails under a static load lower than would be computed from the material ultimate stress and the net remaining section. This notch sensitivity results from the development of an elastic stress concentration in the region at the end of the crack. Figure 133 shows the nature of this concentration as computed by the Redundant Force Method, Reference 7. The figure shows the longitudinal tensile stress existing in one quarter of the plate. The concentration is very localized and severe. These results are discussed in greater detail in a later paragraph.

The highly stressed region of the plate quickly becomes plastic, and failure occurs when the stresses and strains exceed certain limiting values. The plastic behavior of the material is fundamental in the process.

Crichlow (Reference 6) has predicted the residual strength of cracked sheet by a method which combines simplicity with a realistic appreciation of the significant role played by plasticity. The method utilizes an "effective width" which represents the width attained by the plastic region at the end of the crack at the instant of failure. The plastic width is assumed to be a constant of the material for infinitely wide sheet. This viewpoint is adopted in the present study, except that a different method of accounting for plate width is suggested.

Figure 124 shows the assumed stress distribution on a section through the crack. This distribution is an idealization of the actual plastic distribution represented by the dotted line. Equilibrium gives

$$\sigma_R w = \sigma_u \cdot 2 w_e + \sigma_R (w - \ell_c - 2 w_e) \tag{4}$$

where σ_R is the gross section stress at failure, σ_u is the tensile ultimate, and w_e is the effective width.

$$\therefore \quad \frac{\sigma_R}{\sigma_u} = \frac{1}{\ell_c/R_p + 1} \tag{5}$$

where $R_p = 2w_e$. In this equation R_p is assumed to be a constant of the material. The equation has somewhat the correct character since $\sigma_R = \sigma_u$ when the crack length, ℓ_c, is zero, and σ_R decreases as ℓ_c increases. Howewever σ_R should, but does not, become zero when ℓ_c equals the plate width, w. In fact w does not appear in the equation. Crichlow assumes that the effective width, w_e, is a function of the plate width, and gives an expression involving two parameters for this function. A little simpler method of accounting for the effect of plate width is suggested here.

Equation (5) is modified by the introduction of the term $1 - \ell_c/w$, so that

$$\frac{\sigma_R}{\sigma_u} = \frac{1 - \ell_c/w}{1 + \ell_c/R_p} \tag{6}$$

In this expression, σ_R approaches zero when ℓ_c approaches w, which is correct.

Significance of R_p

Equation (6) has the virtue of assuming the form

$$\frac{\sigma_R}{\sigma_u} = 1 - \ell_c/w \tag{7}$$

when $R_p \rightarrow \infty$. Equation (7) evidently gives the residual strength for a cracked plate made of a completely notch-resistant material. Also when

$R_p \rightarrow 0$, $\sigma_R = 0$, which behavior is characteristic of a material without notch resistance. Thus R_p is a measure of the notch resistance of the material. The quantity R_p therefore is termed the "plastic zone notch resistance factor" or simply the "notch resistance factor."

Note that R_p also can be interpreted to mean the effective width of the plastic zone for an infinitely wide sheet. R_p is also the length of crack in an finitely wide sheet which reduces the strength of the sheet by 50%.

Equation (6) can be put in the form

$$\frac{\sigma_R}{\sigma_u} = \frac{1 - \ell_c/w}{1 + \frac{w}{R_p}\frac{\ell_c}{w}} \qquad (8)$$

Comparison of Residual Strength Formula With Test

Figures 125 through 127 show how equation (8) compares with test results. Considering the scatter, the agreement appears satisfactory, especially for PH15-7 Mo. Note that equation (8) contains only the one empirical parameter, R_p. In Figure 125, for example, R_p was determined from a single two-inch panel test point. The rest of the curve for two inch panels, and the remaining panel widths follow.

Figures 128 and 129 show comparisons with data obtained by Crichlow for 24ST and 75ST aluminum alloys. (Reference 6).

Most metals exhibit a period of "slow crack extension" during which the crack grows slowly as the gross section stress is increased. The residual stress, σ_R, in equation (8) is understood to be the gross section stress at the end of the slow growth period at the instant of failure. The length, ℓ_c , is understood to be the crack length at the same instant.

Critical Crack Length

Equation (8) can be solved for ℓ_c to give

$$\frac{\ell_c}{w} = \frac{1 - \sigma_R/\sigma_u}{1 + \frac{w}{R_p}\frac{\sigma_R}{\sigma_u}} \qquad (9)$$

where ℓ_c is the critical crack length corresponding to the gross section stress, σ_R

Correlation of Notch Resistance With Ductility

Figure 130 shows the dependence of the notch resistance factor on material elongation. The figure indicates that some correlation between these two quantities exists. The more ductile materials are more notch resistant. The figure also illustrates the usefulness of the notch resistance factor concept in correlating material properties.

Crack Propagation

The following expression for the rate of damage propagation in the cracking phase is proposed:

$$\frac{d\ell}{dn} = \mu \frac{(\ell / \ell_c)^m}{(1 - \ell / \ell_c)^n} \tag{10}$$

where ℓ_c is the critical crack length and μ is a constant. This equation is based on the following two considerations: (a) As the crack grows in a stress field, more and more stress has to flow around the ends of the crack. Therefore, the rate of propagation should be proportional to some power of the crack length, and (b) when the crack reaches its critical length, the rate of propagation approaches infinity. Therefore, the rate of propagation should be inversely proportional to some power of the difference between the crack length and its critical value.

Preliminary comparisons indicate that the choice of exponents m = n = 1 gives the best correlation with test results. The choice m = 1 also is consistent with the viewpoint, adopted in the discussion of residual strength, that a plastic region is formed proportional to the length of the crack for any given value of the gross stress. Thus solving equation (5) for R_p gives

$$R_p = \frac{\ell_c}{\frac{\sigma_u}{\sigma} - 1} \tag{11}$$

Recall that R_p represents the width of the plastic region for an infinitely wide sheet. If the length of the plastic region is proportional to the length of the crack, then some justification exists for assuming that the rate of cracking likewise is proportional to the crack length.

Equation (10) then becomes

$$\frac{d\ell}{dn} = \mu \frac{\ell}{\ell_c - \ell} \tag{12}$$

Integrating (12) gives

$$\mu n + C = \ell_c \ln \ell - \ell \tag{13}$$

where C is a constant. At $n = n_o$, $\ell = \ell_o$, where n_o and ℓ_o are the number of cycles and the crack length existing at some time shortly after the initiation of the cracking phase.

$$\therefore \quad \mu n_o + C = \ell_c \cdot \ln \ell_o - \ell_o \tag{14}$$

Eliminating C between (13) and (14) gives

$$\mu(n - n_o) = \ell_c \cdot \ln \frac{\ell}{\ell_o} - (\ell - \ell_o) \tag{15}$$

The constant μ can be evaluated by requiring that $\ell = \ell_1$ where ℓ_1 is the length of the crack corresponding to any number of cycles n_1, different from n_o.

$$\therefore \mu(n_1 - n_o) = \ell_c \ln \frac{\ell_1}{\ell_o} - (\ell_1 - \ell_o) \tag{16}$$

$$\therefore \mu = \frac{\ell_c \ln (\ell_1/\ell_o) - (\ell_1 - \ell_o)}{n_1 - n_o} \tag{17}$$

In the particular case when ℓ_1 is equal to the critical crack length ℓ_c, n_1 becomes equal to the fatigue life N.

$$\mu = \frac{\ell_c \ln (\ell_c/\ell_o) - (\ell_c - \ell_o)}{N - n_o} \tag{18}$$

Therefore, the constant μ can be evaluated from the initial conditions ℓ_o and n_o (which for most purposes can be chosen arbitrarily); the critical crack length ℓ_c, which can be evaluated from equation (9); and the fatigue life N. Equation (12) then gives the rate of cracking. The number of cycles n corresponding to any crack length ℓ can be obtained from equation (15).

In the case where the crack length is zero ($\ell = 0$), equation (15) gives $n = -\infty$. This result can be interpreted correctly to mean that the initial phase of damage propagation occupies a very long time. Actually, however, equation (15) does not apply to crack nucleation. A different mechanism, which must be treated separately, operates during the nucleation phase.

Significance of μ

The constant μ has a geometric interpretation. From equation (12), if $\ell = \ell_c/2$

$$\mu = \left(\frac{d\ell}{dn}\right)_{\ell = \ell_c/2} \tag{19}$$

In other words, μ represents the slope of the damage curve when the crack length has reached one half its critical value. The quantity, μ, therefore, is denoted the mean crack rate.

Comparison of Crack Rate Formula With Test

Figure 131 is a comparison between experimental and computed values of $d\ell/dn$ for all of the materials tested. The analytical values were computed from equations (18) and (12). The values of ℓ_o, n_o and N used were taken from the test results. In many cases N had to be estimated because the test was stopped short of failure, so that the specimen could

be used for residual strength determinations. The required values of ℓ_c were obtained from equation (9). The correlation is exceptionally good for fatigue data.

Cumulative Cracking Under Programmed Loads

Cumulative crack lengths were computed for RENE' 41 panels. Curves of crack length versus cycles were constructed from equation (15). These curves are shown in Figure 64 for three test stresses. The curves were computed in such a way as to pass through the points corresponding to $\ell = .6$ and the largest value of ℓ measured in the test, according to the method explained previously. For example the curve for $\sigma = 45{,}000$ psi is based on $n_o = 18.0$, $\ell_o = .6$, $n_1 = 38.2$, $\ell_1 = 1.31$.

Values of the critical crack length for use in equation (15) were obtained from equation (9) using $\sigma_u = 196{,}000$ psi and $R_p = 2.68$. This value of the notch resistance factor R_p is the same as was used in the comparison with test results shown in Figure 127.

Figure 64 shows the agreement obtained between the calculated and measured damage curves for each of the three stress levels. The agreement indicates that the shape of the damage curve is closely approximated by equation (15).

The dotted line shows the method of determining the cumulative crack length. Beginning at a crack length of .6 inches, 7,000 cycles are applied at $\sigma = 45{,}000$ psi, 8,000 cycles are applied at 40,000 psi and 20,500 cycles are applied at 20,500 psi to finally produce a crack length of 1.78 inches. This procedure contains the implicit assumption that the damage curve in the cracking phase for a given stress level is not affected by previous cycles run at a different stress.

Table 5 shows a comparison of experimental and computed results for cumulative crack length. The ratios of calculated to measured results show considerable scatter, but the average value is 0.95.

Digital Analysis of the Elastic Stress Distribution in a Cracked Plate

The elastic stress distribution was computed by the Redundant Force Method. Descriptions of this method can be found in References 7 and 8. The method is applicable to continuous elastic bodies. However, such a body first must be idealized as a discrete structure.

Figure 132 shows the dimensions of the plate and crack. Only one-fourth of the plate has to be analyzed because of symmetry. The figure also shows the idealized structure. The idealization consists of bars carrying axial load and panels carrying shear. The use of such idealizations for elasticity problems has been verified by comparisons with other solutions and test results. (For example, see Appendix B of Reference 11.) Note that the lumping has been made very fine in the region of the crack tip to accomodate the expected high stress gradient.

Figure 133 shows the computed distribution of longitudinal tensile stress. Stress can be measured from the figure, which is to scale. As expected, a large stress concentration appears at the end of the crack. Along the prolongation of the crack the stress rapidly drops to approximately the gross-section stress at the edge of the plate. The stress at the crack in the longitudinal direction is, of course, zero. A complete set of transverse and shearing stresses also was obtained.

The distribution shown is believed to be an accurate representation of the elastic stress distribution in the cracked plate. However the stress at the one point at the tip of the crack is a function of the fineness of the idealization. A finer lumping would give a higher stress. This fact is of little significance in the present study for the following reasons: (a) The purpose of the analysis is to determine the stress and strain environment in the general region of the crack tip and the rest of the plate without going into the microscopic details. (b) The elastic analysis is the basis of the plastic analysis which follows. The result of the plastic analysis is to limit the maximum stress to a value less than or equal to the ultimate for the material.

Figure 134 shows a comparison of the longitudinal stress computed along the transverse plane of symmetry with the theoretical result of Westergaard for an infinitely wide plate (Reference 9). The agreement verifies the analysis.

Plastic Stress Distribution

The plastic analysis is nonlinear because of the nonlinear relation between stress and strain. The nonlinearity requires the performance of an iterative or stepwise solution. This solution utilizes the Redundant Force Method and the Reuss plastic stress-strain equations (References 7 and 10). The elastic analysis discussed previously enters into the solution.

At first the problem was approached by the straightforward iterative method described in Reference 11 where it was used in the plastic analysis of the stress distribution in a plate with a hole. This approach was found to be rather slowly convergent. Therefore, a new, more rapidly convergent approach was sought for the crack problem because the more severe stress concentration aggravates the convergence difficulties.

The new approach employs the Newton-Raphson method for solving nonlinear simultaneous equations. An application of this method to the plastic analysis of structures was given in Reference 12. The method was found to be rapidly convergent, however the solution of a set of equations equal in number to the number of structural elements was required.

The new Newton-Raphson approach requires solving at each iteration a set of equations equal in number only to the number of redundants. For a plastic statically determinate structure, no iterations are required; the solution is given directly. Thus a basic advantage of the Redundant Force Method is utilized. The details of the new technique are presented in Appendix B.

Figure 135 shows the elastic distribution of equivalent stress in the plate at a gross-section of 7,500 psi. The yielding in the plate depends on this equivalent, or octahedral, stress. Where the equivalent

stress is high, more plasticity develops. Figure 135, therefore, gives an idea of how the plasticity develops even though the distribution is elastic. Note the existence of a locus of minimums, or a valley, and two loci of maximums, or ridges, shown by dotted lines extending in approximately opposite directions from the tip of the crack.

The plastic stress distribution in the cracked plate was computed as described above. The results of these computations are given in Appendix D. Time was not available to make extensive calculations. However, enough work was done to demonstrate that the expected trends do in fact develop and that the process is convergent even in the presence of the extreme stress concentration at the end of the crack.

The calculations are based on an equivalent stress-strain curve represented by the Ramberg-Osgood expression with the exponent n equal to 17. A graph of the expression is given in Appendix D. This stress-strain curve was chosen arbitrarily to explore the feasibility of the digital method, and does not represent any particular material. The results of the analysis, therefore, are preliminary and qualitative. In selecting stress-strain curves for future studies, consideration should be given to the fact that strains measured on a 2 inch gauge length may not provide the best information for use in connection with a finely-scaled analysis.

Appendix D contains graphs showing the convergence, the plastic stress distribution and the residual stress remaining after removal of load from the cracked plate.

The significance of a favorable convergence rate is emphasized, because nonlinear problems cannot be solved except by a repetitive process. A method which does not converge satisfactorily has no application.

Studies of the plastic stress distribution such as are presented in Appendix D can be extended to provide information on the width of the plastic zone. This width can be correlated with the stress-strain characteristics of the material and values of the effective width of the plastic zone computed from test with the aid of the empirical formula.

Studies of the variation of plastic stress during a loading cycle can throw light on the fatigue process. Studies of the residual stress variation as a function of gross-section stress can help to explain why cycles of high stress often have a marked effect on the subsequent life under cycles of lower load.

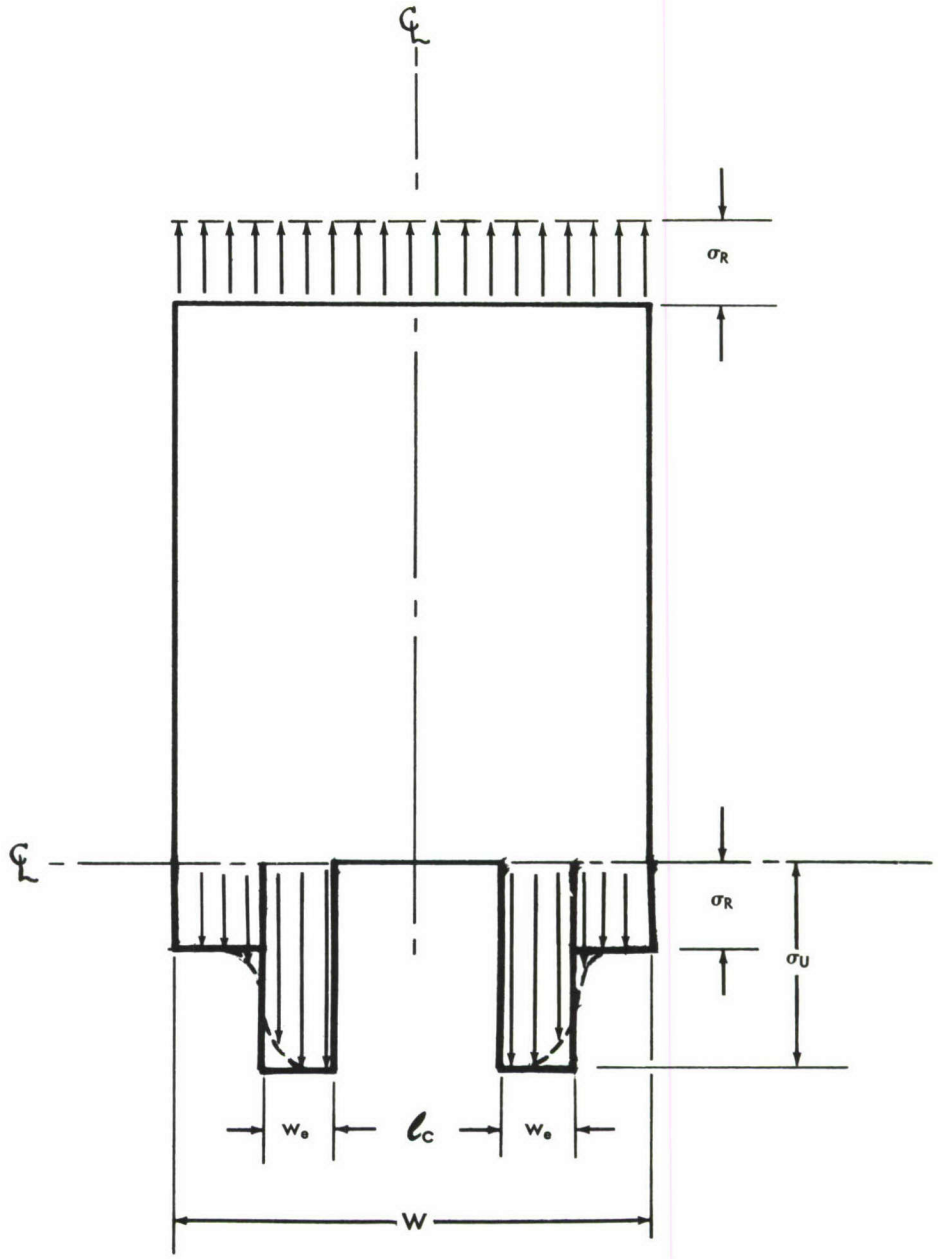


Figure 124. CRACKED PLATE IN EQUILIBRIUM

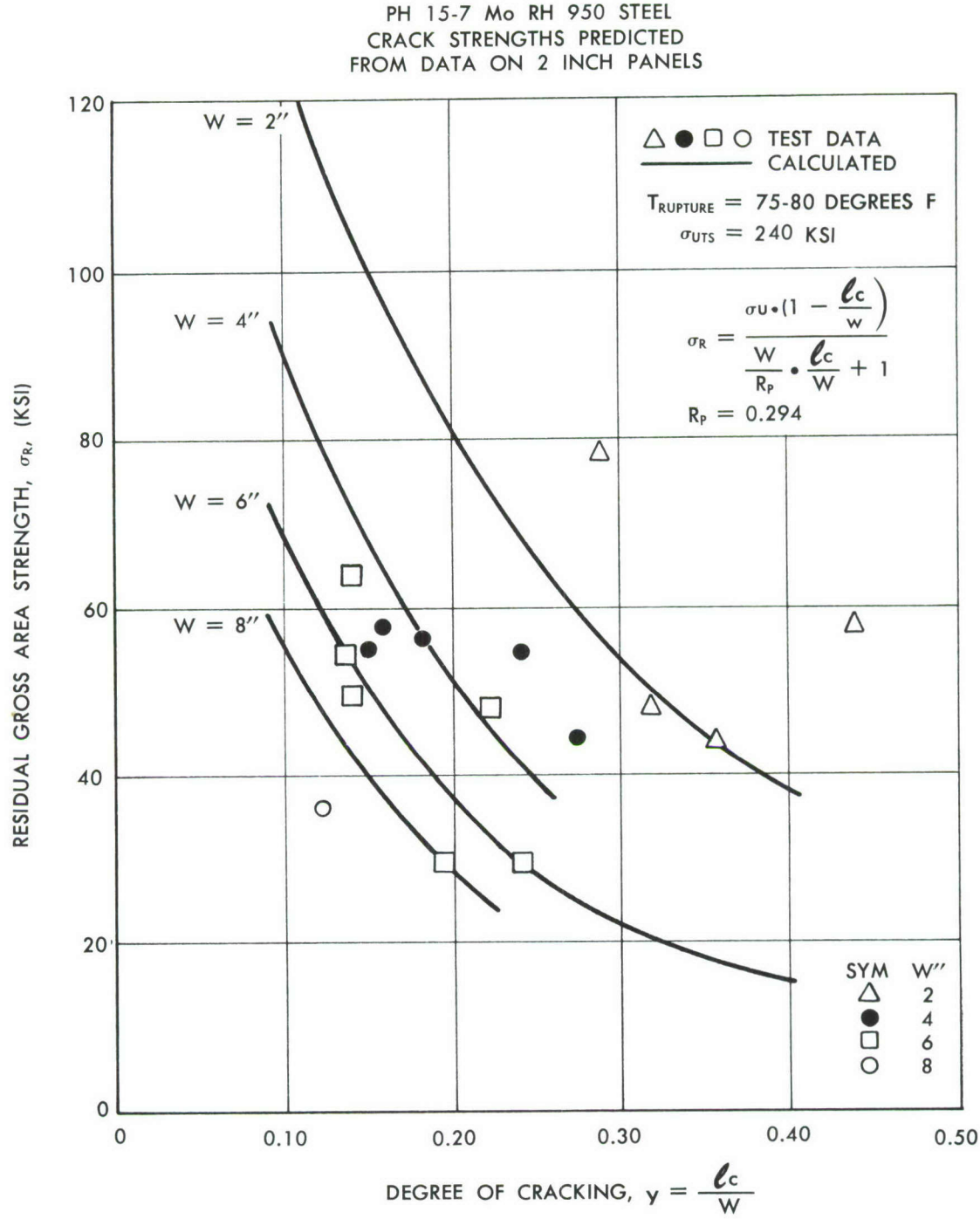


Figure 125. COMPARISON OF RESIDUAL STRENGTH FORMULA WITH TEST FOR PH15-7 MO RH950

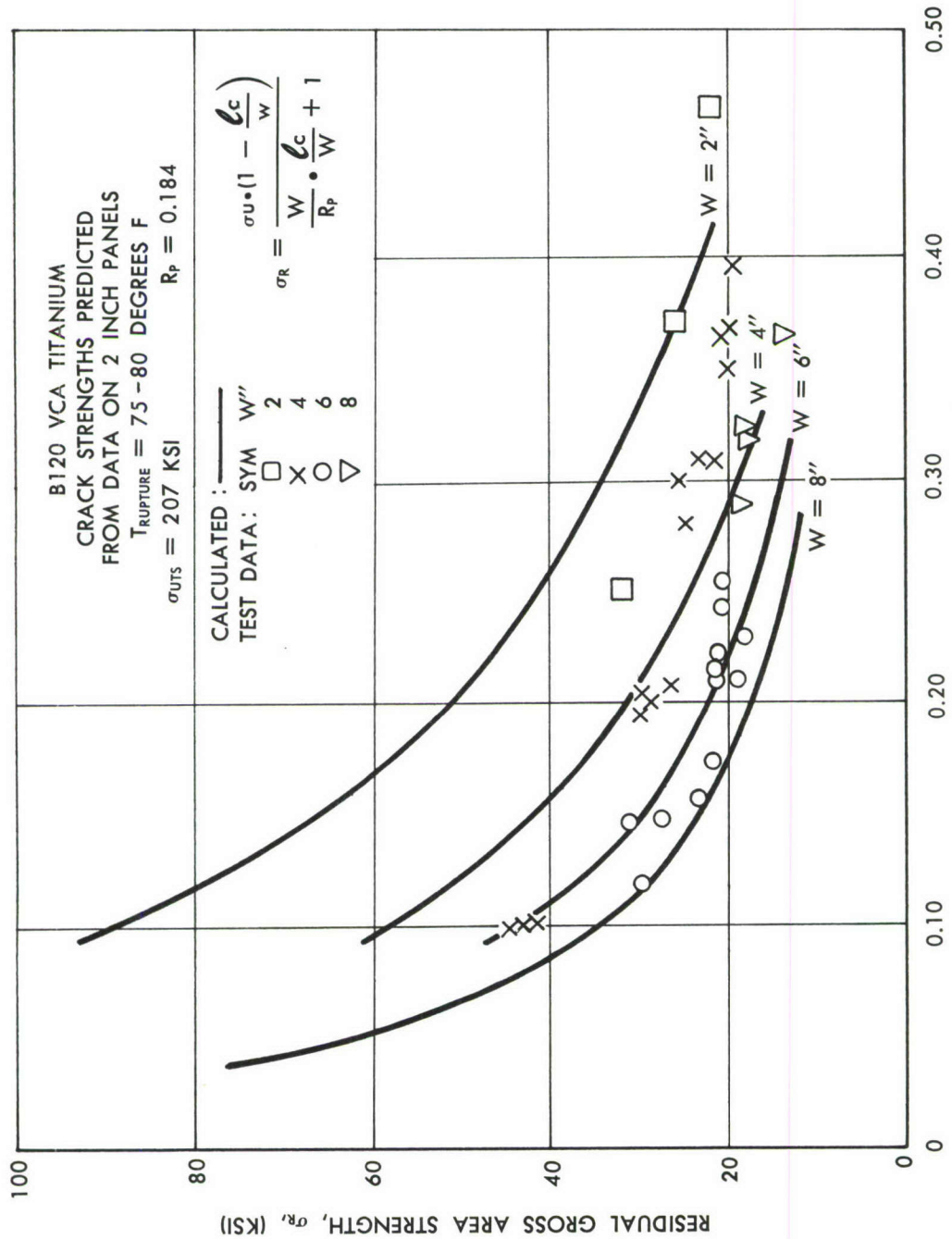


Figure 126. COMPARISON OF RESIDUAL STRENGTH FORMULA WITH TEST FOR B120 VCA TITANIUM

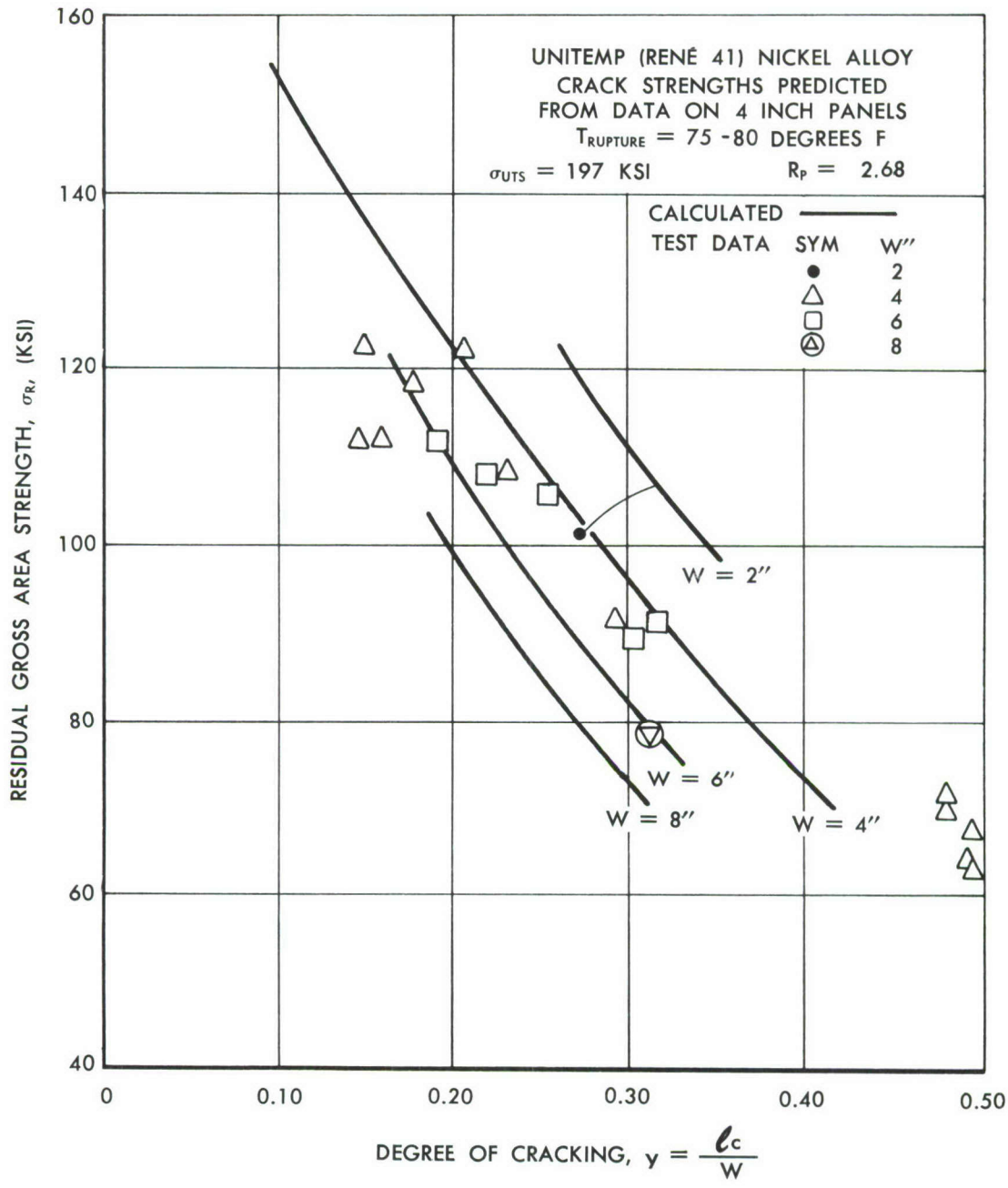


Figure 127. COMPARISON OF RESIDUAL STRENGTH FORMULA WITH TEST FOR RENÉ 41

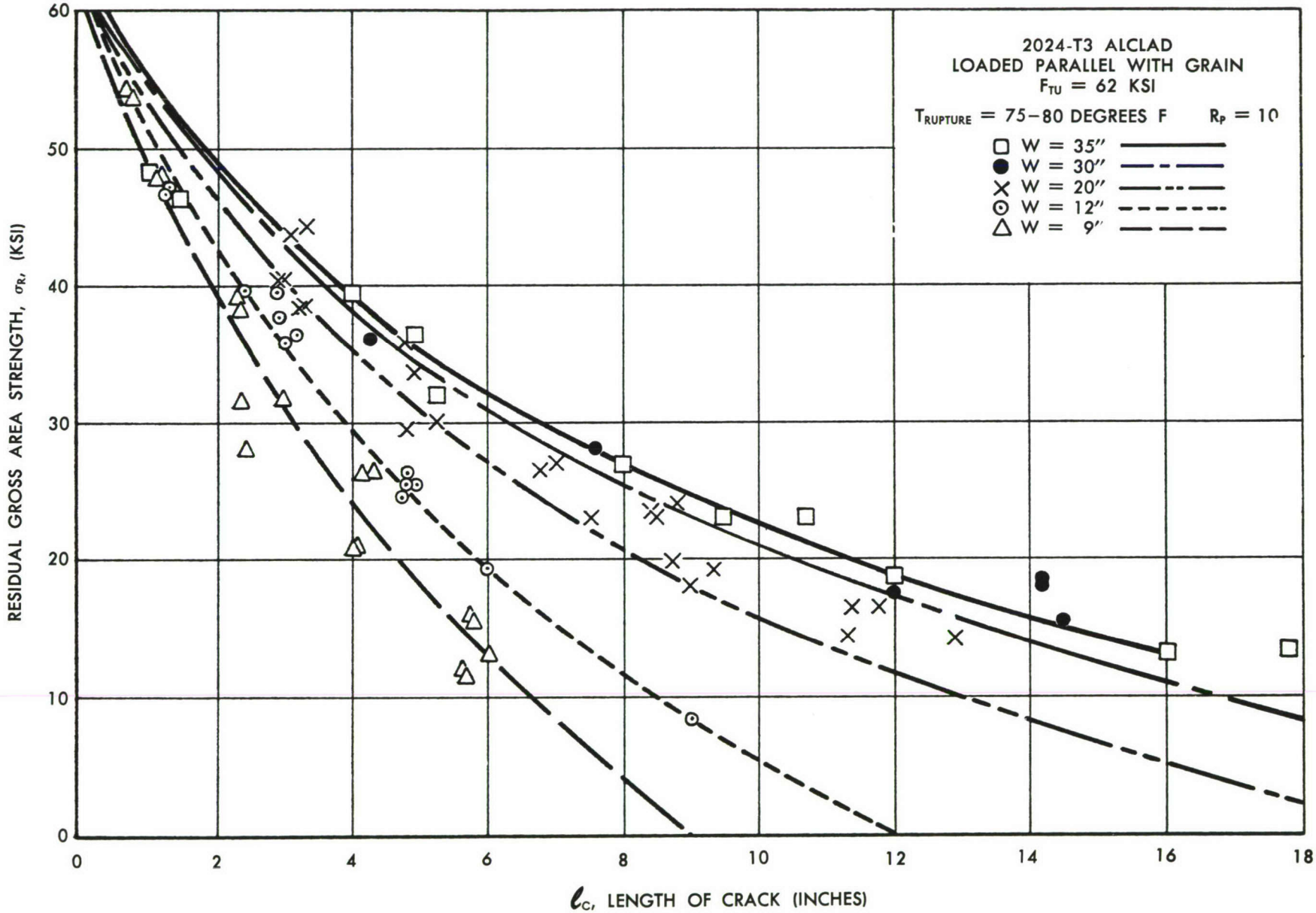


Figure 128. COMPARISON OF RESIDUAL STRENGTH FORMULA WITH TEST FOR 2024-T3 ALCLAD

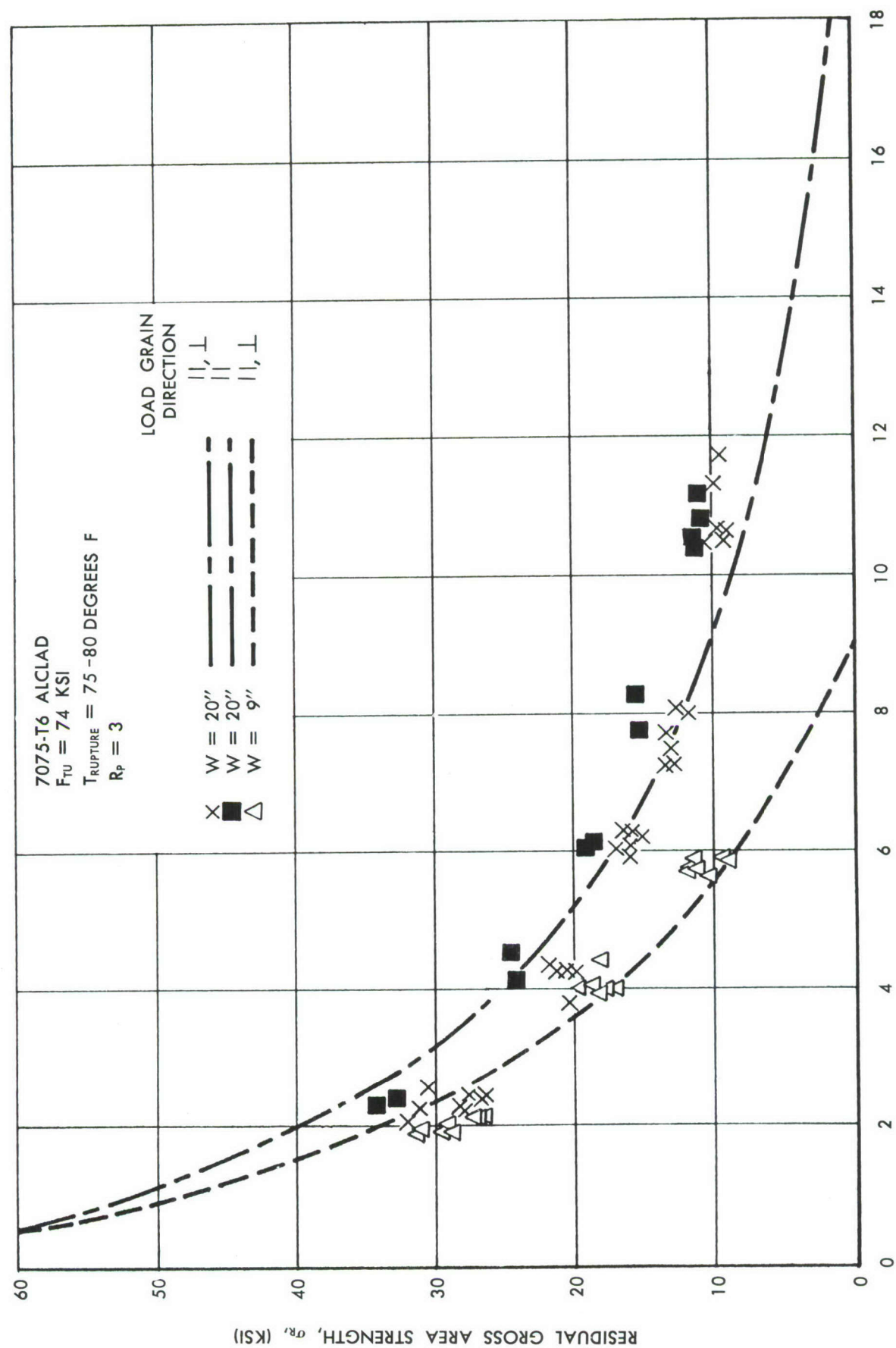


Figure 129. COMPARISON OF RESIDUAL STRENGTH FORMULA WITH TEST FOR 7075-T6 ALCLAD

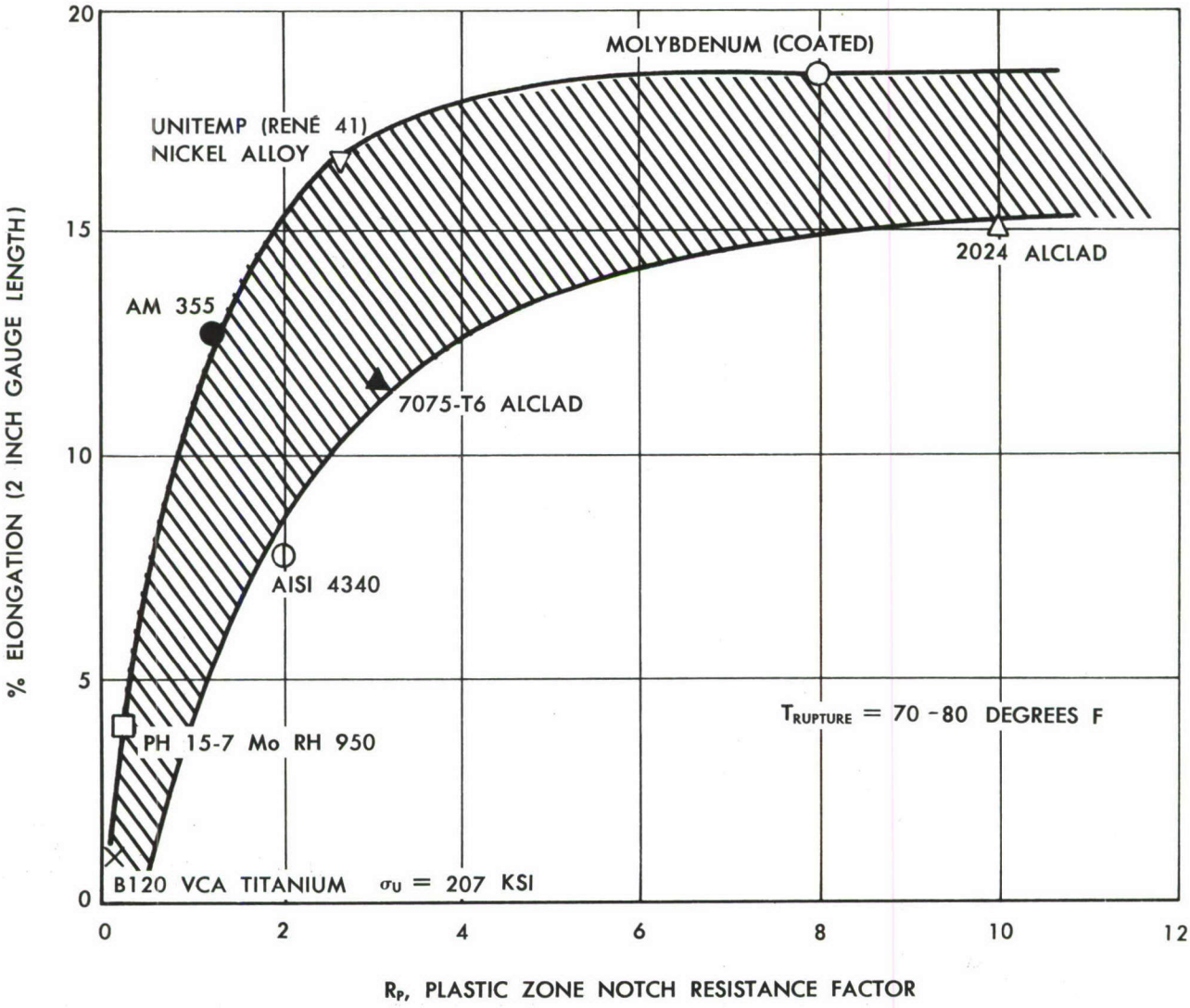


Figure 130. NOTCH RESISTANCE AS FUNCTION OF MATERIAL DUCTILITY

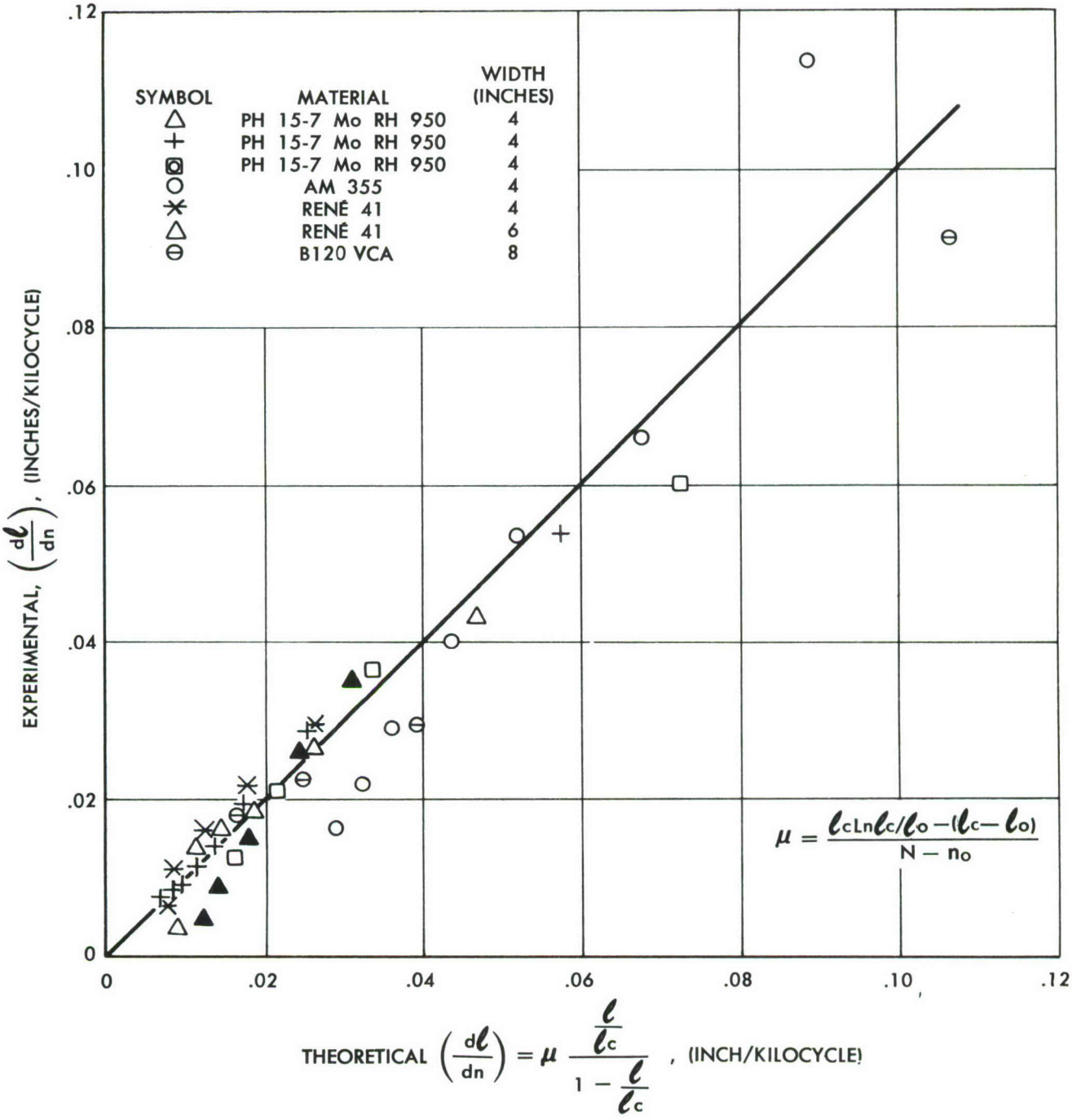


Figure 131. COMPARISON OF THEORETICAL AND EXPERIMENTAL CRACK PROPAGATION RATES

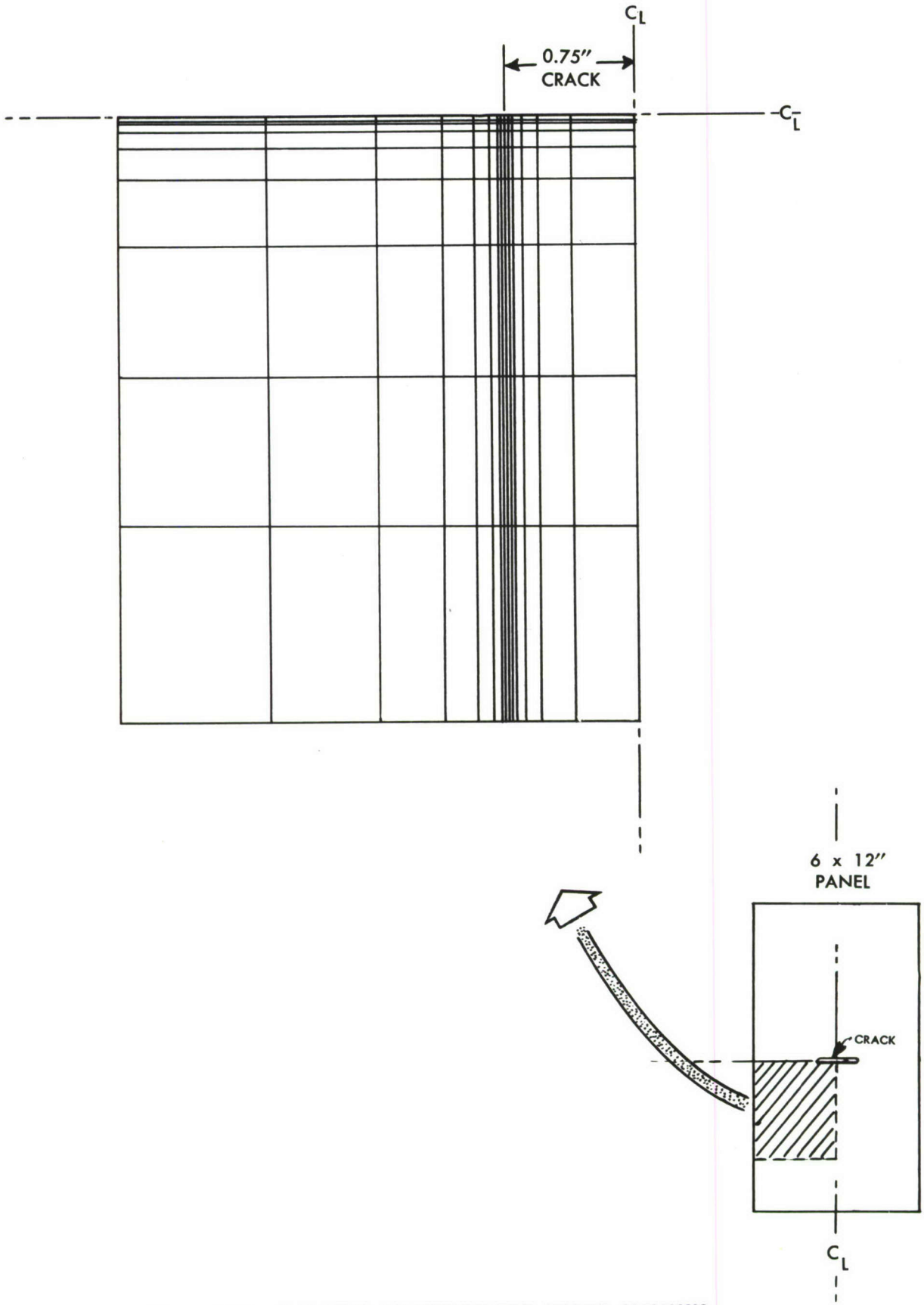


Figure 132. IDEALIZED STRUCTURE FOR CRACK ANALYSIS

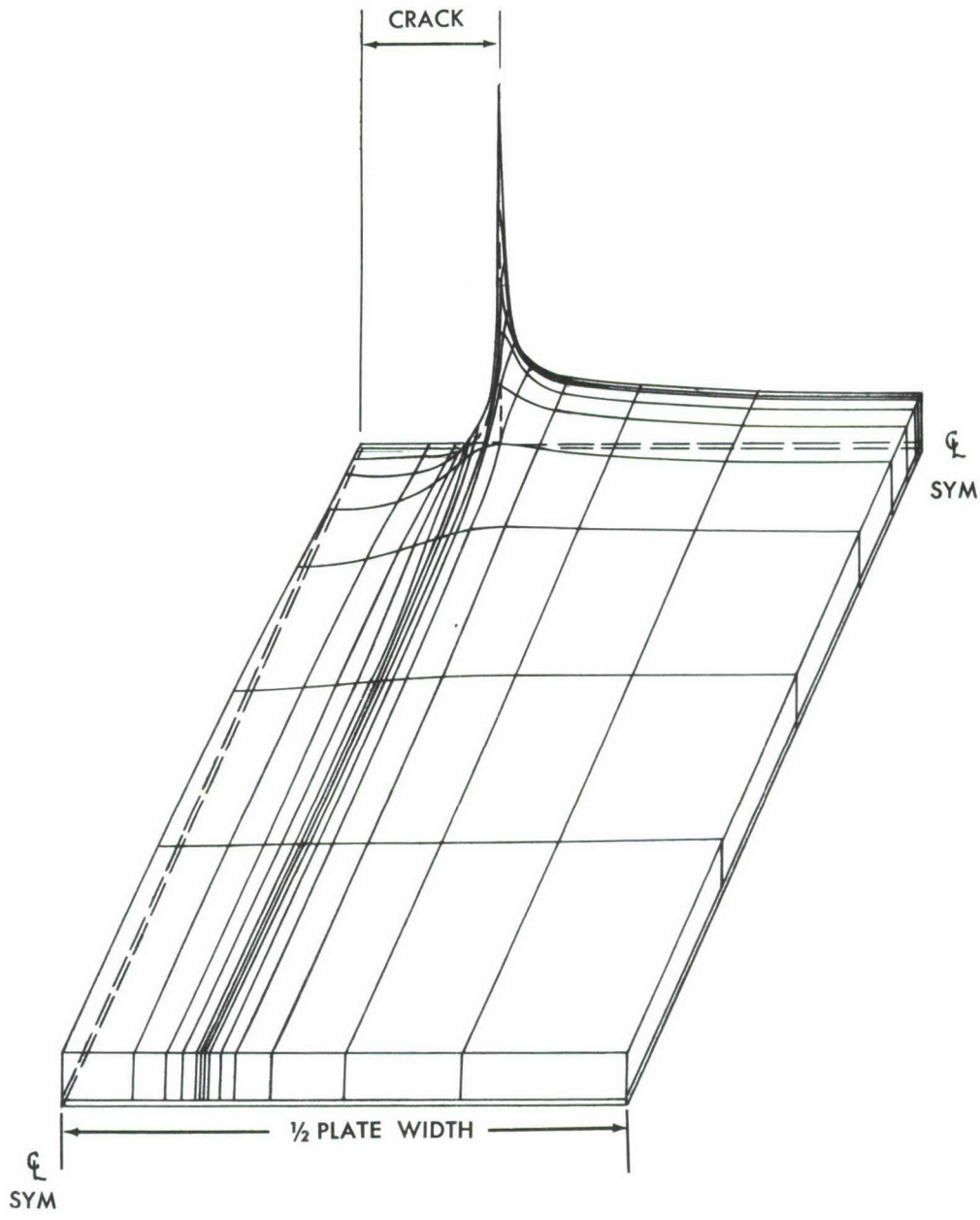


Figure 133. σ_y, **ELASTIC DISTRIBUTION**

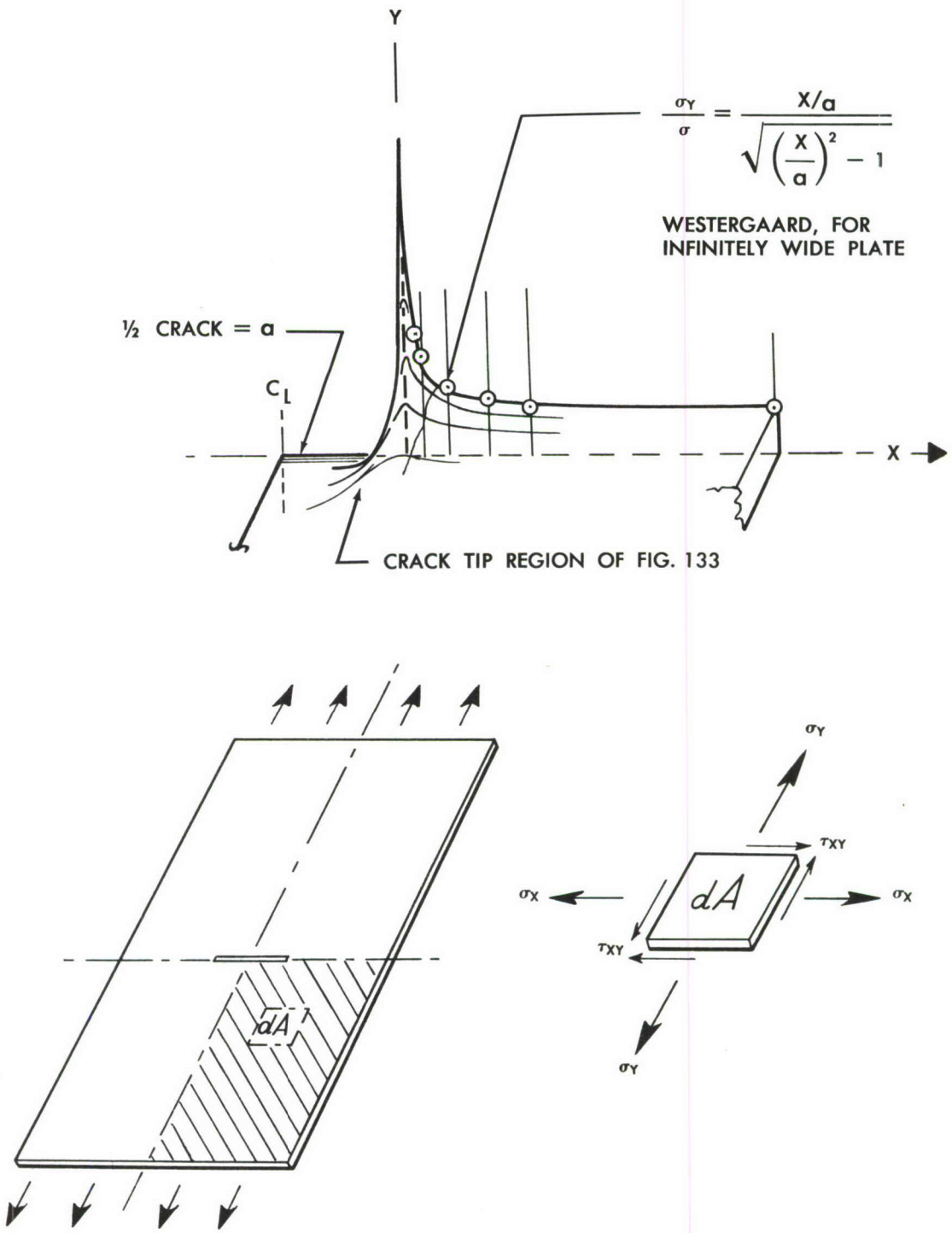


Figure 134. COMPARISON WITH WESTERGAARD'S RESULT

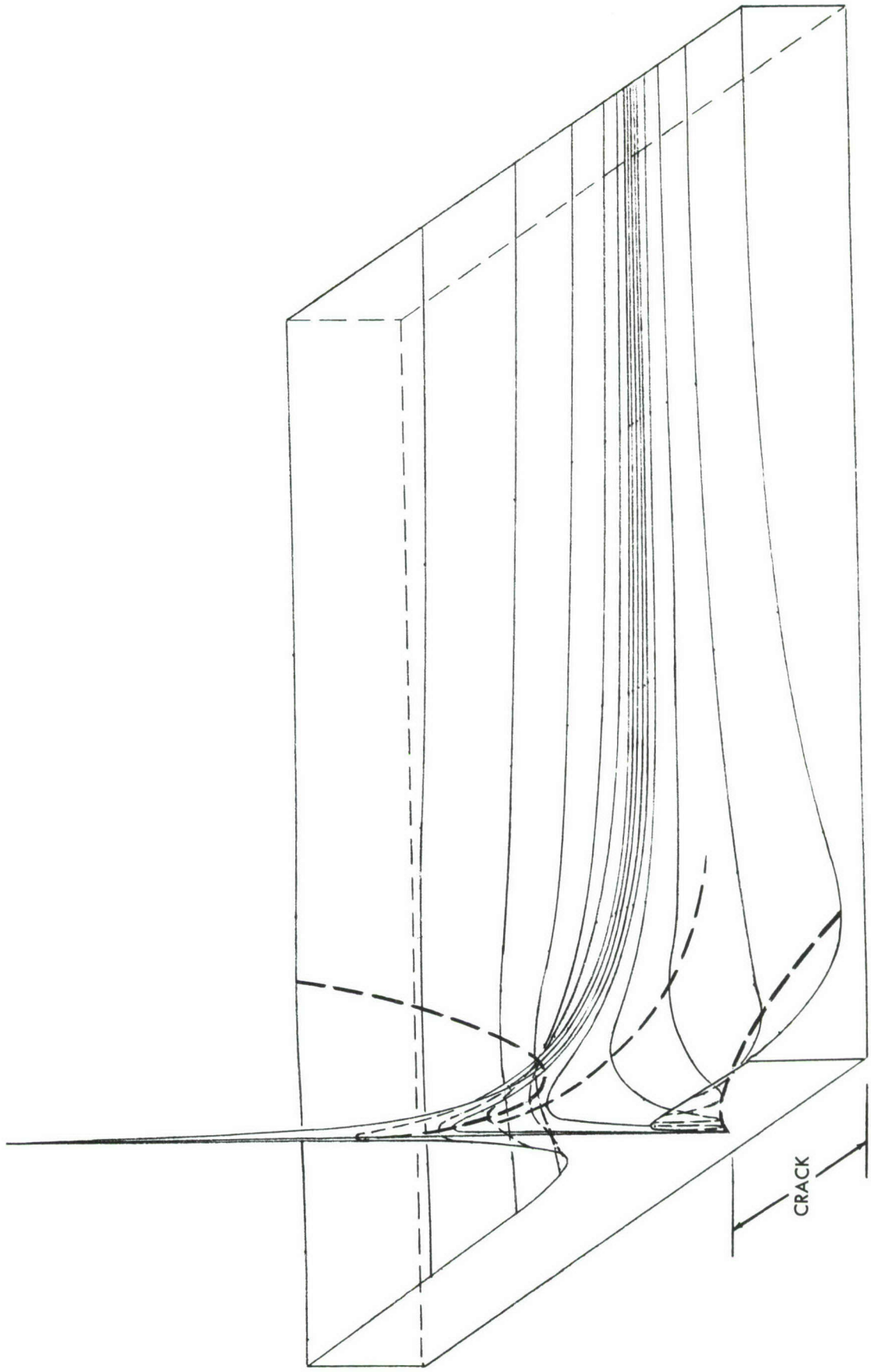


Figure 135. ELASTIC DISTRIBUTION OF EQUIVALENT STRESS

SECTION 15

CONCLUSIONS AND RECOMMENDATIONS

The investigation has brought forth a number of findings which have a bearing on structural design, especially for high speed aircraft and spacecraft. The results of the study again emphasize that the selection of optimum materials for such vehicles is a major problem, because of the broad range of design operating temperatures. This range can result from aerodynamic heating at one extreme, and the need for the containment of cryogenic fuels, or travel in near space, at the other.

In the past, designers have found reliable short-cut testing methods for evaluating structure. The development of such methods for future designs will be more difficult, because many of the strength and deformation properties of materials are time dependent. In particular the crack propagation and residual strength properties depend on time at temperature. These properties, like static properties, must be evaluated as time dependent parameters.

The foregoing considerations apply to the testing of entire structures as well as to coupons, joints and small components. Realistic temperatures and load histories are required during test because of the time dependence. Accelerated tests can be developed, but caution must be observed in their use.

Conclusions

1. A fatigue crack generated by mechanical load stressing is the most severe type of notch that can be formed in a metal, for the range of notches, materials and temperatures that were investigated in the program.

2. Residual strengths associated with cracks formed at low cyclic stress or low temperature tend to be lower than residual strengths associated with cracks formed at higher stress or higher temperature. This effect may result from the development of finer, more acute, cracks at low stress or low temperature, or from the relief, through creep, of residual stresses at elevated temperatures.

3. The residual strength of a cracked plate is correlated with ductility. The more ductile materials tend to be more notch resistant.

4. Fatigue strengths are usually greater at low and cryogenic temperatures than at elevated temperatures. However, once a fatigue crack has been initiated the residual strengths in many of the notch sensitive materials are drastically reduced in low and cryogenic environments.

5. The fatigue strengths of metals in general are decreased by elevated or high temperature exposure. There are some promising metals, however, that have a pronounced decrease in notch sensitivity

with increase in temperature. Beyond the crack inception or nucleation stage in structure many of these metals actually have a slower rate of fatigue crack growth.

6. Crack growth rates appear to be affected by and can be functions of the following conditions: (These effects, however, are not as pronounced in some materials as they are in others).

   a. The greater the ductility (% elongation in a 2" gauge length) the slower the visible crack growth and the longer the crack growth period.

   b. Although the fatigue life is usually decreased by an increase in temperature, the crack growth period beyond the nucleation stage is greater at elevated temperatures than at lower temperatures. However, the greater the material ductility the less pronounced this effect is.

   c. Crack growth depends on intermittent temperature cycling as well as on the total time-of-exposure at temperature under load.

7. The effect of cracks in elevated temperature environments does not appear to be as serious a problem as some may have thought. Probably the effect is less of a problem than at normal temperatures. Subzero environments, however, are far different situations and many material problems may arise. Techniques to mitigate these effects will be necessary.

   There are some components that will tolerate little or no fatigue cracking due to either low structural strength at cryogenic temperatures or for physiological reasons such as loss of atmosphere. The fail-safe design approach will have to be expanded for some of the newer and more complex structures in the anticipated environments of space.

8. The crack growth phase of fatigue damage is more predictable and less subject to scatter than the nucleation phase.

9. At elevated temperatures the cracking is more uniform than at low temperatures, where the cracking of less ductile materials tends to be sporadic.

10. Numerous findings relative to Molybdenum are presented in Section 9. In particular the W-2 and Durak B coatings provide adequate protection at elevated temperatures under steady load. However, the coatings crack and permit oxidation during the development of fatigue cracks.

11. For the biaxially stressed specimens a threshold stress level existed below which the fractures ran in a straight path. Above this threshold the course of the fracture was curved.

12. Within the range of sheet thicknesses and materials investigated the following effects of sheet thickness were observed:

a) For materials of low ductility, fracture strength decreased with an increase in sheet thickness.

b) For materials of high ductility, fracture strength decreased with a decrease in sheet thickness.

13. Electron microscope observations are presented which are expected to be useful in contributing toward a better understanding of fracture mechanics.

14. Empirical formulas for residual strength and rate of crack propagation have been developed. These formulas correlate well with test results.

The formula for residual strength accounts for the effect of plate width, and contains a parameter R_p which is a measure of notch resistance. This parameter is shown to be correlated with material ductility, as mentioned in 3 above.

The formula for crack propagation accounts for the observed approach to infinity of the rate of cracking as the crack length approaches its critical value. The formula contains a parameter μ which represents the rate of crack propagation when the crack reaches one-half its critical value. This parameter may be useful in correlating crack growth data.

The empirical formulas are suitable for use in design.

15. The elastic distribution of stress in a cracked plate has been computed by the digital Redundant Force Method. Results are presented which correlate well with the analytical result of Westergard.

16. A method of computing the plastic stress distribution in a cracked plate has been developed. This analysis combines the Redundant Force Method, the Reuss equations of plasticity, and the Newton-Raphson method of solving simultaneous nonlinear equations.

Preliminary results are presented which demonstrate the convergence of the method, and show qualitative agreement with anticipated trends. Further calculations are expected to provide new information on the mechanisms of fracture, fatigue cracking, and cumulative fatigue damage; and possibly to permit the correlation of empirical constants with basic material properties.

Recommendations

Knowledge relating to the subject of fracture mechanics is accumulating rapidly. Nevertheless much remains to be done, because of the complexity of the subject, and the demands placed on the designer by the increasing performance requirements and extreme environments characteristic of high speed aircraft and aerospace vehicles. If this additional knowledge becomes available soon enough, it will provide relatively inexpensive and efficient means of designing safe structures. Without this knowledge the cost of ensuring structural integrity is bound to be higher.

The following subjects should receive further study:

1. Growth and instability of cracks in biaxial stress fields.

2. Fracture characteristics of larger sheet panel sizes (6 inches wide to 30 inches wide).

3. Use of the electron microscope in examining the shape and contour of the markings on the fracture surface under progressive crack growth due to programmed loading. These studies may lead to a type of calibration chart (Appendix A, page 234) which would be of great use in fracture analysis.

4. Continued correlation and development of the empirical expressions for crack growth and residual strength derived in this report and elsewhere.

5. Further digital studies of the plastic distribution of stress around cracks. An attempt should be made to correlate computed values of effective width of the plastic zone at fracture with experimental results and basic material properties. Such studies also can supply information on the history of plastic and residual stress near a crack during cyclic loading. This information can lead to a better understanding of fatigue cracking and cumulative damage.

SECTION 16

REFERENCES

1. ASTM Bulletin; January and February 1960; pages 18 and 29.

2. ATC Report Nr. ARTC-24; Final Report of Project W-97; July 1960.

3. Anderson, W. E., and Paris, P. C., "Fracture Mechanics Applied to the Evaluation of Aircraft Material Performance".

4. Christensen, R. H., "Fatigue Crack Growth in Metals"; Douglas Engineering Paper #985, April 1960.

5. Bockrath, G. E. and Christensen, R. H., "Master Fatigue Curves"; ASTM Fatigue Session, Ambassador Hotel, Los Angeles; March 1961.

6. Crichlow, W. J., "The Ultimate Strength of Damaged Structure", ICAF-AGARD Symposium on Full-Scale Aircraft Fatigue Testing, Amsterdam Netherlands, 9-11 June 1959.

7. Denke, P. H., "A General Digital Computer Analysis of Statically Indeterminate Structures", AGARD paper, Aachen, Germany, September 1959.

8. Denke, P. H., "A Matric Method of Structural Analysis", Proceedings of the Second U. S. Congress of Applied Mechanics, page 445, June 1954.

9. Westergaard, H. M., "Bearing Pressures and Cracks". Journal of Applied Mechanics, pages A49-A53, June 1939.

10. Hill, R., "The Mathematical Theory of Plasticity", Oxford at the Clarendon Press, 1956.

11. WADD Technical Report 60-410, Part II, "Investigation of Thermal Effects on Structured Fatigue", March 1961.

12. Denke, P. H., "The Matrix Solution of Certain Nonlinear Problems in Structural Analysis", Journal of the Aeronautical Sciences, Vol. 23, No. 3, page 231, 1956.

13. Romauldi and Sanders, "Fracture Arrest by Riveted Stiffeners", Contract AF 49(638)-273, Carnegie Inst. Tech., October 1960.

14. Yen, C. S., Pendleberry, S., "Fracture Strength of High Strength Steels Containing Shallow Cracks"; Douglas Aircraft Company, Inc., Engineering Paper No. 1205; August 1961; To be published.

APPENDIX A

ELECTRON MICROSCOPY IN EXAMINING CRACKED AND FRACTURED METAL SURFACES

The use of the electron microscope for the examination of cracked and fractured surfaces is again rapidly finding wide interest. This section most simply describes the electron microscope, its characteristics, the method of preparing replicas of the surfaces to be examined, examples of fractographs, some of the interesting observations and calculations that have been made and studies that are planned.

The Microscope

The electron microscope proves particularly valuable beyond the resolving power and magnification capabilities of the optical microscope. Two thousand diameters can be considered the useful range of the best optical microscope. Advantages of the electron microscope for this study over the light microscope are higher magnification, greater depth of field and much better resolution. Significant manifestations on the fracture face are revealed which heretofore have remained undiscovered. Magnifications as high as 30,000 diameters have been reached with the RCA EML-1B electron microscope, the instrument used in this program. The external appearance of this instrument is shown in Figure 136. The long, cylindrical structure characteristic of every electron microscope is called the column. It houses the electron gun, magnetic lenses, specimen, fluorescent screen, and photographic plate which make up the optical system.

The electron microscope, which requires a highly evacuated column, uses as its radiation a beam of high speed electrons (instead of light waves) having an equivalent wave length of X-ray dimensions (approximately 0.05 angstrom or one-fifth of a billionth of an inch). It is basically this extremely short wave length which gives the electron microscope its fundamental superiority (high resolution) over the light microscope. These electrons obtain their high velocity and low wave length as a result of their acceleration through about 50,000 volts. The electrons penetrate a specially prepared two-stage plastic carbon replica taken from a fracture face and are then focused by means of magnetic fields so as to form an enlarge image on either a fluorescent screen or a photographic plate.

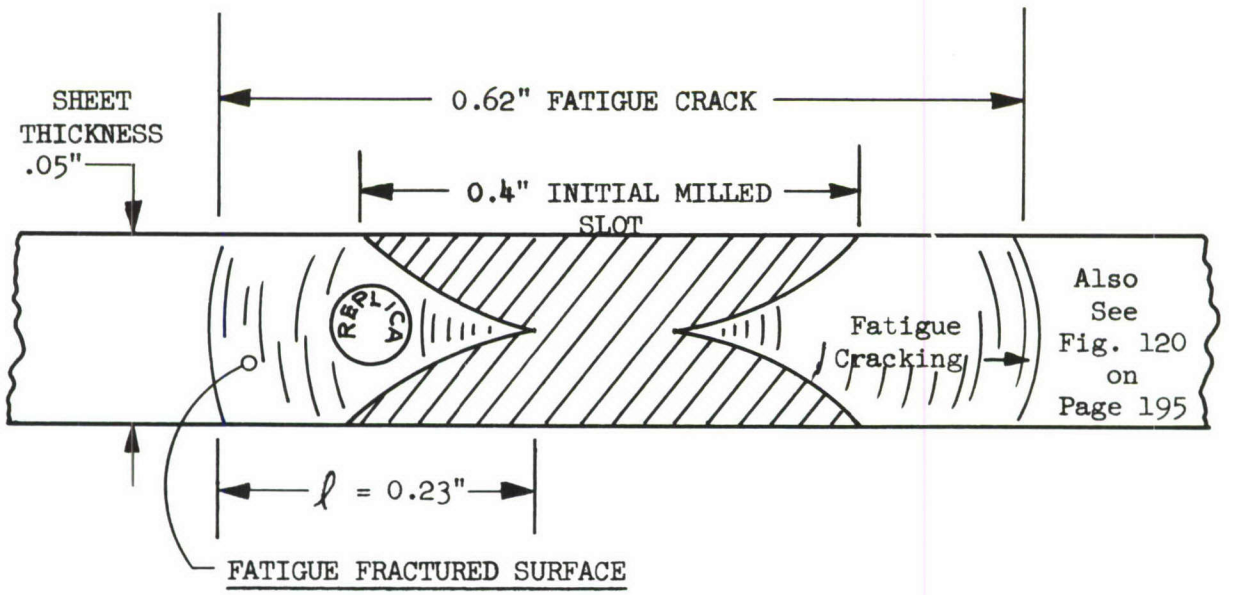
Replication Technique

Microfractorgraphs are prepared from two-stage preshadowed-carbon positive replicas. The two-step procedure consists of first making a plastic negative by pressing a thin cellulose acetate sheet soaked in acetone onto the fracture face. The negative is then dry-stripped and vacuum shadowed with chromium at an angle of 45 degrees to the plane of the replica. This is followed by carbon deposition normal to the replica face. The replica-specimen is next cut into small squares and the plastic negative subsequently dissolved away in acetone, leaving a preshadowed positive replica. The pieces are caught on a 200-mesh copper screen and further washed in vapors of acetone for several hours. The replica specimen is then ready for direct examination in the electron microscope.

The Observations

The electron microfractograph (examples shown in Figures 137 through 142) illustrate the progressive manner in which fatigue fracturing occurs. The surfaces shown are the fracture planes of fatigue cracks and show the "growth arrest" lines of the crack fronts as they have propagated from repeated applications of load.

One of the most striking observations made within this test program (fact of coincidence) concerning the electron microfractograph of the RENE' 41 panel R35 (Figure 137) was that the average "growth arrest line spacing", 8 - micro inches, times the 31,000 test stress cycles equaled the length of the grown crack:



$$\text{Calc. } \ell = \lambda = (.000008)\ (31{,}000) = 0.248"$$

$$\text{Actual } \ell = \text{from test} = 0.23"$$

It is not to be implied that this will always be the case. The observation in this case indicated that materials with greater ductility appear to crack progressively in a fairly uniform manner. High strength and very notch sensitive materials crack in a very sporadic manner showing areas of crack growth lines inter-mixed with large domains of plastic single-load rupture. These materials do not show such good agreement between measured and calculated growths.

Future Studies

Additional studies similar to one that has been made on aluminum alloy, Figure 143, should be carried out. Measurements of growth line spacings under constant amplitude loading as well as under spectrum loading should be made. In this manner it may then be possible, in many marginal cases, to not only identify service fractured surfaces as being due to fatigue action but also the stress levels and stress systems responsible for such deterioration.

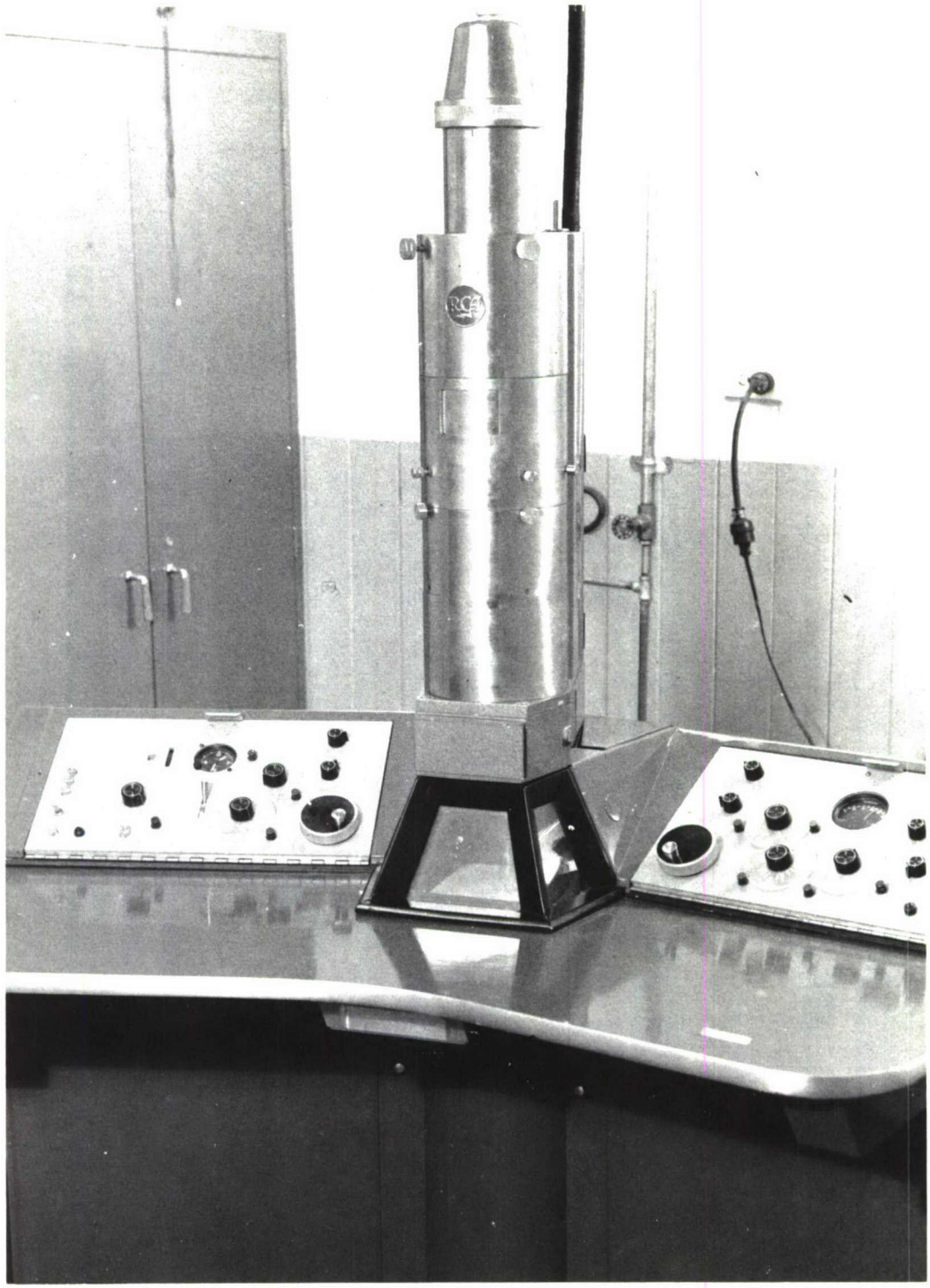


Figure 136. ELECTRON MICROSCOPE



Figure 137. ELECTRON MICROFRACTOGRAPH OF FATIGUE FRACTURED SURFACE — RENE 41 NICKEL ALLOY SHEET MATERIAL

Magnification 24,000X

Progressive fatigue crack growth lines "(λ)" in this specimen were 8 microinches apart (.000008 inches)



Figure 138. ELECTRON MICROGRAPH OF MICROSTRUCTURE — PH15-7 MO RH950

The microstructure shown is a precipitation hardening 15 Cr - 7 Ni- Mo steel, heat treated to the RH 950 condition. The electron micrograph displays a gross grain boundary precipitate. Within the grains thin platelets of a fine precipitate can be observed. These platelets occur along crystallographic planes. The etchant was Vilella's. The specimen was prepared by a preshadowed chromium positive carbon replica. This micrograph represents the rolled surface of the sheet stock.

The microstructure has been enlarged to a magnification of 13,670 X.

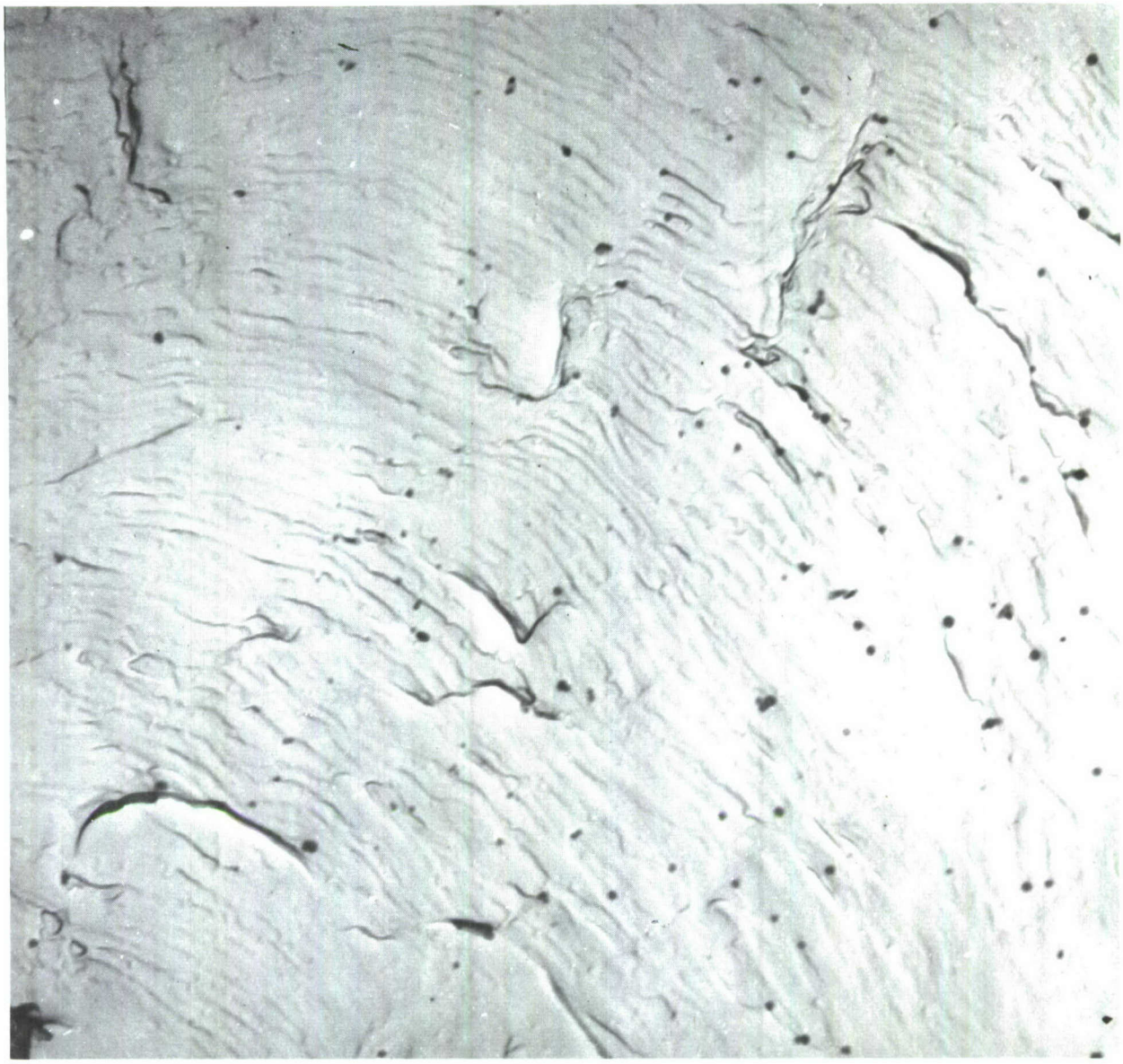


Figure 139. ELECTRON MICROFRACTOGRAPH OF FATIGUE FRACTURED SURFACE IN TANTALUM SHEET STOCK

The fatigue cracking was carried out at a maximum cracking stress of 27,000 psi. Magnification of fractured surface 18,500 X.



Figure 140. ELECTRON MICROFRACTOGRAPH OF FATIGUE FRACTURED SURFACE ALUMINUM

Electron Microfractograph of 7075 Aluminum Alloy illustrates the progressive manner in which fatigue fracturing occurs. The surface shown is the fracture plane of a fatigue crack and shows the "growth" lines of the crack front as it propagated from repeated applications of load. The average distance between "growth" lines in this example is 36 micro-inches (.000036 inches). The area of the fracture which this photo reproduces is within the region, labeled Zone 1, of Figure 114 on page 189 . Magnification 16,000 X.

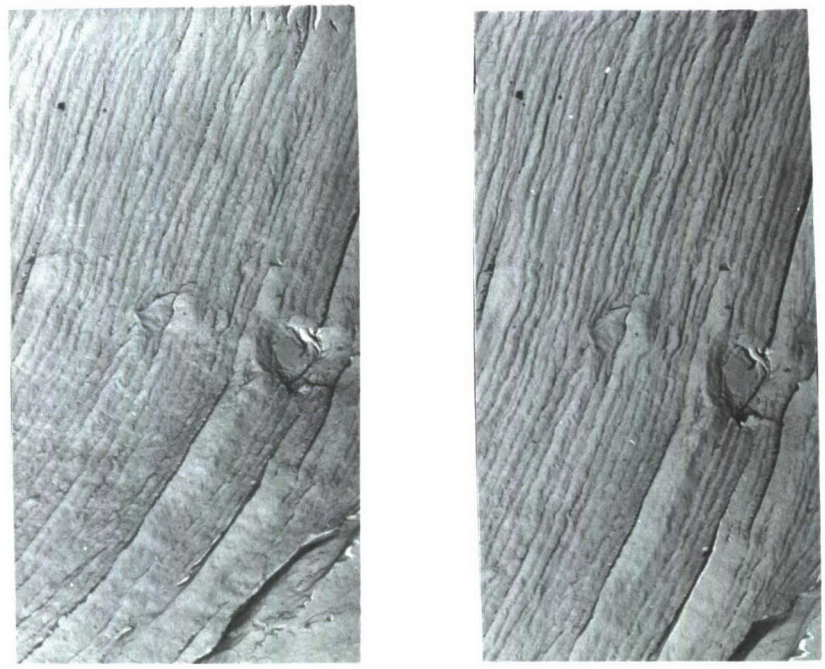


Figure 141. STEREOSCOPIC ELECTRON MICROFRACTOGRAPH OF FATIGUE FRACTURED SURFACE RENE 41

Stereoscopic Electron Microfractograph at 8030 X of the fractured surface of test panel number R35 in the early stages of fatiguing. The maximum cracking stress was 45,000 psi and the cracking temperature + 80° Fahr. The L. H. to R. H. orientation of the stereo prints in this example was 20°.

A three-dimensional effect of the progressive surface fracture can be obtained by viewing the pair of microfractographs with the aid of a map maker's stereoptican viewer.

It is suggested to the viewer that only a small area of the progressively fractured surface be viewed at any one time. Focus and adjustment for ones' own eyes can be best obtained by gradually sliding and rotating the lens over the holder print. It is also interesting to view the microfractographs by rotating them 180°. Ridges become recesses and small craters become mounds. (intaglio effect)

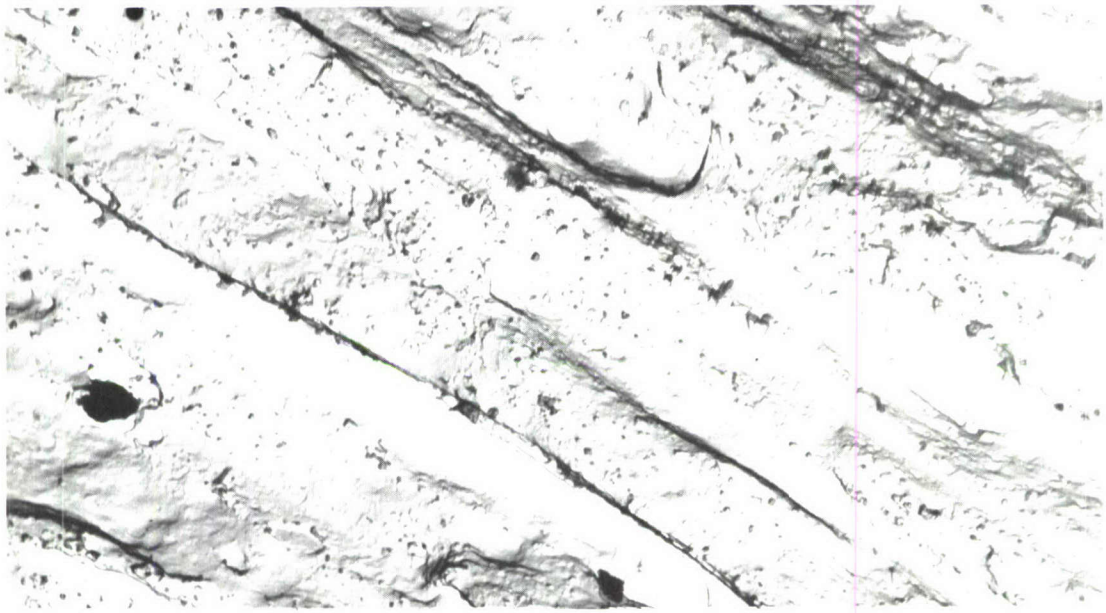


Figure 142. ELECTRON MICROFRACTOGRAPH OF FATIGUE FRACTURED SURFACE OF PURE MOLYBDENUM WROUGHT-SINTERED SHEET

The distinct lines and ridges define the cross-rolled substrate. It is very difficult to discern the fatigue crack growth lines in this metal. The greatest density appears in the center section progressing almost mormal to the substrate boundary lines. Magnification 13,650 X.

A few electron micrographs of the metal PH15-7 Mo and others can be found in Section 13.

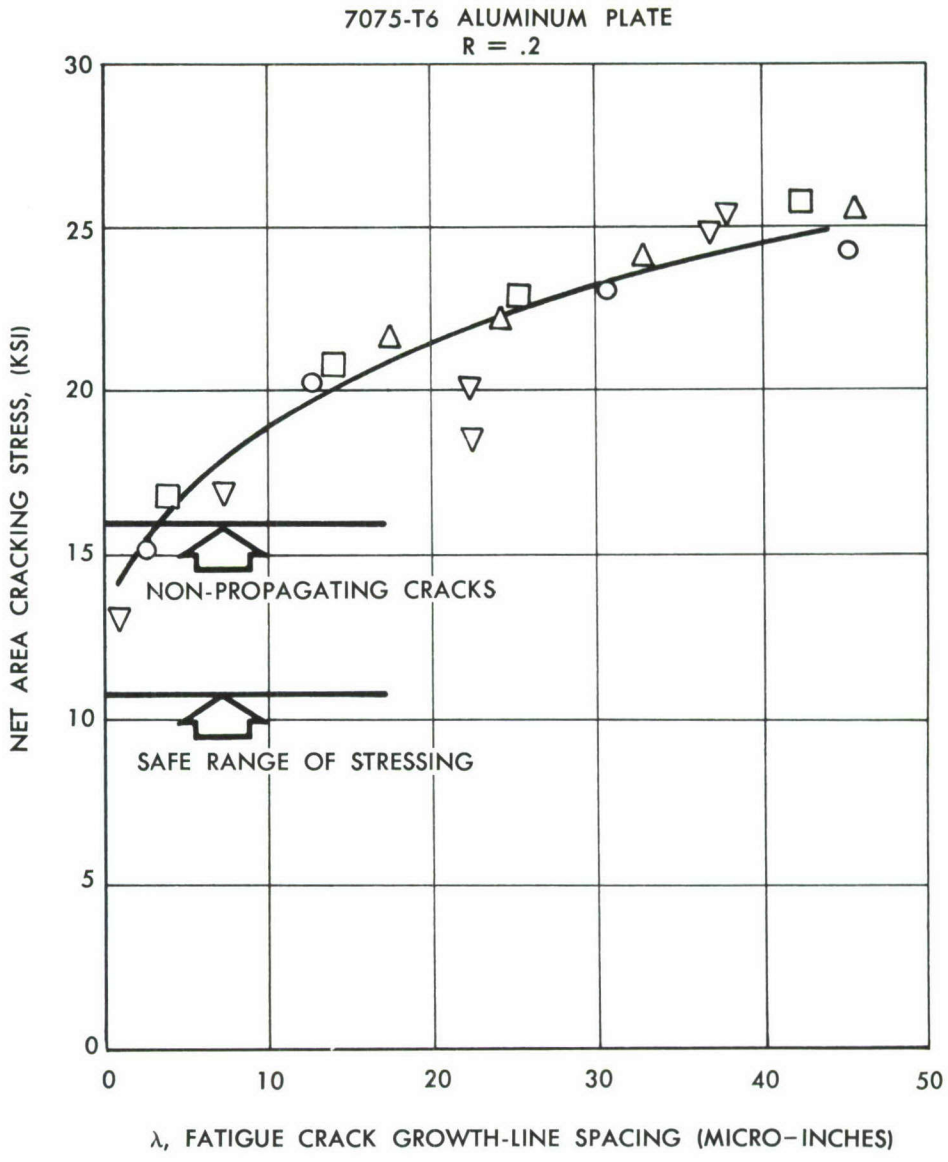


Figure 143. FATIGUE CRACK GROWTH "ARREST" LINES AS A FUNCTION OF NET AREA FATIGUE CRACKING STRESS

APPENDIX B

MATHEMATICAL DERIVATIONS

Plastic Redundant Force Analysis For Biaxial Stress

The following analysis utilizes the notation of Reference 7.

Let Z_i = relative deflection at i^{th} cut.

ΔZ_i = increment in relative deflection at i^{th} cut due to increment in external load.

$$\Delta Z = \left\{\Delta Z_i\right\}$$

Continuity requires that $\Delta Z = 0$ (20)

Now $$\Delta Z = \delta_{xx}\Delta X + \delta_{xo}\Delta\phi + f_x^T \Delta e_p \quad (21)$$

and $$\Delta F = f_x \Delta X + f_o \Delta\phi \quad (22)$$

The incremental plastic element deformations Δe_{pij} are related to the incremental element forces through the Reuss equations. This relation may be written:

$$\Delta e_p = \Delta e_p(\Delta F) \quad (23)$$

Equation (23) is nonlinear, therefore equation (20) is nonlinear. Equation (20) can be solved by the Newton-Raphson method as follows:

$$\Delta X_{(i,j+1)} = \Delta X_{(i,j)} - A^{-1}_{(i,j)} \Delta Z^{*}_{(i,j)} \quad (24)$$

where

$$A_{(i,j)} = \Delta Z_{(i,j)} \partial \quad (25)$$

and

$$\partial = \left[\frac{\partial}{\partial \Delta X_1}, \frac{\partial}{\partial \Delta X_2} \cdots\cdots \frac{\partial}{\partial \Delta X_{\eta_R}}\right] \quad (26)$$

The matrix A is square of order η_R,

where η_R is the number of redundants. Combining (25) and (21) gives

$$A = \delta_{xx}\Delta X\partial + \delta_{xo}\Delta\phi\partial + f_x^T \Delta e_p \partial = \delta_{xx} + f_x^T \Delta e_p \partial \quad (27)$$

* First subscript denotes increment; second subscript denotes iteration.

The jth incremental element deformation is a function of the incremental element forces, from (23), as follows:

$$\Delta e_{p_j} = \Delta e_{p_j} (\Delta F_1, \Delta F_2, \ldots \Delta F_\alpha \ldots) \tag{28}$$

Therefore, according to the rules of partial differentiation,

$$\frac{\partial \Delta e_{p_j}}{\partial \Delta X_k} = \sum_\alpha \frac{\partial \Delta e_{p_j}}{\partial \Delta F_\alpha} \frac{\partial \Delta F_\alpha}{\partial \Delta X_k} \tag{29}$$

but, from (22),

$$\Delta F_\alpha = \sum_\beta f_{x_{\alpha\beta}} \cdot \Delta X_\beta + \sum_\beta f_{\circ_{\alpha\beta}} \Delta \phi_\beta \tag{30}$$

$$\therefore \quad \frac{\partial \Delta F_\alpha}{\partial \Delta X_k} = f_{x_{\alpha k}} \tag{31}$$

$$\therefore \quad \frac{\partial e_{p_j}}{\partial \Delta X_k} = \sum_\alpha \frac{\partial e_{p_j}}{\partial \Delta F_\alpha} f_{x_{\alpha k}} = \sum_\alpha \frac{\partial e_{p_j}}{\partial F_\alpha} f_{x_{\alpha k}} \tag{32}$$

$$\therefore \quad \Delta e_p \partial = B f_x \quad \text{where} \quad B = \left[B_{j\alpha} \right] \quad \text{and} \quad B_{j\alpha} = \frac{\partial e_{p_j}}{\partial F_\alpha} \tag{33}$$

$$\therefore \quad A = \delta_{xx} + f_x^T B f_x \tag{34}$$

Summary

The ith increment occurs between the ith load level and the $i+1^{th}$ load level.

$$\Delta F_{(i,j)} = f_x \Delta X_{(i,j)} + f_\circ \Delta \phi_{(i)} \tag{35}$$

$$\text{Take } \Delta X_{(i,1)} = \Delta X_{(i,e)}^{*} \tag{36}$$

$$F_{(i+1,j)} = F_{(i,n)} + \Delta F_{(i,j)}^{**} \tag{37}$$

* e = elastic
** n = final iteration

At each joint extract σ_x, σ_y, and τ_{xy} from F(i+1,j). τ_{xy} is obtained by averaging the shear stresses in the four panels adjacent to the joint.

$$\sigma'_{11} = \frac{2\sigma_x - \sigma_y}{3} \qquad \sigma'_{22} = \frac{2\sigma_y - \sigma_x}{3} \qquad \sigma'_{12} = \tau_{xy} \qquad \ldots\ldots (i+1, j) \tag{38}$$

$$\bar{\sigma}_{(i+1,j)} = \left(\sqrt{\sigma_x^2 - \sigma_x\sigma_y + \sigma_y^2 + 3\tau_{xy}^2}\right)_{(i+1,j)} \tag{39}$$

$$\bar{\epsilon}^{\,p}_{(i+1,j)} = \bar{\epsilon}^{\,p}_1 \left[\frac{\bar{\sigma}_{(i+1,j)}}{\bar{\sigma}_1}\right]^{n} \quad * \tag{40}$$

$$\Delta\bar{\epsilon}^{\,p}_{(i,j)} = \bar{\epsilon}^{\,p}_{(i+1,j)} - \bar{\epsilon}^{\,p}_{(i,j)} \tag{41}$$

$$\omega_1 = \frac{3}{2}\frac{\sigma'_{11}}{\bar{\sigma}} \qquad \Delta\epsilon^p_{x(i,j)} = \omega_{1(i,n)}\Delta\bar{\epsilon}^{\,p}_{(i,j)} \tag{42}$$

$$\omega_2 = \frac{3}{2}\frac{\sigma'_{22}}{\bar{\sigma}} \qquad \Delta\epsilon^p_{y(i,j)} = \omega_{2(i,n)}\Delta\bar{\epsilon}^{\,p}_{(i,j)} \tag{43}$$

$$\omega_3 = 3\frac{\sigma'_{12}}{\bar{\sigma}} \qquad \Delta\gamma^p_{xy(i,j)} = \omega_{3(i,n)}\Delta\bar{\epsilon}^{\,p}_{(i,j)} \tag{44}$$

Assemble $\Delta e_{p(i,j)}$ from the $\Delta\epsilon^p_{x(i,j)}$, $\Delta\epsilon^p_{y(i,j)}$ and $\gamma^p_{xy(i,j)}$

$$\Delta Z_{(i,j)} = \delta_{xx}\Delta X_{(i,j)} + \delta_{xo}\Delta\phi_{(i,j)} + f_x^t\Delta e_{p(i,j)} \tag{45}$$

$$\left(\frac{d\bar{\epsilon}^{\,p}}{d\bar{\sigma}}\right)_{ij} = n\frac{\bar{\epsilon}_1}{\bar{\sigma}_1}\left[\frac{\bar{\sigma}_{(i+1,j)}}{\bar{\sigma}_1}\right]^{n-1} ** = C_{ij} \tag{46}$$

* Ramberg-Osgood stress-strain formula. Other expressions can be used.

** ΔZ_{ij} corresponds to $\bar{\sigma}_{i+1,j}$

$$\left(\frac{\partial \epsilon_x^p}{\partial \sigma_x}\right)_{ij} = \omega^2_{1(i+1,j)} C_{ij} \tag{47}$$

$$\left(\frac{\partial \epsilon_y^p}{\partial \sigma_y}\right)_{ij} = \omega^2_{2(i+1,j)} C_{ij} \tag{48}$$

$$\left(\frac{\partial \gamma_{xy}^p}{\partial \tau_{xy}}\right)_{ij} = \omega^2_{3(i+1,j)} C_{ij} \tag{49}$$

$$\left(\frac{\partial \epsilon_x^p}{\partial \sigma_y}\right)_{ij} = \left(\frac{\partial \epsilon_y^p}{\partial \sigma_x}\right)_{ij} = (\omega_1 \omega_2)_{(i+1,j)} C_{ij} \tag{50}$$

$$\left(\frac{\partial \epsilon_y^p}{\partial \tau_{xy}}\right)_{ij} = \left(\frac{\partial \gamma_{xy}^p}{\partial \sigma_y}\right)_{ij} = (\omega_2 \omega_3)_{(i+1,j)} C_{ij} \tag{51}$$

$$\left(\frac{\partial \gamma_{xy}^p}{\partial \sigma_x}\right)_{ij} = \left(\frac{\partial \epsilon_x^p}{\partial \tau_{xy}}\right)_{ij} = (\omega_3 \omega_1)_{(i+1,j)} C_{ij} \tag{52}$$

Assemble the matrix $B_{(ij)} = [B_{k\alpha}]$ where $B_{k\alpha} = \dfrac{\partial e_{p_k}}{\partial F_\alpha}$ (53)

$$A_{(i,j)} = \delta_{xx} + f_x^t B_{(ij)} f_x \tag{54}$$

$$\Delta X_{(i,j+1)} = \Delta X_{(i,j)} - A^{-1}_{(i,j)} \Delta Z_{(i,j)} \tag{55}$$

$$e_{p_{(i+1,n)}} = e_{p_{(i,n)}} + \Delta e_{p_{(i,n)}} \tag{56}$$

$$e_{(i+1,n)} = e_{p_{(i+1,n)}} + DF_{(i+1,n)} \tag{57}$$

APPENDIX C

ELECTRIC - ARC DISCHARGE METHOD OF FORMING STARTER CRACKS

An alternative method of producing starter cracks in the test panels was by the electric-arc discharge method. This method was found particularly adaptable for the hard to machine metals that possessed toughnesses that were too difficult for the very thin high-speed steel jewelers slotting saws. The electric-arc discharge method was found particularly useful for slotting the steel AM355 as well as the biaxial-test bulge panels in both PH15-7 Mo RH950 steel and RENE' 41 alloy. Through-slots or slot widths in the order of 5 to 8 thousandths of an inch can be eroded into the metal panels by this technique.

In this test program a relatively new machine tool and technique for machining hard metals called the Agietron was used.

The Agietron process embodies a relatively new and unique approach to machining hard metals by spark erosion. An additional important factor as far as these experiments were concerned is that it produced extremely thin slot widths. The Agietron technique produces a high frequency spark discharge with pure alternating current by using resistors and condensers. No tubes or rectifiers are required in the entire circuit of the machine. The cutting procedure is carried out in oil immersion of the test piece.

The photographs in Figures 144 and 145 show a general view of the machine with the oil immersion cutting bath and a close-up of the electrode used to cut a starter crack .006" wide by 0.7" long in the crown of one of the bulge panels.

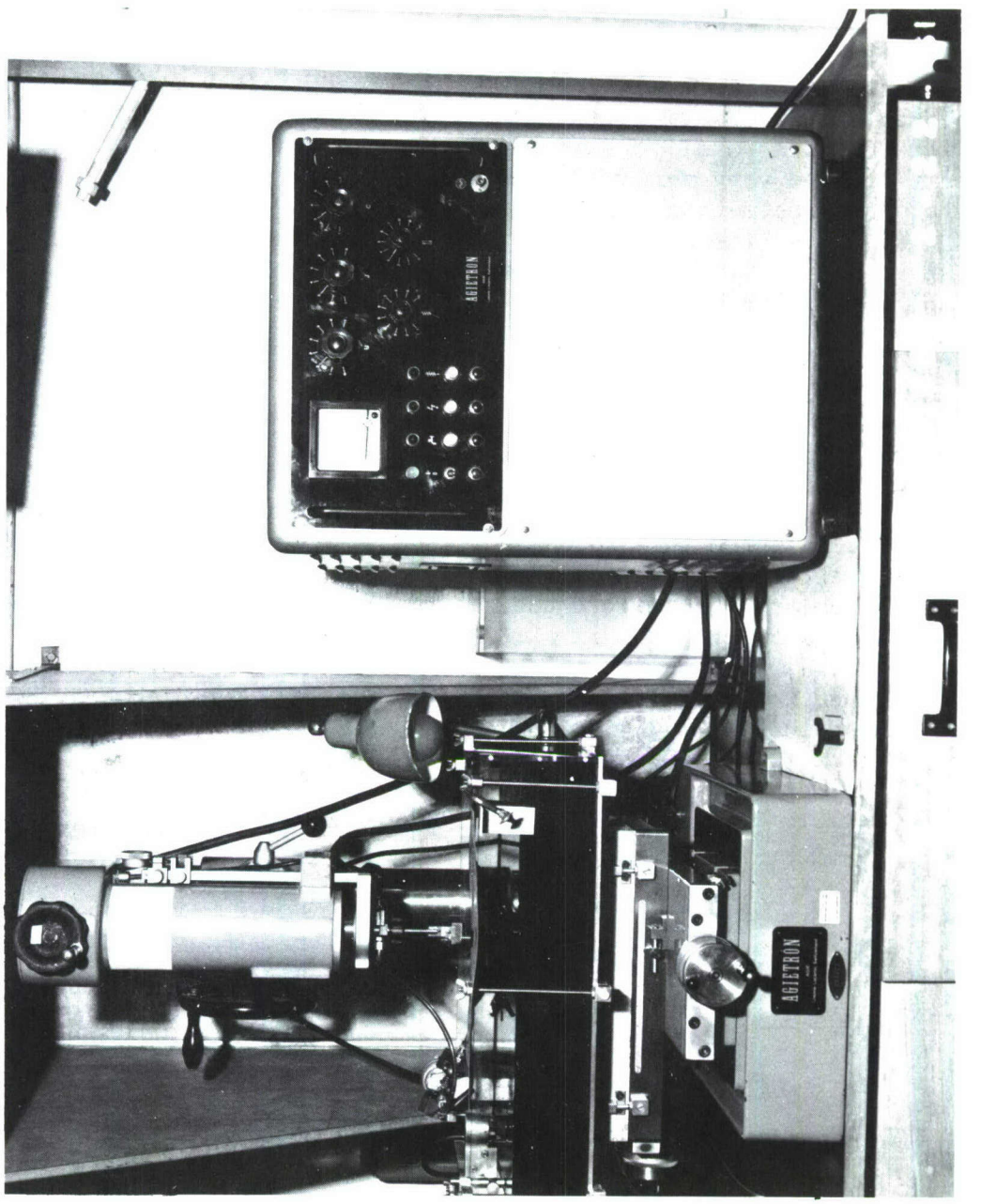


Figure 144. AGIETRON MACHINE TOOL

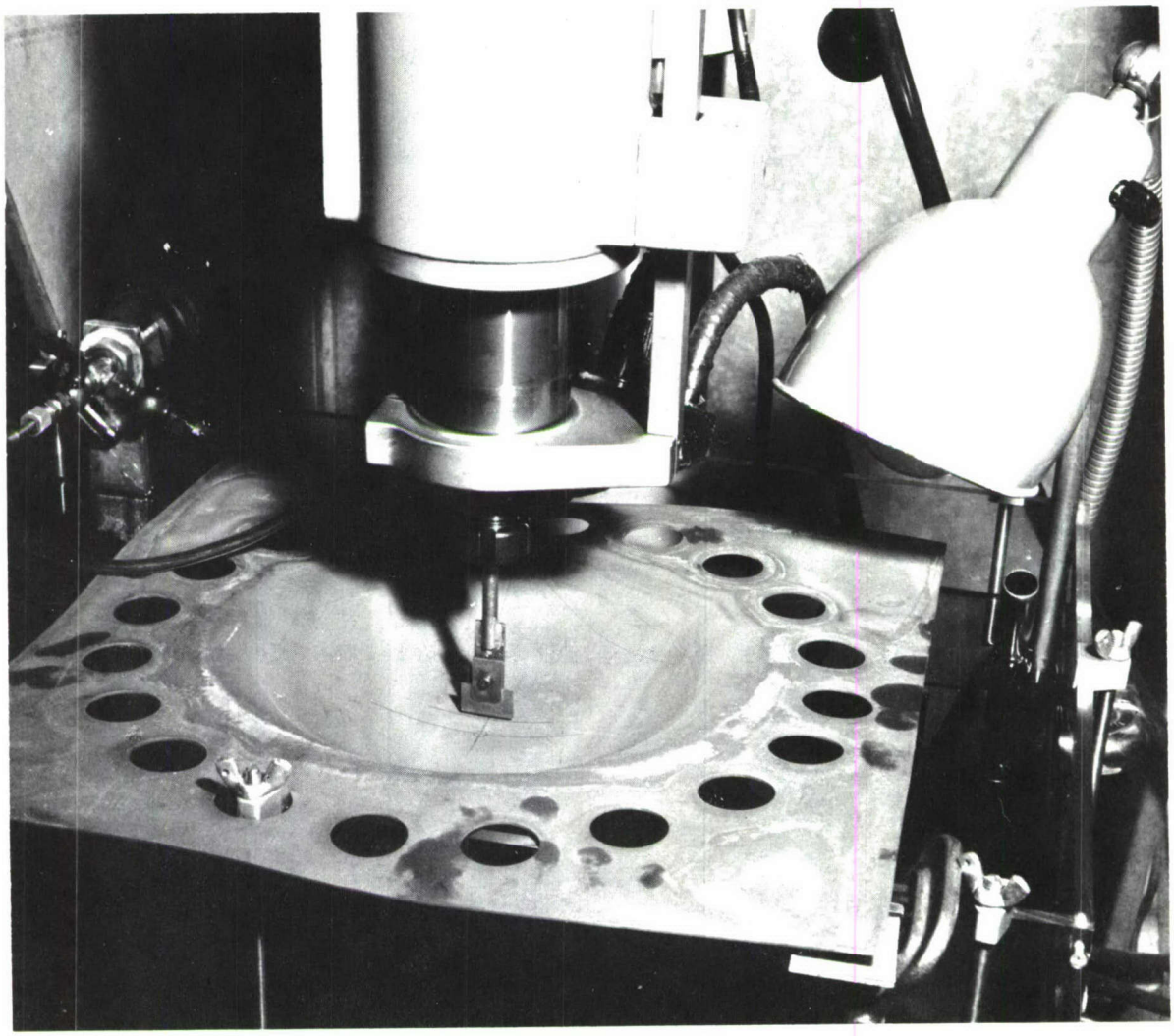


Figure 145. VIEW SHOWING A BULGE PANEL IN POSITION FOR FORMING FINE (.006 INCH) SLIT IN CROWN OF TEST SPECIMEN

Oil, submerging electrode and test specimen has been eliminated in this photo for purposes of clarity.

APPENDIX D

RESULTS OF THE PLASTIC ANALYSIS

The equation for the equivalent stress-equivalent plastic strain curve is given by the Ramberg-Osgood equation:

$$\bar{\epsilon}^{p} = .019776(10^{-5}\,\bar{\sigma})^{17} \tag{58}$$

Figure 146 is a graph of this equation.

Figure 147 shows how the equivalent stress at the most highly stressed point converges with iteration number. The convergence is satisfactory.

Figure 148 shows the plastic distribution of longitudinal stress at a transverse section through the crack. The elastic distribution is shown for comparison. Figure 149 shows the residual stress under zero load at the same section.

Figure 150 is a graph of the residual stress in the plate.

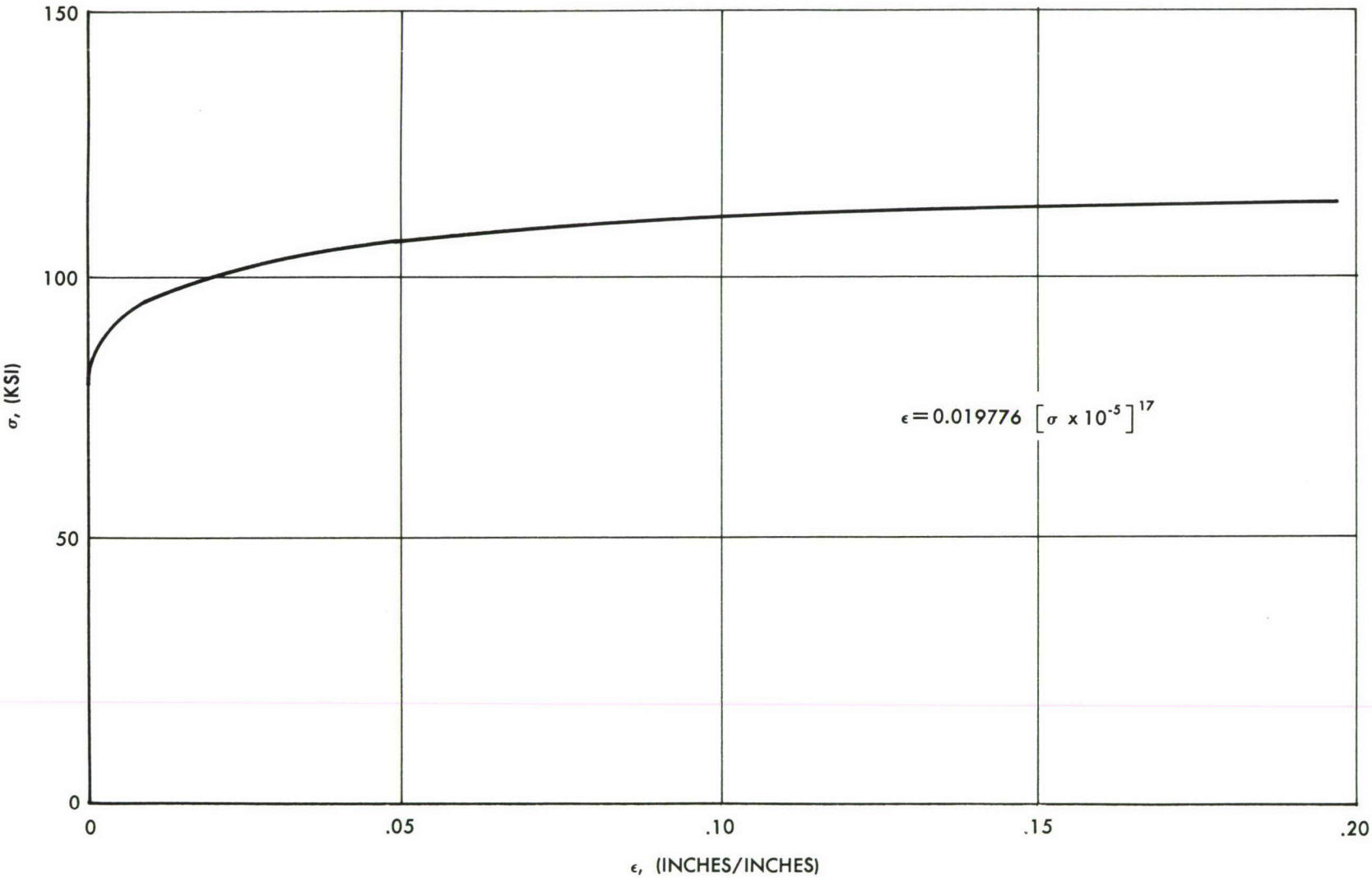


Figure 146. EQUIVALENT STRESS-EQUIVALENT PLASTIC STRAIN CURVE

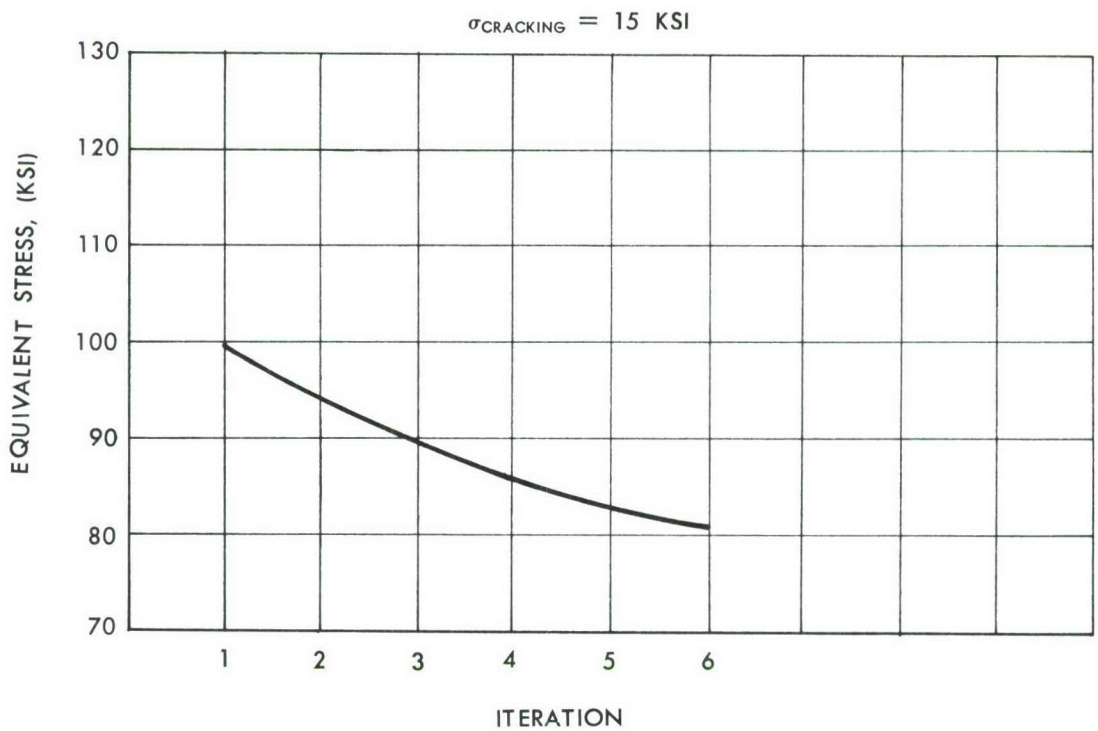


Figure 147. CONVERGENCE OF THE NEWTON-RAPHSON PROCESS

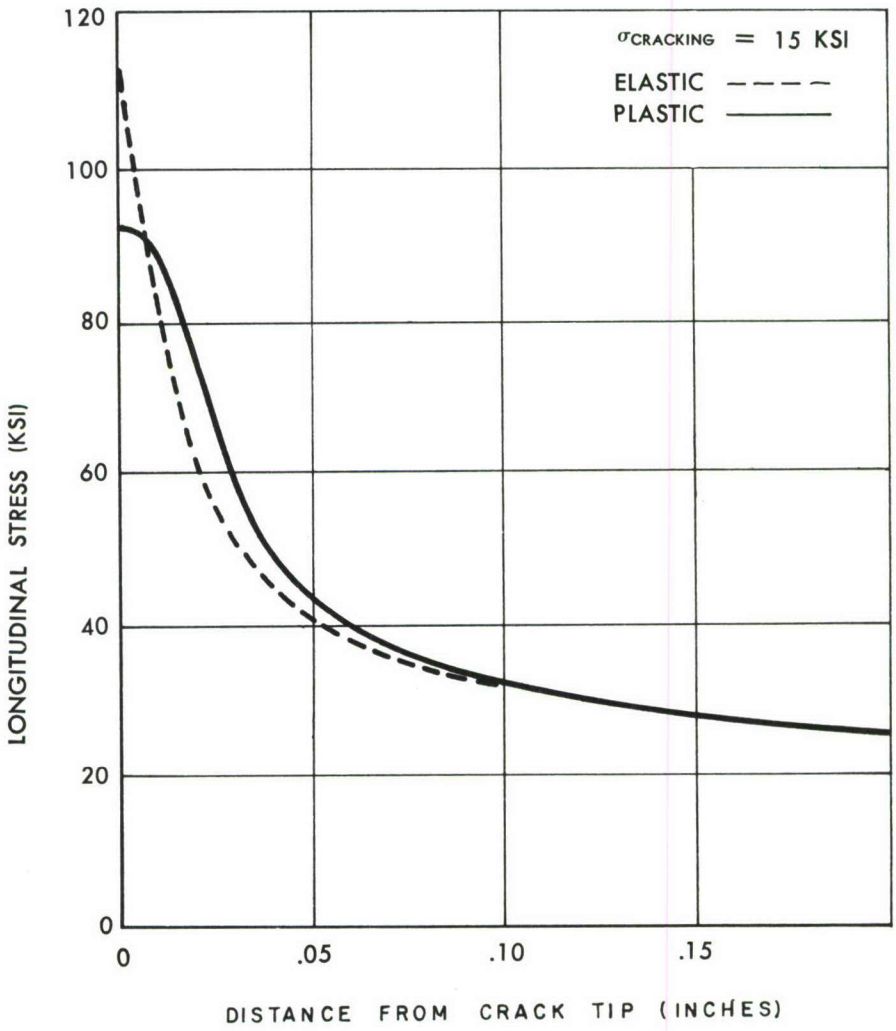


Figure 148. DISTRIBUTION OF LONGITUDINAL STRESS AT A TRANSVERSE SECTION THROUGH THE CRACK

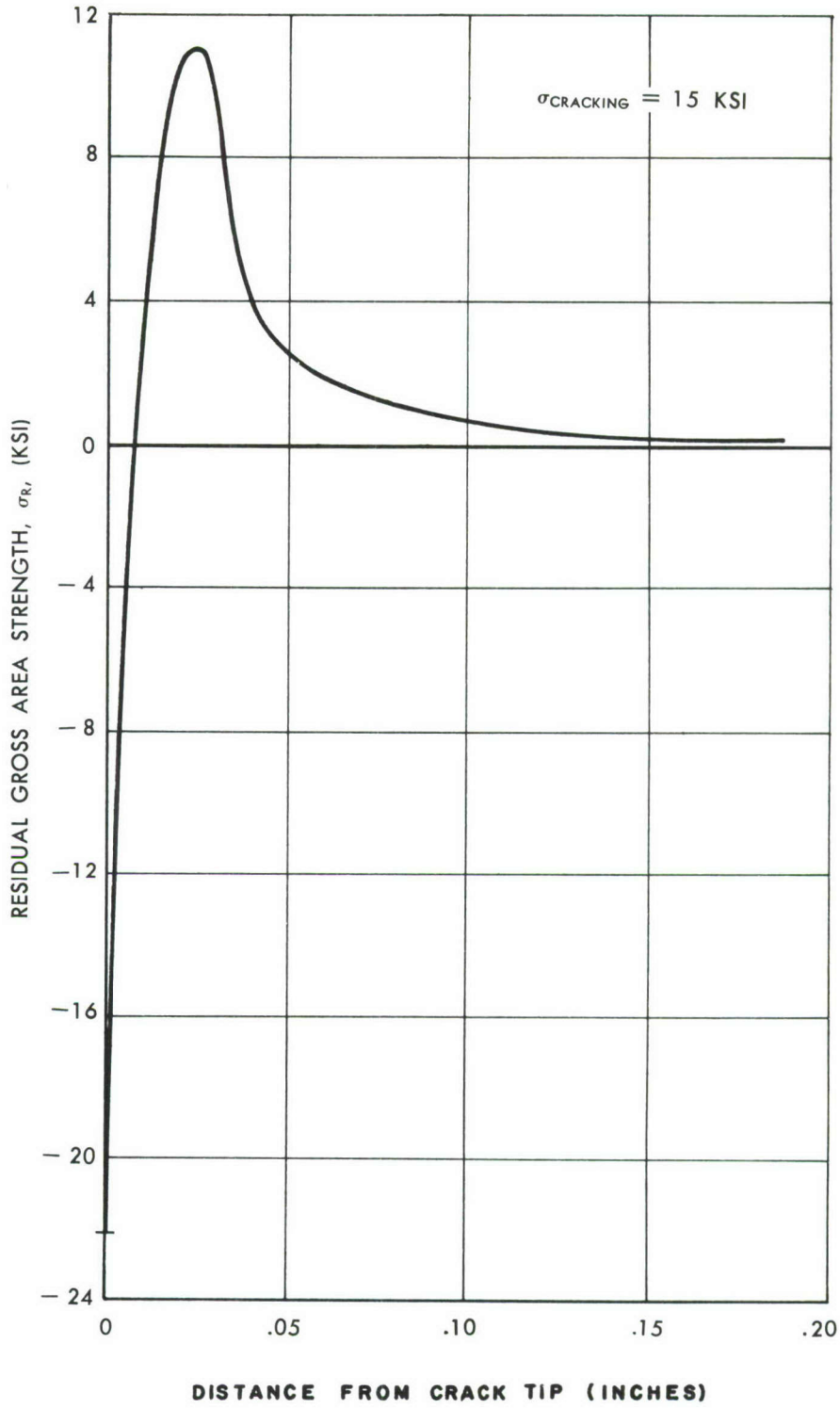
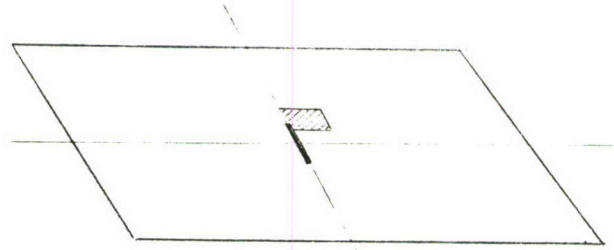


Figure 149. RESIDUAL STRESS AT ZERO LOAD

RESIDUAL STRESS RESULTING FROM
15,000 PSI GROSS APPLIED STRESS



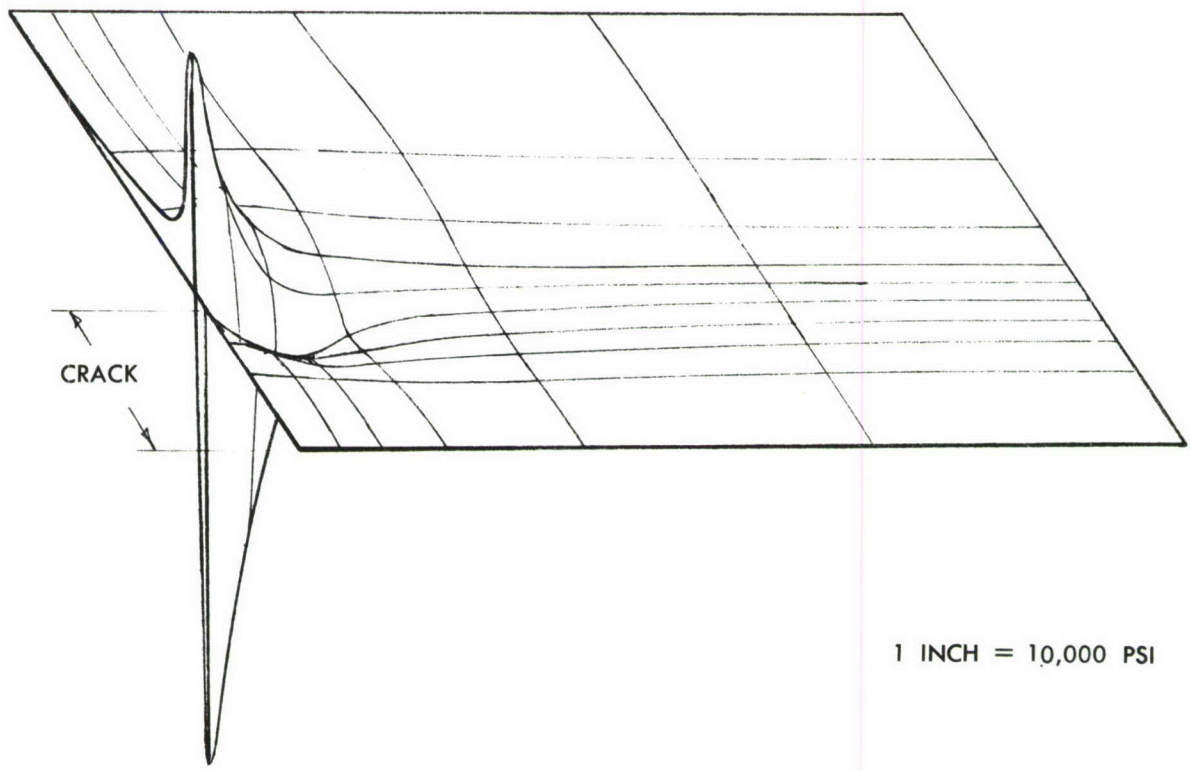


Figure 150. LONGITUDINAL RESIDUAL STRESS DISTRIBUTION

APPENDIX E

USE OF THE EMPIRICAL FORMULAS

RESIDUAL STRENGTH

A sheet of PH15-7MO, RH950, 5 inches wide and .040 inches thick contains a crack 1 inch long. Estimate the residual strength. Use σ_u = 240,000 psi.

From equation 8

$$\sigma_R = \frac{\sigma_u (1 - \ell_c/w)}{1 + \ell_c/R_p} \tag{59}$$

From Figure 125, R_p = .294 (See also Figures 126 to 130 inclusive)

$$\therefore \quad \sigma_R = \frac{240{,}000\ (1 - 1/5)}{1 + 1/.294} = 43{,}600 \text{ psi} \tag{60}$$

This stress, which is the gross section stress required to fail the cracked sheet, represents only 18% of the strength of the uncracked sheet. The above value of σ_R can also be read from Figure 125.

CRACK PROPAGATION

Estimate the rate of crack propagation for the sheet of the preceding example, if the sheet is subjected to a cyclic load for which

$$\sigma_{max} = 35{,}000 \text{ psi}, \quad R = .2. \tag{61}$$

From equation 9, the critical crack length is given by

$$\ell_c = \frac{w(1 - \sigma_R/\sigma_u)}{1 + \frac{w}{R_p}\frac{\sigma_R}{\sigma_u}}$$

$$= \frac{5(1 - 35{,}000/240{,}000)}{1 + \frac{5}{.294} \times \frac{35{,}000}{240{,}000}} = 1.228 \text{ inches} \tag{62}$$

This value can also be obtained from Figure 125.

From equation 12, the crack propagation rate is given by

$$\frac{d\ell}{dn} = \mu \frac{\ell}{\ell_c - \ell} \tag{12}$$

Table 11 contains values of the mean crack rate μ determined from test. From this table, μ is estimated to be .021 in/kilocycle

$$\therefore \quad \frac{d\ell}{dn} = \frac{.021 \times 1.000}{1.228 - 1.000} = .0921 \text{ in/K.C.} \tag{63}$$

This is the crack rate when the crack is 1 inch long. Plot a graph of the subsequent and previous development of the crack (crack length versus cycles).

From equation 15

$$n = n_o + \frac{1}{\mu} \left(\ell_c \ln \frac{\ell}{\ell_o} - \ell + \ell_o \right) \tag{64}$$

Start counting the cycles from the time the crack is 1 inch long (this choice can be made arbitrarily) so that $n_o = 0$, $\ell_o = 1$.

$$\therefore \quad n = \frac{1}{.021} \left(1.228 \times 2.30 \log_{10} \frac{\ell}{1} - \ell + 1 \right) \tag{65}$$

$$= \frac{2.83 \log_{10} \ell - \ell + 1}{.021} \quad \text{K.C.}$$

The graph of this equation is shown in Figure 151. The calculation is shown in Table 12.

Note that the range of values of the mean crack rate, μ, in Table 11 is between .0159 and .0859. This range is very small compared to the range in values of the fatigue life N for specimens tested under the same conditions. These facts emphasize again that the predictability of fatigue damage in the cracking phase is greater than in the nucleation phase.

TABLE 11

MEAN CRACK RATES

Material	σ_u KSI	σ_{Max} (KSI)	R	W	T (oF)	t	μin/KC
Ph15-7 Mo	240	35	.20	6	75°	.040	.0210
"	240	35	.20	6	75°	.020	.0159
"	240	35	.20	6	75°	.030	.0317
Rene' 41	193	40	.20	6	75°	.050	.0859
"	193	40	.20	6	75°	.050	.0763
"	193	37	.20	4	75°	.050	.0392
"	193	40	.20	4	75°	.050	.0371
"	193	45	.20	4	75°	.050	.0533
AM355	210	40	.20	4	75°	.050	.0789
Titanium B120VCA							
"	207	20	.20	2	75°	.050	.0217
"	207	20	.20	2	75°	.050	.0220
"	207	20	.20	4	75°	.050	.0233
"	207	20	.20	4	75°	.050	.0254
"	207	18	.20	4	75°	.050	.0233
"	207	20	.20	4	75°	.050	.0174
"	207	20	.20	4	75°	.050	.0186
"	207	20	.20	4	75°	.050	.0173
"	207	16	.20	4	75°	.050	.0167
"	207	20	.20	6	75°	.050	.0264
"	207	20	.20	8	75°	.050	.0404

TABLE 12

CALCULATION OF CRACK PROPAGATION CURVE

ℓ	1	1.05	1.10	1.15	1.20	1.228	.80
$\log_{10} \ell$	0	.212	.0414	.0607	.0792	.0892	-.0969
$\ell - 1$	0	.05	.10	.15	.20	.228	-.20
$2.83 \log_{10} \ell$	0	.0600	.1170	.1720	.224	.252	-.274
$2.83 \log_{10} \ell - (\ell - 1)$	0	.0100	.0170	.0220	.024	.024	-.074
n KC	0	.476	.810	1.048	1.143	1.143	-3.52

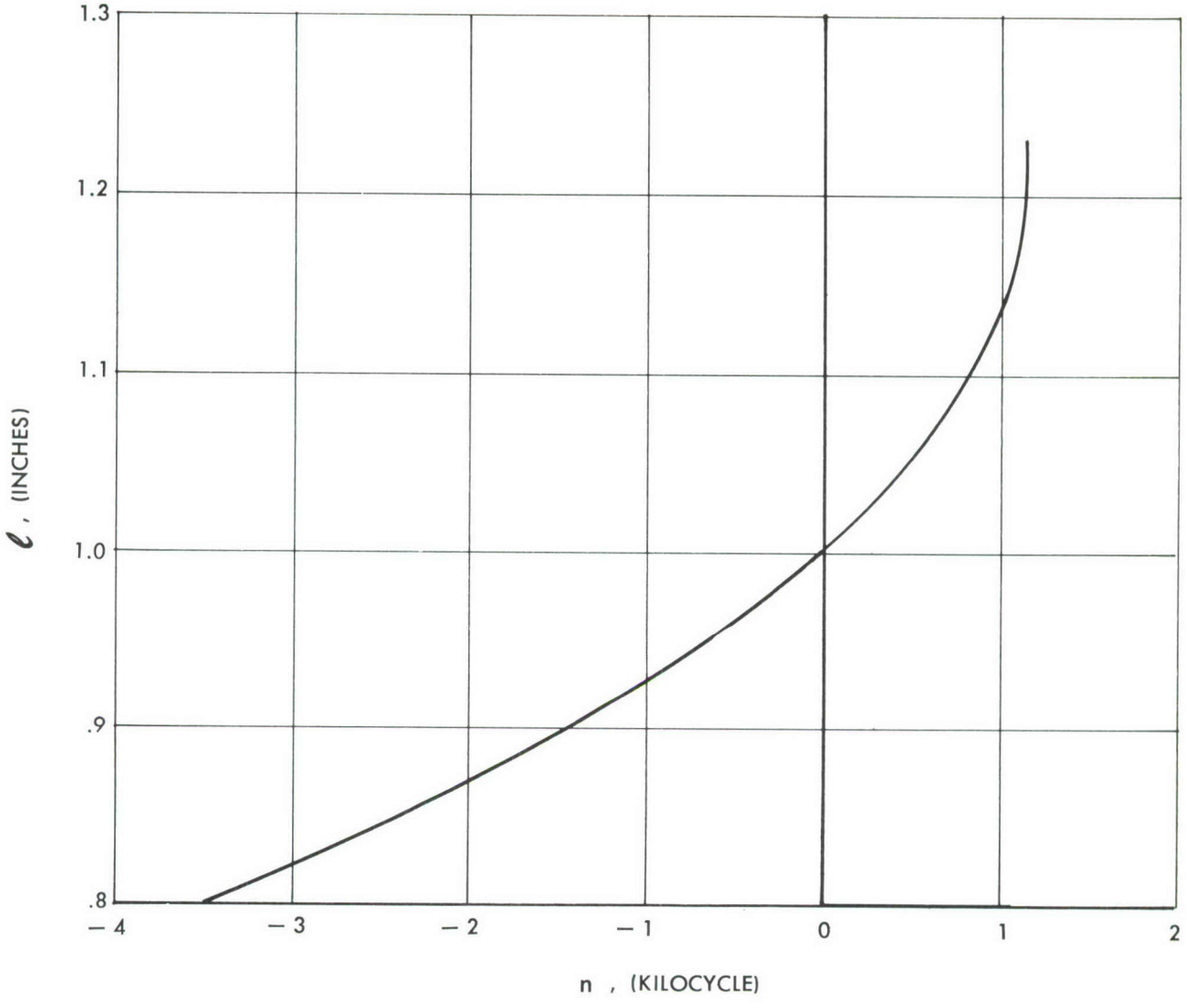


Figure 151. EXAMPLE OF FATIGUE CRACK PROPAGATION

APPENDIX F

SUPPLEMENTARY ANALYSIS OF RESIDUAL STRENGTH

Toward the close of the research program other formulas for residual strength were found which fit the data in some cases better than formula (6) of Section 14. One of these formulas is obtained by introducing an empirical exponent α in the denominator of (6) so that

$$\frac{\sigma_R}{\sigma_u} = \frac{1 - \ell_c/w}{1 + (\ell_c/R_p)^{\alpha}} \tag{66}$$

This formula usually can be made to fit the data very closely by proper choice of the two empirical constants α and R_p.

Another formula can be derived which fits the data about as well as (66). This new formula has a sounder physical basis than either (6) or (66), and contains only one empirical constant. This new formula is based on an assumed stress distribution on the cracked section as shown in Figure 152. In the figure, σ_y is the longitudinal tensile stress, x is the distance from the center of the cracked panel, and a is one half the length of the crack. As in Crichlow's analysis, a plastic zone of width w_e, in which the stress is equal to σ_u, is assumed to exist at the end of the crack. The rest of the stress distribution is assumed to be the theoretical elastic distribution, contrary to Crichlow's assumption.

For equilibrium the area under the rectangle marked "plastic zone" must be equal to the area under the dotted portion of the elastic stress distribution curve.

$$\therefore \quad \sigma_u w_e = \int_a^{a+w_e} \sigma_y \, dx \tag{67}$$

but

$$\frac{\sigma_y}{\sigma_R} = \frac{x/a}{\sqrt{(x/a)^2 - 1}} \tag{68}$$

where σ_R is the gross-section stress. Equation (68) gives the elastic stress distribution in a wide sheet, according to Westergaard (Reference 9).

$$\therefore \quad \sigma_u w_e = \int_a^{a+w_e} \frac{\sigma_R \, x/a}{\sqrt{(x/a)^2 - 1}} \, dx \tag{69}$$

Integrating (69) and solving for σ_R/σ_u gives

$$\frac{\sigma_R}{\sigma_u} = \frac{1}{\sqrt{1 + 3\ell_c/R'_p}} \tag{70}$$

where $R'_p = 3\, w_e$ and $\ell_c = 2a$. Introducing a correction for panel width as in Section 14 gives

$$\frac{\sigma_R}{\sigma_u} = \frac{1 - \ell_c/w}{\sqrt{1 + 3\ell_c/R'_p}} \tag{71}$$

The symbol R'_p represents the crack length which reduces the strength of an infinitely wide sheet to one half the tensile ultimate, since $\sigma_R/\sigma_u = 1/2$ when $w = \infty$ and $\ell_c = R'_p$. Thus R'_p has the same physical significance as R_p.

The use of equations (66) and(71) is essentially the same as the use of equation (6), as demonstrated in Appendix E.

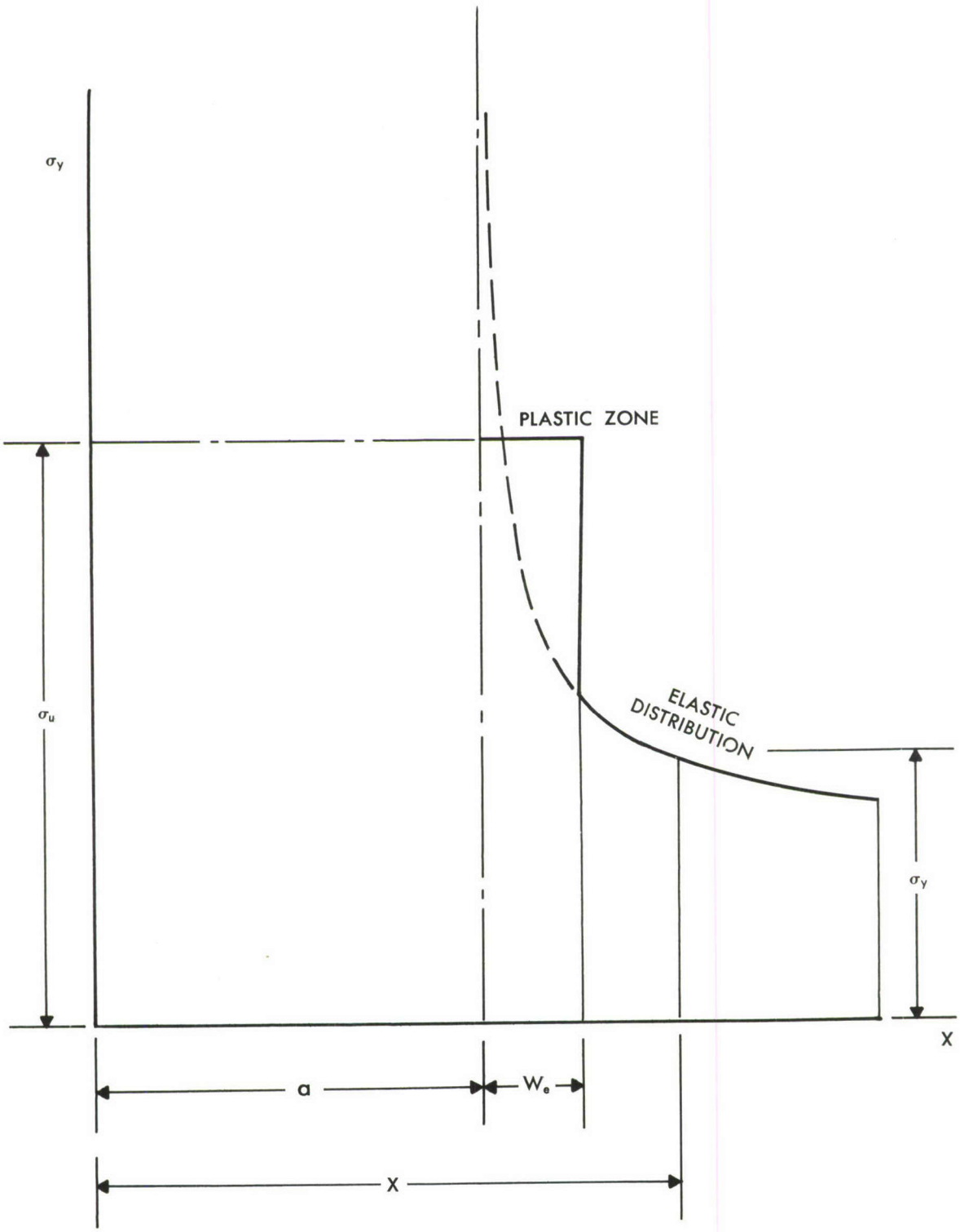


Figure 152. MODIFIED ASSUMPTION FOR STRESS DISTRIBUTION

BIBLIOGRAPHY

1. Bergeron, C. G., Tennery, V. J., Friedberg, A. L., Maroney, D. M., Shannon, R. D.; "Protective Coatings for Refractory Metals"; University of Illinois; WADD TR 59-526; August, 1960.

2. Bernstein, H., Weinberg, H.; "Progress Report on Fracture Toughness Tests of High-Strength Sheet Metals"; NAVORD Report 6496 and Part II, May 1959, January 1960.

3. Brock, G., Sinclair, G.; "Elevated-Temperature Tensile and Fatigue Behavior of Unalloyed Arc-Cast Molybdenum"; ASTM Preprint 64; Atlantic City, New Jersey, July 1960.

4. Campbell, J. C., Rice, L. P.; "Properties of the Precipitation-Hardening Stainless Steels and Low-Alloy High-Strength Steels at Very Low Temperatures"; Battelle Mem. Inst. Preprint; ASTM Annual Meeting, Atlantic City, New Jersey, July 1960.

5. Christensen, R. H.; "Some Fatigue Design Requirements for Future Air and Space Vehicles"; WADD TR 60-507; August 1959, page 777.

6. Christensen, R. H.; "Fatigue Damage, Fatigue Cracking and Their Detection"; Metal Fatigue, book published by McGraw Hill Book Co., 1959.

7. D.M.I.C. Report R 126; "Structural Damage in Thermally Cycled Rene' 41".

8. Dow, N. F., Editor, with NASA Advisory Committee on Strucutral Design; "Important Research Problems in Advanced Flight Structures Design - 1960"; NASA TN D-518, June 1960.

9. Fisher, Gideon, McClure, Grover, Carlson, Manning; "Development of Methods and Insturments for Mechanical Evaluation of Refractory Materials at Very High Temperatures"; WADD TR 60-155 June 1960.

10. Giemza, C. J.; "Experimentation, Analysis, and Prediction for Environmental Creep"; WADD TR 60-777, Nov. 1960.

11. Gluck and Freeman; "Effect of Prior Creep on Short-Time Mechanical Properties of C110 M Titanium with Emphasis on the BAUSCHINGER Effect"; WADC TR 59-681, February 1960.

12. Grosskreutz, J. C.; "Research on the Mechanisms of Fatigue"; WADD TR 60-313, April 1960.

13. Hanson, M. P.; "Smooth and Sharp-Notch Tensile Properties of Cold-Reduced AISI 301 and 304 L Stainless Steel Sheet at 75°F, -320°F, and -423°F"; NASA TN D-592; February 1961.

14. Illg, W., McEvily, A. J.; "The Rate of Fatigue-Crack Propagation for Two Aluminum Alloys Under Completely Reversed Loading"; NASA TN D-52; October 1959.

15. Imgram, A. G., Holden, F. C., Ogden, H. R., Jaffe, R. I.; "Notch Sensitivity of Refractory Metals"; Battelle Memorial Institute; WADD TR 60-278; September 1960.

16. Imgram, A. G., "Strain Aging of Refractory Metals"; DMIC Report 134; Battelle Memorial Institute; August 1960.

17. Irwin, G. R.; "Fracture Testing of High-Strength Sheet Materials Under Conditions Appropriate for Stress Anslysis"; NRL Report 5486; July 1960.

18. Jacobsen, M. M.; "Notch Sensitivity in High-Strength Sheet Materials"; Watertown Arsenal Progress Reports; May, Sept. 1960.

19. Kies, J. A., Smith, H. L., Romine, H., Bernstein, H.; "Minimum Toughness Requirements for High-Strength Sheet Steel"; NRL Report 5521, Oct. 1960.

20. Kikukawa, M.; "Factors of Stress Concentration for Notched Bars Under Tension and Bending"; Tenth Congress Appl. Mech.; Stresa, Italy, 1960

21. Lardenoit, V. F.; "Effective Stress Concentration Factors for Flight Vehicle Materials Under Various Conditions During Fatigue Testing"; Materials Central WADD; WADD TR 60-419, October 1960.

22. Leybold, H.; "Axial Load Fatigue Tests on 17-7 PH Stainless Steel Under Constant-Amplitude Loading"; NASA TN D-439, October 1960.

23. Mathauser, E., Stein, B., Rummler, D.; "Investigation of Problems Associated with the Use of Alloyed Molybdenum Sheet in Structures at Elevated Temperatures"; NASA TN D-447; October 1960.

24. Mittenbergs, A.A., Williams, D. N., Jaffe, R. I., Grover, H. J.; "Investigation of the Fatigue Properties of Molybdenum Under Various Conditions of Temperature, Coatings, and Stress Concentration"; Battelle Memorial Institute; WADD TR 60-427; October 1960.

25. NASA TR R-44; "A Phenomenological Theory for the Transient Creep of Metals at Elevated Temperatures; 1959.

26. Romine, H. E.; "Critical Crack Extension Force Determinations"; U.S. Naval Proving Ground Technical Reports; T27-59, T3-59, T13-59, T22-58, and T8-60.

27. Romauldi and Sanders; "Fracture Arrest by Riveted Stiffeners"; Contract AF 49(638)-273; Carnegie Inst. Tech.; October 1960.

28. Schijve, J.; "Fatigue Crack Propagation in Light Alloy Sheet Material and Structures"; National Aeronautical Research Institute, Amsterdam; Report MP.195; August 1960.

29. Shrier, A., Weissmann, S., Slade, J. J.; "X-ray Study of Lattice Defects in Fatigued Single Crystals"; AFOSR TN 60-519; July 1960.

30. Smith, R. W., Smith, G. T.; "Thermal-Fatigue Crack-Growth Characteristics and Mechanical Strain Cycling Behavior of A-286 and 16-25-6 Steels"; NASA TN D-479; October 1960.

31. Voorhees, H. R., Freeman, J. W.; "Notch Sensitivity of High-Temperature Alloys"; WADD TR 59-470, March 1960.

32. WADD TR 60-310; "The Effect of Several Geometrical Variables on the Notch Tensile Strength of 4340 Steel Sheet Heat Treated to Three Strength Levels"; Syracuse University Res. Inst.; September 1960.

33. WADD TR 60-410; "Investigation of Thermal Effects in Fatigue"; Part I, August 1960.

34. Whaley, R. E., Kurzahls, P. R.; "Fatigue Crack Propagation in Aluminum-Alloy Tension Panels"; NASA TN D-543, November 1960.

35. Williams, T. R. G.; "The Problem of Cumulative Fatigue Damage in Sheet"; Sheet Metal Industries, September 1960, page 653.